Investigation of the Functionality of White Soft Paraffin with Regards to Ointments

Phillip John Bentley

Submitted in accordance with the requirements for the degree of Doctor of Philosophy

University of Leeds

School of Food Science and Nutrition

August 2017

The candidate confirms that the work submitted is his/her/their own and that appropriate credit has been given where reference has been made to the work of others.

Acknowledgements

I would like to start by thanking my two supervisors, Professor Brent Murray and Professor Nikil Kapur, for their continued support advice and guidance throughout my thesis. Your knowledge was invaluable as I advanced with what we all found to be a complicated material.

I would also like to thank Dr Eloise Welfare and GlaxoSmithKline for bringing this project to my attention. Dr Welfare's advice and first-hand knowledge of white soft paraffin was crucial times and her continued assistance from the other side of the world, in Kuala Lumpur, was greatly appreciated.

I would like to thank the multiple people who have helped me at GlaxoSmithKline with support and advice throughout my thesis project; Brian McBride, Gordon Scott and Tim Sabey.

I also want to thank Dr Anuradha Pallipurath (National University of Ireland Galway) for her help with Raman spectroscopy analysis of my samples. Mahmood Akhtar, Ian Hardy and Miles Radcliffe, along with all the staff at Leeds School of Food Science and Nutrition for their assistance with my consistent distractions of their work, so I could complete my own lab practices.

Finally, I want to thank my mum, Elaine Bentley for her support throughout this entire process. My greatest thanks go to my love, Laura Laguna Cruañes for her support, encouragement and understanding throughout all my highs and lows. Her constant praise and belief has got me through to the end, this work is as much for her as it was for me.

Thank you all.

Abstract

Within the pharmaceutical industry, paraffin products are used as functional ingredients to produce ointment products, suitable for consumer end use. Paraffin wax is a complex material, itself describes an entire group of alkanes ranging from C10 to C60. It was the aim of this project to characterise the paraffin constituent components (oils and waxes) and their combinations (creating white soft paraffin (WSP)). Using a wide range of instrumental characterisation such as cone penetration, viscosity, oscillation rheology and cross polar optical microscopy; thermal characterisation: differential scanning calorimetry: and chemical characterisation: solubility parameters and Raman spectroscopy, the functionality of WSP products will be examined. Finally using WSP blends and constituent components, long term stability was tested as well as overload process testing on model WSP blends.

Waxes with high congeal points were found to have greater penetration forces and viscosities (MWM = 281.62 N, MWH = 273.67 N), model WSP blends containing different wax materials showed similar penetration values corresponding to wax forces (WSP9, a combination of PWH and MWH = 29.92 N). Similarities in waxes and WSP blends seen in penetration and rheology are not seen in DSC thermographs, loss of energy from wax components within the WSP blends were evident (PWL; 295.08 mJ + MWM; 134.58 mJ ≠ WSP5; 23.42 mJ). The progression of solubility parameters saw that there were similarities in expected WSP blends and correlation between wax components, indicating that miscibility has a role to play in WSP production.

Processing testing and microscopic analysis showed that long term storage crystals decrease in size affecting the packing density, reducing penetration forces and G’ stiffness in samples, ultimately indicating the need for greater wax ratio mixes to be developed for consumer end use suitability.

List of Figures

List of Tables

Abbreviations

WSP	White soft paraffin
PW	Paraffin wax
PWL	Paraffin wax low congeal point
PWM	Paraffin wax medium congeal point
PWH	Paraffin wax high congeal point
MW	Microcrystalline wax
MWL	Microcrystalline wax low congeal point
MWM	Microcrystalline wax medium congeal point
MWH	Microcrystalline wax high congeal point
LO	Low viscosity oil
HO	High viscosity oil
LP	Liquid paraffin
BP	British Pharmacopoeia
EP	European Pharmacopoeia
USP	United States of America Pharmacopoeia
FDA	Federal drug agency
JP	Japan Pharmacopoeia
MHRA	Medicines and Healthcare Products Regulatory Agency
API	Active pharmaceutical ingredient
GSK	GlaxoSmithKline
Mw	Molecular weight
PCM	Phase change material
DNA	Deoxyribonucleic acid
RNA	Ribonucleic acid
PCR	Polymerase chain reaction
LVER	Linear viscoelastic region
DSC	Differential scanning calorimetry
SEM	Scanning electron microscope
TEM	Transmission electron microscope
CLSM	Confocal laser scanning microscopy
AFM	Atomic force microscope
FIMS	Field Ionisation Mass Spectrometry
H-NMR	Nuclear Magnetic Resonance Spectroscopy
HP	Hildebrand solubility parameter
HSP	Hansen solubility parameter
GCMS	Gas chromatography mass spectrometer
RS	Raman spectrometer
GC-FIMS	Gas chromatography field ionisation mass spectroscopy
-E	Cohesive energy density
RED	Relative energy density
IR	Infrared
CGP	Congeal point
MSDS	Material Safety Data Sheet
UV/Vis	Ultraviolet/Visible

PTFE	Polytetrafluoroethylene
λMAX	Wavenumber of maximum absorbance
δd	Dispersion forces
δp	Intermolecular forces
δh	Hydrogen bond forces
CARS	Coherent Anti-Stokes Spectroscopy

Units

N	Newtons
mJ	Millijoules
kJ	Kilojoules
J	Joule
kg	Kilograms
K	Kelvin
Jg^{-1}	Joules per gram
°C	Degrees Celsius
Pa	Pascal
dyn cm^{-2}	Dyne per centimetre squared
N m^2	Newton metres squared
mm	Millimetre
mW	Milliwatt
$MPa^{1/2}$	$Megapascal^{1/2}$
cm^3 mol^{-1}	Centimetre cubed per mol
cSt	Centistokes
Pa s	Pascal seconds
ml	Millilitre
h	Hours
mm s^{-1}	Millimetre per second
s^{-1}	Per second
Hz	Herts
µl	Microliter
°C min^{-1}	Degrees Celsius per minute
mg	Milligram
g	Gram
nm	Nanometre
µm	Micrometre
cm	Centimetre
cm^{-1}	Per centimetre

Table of Contents

Chapter 1 Introduction

1.1 Context

The pharmaceutical industry is one of the largest manufacturing sectors in the world with the top 10 pharmaceutical companies generating $ 405.4 billion in 2015 (Statista, 2016). The pharmaceutical industry manufactures many products designed for medical and healthcare purposes. Whilst there are many thousands of products only a limited range of administration routes. These methods are enteral for example, oral tablets like paracetamol; parenteral, injection to the bloodstream for example intravenous drugs such as vaccinations; and a variety of methods including drug administration through intranasal, topical, inhalation, or rectal means.

In the 1960s the administration of Thalidomide to pregnant mothers was linked to the cause congenital abnormalities in their children (McBride, 1961). This case of harm to health as a result of Thalidomide has driven the installation of regulations for monitoring of control and monitoring of manufacturing, under international laws and regulations, given by organisations such as the Federal Drug Administration (FDA) and British Pharmacopoeia (BP), European Pharmacopoeia (EP), United States of America Pharmacopoeia (USP), Japanese Pharmacopoeia (JP) and the Medicines and Healthcare Products Regulatory Agency (MHRA).

To be able to control the manufacturing of pharmaceutical drug products the chemical and physical characteristics of both raw material and the final product must be understood to be able to offer consumers the safe products for their specific medical needs. As already discussed these drugs can be administered by different routes, however, this project has been completed to address the process of manufacture of white soft paraffin (WSP), fundamental to the manufacture of ointments, a product that is applied as a topical, dermatological product.

In most occurrences of pharmaceutical ointment manufacture, the product is designed as a base to carry a range of medicinal ingredients called active pharmaceutical ingredients (APIs), to be applied topically and absorbed through the skin/dermis. Ointment products can also be used solely for hydration

purposes, although not an ointment, Vaseline® is used for hydration purposes and is a pure petrolatum, also known as, WSP. Production of ointments is varied depending on their certain demands, research into combining raw ingredients for these ointments has previously been carried out, and a number of sources give good accounts of how to make these mixes with required chemical and physical characteristics (Barry and Grace, 1971c; Chang et al., 2003; Vilasau et al., 2011; Deman and Beers, 1987).

Ointments are generally a mixture of hydrocarbons, waxes and/or polyethylene glycols which act as the base carrier material for other active or non-active products. Ointments can also include up to 20 % water to produce an emulsion mixture (Buhse et al., 2005). Paraffin waxes and microcrystalline waxes are often the main base product used in ointment products (Barry and Grace, 1971c). White soft paraffin is a combination of these individual waxes along with paraffin/mineral oils and is the general term used for the mixture of paraffin products used.

This project has been carried out to better understand the characteristics of the base materials in the use of ointment production at GlaxoSmithKline (GSK), with the focus being for white soft paraffin (WSP), and paraffin products, the main materials that make up the final ointments. WSP is the main component of cream and ointment products formed at GSK, however, there are other materials that also could be considered when characterising WSP under different processing and experimental conditions. The active pharmaceutical ingredient (API) and water are both frequently used in the formulation. API's are generally added at less than 1 % into ointments but can reach up to 5 % in some very specific products. As stated previously water can be added up to 20 % of the total (Buhse et al., 2005). In addition, structuring agents such as hydrocolloids can also be incorporated along with surfactants for stability and bactericides. The focus of this work will be on ointments of a WSP and oil base without the additional complexity of other materials.

1.2 Structure of WSP

Paraffin is a group of higher molecular weight (Mw) alkanes with the general formula (C_nH_{2n+2}). All of them are extracted from crude oil refinery via fraction distillation and have many uses within multiple industries. Some of the

uses and the industries that use paraffin products will be later discussed in section 1.3 Uses and Functions.

The products that pharmaceutical companies are primarily interested in for the manufacture of ointments include the following;

- Liquid paraffin (LP)
- Macrocrystalline/Paraffin wax (PW)
- Microcrystalline wax (MW)

The degree of carbon content increases from liquid paraffin to microcrystalline waxes, liquid paraffin contains between C_{10}-C_{18}, macrocrystalline wax contains C_{18}-C_{30} and microcrystalline wax contains between C_{40}-C_{55}. Soft paraffin/petroleum jellies are the same in makeup but contain a different mixture of solid waxes and liquid paraffin depending on grade variations but can range in carbon content between C_{20}-C_{40}. White soft paraffin is a blend of various paraffin derivatives and depending on the need for the final product and the mixture ratio there will be specifications for suppliers to produce these blends to produce ointments. As part of this report, the formulation of blends and the specifications for these certain blends will be covered. Figure 1.1 shows a flowchart of paraffin derivative products available by various methods of production; the key materials from this will be highlighted in the following sections.

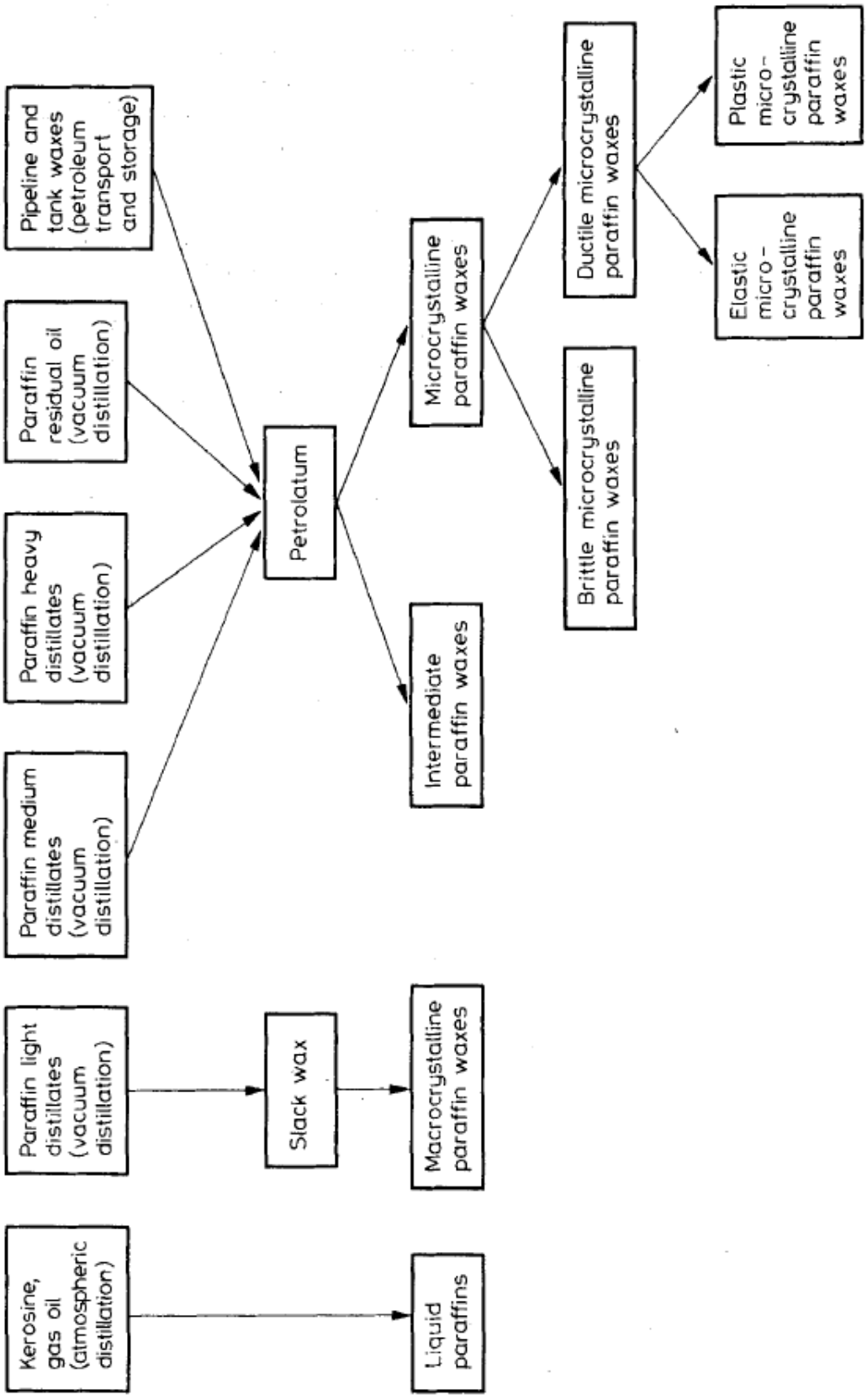

Figure 1.1 – Flowchart showing the steps of formation for different paraffin derivatives (Freund et al., 1982).

1.2.1 Liquid Paraffin/Paraffin Oil/Mineral Oil

White soft paraffin by nature is a blend of many grades of paraffin derivatives, one of which is liquid paraffin, as such the scope of this project also includes investigation of liquid paraffin (mineral oil).

Liquid paraffin is a light fraction of kerosene and gas oil obtained from crude petroleum distillation and is a mixture of hydrocarbon alkane molecules ranging from C_{11}-C_{24} (Freund et al., 1982). The alkane mixture is liquid at room temperature and atmospheric pressure due to the chemical nature of the hydrocarbon chains in the liquid paraffin. As the chain length of the hydrocarbons is so low (between C_{11}-C_{24}) there is no ability to form crystals (waxes) in the mixture and lowering the temperature will only cause an increase in viscosity rather than formation of crystalline waxes.

An increase in liquid paraffin viscosity is observed as the molecular weight increases (Freund et al., 1982). This can be explained by the increasing number of hydrocarbon chain length within the liquid paraffin, which in turn causes a greater number of interactions between countering hydrocarbon chains. On a molecular level hydrocarbons can interact between neighbouring molecules via weak attractive forces, causing the change. This phenomenon is well known and is the reason for the addition to crystalline wax blends that ultimately make up white soft paraffin. Liquid paraffin is added to white soft paraffin and is trapped within a three-dimensional crystal network made by crystalline waxes. When more liquid paraffin is added, greater slip qualities occur within the white soft paraffin allowing for a less viscous, more fluid, white soft paraffin to be produced.

Liquid paraffin is mostly made up of n-alkanes (96.4 wt.%) but does contain some iso-/cyclo-alkane content (3.4 wt.%) and very small amounts of aromatic (phenyl) alkanes (0.2 wt.%) (Freund et al., 1982). This supports why the paraffin is liquid at room temperature and atmospheric pressure as most of the liquid paraffin contains short chain n-alkane molecules and lacks the quantity of molecules to form interactions, therefore, liquid paraffin lacks weak interaction force between molecules.

1.2.2 Macrocrystalline Wax/Paraffin Wax

Macrocrystalline wax (also known as paraffin wax), like all paraffin products, consists of a mixture of hydrocarbons ranging in molecular weight between 250 and 450 where chain lengths range between C_{18}–C_{30} (Freund et al., 1982). The melting points of macrocrystalline waxes are in the range 40-60 °C with further classification of soft paraffin ≤ 45 °C and hard paraffin 45-60 °C

Macrocrystalline wax will consist of plate and needle shape crystal habits. These habits will allow for certain packing formation and crystal interaction for the paraffin wax, this, in turn, determines the physical properties of the wax (note rheological and thermal properties are given in Chapter 3 and Chapter 4). Macrocrystalline wax consists mainly of saturated hydrocarbon alkane chains but will contain some low molecular weight aromatic hydrocarbons, formed mainly as alkylbenzene derivatives. The alkylbenzenes have a very little effect on the macrocrystalline wax in terms of rheological and thermal determination but could cause a health risk to the consumer if contained within the final products due to the reactive nature of the aromatic hydrocarbon. Macrocrystalline wax will form three dimensional crystals as the paraffin is cooled across a temperature range, the blend of waxes present will determine the temperature at which the blend will crystallise. A similar process is seen in fatty spreads and chocolate in the food industry with ranges of melting points for blends of lipids depending on the molecular weight of the lipids and the weight percentage of the product (Heertje et al., 1997). Physically, macrocrystalline wax is a brittle substance with very little elasticity; the wax will almost “flake” and will break immediately upon application of force. Increasing the ratio of branched hydrocarbon content, often contained within microcrystalline wax, will change the macrocrystalline wax. Increasing branched content in liquid paraffin form will cause the wax to soften, reducing cohesion stress. However, adding branched content in solid form will plasticise the wax, reducing the brittle nature of the macrocrystalline wax by filling the gaps between the straight chain hydrocarbons present within macrocrystalline waxes (Freund et al., 1982).

1.2.3 Microcrystalline Wax

Microcrystalline waxes are like macrocrystalline wax but contain a greater proportion of iso-alkanes and cycloalkanes (naphthalene) with large numbers of

long hydrocarbon side chains. Chain lengths of microcrystalline waxes range between C_{40}-C_{55}. These factors result in a finer crystal network with a great packing amount and consequently a higher molecular weight. Melting points can range between 60-80 °C (laminating grade), 80-93 °C (hardening grade). The waxy alkane hydrocarbons cooled below their melting points form crystals, producing a three-dimensional network, much like for the macrocrystalline waxes. The three-dimensional lattice network that is formed can trap liquid paraffin within the network due to the microcrystalline nature of the wax is much smaller than that of the macrocrystalline there is less liquid paraffin that can be trapped, resulting in the microcrystalline wax blend being more viscous and solid compared to the macrocrystalline. The presence within the network of liquid paraffin will allow for some flow properties accredited to the waxes. Depending on the degree of crystal growth and crystal habit will determine the flow properties, or rheology, of the wax.

1.2.4 White Soft Paraffin

White soft paraffin (WSP) is defined in "*British Pharmacopoeia"* as (Freund et al., 1982):

"Purified and wholly or nearly decolourised mixture of semi-solid hydrocarbons, obtained from petroleum. It may contain suitable antioxidant."

WSP is a soft unctuous mass and is poorly soluble in water and alcohols but is soluble in methylene chloride. As such it is a useful product to use in liquids, creams, emulsions and ointments, of which, ointments will only be considered within this body of work. WSP is an excellent carrier material (base) for active dermatological ingredients as well as acting as a barrier to the environment, providing moisturising trapping, oily characteristics preventing evaporation of water to the environment. WSP is a mixture of hydrocarbons derived from petroleum. More accurately paraffin is a name given to a range of high molecular weight (Mw) alkanes with molecular formula C_nH_{2n+2}. Paraffin can range from light liquid paraffin to microcrystalline waxes with the characteristics of the paraffin product being determined by the alkane length, carbon number and saturation within the chain.

White soft paraffin is determined by the final aspects of the blending paraffin derivatives of liquid paraffin, paraffin wax and microcrystalline wax, and

depend on the requirement of the product being manufactured which will determine the ratio of paraffin derivative used. A crucial factor to consider in the wax blend related to its physical stability is the ratio of the derivatives, with at least 12 % and up to 15 % being microcrystalline wax. This figure is critical as any less than 12 % and there will not be sufficient microcrystalline to “hold” the liquid paraffin within the WSP lattice network, based on information obtained from one WSP suppliers, Fuchs Lubricants (UK) plc, and the liquid paraffin will leave the blend with ease (squeezing with hand force or leaving over time will cause the liquid paraffin to separate from the bulk). Other considerations are the type of crystals that are present in the waxes these can be hexagonal or orthorhombic. Alkanes between C_{19}-C_{29} with an odd number of carbon atoms tend to be orthorhombic, alkanes between C_{18}-C_{26} with an even number of carbons are triclinic and those between C_{28}-C_{36} are monoclinic (Freund et al., 1982). Upon growth of crystals, the packing of the crystals can also determine the viscosity of the wax. Hexagonal packed crystals tend to flow more readily than orthorhombic crystals due to the ability of the hydrocarbon chains being able to rotate around their axis. Due to the packing nature of the orthorhombic crystals, these are not allowed to rotate about their axis when in a packed structure. A diagrammatic representation is shown in figure 1.2a and 1.2b.

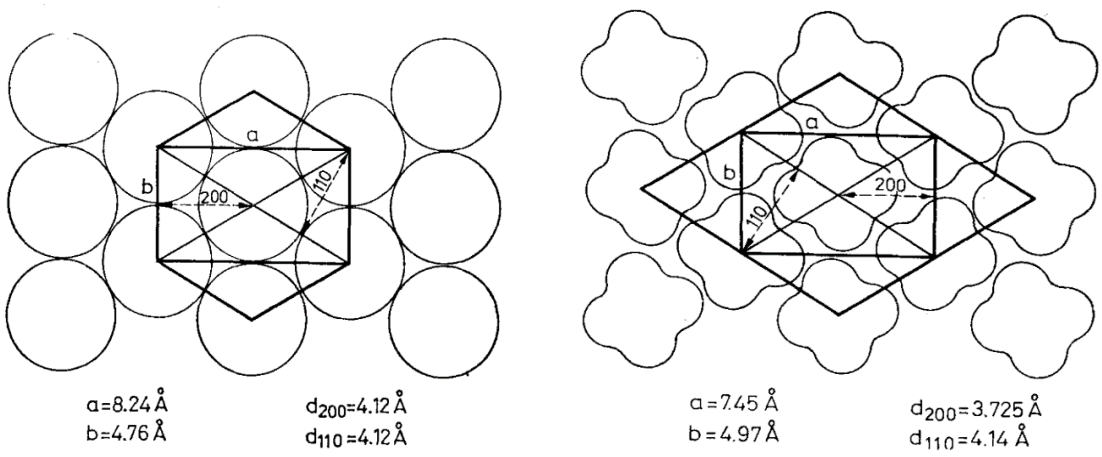

Figure 1.2a (left) – Hexagonal structure of paraffin wax crystals. (Freund et al., 1982) **Figure 1.2b (right)** – Orthorhombic structure of paraffin wax crystals. (Freund et al., 1982)

When considering paraffin waxes, it is also important to understand the phase transitions of the wax crystals. As discussed, the different paraffin derivatives have different melting points. This is related to the latent heat of fusion which is the amount of energy required per kilogram of product to effect a change to another phase state. The waxes also exhibit different crystal phases

upon changes to the latent heat of fusion, much like in chocolate with six different crystal phases, macrocrystalline waxes have 2 crystal phases (α- and β-) (Freund et al., 1982). Within macrocrystalline waxes, α-crystals are more predominant but it has been determined that increasing carbon chain length within the alkanes causes a modification to β-crystals. Lowering temperature of the wax will also cause a shift to the β-crystal phase. The variation in polymorphism in macrocrystalline waxes is another reason for why there is such variability in the viscosity of the wax. Due to the large molecular weight and high carbon length in microcrystalline wax chain lengths, there is less variation, therefore the waxes are much more solid under ambient conditions.

When blending paraffin derivatives to produce WSP it will often require multiple types of waxes and oils to obtain the correct consistency that would be required by an end user.

From discussion with suppliers, mixing two paraffin waxes with different congeal points is often required to give solid properties to the wax blend. Addition of one or multiple microcrystalline waxes with different congealing points are used to introduce elastic properties, followed by liquid paraffin to give a product the physical properties that would be required. The congealing point is an international testing method for paraffin wax blends; it is the highest temperature at which a melted solid (wax blend) will solidify. The congealing point is affected by the carbon chain length and saturation of the hydrocarbon present in the paraffin fraction; it is these factors that also help the blending process when producing white soft paraffin wax blends.

One final aspect that could influence the waxes properties are the habits of the crystals within the wax. It has been shown that three habits exist, needle, plate and mal types. Figure 1.3 shows a diagram of the 3 crystal types that can be found.

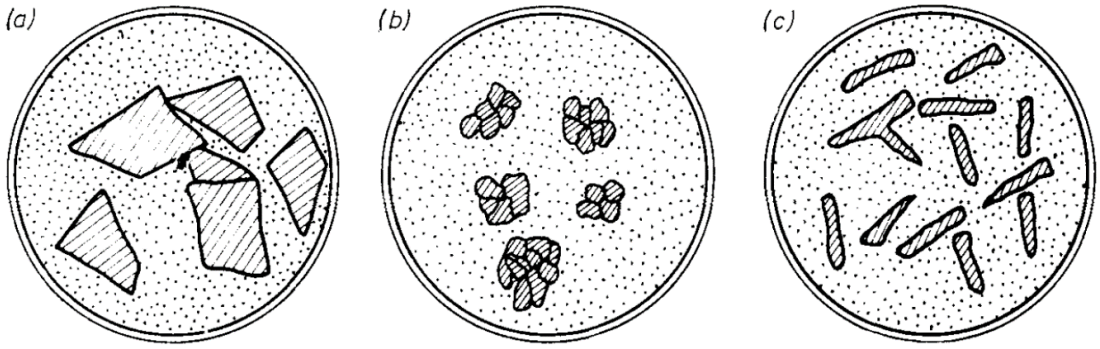

Figure 1.3 – Diagram showing 3 crystal habits of paraffin waxes. (a) *plate crystals,* (b) *mal crystals,* (c) *needle crystals* (Freund et al., 1982).

Macrocrystalline waxes contain mostly plate crystals and as such can form stable lattice microstructures with the capability to pack in liquid paraffin in these gaps, allowing for greater variation in the blends of the wax. Evidence of how a wax structure made of plate crystals is shown by (Jafari Ansaroudi et al., 2013) when testing wax deposition in control flow loops. (Ashbaugh et al., 2002) and (Imai et al., 2001) also show images of how plates crystals form, introducing the term ‘house of cards’ to describe how the crystals will for a 3D network. Microcrystalline waxes contain a high ratio of mal and needle crystal types, therefore, have a greater packing density not allowing for the inclusion of liquid paraffin making the wax more solid with less flowing properties.

For a crystal lattice to form the temperature of the wax would have to be reduced to below its melting point, and further to a supercritical temperature point at which supersaturation will occur in the wax melt. At this point nucleation will take place in the wax melt, this occurs due to microscopic crystals presence and the effect of Brownian motion occurring. Attractive forces between the crystals become greater than the energy in the force of motion allowing the crystals to form connections, and grow. As previously stated most wax materials are made of plate crystals and as such build lamellar layers to form 3D structures. Depending on wax boundary orientation the crystals can grow in various directions and can also form a ‘house of cards’ structure. These small crystals will always grow to reach mass volume expansion due to small crystals requiring large amounts of energy to hold their stability at a small size. Interfacial energies between the crystal molecule and the surrounding melt will be large, therefore the atoms in the melt will be greatly attracted to the crystal causing the growth with time. If the temperature is further reduced beyond nucleation temperature

the crystals will grow at greater rates, this rate of growth will then also affect the crystal habit and size, and therefore wax stability.

Although there has not been much recent investigation, authors (Ferris and Cowles, 1945) show how individual crystal types can form connections and grown as 3D lattice networks in wax samples. (Freund et al., 1982) states sizes of some hydrocarbon lengths are; $C_{15}H_{32}$ 21.0 Å, $C_{17}H_{36}$ 23.6 Å, $C_{19}H_{40}$ 26.2 Å, and $C_{29}H_{60}$ 38.6 Å however does not indicate the distances between wax crystals. Multiple authors throughout this thesis will indicate the size of various crystal growths as well as evidence shown in this investigation that crystal sizes can reach up to 50 – 100 µm. (Pahlavan et al., 2016) model how wax-doped asphaltenes can form a variety wax crystals and effect the wax behaviour based on wax percentage. This model also helps to show the behaviour of the fracturing between wax masses when a shear force is applied.

Fracturing of wax crystals due to the weak interactive forces between the crystals, these being Van der Waal forces. These forces can keep crystal structures in place without agitation due to the number of attraction points available, however, under relatively small force application these crystals will shear and fracture, Van der Waal forces (or London dispersion forces) are the weakest and arise from temporary molecular charge instigated by electron cloud movement around atoms and molecules and are spontaneous in occurrence. Dipole-dipole forces, which occur in compounds with permanent compound charge distribution. For example, hydrochloric acid where hydrogen and chlorine have different electron densities, giving rise to partial charge development. Hydrogen bonding, the strongest of the molecular interactive forces. Hydrogen bonding occurs between molecules that have hydrogen atoms bonded to an electronegative atom, e.g. oxygen or nitrogen, this then develops a charge difference in the molecule. In paraffin waxes, only London forces will be encounters, as only pure hydrocarbons would be useful in wax, other atoms that would cause dipole-dipole attractions and hydrogen bonding could cause further chemical breakdown and oxidation of paraffin waxes for future stability.

1.3 Uses and Functions

Paraffin waxes, a component of white soft paraffin (WSP) blends have a variety of uses in many industries including: “*pharmaceuticals, cosmetics, paper*

manufacturing, candle making, electrical goods, rubber compounding, and *textiles"* (Freund et al., 1982).

1.3.1 Pharmaceuticals

Paraffin wax and more commonly white soft paraffin is a product used as a base for production of emulsions, creams and ointments within the pharmaceutical industry. What makes WSP especially useful is that the it can be a relatively stable product and does not react with other active ingredients, such as the API or other components. That said, paraffin wax is a mixture of long chain hydrocarbons and it should be recognised that the hydrocarbon chain is unsaturated and can undergo oxidation to create peroxides, which can be very reactive species and can cause problems with other active ingredients mixed in with the white soft paraffin.

Oxidation of active pharmaceutical ingredients in ointments has been evident for many years (Freund et al., 1982). Not only is it important to control the molecular components of white soft paraffin, but also the mixing process. When developing formulations for ointments the ratio of drug to WSP and water should all be considered. It has been shown that making a primary mixture of an ointment base and a second mixture with the API component in an oil phase, or contained in propylene glycol can prove efficient, helping to prevent oxidation of the API, improving product stability.

White soft paraffin is often used as the base ingredient in ointments, creams and emulsions. Alongside the API, surfactants are vital to formulation with the purpose of increasing stability and emulsification ability for creams and emulsions, surfactants and stabilisers can be added in various forms, (Freund et al., 1982) using fatty amphiphiles to help stabilise wax emulsions by creating interfacial surfaces on oil droplets present in the emulsion. The presence of the several types of fatty amphiphiles can also modify the rheological properties through the altering of the viscosity of the emulsions depending on the requirement by increasing or decreasing the ratio of amphiphile.

1.3.2 Phase Change Material Technology

Paraffin wax has seen the application as a phase change material (PCM) with energy management. The advantages of the paraffin waxes as a PCM are

due to the latent heat of fusion. This latent heat allows the wax to hold a large amount of heat in the system. At this point, this heat can transfer to or from surrounding materials, such as clothing items or most commonly as part of insulated wall panels within buildings. The specific heat capacity (C_p) of paraffin wax has been measured at around 2.1 kJ kg^{-1} K^{-1} with the melting enthalpy ranging between 180 – 230 kJ kg^{-1} (Luyt et al., 2010). As a comparison air has a C_p of 1 kJ kg^{-1} K^{-1} (Al-shemmeri, 2010), oxygen has a C_p of 0.918 kJ kg^{-1} K^{-1}, carbon has a C_p of 0.709 kJ kg^{-1} K^{-1} and water has a C_p of 4.187 kJ kg^{-1} K^{-1} (Lide, 2003). It is the high capacities of paraffin wax that benefit the PCM aspects of paraffin wax as the heat input into the system will be retained for a considerable amount of time, slowly releasing the heat back into the surroundings.

It was believed (Luyt et al., 2010) that polyamide 12 and maleic anhydride could have been blended with paraffin wax to aid with the latent heat properties of the paraffin wax increasing efficiencies and use of the blends as a phase change material. In principle, this would have helped to improve the stability of the paraffin wax and PCM. However, it was found that upon blending it was difficult to incorporate more than 30 % paraffin wax within the product matrix.

Another use for paraffin wax as a phase change material is within the textiles industry creating thermo-regulating clothing by means of microencapsulating paraffin wax (Sánchez et al., 2010). The wax was encapsulated since due to the melting points of the paraffin the waxes would simply melt out of the textile material during production. As such the paraffin wax was encapsulated within a polymer coating to protect the properties of the paraffin wax and to keep it fixed in place. The encapsulated PCM particles were incorporated into the textile material which underwent certain thermal tests to determine the acceptability and endurance of the microencapsulated PCM. Although only 35 % of fabric could be coated with the microcapsules heat absorption of 7.6 J g^{-1} was attained. However, it was discovered that under regular treatment processes such as washing and ironing of the fabric there was a significant loss of microcapsules and therefore loss of heat storage capacity of the fabric and acting PCM.

A further example of paraffin wax as a phase change material is with use within solar heat storage panels (Hawlader et al., 2003). Due to the excellent

heat capacity of the paraffin wax along with microencapsulation the paraffin wax can act as an insulator. In work conducted by (Hawlader et al., 2003), gum Arabic and gelatin powder were used to encapsulate paraffin wax with a melting point of between 60 °C and 62 °C consisting mainly of n-alkane. This would indicate the use of a hard paraffin macrocrystalline wax. The work used two methods of producing the microencapsulation upon the solar panel, spray-drying and coacervation. Results showed that depending on material ratio mixing and production type, energy storage capacities ranged between 145.28 J g^{-1} to 239.78 J g^{-1}, and energy release capacities ranged between 148.32 J g^{-1} to 234.05 J g^{-1}. The results obtained showed promise with excellent storage capacity for heat energy. Depending on the method of encapsulation and treatment of the PCM better ability as an energy storage medium within the solar panels was discovered.

One possible way of improving phase change materials has been discussed by (Babaei et al., 2013). It was proposed that with the addition of graphene and carbon nanotubes into a paraffin wax the thermal properties of the wax could be improved, as used as a phase change material. In the paper, it was discovered using computer modelling that thermal conductivity could be improved within the paraffin wax, however, there seemed to be a dispute as to how the improvement was achieved, with some evidence that the improved ordering of the structure of the paraffin crystal lattice enhanced the thermal conductivity. Other variations on nano-carbon composites introduced to paraffin wax to improve thermal properties have been investigated (Xiang and Drzal, 2011; Zhang et al., 2013).

1.3.3 Medical Research

Paraffin waxes have found a use for DNA/RNA extraction in PCR investigations (Lehmann and Kreipe, 2001). With limited success paraffin wax, could be used as an embedded medium for the extraction of RNA, however, methods were often based on techniques of specific investigation/research and could not be given a generalised methodology at this time. Further research into the use of paraffin wax as a growth medium would have to be carried out before confidence could be given as a standard method of use.

1.3.4 Encapsulation Technology

(Ibrahim and Jibril, 2005) and (Al-Zahrani, 2000) conducted work on the encapsulation of fertilizers with the use of paraffin wax in combination with other polymer waxes in order to cause a timed release of fertilizer. Paraffin wax was believed to be a suitable product due to the stable nature of the hydrocarbon alkanes present in the paraffin. There is always a chance that auto-oxidation can take place however the risk is so low that it would have a negligible effect on the fertiliser and surrounding environment. Through investigation it was found that the paraffin wax did delay the release of the fertiliser in question, however, it was less efficient at delaying than other polymer waxes that were under consideration. It is plausible that paraffin wax can be used as a delayed released mechanism for certain products depending on the requirement.

1.3.5 Paper Manufacturing

Paraffin wax is one of the more important materials used in the production of paper. Although used specifically in paper products it is also used in the production of cardboard and corrugated paperboard. The specific use of paraffin wax within the paper industry is for impregnation, coatings and laminating (Freund et al., 1982).

1.4 Characterisation Techniques

WSP is a complex material used within a regulated industry. The characterization of the material is therefore important.

1.4.1 Rheology

Due to the nature of WSP, the crystalline networks can be deformed easily under force. Depending on the temperature of the test carried out the WSP can act as a Newtonian fluid (i.e. when the WSP is (≥ 80 °C) molten) or as a sort of solid. Rheological characterization defined as (Schramm, 1994);

“Deformation of a body under the influence of stresses”

It is one of the most important investigative tools that can be used for analysing white soft paraffin. Typically, rheometers are used to perform a variety of small deformation tests, including shear stress, shear strain, viscosity plus other oscillatory tests depending on the requirement of the product (Barry and

Grace, 1971a). For large deformation testing, penetration testing often using drop cone penetrometers (Pharmacopoeia, 2005), texture analysers or viscometers are used to test bulk material characteristics of products. Each one of these tests has its benefits and drawbacks and depending on the specific blend of white soft paraffin in question may determine the type of test to be used. These tests can also be separated into two separate forms of characterisation, small deformation and large deformation rheology. Frequency sweeps and amplitude sweeps are classed as small deformation rheology due to imparting only small forces on the sample. Penetration tests are an example of large deformation rheology, this information will record much larger magnitudes of force, such as maximum values of stiffness and penetration of samples, but results can be much more variable as the interaction of the materials on a chemical level are much more subjective. Continuous shear viscometry and creep viscometry can be tested under both small and large deformation, depending on the material tested and the size of deformation performed on the material. For example, applying a shear rate of 1 s^{-1} to liquid paraffin could result in a large deformation, however applying 1 s^{-1} on a solid wax could result in a small deformation.

An ideal (Hookean) solid will, under given stress, deform with linear proportionality to the applied stress instantly and will remain deformed until the stress is removed. Removal of a stress will cause the solid to return to its original condition instantaneously. An ideal liquid will flow and will deform under any given stress without the ability to reform energies independently and will be lost to heat energy. Many materials exhibit mixtures of solid and liquid properties- these are termed viscoelastic. These materials will flow to a certain degree, the factor which determines the response is applied force and time. When considering a solid or liquid there are two time factors to be considered;

- Characteristic relaxation time factor (λ)
- Characteristic observation time value (t)

These two factors of a solid or liquid will give an important figure when considering the type of material being described; this is the Deborah number and is given in the following equation:

$$Deborah\ Number = \frac{\lambda}{t}$$

High values for the Deborah number will describe solid like products that are resistance to fast flow (may take centuries to flow), while low values will describe liquid like products and will flow very rapidly and easily (such as water, $\lambda_w = 10^{-12}$ s) (Schramm, 1994).

1.4.1.1 Modulus of Elasticity

As seen previously solids do not flow and there is a relationship between the stress and strain. Shear modulus is used to characterise such materials.

$$\tau = G \cdot \frac{dL}{dy} = G \cdot tan_{\gamma} \approx G \cdot \gamma$$

- τ = shear stress (= force/area) $\left[\frac{N}{m^2} = Pa\right]$
- G = shear modulus (relating to the stiffness of a solid $\left[\frac{N}{m^2}\right]$
- $\gamma = \frac{dL}{y}$ = strain
- y = height of the solid body [m]
- ΔL = deformation of the body due to shear stress [m]

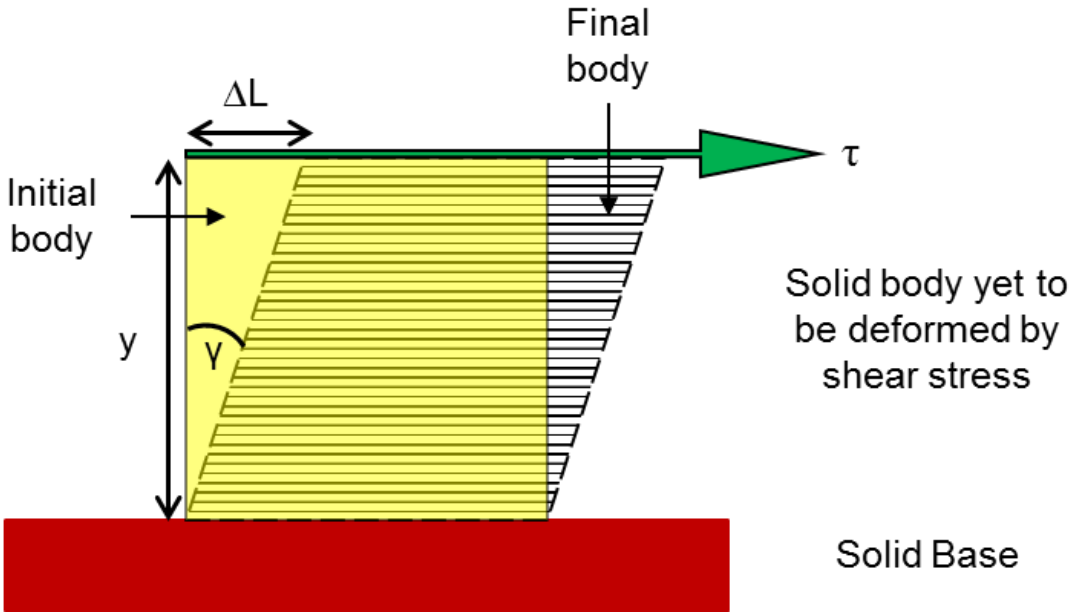

Figure 1.4 – Diagram of body of movement describing shear modulus.

1.4.1.2 Viscosity

When considering an ideal liquid (Newtonian liquid), a shear stress force is applied to the liquid and the deformation rate will increase linearly in proportion

to the force. Once the force is removed the liquid in its new state of deformation remains unchanged until a new shear stress force is applied. The following equation will show the relation for a Newtonian liquid (Schramm, 1994).

$$\eta = \frac{\tau}{\dot{\gamma}}$$

- τ = shear stress (Nm^{-2})
- η = viscosity (Pa s)
- $\dot{\gamma}$ = shear rate (ms^{-1})

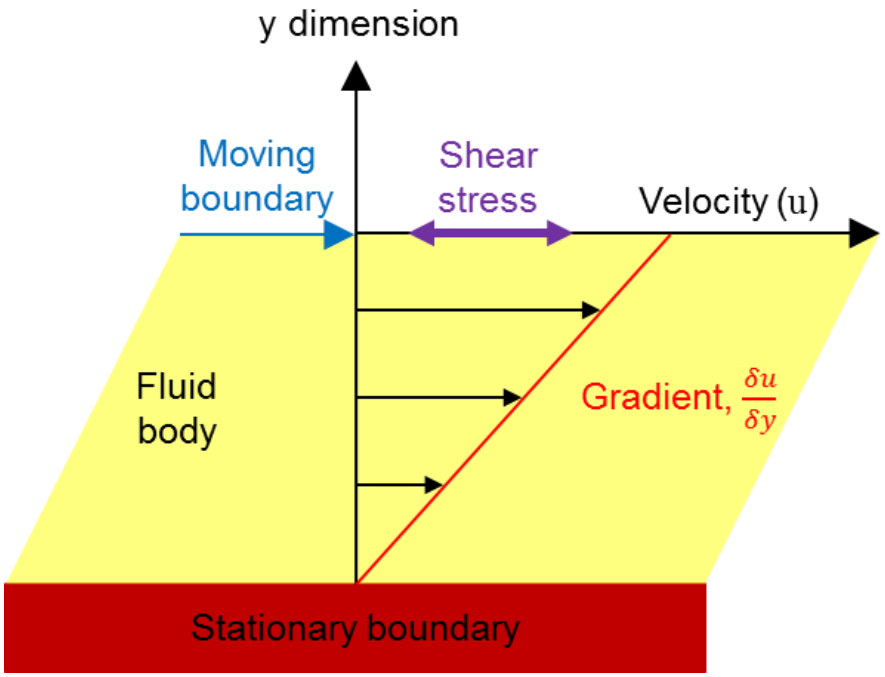

Figure 1.5 – Diagram showing the actions of shear viscosity following planer Couette flow.

The previous equation and figure 1.5 describe the shear viscosity of a body, this is the measurement of the resistance to flow. As a shear stress (τ) is applied to a fluid body then the body will effectively move in planes at greater velocity (u) the further away from a stationary phase. The distance travelled by a point over a measured amount of time will give the shear rate ($\dot{\gamma}$), indicated by the gradient in figure 1.5.

Continuous shear viscometry testing is a method that will provide data about the viscosity of the white soft paraffin, while oscillatory tests can provide data on viscoelastic modulus. Under continuous shear, care must be taken when testing materials as this method is in its nature is destructive, where increasing

the shear rate will cause a greater amount of breakdown in the materials microstructure. It is also possible if using a cone and plate method that the white soft paraffin can be squeezed out of the gap of the equipment which can cause erroneous results when sampling the white soft paraffin. Therefore, following the equipment's standard operating procedures is crucial when carrying out testing.

Another common test that can be used to determine consistency at a production plant level is the Falling-Ball viscometers. This type of viscometer operates on the principle of measuring the time for a ball to fall through a liquid, or a semisolid in this case, under the influence of gravity. The falling ball reaches its terminal velocity when the acceleration due to the force of gravity is exactly compensated for by the friction of the fluid on the ball (Bourne and Bourne, 2002). In this test, a large graduated glass cylinder is filled and a steel ball is gently dropped in the centre of the cylinder. Then, with the use of a stopwatch, the velocity of the fall of the ball is measured.

1.4.1.3 Viscoelastic Response

Ointments are a type of material that are considered non-ideal, they are neither fully solid or fully liquid but instead, contain both mechanical concepts within their physical properties. To represent the viscoelastic response of materials two models were developed by considering a spring and dashpot (Schramm, 1994).

- Kelvin-Voigt model (for solids)
- Maxwell model (for liquids)

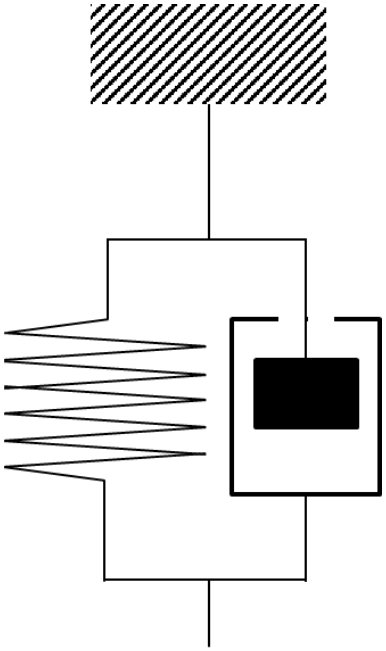

Figure 1.6 – Schematic of Kelvin-Voigt model of spring and dashpot response for viscoelastic solid materials (Schramm, 1994).

The Kelvin-Voigt model (figure 1.6) considers a spring and dashpot model that will relate to a simple viscoelastic solid. The strain in both elements must be the same, therefore the stresses shared unequally. The force applied to both spring and dashpot will result in an immediate response shown in the spring, which will be delayed and slowed by the dashpot present. Over time a larger deformation will occur at a slower rate as the dashpot experiences a response to the force applied. When the force is removed, the spring will have a large initial deformation while the dashpot will again offer resistance slowing the response from the loss of force. The response of force applied and the material extensional response is shown graphically in figure 1.7.

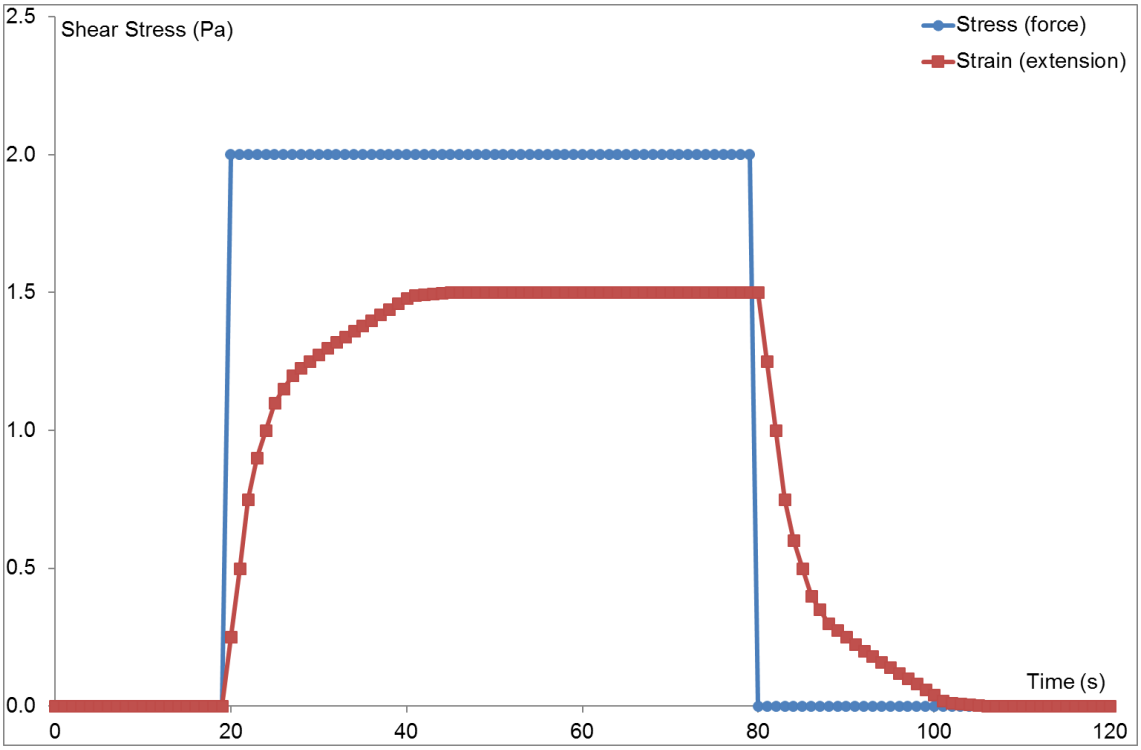

Figure 1.7 – A graph showing the Kelvin-Voigt model for a solid (Schramm, 1994).

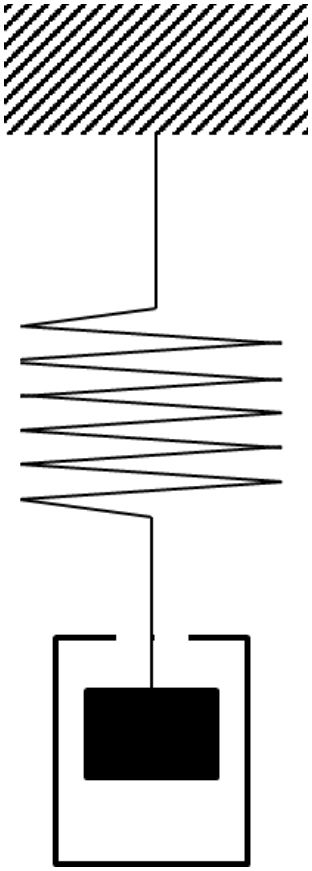

Figure 1.8 – Schematic of Maxwell model of spring and dashpot in series response for viscoelastic liquid materials (Schramm, 1994).

For a Maxwell model system (figure 1.8), when a force is applied, the spring will deform over a small time period with immediate effect while a delayed,

longer time, the response from the dashpot will be observed. The strain in both elements can be different but the stress over each element is the same. After the initial response from the spring, the deformation would increase uniformly with time, as force would be applied in proportion. On removal of the force, there will be an initial and immediate reduction in the shear stress experienced by the spring over a short time, followed by a delayed, longer time response from the dashpot. The response of force applied and the material extensional response is graphically represented in figure 1.9.

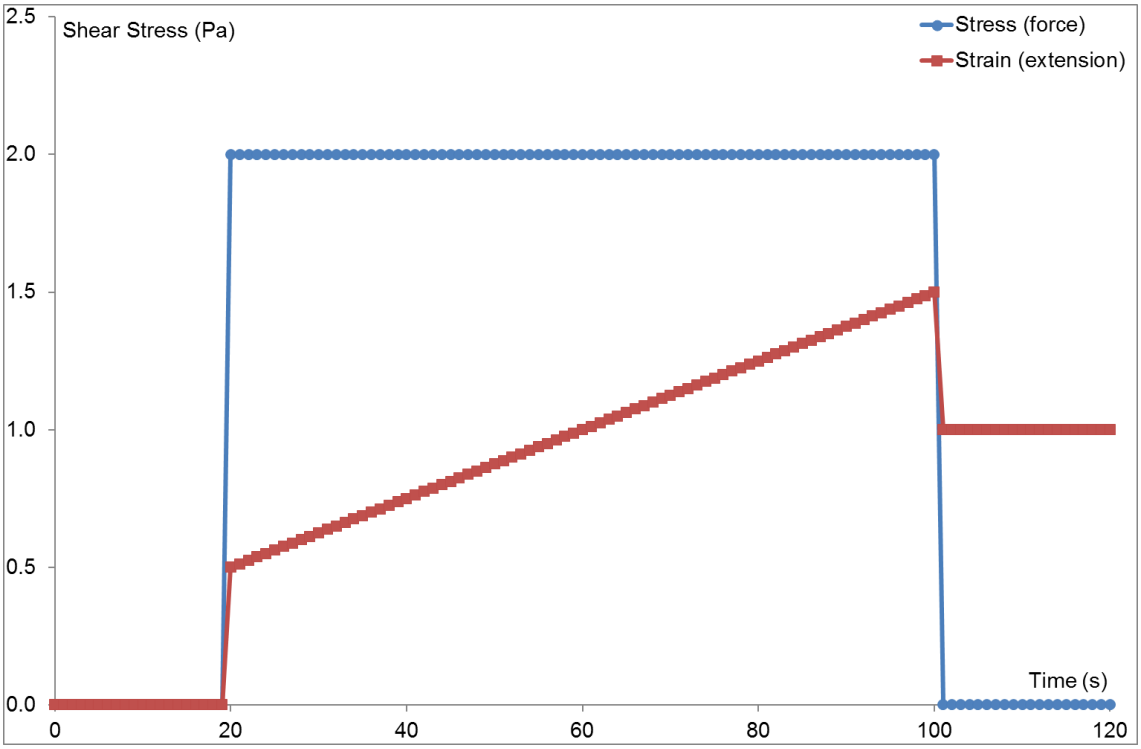

Figure 1.9 – A graph showing the Maxwell model for a liquid. (Schramm, 1994)

Kelvin-Voigt and Maxwell models test the viscoelastic response of a material in extreme states of solids and liquid, respectively, but still only consider the creep and recovery response of which is still a static test model. Together a 'real' viscoelastic model would be considered in figure 1.10.

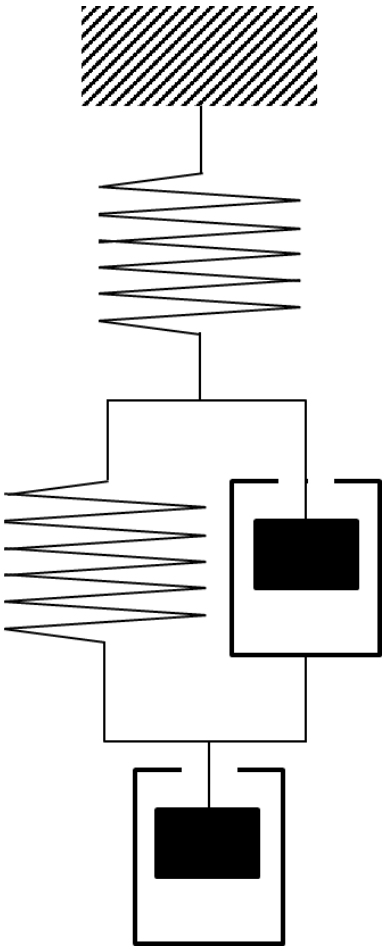

Figure 1.10 – Schematic of Burgers real viscoelastic model taking both Kelvin-Voigt and Maxwell models into account (Schramm, 1994).

. The real viscoelastic tests would be found using oscillatory model tests which consider the more dynamic factors. Oscillatory tests measure the small deformations in the material, giving a more real or dynamic simulation, which would govern changes experienced in a viscoelastic material. Due to the chemical nature, it is possible to go beyond the yield point when testing with creep and recovery tests and break the material and further testing possibilities.

1.4.1.4 Oscillatory testing

Testing using oscillatory methods will exert a shear force on a material with small deformations using a sinusoidal motion. A common method is on a rheometer where a cone attached to a motor on the rheometer will oscillate at different frequencies and with varying shear stress/strains (amplitude). As previously mentioned frequency and amplitude sweep tests are commonly used oscillatory methods. A frequency sweep would apply an oscillatory deformation to a material, where one frequency step would involve one sinusoidal motion and the sweep would increase the number of sinusoidal deformations per frequency

step increase. An amplitude sweep would incur an oscillatory test that per step increase the force applied to a sample will increase. Figure 1.11a and figure 1.11b give examples of the waveforms expected from these types of tests.

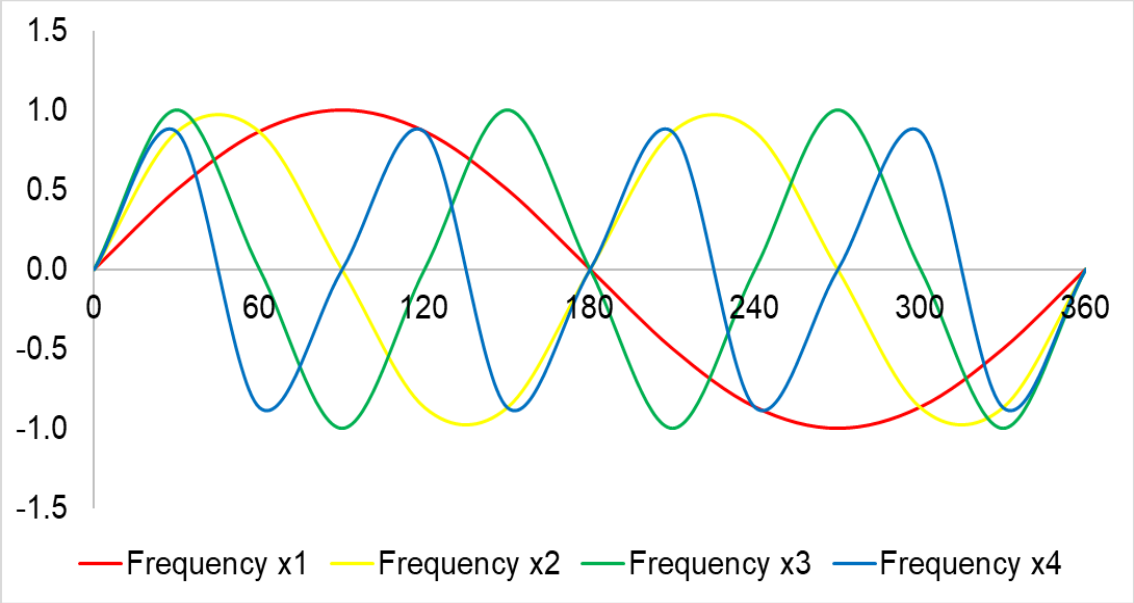

Figure 1.11a – Plot of sinusoidal waveform for changing frequencies.

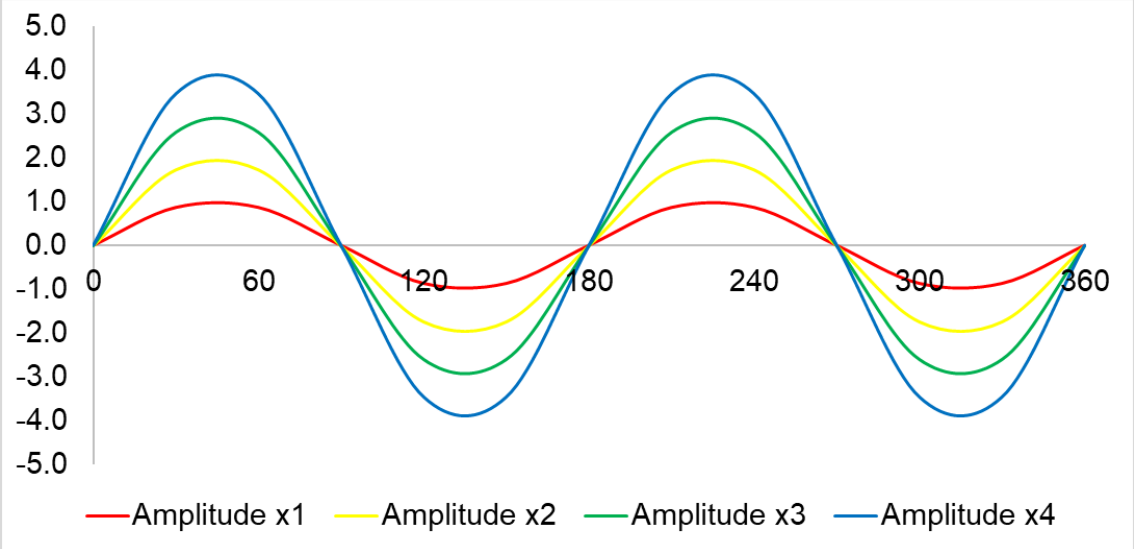

Figure 1.11b – Plot of sinusoidal waveform for changing amplitudes.

Figure 1.12 shows a typical rheometer with a cone and plate setup and a diagram of typical expected force application and response.

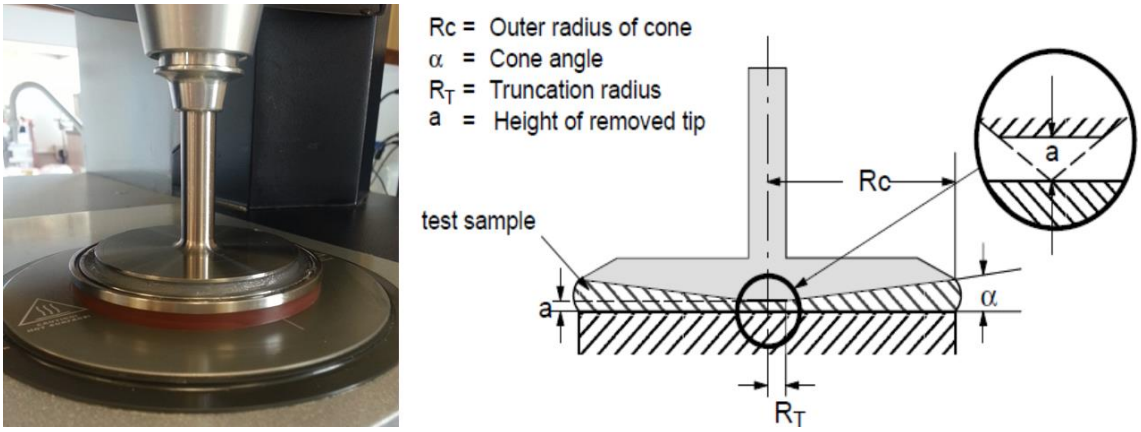

Figure 1.12 – Representation of cone and plate rheometer (Schramm, 1994)

This sinusoidal motion will generate a viscoelastic response from the tested material sample which will give information of a phase angle (σ) based on graphical representation from the degree of amplitude exerted on the material from the rheometer and the delay in response detected from the material. The degree of phase angle is an indication of the material property, whether it is solid like (σ = 0°) or liquid like (σ = 90°). This method can be illustrated in a similar way to the Kelvin-Voigt and Maxwell model where the behaviour of a purely elastic material would give the response strain in figure 1.07, for a Newtonian liquid the response is shown in figure 1.09.

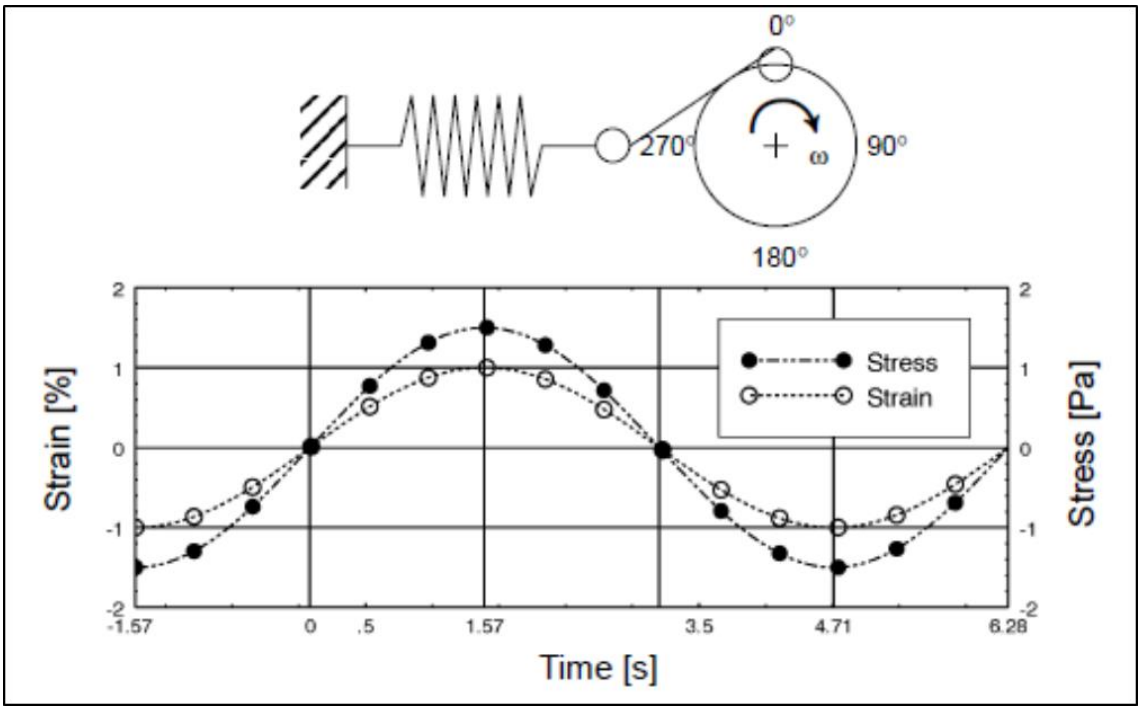

Figure 1.13 – Graphical representation of a spring model system determining the strain/stress response of an ideal solid against time (Schramm, 1994).

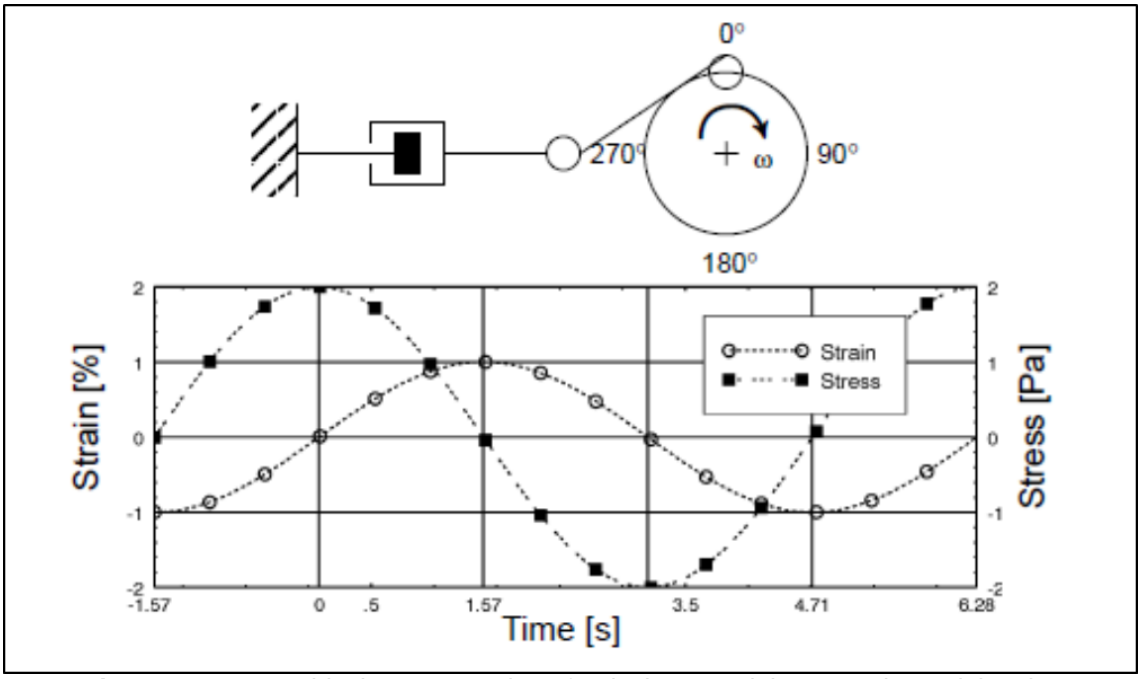

Figure 1.14 – Graphical representation of a dashpot model system determining the strain/stress response of a Newtonian liquid against time (Schramm, 1994).

As can be seen in figure 1.13 an ideal solid will act with an immediate strain response when a shear force is exerted on the sample material, this indicates that there is no phase angle ($\sigma = 0°$) experienced by the sample, therefore, showing an entirely elastic solid. Figure 1.14 shows a Newtonian liquid where there is a maximum phase angle present ($\sigma = 90°$). When a material demonstrates this phase angle it is a pure liquid. With white soft paraffin, a

viscoelastic material phase angle between 0° and 90° will be expected, i.e. a mix of viscous and elastic response.

Further parameters from carrying out oscillation testing are the complex modulus (G*) of a material. The complex modulus is an indication of the total resistance of a material when a force is applied to the material and strain is experienced, τ_0 represents the stress applied at 0 phase angle, γ_0 represents the strain experienced at 0 phase angle. G* is defined by the following equation;

$$G^* = \frac{\tau_0}{\gamma_0}$$

With the knowledge of phase angle, the complex modulus and the input of angular velocity/frequency it is possible to calculate two factors;

- G’ – The elastic modulus (storage modulus)
- G’’ – The viscous modulus (loss modulus)

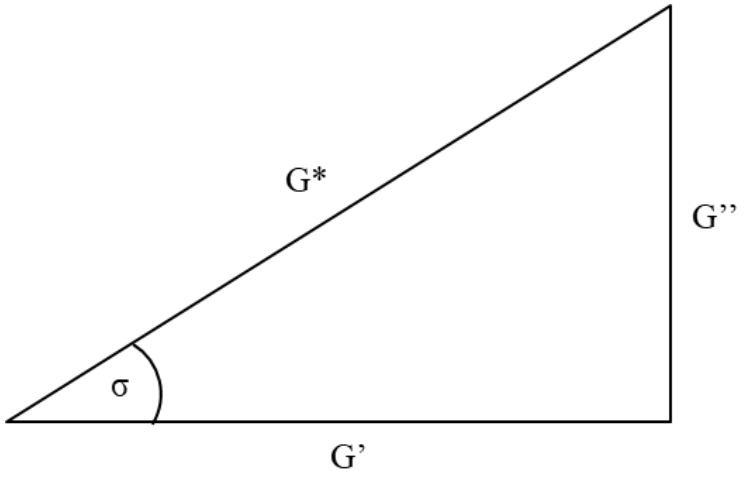

Figure 1.15 – Diagram representing the calculation of phase angles based on the data for G’ (elastic modulus) and G’’ (viscous modulus). Using Pythagoras theory of $a^2 + b^2 = c^2$.

As the names indicate the elastic modulus is a value that will correspond to the degree of elasticity that a material will have and the more solid like it may be. The viscous modulus is a value corresponding to the viscosity of a material an indication of how liquid like a material is. The connection between elastic, viscous and complex modulus is as follows (Schramm, 1994):

$$G^* = G' + i \cdot G''$$

From the determination of the complex modulus it is then possible to calculate the elastic and viscous moduli (Schramm, 1994):

$$G' = G^* cos\sigma = \frac{\tau_0}{\gamma_0} \cdot cos\sigma$$

$$G'' = G^* sin\sigma = \frac{\tau_0}{\gamma_0} \cdot sin\sigma$$

When carrying out oscillatory viscoelastic tests, measurements are ideally reported in the linear viscoelastic region (LVER). This is where the moduli are constant and independent of the magnitude of strain. Due to the nature of the WSP being investigated determination of LVER is important to consider before carrying out further oscillatory rheological tests, to ensure reproducible data. It is also important to consider the angular frequency of testing for WSP, and a frequency sweep will be carried while testing WSP. Changing the angular frequency will change G' and G'' response in a viscoelastic material, shown previous by (Park and Song, 2010). By increasing the frequency of testing interactions between particles within the WSP can be disrupted increasing the fluid nature of the material, showing an increase in G'' values. Figure 1.16 shows a plot of a material that has undergone an amplitude sweep test to determine the LVER.

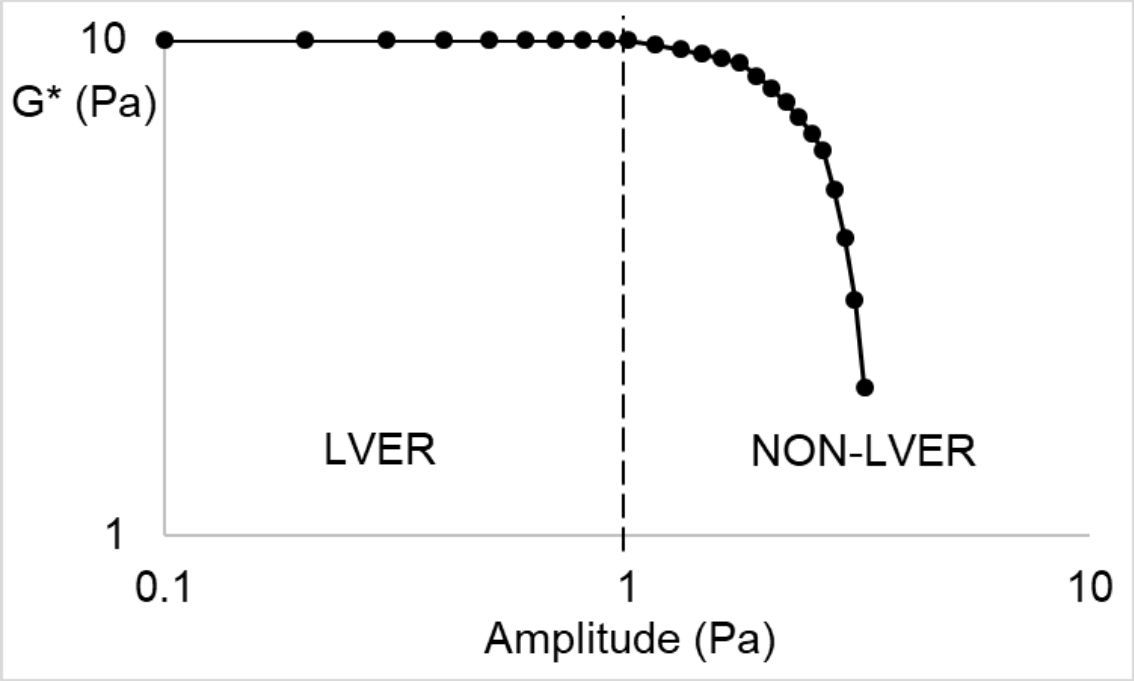

Figure 1.16 – Plot showing an exact example of a materials linear viscoelastic and non-linear viscoelastic response to an amplitude sweep test.

When testing future materials, LVER regions should always be used for parameter setup, when materials are tested in the NON-LVER it is more likely that the material can deform beyond that force applied by the equipment in use. Such as the strain experienced by a material will not behave with a linear response to the stress. Therefore, results of frequency tests would not be representative of true results as the error possibilities are large and unknown.

When testing dissimilar materials, it is also important to re-test the LVER, this is due to varied materials having different molecular interactions, a liquid oil sample would have much less interaction compared to a solid wax sample, and as such a liquid material is likely to have an LVER in a region of less amplitude force. When testing materials, it is then valid to explain a force applied as proportional to the material, due to the molecular interaction of one material to another.

1.4.1.5 Creep viscometry

Creep viscometry can provide reproducible data as the test does not damage the sample under testing. Creep viscometry has been used to test the viscoelastic region of white soft paraffin (Genovese and Shanks, 2007). The test is carried out by applying step strain and maintained for a period of time and the recorded data of strain response versus time determines a creep curve.

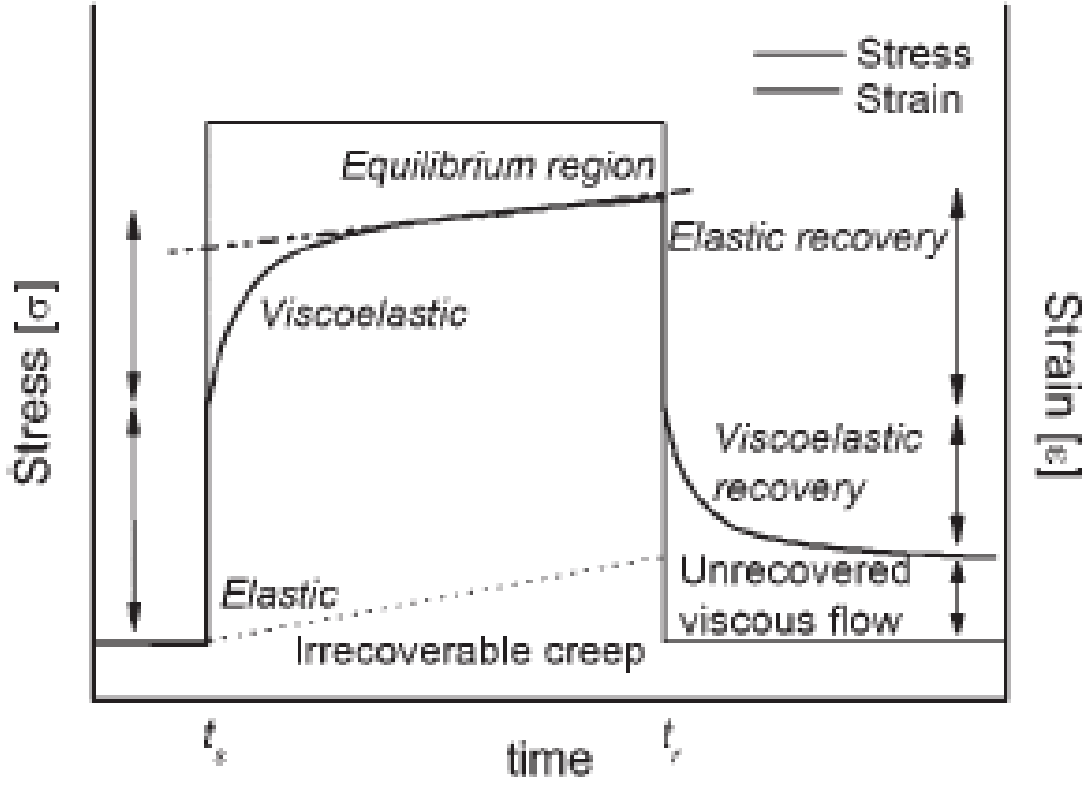

Figure 1.17 – Graph showing a standard creep curve (Genovese and Shanks, 2007).

A previous study has shown viscoelastic behaviour was found in White Soft Paraffin B.P. (Barry and Grace, 1971b) where creep tests conducted up to and including 25 °C showed linear viscosity at 900 dyn cm^{-2} (90 N m^2). Between 30 °C and 40 °C linear viscosity existed for stresses up to 150 dyn cm^{-2} (15 N m^2) however become non-linear above 150 dyn cm^{-2} (15 N m^2). At 45 °C stress of 100 dyn cm^{-2} (10 N m^2) showed evidence of non-linear viscosity and for temperature 50 °C and above non-linear viscosity was almost instant where the white soft paraffin could only withstand 1.5 dyn cm^{-2} (0.15 N m^2). While different techniques may play a role, it is also evident that temperature plays a significant role in white soft paraffin behaviour.

1.4.1.6 Large Deformation Rheology

In addition to fundamental rheological analysis, other empirical tests are typically performed to assess the mechanical properties of WSP. Large deformation analysis in WSP is needed because during transportation or use (i.e. removal from a container or a tube and application to the human body or skin) WSP experiences a wide range of stresses (Park and Song, 2010). Due to its paramount importance in pharmaceutical and cosmetic industries, many

attempts have been made to investigate the large deformation properties of WSP. The ASTM (ASTM, 2016) provides a Standard Test Method for Needle Penetration of Petroleum Waxes. (Pharmacopoeia, 2005) also shows British standard testing for penetration tests for paraffin wax, used within the pharmaceutical industry for products designed for use in the UK and an example of equipment used is seen in figure 1.18.

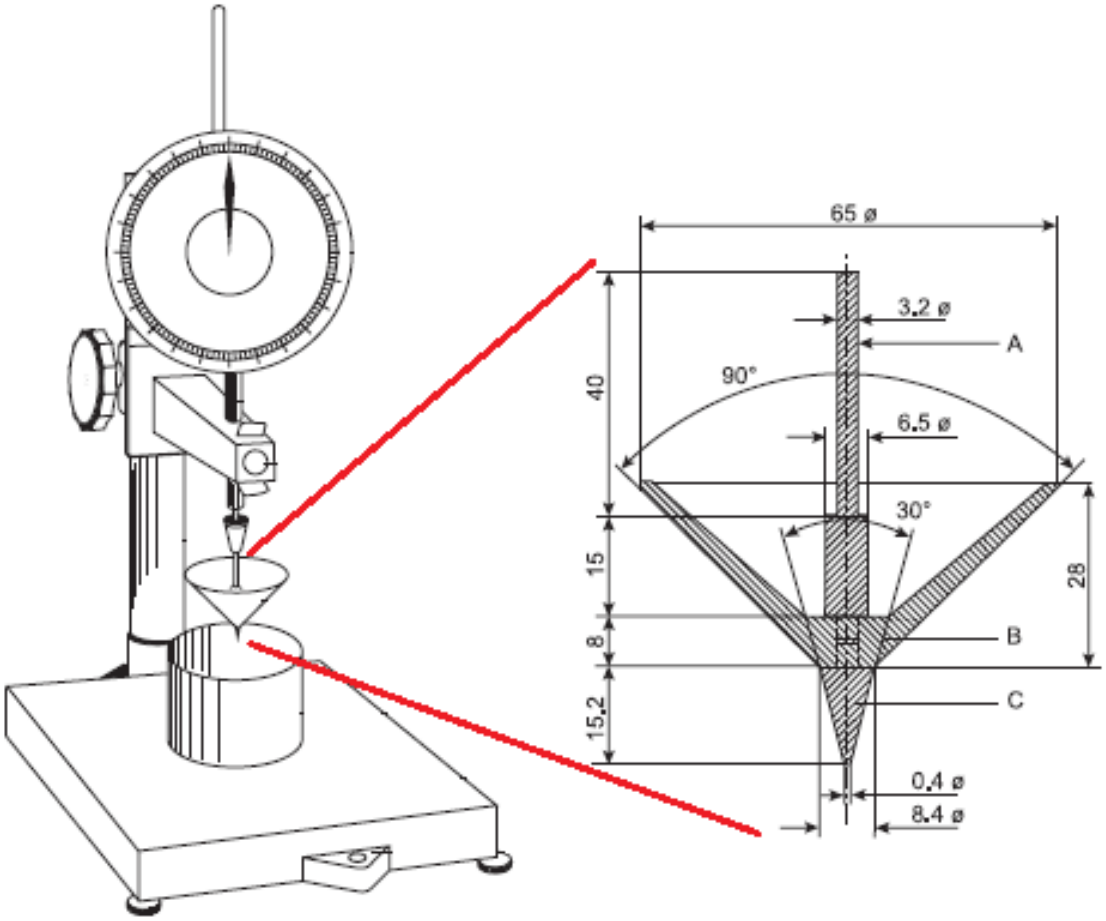

Figure 1.18 – Diagram of equipment used for penetration testing (Pharmacopoeia, 2005).

To test a sample, three sample will be prepared in containers using one of three methods detailed in the standardised test. The sample will then be placed on the base of the penetrometer ensuring the sample is flat and perpendicular to the testing probe. In this test, all penetrations are to be carried out where the sample and the penetration tip is equilibrated to 25 °C ± 0.5 °C. the tip will be adjusted so that it just touches the surface of the sample. The penetrator will then be released and allowed to penetrate the sample, where it will be left for five seconds before being clamped in place so an accurate reading of penetration depth can be measured. Results are given in tenth of millimetres

as a mean of the three sample container measurements, and if results deviate by greater than 3 %, the experiment must be repeated.

Penetrometer tests are relatively easy to use as a technique in comparison to small deformation tests carried out on a rheometer. There are a number of studies that have evaluated WSP in this way. (Van Ooteghem, 1965) derived yield values for petrolatum and (Berneis et al., 1964) found a linear correlation between penetration data and the dilution of petrolatum with liquid paraffin. Later (Delonca et al., 1967) employed a modified form of penetrometer to determine the thixotropy of petrolatum. (Cerezo and Suñe, 1970) used penetrometer tests to evaluate semisolid preparations for topical application. The effect of temperature on the penetration depth of petrolatum was also investigated (Mutimer et al., 1956). Later authors studied the dependence of penetration on temperature and composition of paraffin waxes (Matthäi et al., 2001), it was found that at 25 °C penetration depth ranged between 0.14 to 0.21 mm for macrocrystalline waxes and 0.15 to 0.29 mm for microcrystalline wax. As temperatures were increased to 45 °C penetration depth reached up to 1.69 mm for macrocrystalline wax and 0.57 mm for microcrystalline wax.

In this work, the relationship of small and large deformation will be explored with the aim to improve the knowledge of their relationship and to establish the feasibility and information of each one of the techniques. Until now research has not related the findings of small and large deformation rheology in white soft paraffin.

1.4.2 Differential Scanning Calorimetry

Differential scanning calorimetry is a method of thermal analysis often used on samples that display changes in phases and states of matter against a function of temperature. White soft paraffin is such a product and depending on WSP type and blend can contain few or many changes in phases. These phase changes, indicate crystal melting or crystallisation of WSP. DSC measures the change in heat flow within the test material as a function of time. After analysis, a measured curve (see figure 1.19) will be produced showing change in heat flow (for the differences between the sample and reference furnaces), measured in milliwatts (mW) against time in seconds (s). In figure 1.19 the measured curve

shows a typical endothermic response from the DSC analysis, this would indicate the crystallisation process in WSP.

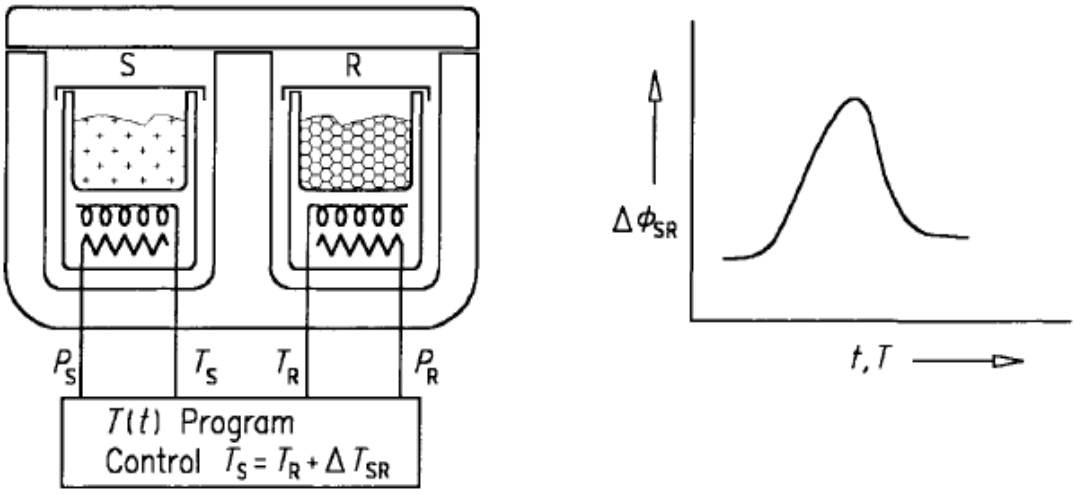

Figure 1.19 – Example of a power compensated DSC furnace and a typical thermograph (Gallagher et al., 1998).

Figure 1.19 is an example of a double furnace power compensated DSC. In a power compensating DSC, the tested samples are placed in two furnaces both with their own heating unit and temperature sensors (figure 1.19). As such the two furnaces are temperature controlled by power control loops (P) that will aid in keeping temperature difference between the sample and reference furnaces to a minimum. Measurement of thermal analysis is possible as the control of power is measured so that there is always a residual temperature difference between the sample and reference furnaces. If the differences have thermal symmetry, then the recording data is shown as a standard heating change in the reference and sample furnaces and proportional to the difference in heating powers to the system. If thermal differences are recorded due to the difference in heat capacity or endothermic/exothermic phase transitions in reference and samples furnaces, the difference is proportional to the additional power required (to maintain a minimum difference in temperature between sample and reference furnace). Heat flow rates supplied to the sample and reference furnaces ($\Delta\phi_{SR}$) are given by:

$$\Delta\phi_{SR} = \Delta C_p \times \beta \propto \Delta\phi_{trs} \qquad \text{Equation 1}$$

Where ΔC_p= change in heat capacity and β = heat/cooling rate. This is also proportional to the heat flow rate of transition ($\Delta\phi_{trs}$) (Gallagher et al., 1998).

Equation 1 is specific to power compensated DSC, in general equation 2 gives the thermodynamic heat flow equation for all DSC. When heat flow from a sample is experiencing a linear (constant) heating, or cooling, the sample will comprise of a heat capacity component and a contribution from a thermal event, the total heat flow is therefore shown by the following equation. Where δq is the change in heat, δt is the change in time, Cp is the heat capacity of the sample and δT is the change in temperature experienced by the sample/system.

$$\frac{\delta q}{\delta t} = C_p \times \frac{\delta T}{\delta t} \qquad \text{Equation 2}$$

The thermal data changes will be recorded by the DSC program software and measured curves will be represented graphically, shown in a similar fashion to those shown in (figure 1.20 and figure 1.21). When considering the known mass of a substance the equation can be written as follows. Q is the energy transferred, m is the mass of the sample, C_p is the heat capacity of the sample and ΔT is the change in temperature.

$$Q = m \times C_p \times \Delta T$$

DSC has many uses and has been used by many researchers for investigation into thermal properties of polymers (Flaherty, 1971; He et al., 2004; Matthäi et al., 2001; Hawlader et al., 2003). DSC is frequently used with other tests to provide results for polymer characteristics, and it has been shown that DSC is capable of correlating differences in penetration tests for petrolatum (Matthäi et al., 2001). In this work, DSC testing helps to define the crystalline structure of the WSP in question, indicating that as crystal lattices grow in number, penetration depths are not as deep, this indicates that there is greater hardness in the paraffin wax.

An important use of DSC testing can be seen when considering phase change materials for energy storage devices (Hawlader et al., 2003). DSC scans will show the difference in phase changes within the product often indicating an increase in heat flow as an endothermic change, such as melting points of crystals within paraffin wax, and exothermic changes, such as crystallisation of paraffin wax phases. Figures 1.20 and 1.21 show DSC scans for heating and cooling stages respectively. Previous authors have also studied the effect of phase change materials (PCM) when analysed by DSC, based on ratio

composition of paraffin waxes in the PCM (Zhang et al., 2013). The authors found that increasing wax ratio into the PCM blends increased potential for latent heat storage, a key factor in PCM’s.

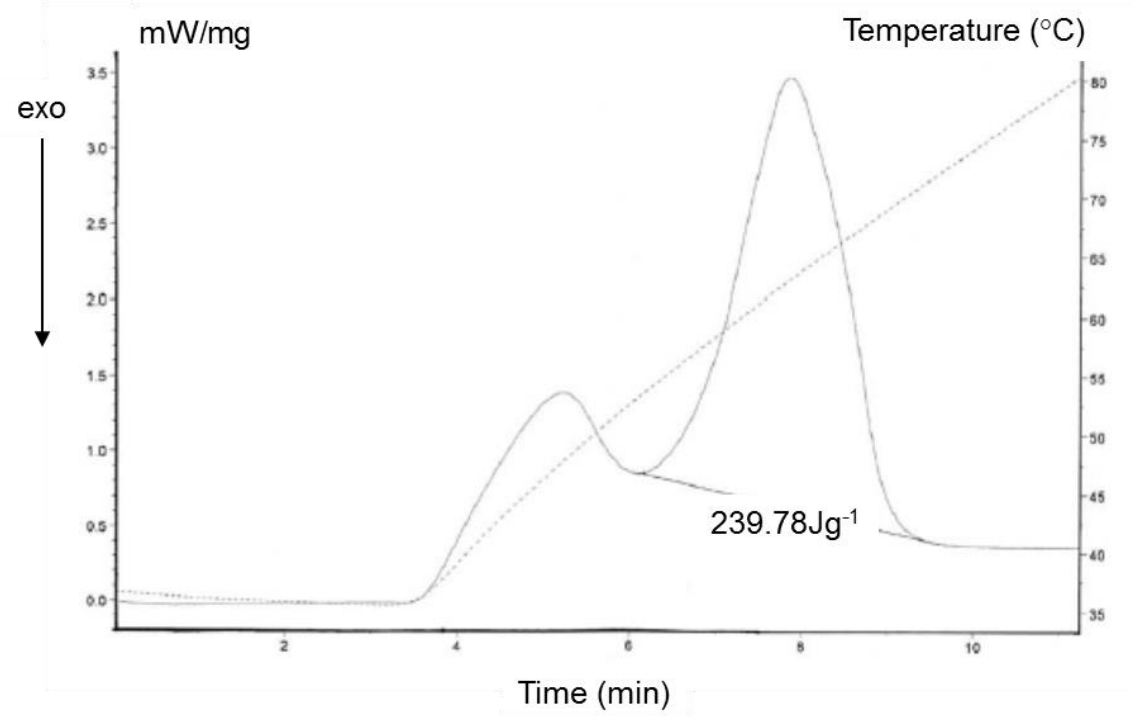

Figure 1.20 – DSC of a heating cycle for a phase change material (Hawlader et al., 2003).

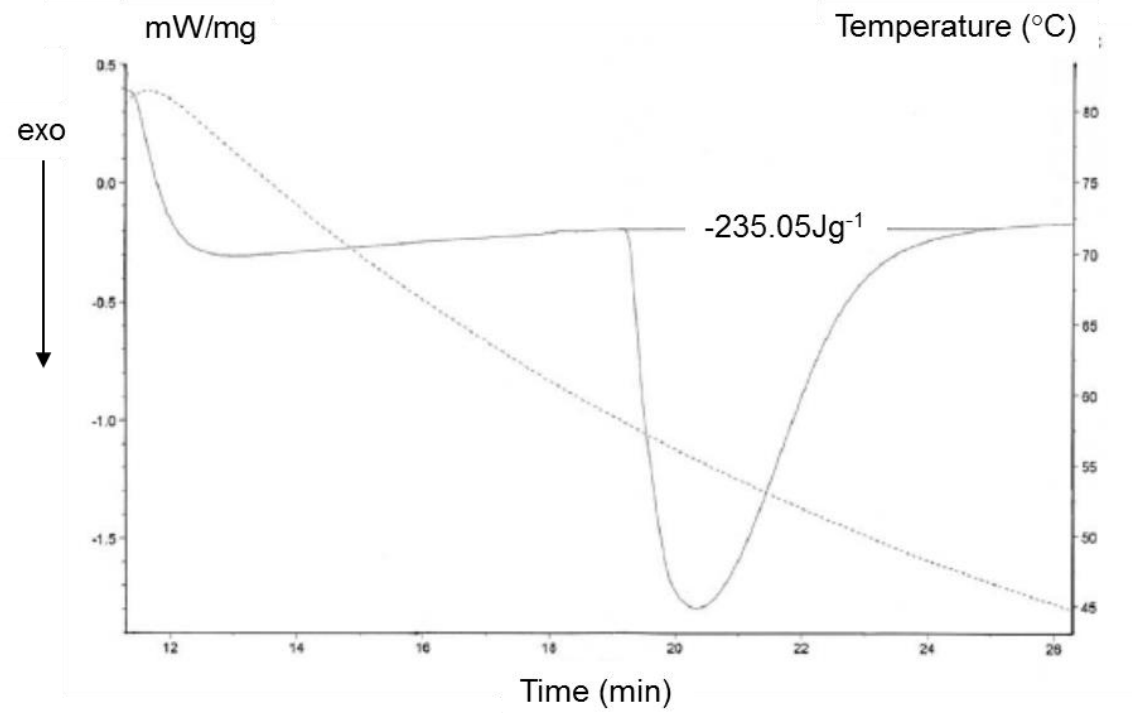

Figure 1.21 – DSC of a cooling cycle for a phase change material (Hawlader et al., 2003).

As can be seen in figures 1.20 and 1.21 areas under peaks for both endothermic (figure 1.20) and exothermic (figure 1.21) can be calculated giving the enthalpy of that thermal event recorded. These peaks will give an indication of the total energy required by the sample/system to cause a phase change to

the material. Depending on the sample being tested the enthalpy changes can be indicated by large or small energies. It would be expected that high molecular weight samples would require a greater enthalpy to apply a phase change due to the greater number of chemical bonds present within the sample. As such samples, such as the paraffin oil would require a small enthalpy when high Mw samples like microcrystalline wax would require a large enthalpy.

1.4.3 Microscopy

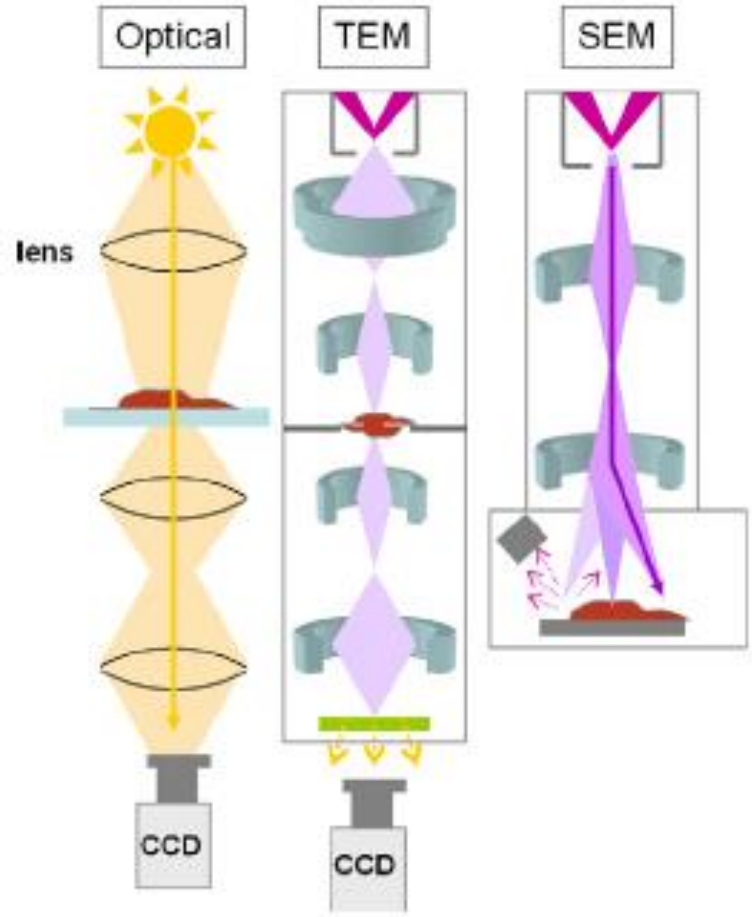

Figure 1.22 – Image of microscopy techniques used by optical microscopy, SEM and TEM (Dudkiewicz et al., 2011)

1.4.3.1 Scanning Electron Microscope (SEM)

SEM is an electron microscope that will generate images by scanning products with a focused beam of electrons, which will interact with atoms within the sample to produce signals that will be detected by a sensor and will display a rendered image of the surface of the products atoms that is being viewed. SEM has a resolution of approximately 1 nm (Dudkiewicz et al., 2011) allowing for high magnification images indicating the structural makeup of the product in question, although electron beam damage can be a problem. Generally, samples are

imaged under vacuum or low pressure in the case of the Environmental SEM. Previous authors (Luyt et al., 2010; Hawlader et al., 2003; Krupa et al., 2007) have used SEM to image paraffin waxes for use in phase change materials. (Laux et al., 2005) used SEM to correlate to other characterisation techniques to analysis paraffin wax.

1.4.3.2 Transmission Electron Microscope (TEM)

TEM is a microscopy technique like SEM, however, in TEM a beam of electrons is transmitted through a sample that has been layered out onto a medium with a very small thickness. The electron beam will interact with the sample as it passes through it. An image is then formed from the interaction of the electrons with the sample and is projected onto a detection device such as a fluorescent screen. TEM has a very good resolution of samples and can achieve resolution around 0.07 nm (Dudkiewicz et al., 2011). It is possible for the TEM to scan a single layer of atoms due to de Broglie wavelength of electrons. TEM can also be used to observe modulations in chemical identity, crystal orientation, electronic structure and sample induced electron phase shift as well as the regular absorption based imaging, these will help to define the different blends white soft paraffin on a molecular level. However, could not be used on a regular basis due to time consumption and difficulty in preparing samples for routine measurements. Previous work has shown paraffin wax crystal morphology in crude oils through use of TEM (Kané et al., 2003) and gives a good indication of the different types of crystals present in paraffin products.

1.4.3.3 Optical Microscopy

This is the simplest form of microscopy available and is dependent on light transmittance from a sample. The resolutions of optical microscopes are very limited in comparison with electron microscopy, the best being around 1 µm. It is often recommended that the use of polarised filters should be used with optical microscopy when working with wax hydrocarbon products as this will help to define the crystals present much more effectively. (Mahmoud et al., 2005) showed that asphaltenes, a paraffin product, is visible at x100 magnification under optical microscopes

1.4.3.4 Confocal Microscopy

Confocal laser scanning microscopy (CLSM) is used for obtaining high-resolution images with the ability to scan into and through required depths of a sample, known as optical sectioning. Images are obtained point-by-point and the data is analysed by computer software that will render an image on the computer's display. Analysis by a computer can allow for complex 3D images of the topology of the sample. CLSM can scan through images with use of a laser this would be useful for some blends of white soft paraffin as the CLSM could provide a detailed 3D image of the interior of the crystalline network. Work carried out by (Pu and Severtson, 2009) helps to correlate thermal techniques and confocal microscopy by using Raman confocal microscope analysis to determine crystallinity in paraffin wax before and after heat treatment.

1.4.3.5 Atomic Force Microscope (AFM)

AFM is a very high-resolution type of scanning probe microscope, reaching resolutions as small as fractions of nanometres. The AFM works by feeling the surface with a mechanical probe and collecting the data of the surface topology. Piezoelectric elements allow small precise movements on (electronic) command, enabling the very precise scanning. The data is then analysed computationally and an image is generated and displayed to give an accurate render of the sample surface often showing molecular detail. Figure 1.23 shows the setup of an AFM instrument. The AFM consists of four major components; a cantilever with a sharp tip (typically silicon), a piezo-scanner that drives the cantilever, based on a voltage passing through the piezo-material, moving the cantilever; a laser diode and a position sensitive detector. AFM consists of three mode types, (i) non-contact mode, (ii) contact mode, and (iii) tapping mode (Jalili and Laxminarayana, 2004). The cantilever tip will move over the surface of a material in contact mode, tapping the surface, or will hover just over the surface in non-contact mode. With the cantilever being attached to a piezoelectric element, the attractive interactions with the material cause a natural resonance in the piezoelectric element allowing the measurement of the surface of the material. As the tip is displaced a weak laser beam measures the surface contours, this is detected by a reflection of the laser beam movement by a photodiode detector. The movement of the laser then allows computational

software to create topographic images of the surface of the material (Chang et al., 2012)(Jalili and Laxminarayana, 2004).

Figure 1.24 shows an image of paraffin wax mounted a testing plate for AFM analysis (Zbik et al., 2006), the study was carried out to observe the surface roughness of paraffin wax detected by AFM analysis when using different mounting materials with the paraffin wax. (Pu and Severtson, 2009) also showed how AFM can be used in correlation with other microscopic and thermal analysis techniques. Work by (Li et al., 2009) shows the use of multiple microscopy techniques to analyse the use of paraffin wax as a stabilising material in emulsions, including optical cross polar microscopy, TEM and confocal microscopy.

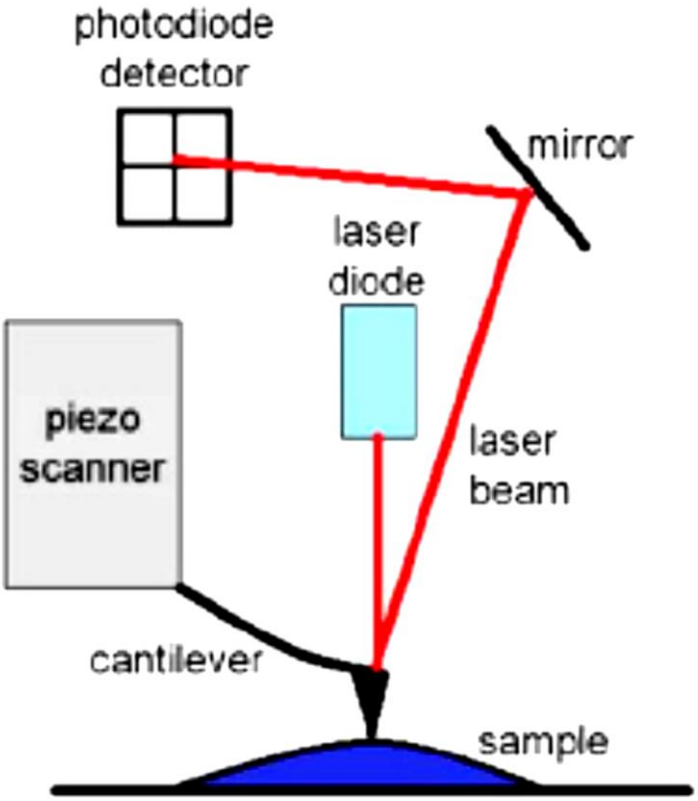

Figure 1.23 – Schematic diagram of a typical AFM setup (Chang et al., 2012).

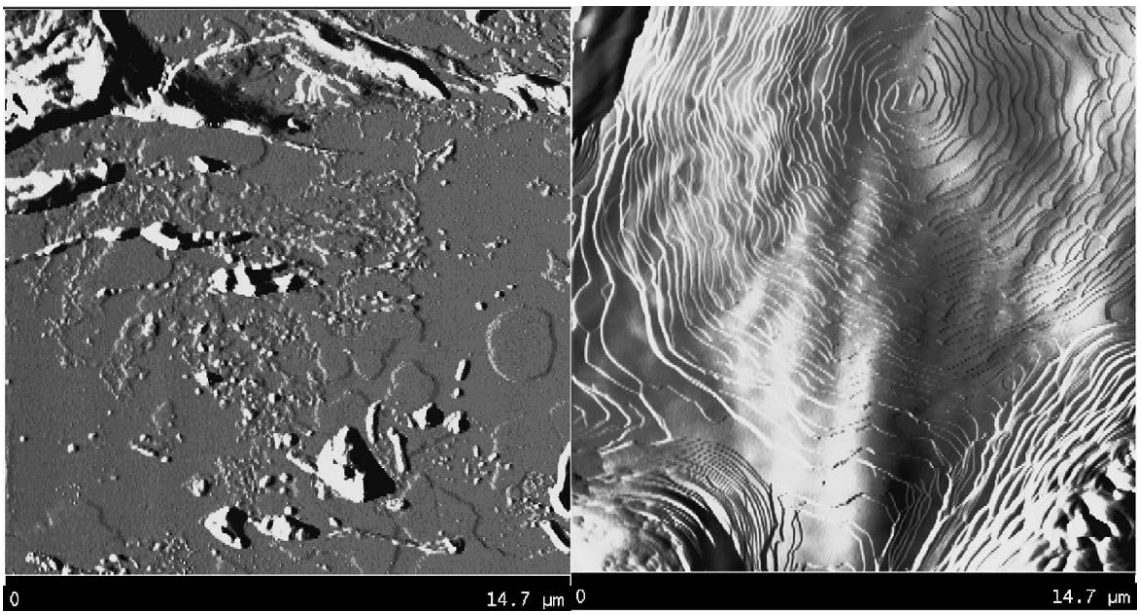

Figure 1.24 – AFM image of paraffin wax mounted on a Slygard cast, mounted on a silicon wafer (Zbik et al., 2006).

1.4.4 Chemical Analysis

There are multiple methods used for chemical characterisation of paraffin waxes (Speight, 2011). Some more specialist techniques used mainly in the petrochemical industry include Field Ionisation Mass Spectrometry (FIMS) and Nuclear Magnetic Resonance Spectroscopy (H-NMR), these offer a highly

accurate form of compound analysis within petrochemicals and paraffin derivatives, these methods are easily able to identify impurities within samples compared with other chemical analysis techniques. Other methods implemented include solubility based testing including Hildebrand and Hansen Solubility Parameters (HP and HSP). Solubility parameters have been introduced with the idea of “like dissolves like” and the use of solvents to dissolve other chemicals, most specifically hydrocarbons. As solubility is a possibility this also allows the use of spectrometry methods, such as Gas Chromatography Mass Spectrometry (GCMS) or High Temperature-GCMS, Raman Spectroscopy (RS) and with some effectiveness photospectrometry. While these techniques offer quality analysis, they may lack some finer identification tools that are implemented by FIMS and H-NMR.

1.4.4.1 Field Ionisation Mass Spectrometry (FIMS)

Used mainly in petrochemical industry, it gives detailed carbon chain length and characteristics which make up the variety of alkane hydrocarbons that form paraffin. FIMS works by supplying energy to the molecules of the sample being tested producing molecular ions and therefore reduces the amount of fragmentation of the sample giving a higher molecular analysis compared to methods of electron ionisation analysis (Briker et al., 2001). Gas chromatography field ionisation mass spectroscopy (GC-FIMS) can determine iso- and normal paraffin separately and as stated can analyse separate molecules with the use of chromatograms obtained from gas chromatography. The analysis of hydrocarbon mixtures is based on the z-number where C_nH_{2n+z} in a hydrocarbon molecular formula (Briker et al., 2001). The requirement of gas chromatography is evident when hydrocarbons can have the same mass but have differing structure (e.g. nonane and naphthalene). FIMS is not a sufficient tool to separate out the two hydrocarbon isomers but with GC separation will occur giving definition to the isomer (Briker et al., 2001). Figure 1.25 shows an example of an ion chromatogram of a hydrocarbon mixture with C13-C16.

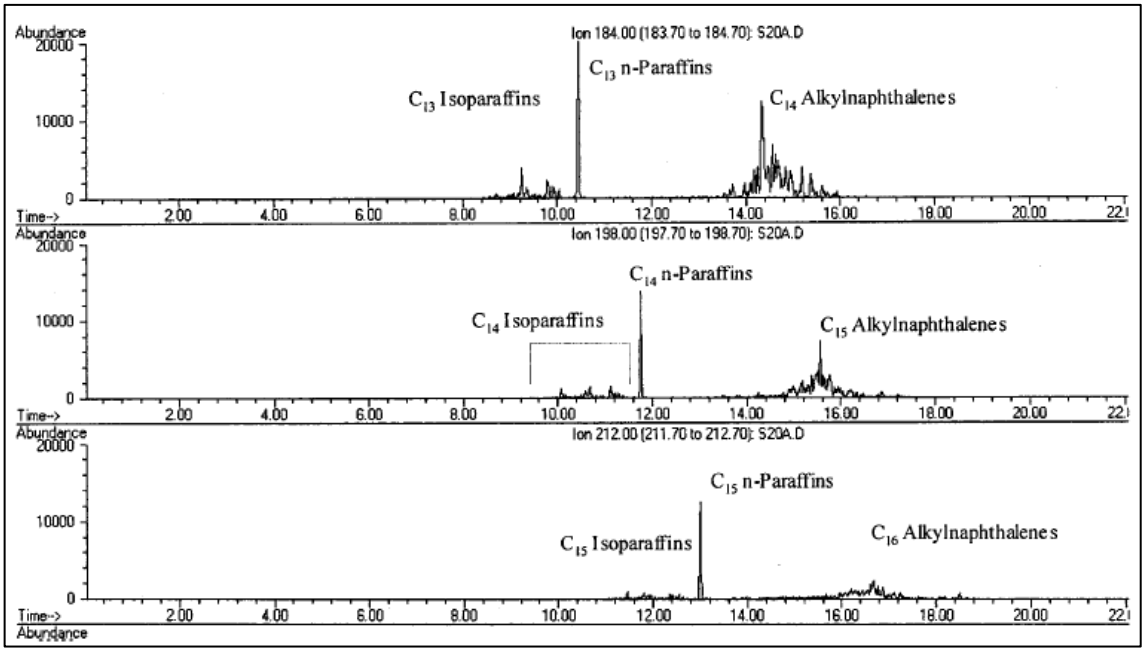

Figure 1.25 – Ion chromatogram showing short and long retention times for a hydrocarbon mixture of C13-C16 (Briker et al., 2001).

1.4.4.2 Nuclear Magnetic Resonance Spectroscopy (H-NMR)

This is a testing method used to analyse the type of carbon bonds present in the paraffin products. H-NMR is a useful tool to determine the chemical makeup of the white soft paraffin and can be used alongside other tests to show the types of bonds present possibly indicating any degree of crystalline structure.

- Aliphatic (in the high field, 0.4 – 4.2 ppm).
  - These contain no carbon double bonds and can be cyclic or acyclic.
- Olefinic (in the mid field, 4.5 – 5.3 ppm).
  - These are linear carbon chain molecules with areas of carbon double bond unsaturation.
- Aromatic (in the low field, 7 – 8 ppm).
  - These structures tend to be cyclic, planer and contain a high amount of conjugation.

Although H-NMR is a very useful technique and is highly accurate, it is an expensive test and is not used to carry out quantitative measurement of white soft paraffin. H-NMR has been used in the petroleum industry to detect for the makeup of wax deposits present from crude oils (Musser and Kilpatrick, 1998), and other crude oil fractions (Martos et al., 2008). H-NMR may be a useful

method to understand the underlying structure of WSP as part of a detailed scientific study but is unlikely to become a pharmaceutical industry standard test.

1.4.4.3 Hildebrand Solubility Parameters (HP)

Solubility parameters are a way of measuring the ability for at least two or more substances to be miscible within each other or a combination of various solvents. A solute is generally the material under test mixed with either one or a combination of solvents, solubility parameters will determine the solutes solubility. Whilst there are many solubility parameter theories, the focus of this work will be the Hildebrand Solubility Parameters (HP) and Hansen Solubility Parameters (HSP). The overall idea of mixing solutes and solvents is that 'like dissolves like' and products that are similar will be miscible (Hansen, 2000; Barton, 1975).

Even though the experimental work carried out in this thesis will focus mainly on Hansen Solubility Parameters (HSP), before working with HSP, understanding of previous work by (Hildebrand, 1916) is required. It was shown in previous work that initial derivation of Solubility parameters (SP(δ)) are a measure of cohesive energy density and can be shown in equation 3 (Barton, 1975);

$$\delta = \left(\frac{E}{V}\right)^{1/2} \qquad \text{Equation 3}$$

Values for E determine the measurable energy of vaporisation and V determines the molar volume of the tested solvent, the SI units of solubility parameters are $Pa^{1/2}$. In normal practice liquid-liquid or liquid-solids are considered with measurable solubility parameters, this is due to the condensed nature of the molecules within the solute/solvent. As such this creates strong attractive forces between molecules, leading to strong negative potential energy, this is the molar cohesive energy, -E (J), (also commonly written as E in equation 3) (Barton, 1975).

From equation 3 it can be seen that solubility parameters are derived from thermodynamic laws based on vaporisation energies, molar fractions and temperature changes based on previous work by (Hildebrand, 1979; Hildebrand and Lamoreaux, 1974; Hildebrand, 1934; Hildebrand, 1916; Hildebrand and

Scott, 1979). The following series of equations (4-8) (Barton, 1975) will show the steps to reach that of equation 3, all which have been derived from the previous various sources.

$$-E = \Delta_i^g U + \int_{V=V_{vap}}^{V=\infty} (\partial U/\partial V)_T d\,V \qquad \text{Equation 4}$$

Molar cohesive energy, -E (J), consists of two components, energy needed for vaporisation of a liquid to saturation point ($\Delta_i^g U$), and the isothermal energy needed for expansion of volume, infinitely, for saturated vapour to fill ($\int_{V=V_{vap}}^{V=\infty} (\partial U/\partial V)_T d\,V$). When the temperature of the system is less than the boiling point of the solvent, the isothermal energy for expansion of vapour can be ignored, giving equation 5.

$$-E \approx \Delta_i^g U \qquad \text{Equation 5}$$

If the rules of ideal gas constants are followed, then equation 6 can be considered as correct as the change of volume or pressure will not influence the energy of the system, which is demonstrated in the equation below, leading to equation 6.

$$-\int_{V_{vap}}^{V=\infty} \frac{RT}{V}\,dV = -\ln\frac{V_f}{V_i}$$

$$-E \approx \Delta_i^g H - RT \qquad \text{Equation 6}$$

The cohesive energy density is defined in equation 7, where V is the molar volume ($cm^3\ mol^{-1}$) and as such with relation to ideal gas equations is also approximate to the solubility parameter in equation 8.

$$c = \frac{-E}{V} \qquad \text{Equation 7}$$

$$\delta^2 = c \approx \frac{\Delta_i^g U}{V} \qquad \text{Equation 8}$$

Hansen Solubility Parameters (HSP) – As defined by Hildebrand the solubility parameter in equation 8 it has also been stated by Hansen that the cohesive energy density is made of three (Barton, 1975; Abbott et al., 2013; Sato

et al., 2014), (i) dispersion (London) forces (dispersion cohesive energy, E_d) that arise from fluctuating dipole movements between atoms in molecules, (ii) polar interactions such as permanent dipole-permanent dipole interactions (polar cohesive energy, E_p) caused by sharing of charge between positive and negative dipole in separate molecules, (iii) hydrogen bonding (E_h).

$$E = E_d + E_p + E_h \quad \text{Equation 9}$$

The total energy is made of the three components indicated by Hansen. If we take equation 7 and 8 stated by Hildebrand and divide the energies in equation 9 by the molar volume, we can state equations 10 and 11 are true (Sato et al., 2014; Abbott et al., 2013).

$$\frac{E}{V} = \frac{E_d}{V} + \frac{E_p}{V} + \frac{E_h}{V} \quad \text{Equation 10}$$

$$\delta^2 = {\delta_d}^2 + {\delta_p}^2 + {\delta_h}^2 \quad \text{Equation 11}$$

Due to the statement that the cohesive energy density of a molecule could be separated into three components, it would then be possible to test these individual energies with a variety of solvents, with solvent selection based on the type of interaction for the specified cohesive energy. It is possible to plot the solubility parameter of the various solvents on a 3D axis of x, y, z with δ_d vs. δ_p vs. δ_h. Based on how the solute dissolves in the respective solvents if a solute is fully dissolved a mark of 1 is give and a solute not dissolved is marked 0, as bad. The good solvents used for a particular solute are important as they will drive the production of a solubility sphere. The distance of the good solvents (of known HSP) will allow the calculation of the sphere, for example, the middle point of the two maximum solvents will give the centre of that solute's HSP sphere, the greater the number of solvents used with good solubility will give greater distance calculations to give a better accuracy of the solutes HSP sphere. When the plot is produced either by computer software or by manual calculation it is required and possible to find the distance between the solute and solvent, based on the solubility of the two materials, to calculate this distance of HSP (R_a ($MPa^{1/2}$)) we can use the equation 12 (Sato et al., 2014; Abbott et al., 2013).

$$R_a = \left[4(\delta_{d1} - \delta_{d2})^2 + \left(\delta_{p1} - \delta_{p2}\right)^2 + (\delta_{h1} - \delta_{h2})^2\right]^{1/2} \quad \text{Equation 12}$$

Small R_a values will favour solubility of the material in the inspected solvent, and subsequently, the opposite is true of large R_a values. Figure 1.26 shows an example of a Hansen Solubility Parameter sphere that has been created using the software package from Hansen and his team (Abbott et al., 2013).

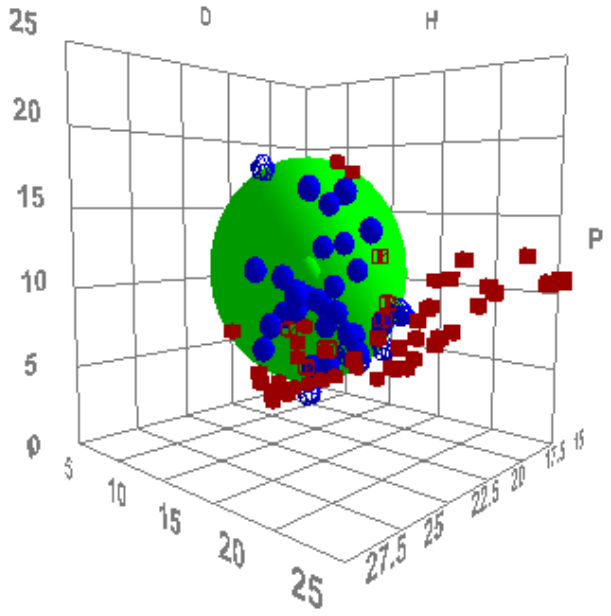

Figure 1.26 – Plot of a Hansen Solubility Parameter sphere (Abbott et al., 2013).

This example of a solubility sphere in figure 1.26 shows red squares that represent poor solvents, mostly found outside the green sphere, and blue small spheres indicating good solvents, often found inside the green sphere, the green sphere indicates the solute material (small green sphere) at the centre of the large green sphere (distance of HSP ability). The relevant software used to create this plot will use equation 12 to calculate the maximum solubility distance for various solvents tested with the solute under investigation.

$$RED = \frac{R_a}{R_o} \qquad \text{Equation 13}$$

The radius (R_o (M $Pa^{1/2}$)) of this sphere is the indication for solvents of good and bad solubility, based in and out of the sphere respectively using the radius and the distance of HSP (equation 12) the relative energy density (RED) can be calculated (equation 13), this is a useful technique the can be used by software to calculate good and bad solubilities when using large datasets that may reach into the 100's. When calculating the RED, a value of 0 indicates there is no energy difference between solute and solvent and the solubility is good, a

RED value above 1 and increasing are poor, with reducing affinities the large the number becomes. Values close to but below 1 are solvents close to the boundary regions (Sato et al., 2014; Abbott et al., 2013).

1.4.4.4 Raman spectroscopy (RS)

This is a method of vibrational spectroscopy allowing identification molecules and their structure, even when testing large or microscopic sample amounts. To identify samples, changes in energy of molecules are measured by observing the changes in vibrational states induced in molecular bonds due to the energy increase or decrease caused by incident photons directed at the samples (Larkin, 2011; Lide, 2003). Raman spectroscopy is a process that will require two photons of light and is a measure of the inelastic light scattering between the photons and sample matter. That being, as the photon incident on the sample interacts with the sample and energy is passed to and absorbed by the sample from the photon, causing the molecule to vibrate about the connecting bonds present within the molecule. The energy not absorbed is then scattered away from the sample as a photon with reduced frequency, indicating the energy absorbed and identifying the molecules and bonding present in the sample (Larkin, 2011). Raman spectroscopy is often used as a fingerprint method of identification for samples since all molecules are unique to themselves and the bonding within these molecules, also being unique, will allow for easier identification. The energy of molecular bonding as already stated can act as a fingerprint for most different bond types present. Figure 1.27 shows the energy wavenumber that will best represent the molecules and bonding present in samples being tested.

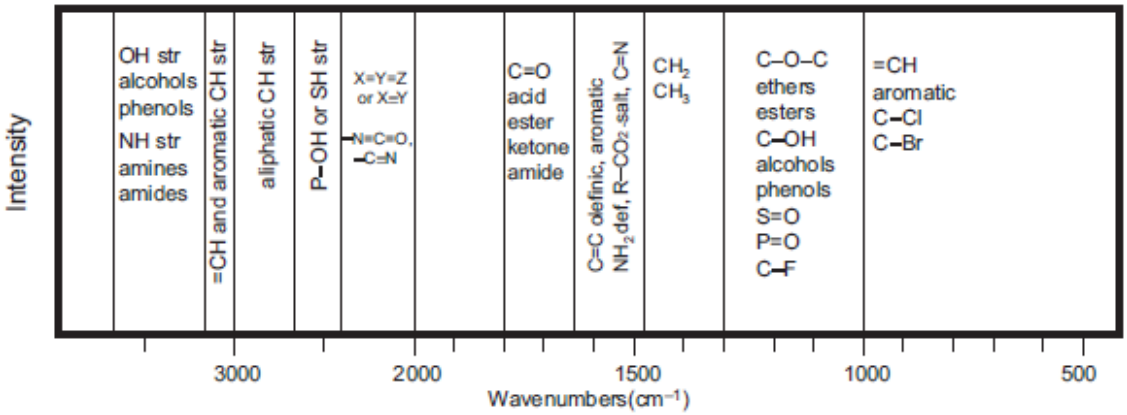

Figure 1.27 – Regions of the fundamental vibrational spectrum with some named characteristic group frequencies (Larkin, 2011).

Due to working with samples of paraffin waxes and their blends it would be expected that most wavelength number will be found around 3000 cm^{-1} to symbolise aromatic and aliphatic –CH, and 1500 cm^{-1} to symbolise CH_2 and CH_3 that would be expected a part of paraffinic hydrocarbons. Other sources, (Zheng and Du, 2006; Edwards and Falk, 1997), also collaborate that this would be expected from paraffinic samples tested as part of this project.

Often classified along with infrared (IR) as they are a part of the electromagnetic spectrum and are techniques used to characterise chemicals based on the vibrational movements from the induction of energy upon the chemical being characterised when using RS only the electrical field of the spectrum is considered.

Previous authors have used Raman spectroscopy to help characterise paraffin waxes, (Clavell-Grunbaum et al., 1997) used Raman to determine physical characteristics of n-alkane waxes and model combinations of multiples of those waxes. Saturated and unsaturated waxes were analysed with Raman spectroscopy, determining the difference in peaks and band spectra between multiple plant based waxes (Edwards and Falk, 1997). Later (O Faolain, 2005) used Raman spectroscopy to determine the ability of dewaxing agents on formalin-fixed paraffin processed tissue sections, using different solvents to dewax the tissue sections Raman was then used to analyze the different solvent treatments. In 2006 (Zheng and Du, 2006) used Raman spectroscopy to identify multi-component paraffin waxes, with the identification of phase behaviour being apparent within Raman spectroscopy scans.

1.5 Project Considerations

When considering the makeup of the ointment mixtures, there are many variables that must be considered including materials/ingredients and production processes which all have a direct impact on the final product. When mixing ingredients to produce ointments the source of the raw materials and their chemical nature may vary depending on the source, this can cause different characteristic of the final ointment product. For example, obtaining stocks of WSP from two different suppliers can result in two completely separate products on a microstructural level (GlaxoSmithKline, 2013). This would influence the mixing ratios of ingredients, such as water and API when making the final products.

Considering the many variables of product manufacture, focusing on ointments, within this project the following key areas will be considered.

- *Supply*
    - Who is the supplier?
    - What is the supplier's specification?
        - Is this transferred to the pharmaceutical company?
        - How far back does due diligence go?
    - What is the variability in the batches from the supplier?
        - Can this be standardised or reverse engineered to give a required specification?
- *Formulation*
    - What purpose is the product designed for?
    - What raw materials are included in the WSP?
        - What ratios are used?
    - What are the concentrations of WSP and other ingredients?
- *Process*
    - What steps are involved and how does it affect the WSP and other ingredients?
        - Storage
        - Heating
        - Cooling

        - Do repeat temperature cycles cause degradation of WSP?
        - Do cooling rate effect the WSP?
    - Mixing
    - Filling/finishing
- *Stability/Storage*
    - How long will the product store?
    - Does the product separate under different conditions?
    - What keeps the product stable?
- Patient Consideration
    - What is the appearance of the product?
    - What is the texture of the product?
    - How does the product feel?
    - How does the product flow?
    - What is the efficacy of the product?

Due to the nature of these products and their roles within the pharmaceutical market, the scope of this project must consider the patient, and their experience when using the final product. A patient-centric focus requires, for example, that a material substitution still gives a product close to those already represented on the market. Therefore, it is important that any characterisation is representative of current models and recipe ratios already used as standard and that testing must be compared with the commercial pharmaceutical grade WSP.

1.6 Research Objectives

The aim of the project is to apply a range of characterisation techniques to both white soft paraffin and its constituent components to define a basis for a functional specification. As paraffin products are a range of hydrocarbon alkanes, the belief that characterisation will allow the combination of these constituent components to produce WSP blends. It is proposed that paraffin products of different carbon length when combined will change the physical and chemical characteristics of the blended WSP. Paraffin oil, macrocrystalline and microcrystalline waxes when combined will lead to a range of WSP products with different stiffness and rheology properties. this theory will be investigated within

the scope of this thesis by using the objectives mentioned below. By also relating the characteristics of the constituent components to the WSP blends made of those components it should be possible to test unknown WSP blends and reverse engineer or hypothesis the components contained within those WSP blends. It should be possible with understanding the characteristics of components to be able to model specific blend types suitable for consumer end products, such as with use in an ointment relating to a pharmaceutical product, within the scope of this thesis.

The objectives are:

1. To use a range of techniques to explore physical characteristics of WSP
    a. Rheology
    b. DSC
    c. Microscopy
2. To address the chemical makeup and characterisation of WSP using:
    a. Raman spectroscopy
    b. Solubility
3. To explore the blending of WSP from constituent components. This will necessitate the study of both underlying components and formulated material
4. To relate WSP materials to key requirements of stability and process changes.

In this report, several topics will be covered giving an overview of the relevant research that has been completed. White soft paraffin products, their derivatives and their use in the production of ointments. The range of low molecular weight liquid paraffin to high molecular weight microcrystalline paraffin will be detailed in this report also. Showing what has been covered previously, the types of products that have been discovered and the makeup of those products will be explained. The chemical and physical nature will also be discussed to show how the differences in white soft paraffin can be determined, while also considering what these differences will mean for the final product being made.

1.6.1 Thesis Makeup

Chapter one will introduce background information about paraffin products and white soft paraffin. Covered in this chapter will be techniques already implemented to characterise these and similar materials/derivatives. Information will be given about how the techniques used could help this project to achieve its objectives to be able to characterise WSP in the scope of ointments.

The second chapter will focus on the blending of constituent components to produce WSP blends made to simulate those of commercial grade. These blends will be used to mimic commercial blends to determine if quality assurance techniques currently in use could be improved or extended to aid in the manufacture of WSP in the future.

The third chapter will explain the rheological characterisation of WSP and constituent components, this will include large deformation rheology; cone penetration testing and small deformation rheology; oscillation cone and plate rheology. Viscosity testing will also be carried out as a comparison with existing standardised methods used for paraffin like materials.

Chapter four will focus on the thermal analysis of WSP and constituent components by use of differential scanning calorimetry. Analysis of the latent heats contained within samples will be carried out and comparisons will be made between the constituent components and the WSP blends made from them. WSP blends made within the laboratory will also be compared against commercial WSP blends, to help distinguish energy differences between the samples, this will be with the hope of determining a quality method of identification, possibly a fingerprint for a WSP or constituent component type.

In chapter five chemical analysis will take place, investigating the solubility of the constituent components and WSP samples, this will help to explain the homogeneity of the paraffin products, based on the idea of “like dissolve like”. Within this chapter, Raman spectroscopy will also be carried out with the hope of further analysis these compounds contained within the paraffin products. The observation of specific compounds could also aid in the identification of impurities or atypical compounds prevalent in paraffin products that would help the manufacture of WSP blends.

The sixth chapter will concentrate on stability and storage testing carried out on selected commercial WSP and model WSP blends. Within the pharmaceutical industry, storage testing will take place over several years, to successfully pass quality assurance so products are suitable for consumer use. Although in industry WSP would be tested over numerous years, this is not possible within the scope of this project due to time limitations. Therefore, an accelerated test will be performed over the space of 12 months allowing for the rise of potential problems with physical and chemical stability within the sample. WSP blends will undergo full characterisation testing, that has previously been explained, allowing for a full comparison of before and after storage conditions.

Chapter six will also concentrate on factory processing and how it impacts on the model WSP blends. The exact process cannot be replicated due to lack of manufacturing equipment, however, a close example of process mixing times and temperatures, and mixing ratios will be investigated. At this point of the investigation carrying out purposefully destructive experiments by overloading the blends with excess excipients, will be carried out. The purpose of this is also to investigate the stability of the WSP blends available and to find the limitations of the blends within the protocols of the factory processes deciding upon for these experiments. The purpose of this chapter is to investigate how the materials and blends made up will affect the process of mixing, theoretically, this could then influence the factory equipment if the wrong materials were used, or materials that do not follow quality assurance protocols are used.

1.7 Conclusions

The evaluation of white soft paraffin (WSP) and paraffin derived materials (paraffin and microcrystalline wax) will be mostly based on rheological properties, this is due to the viscoelastic nature of WSP, however, due to the chemical nature of the wax materials, chemical and thermal analysis are also a requirement.

With a combination of rheological, thermal and chemical analysis it is hoped that a fingerprint of material characteristics can be achieved, to aid in the manufacture of WSP within an industry setting.

Paraffin wax materials and their derivatives are not simple materials, and the production of WSP is not as simple as mixing the waxes together with the hope they will produce a consumer safe material. With this in mind the analysis will help to guide blending of wax materials in the production of model WSP blends to mimic commercial blends, to be able to describe the differences between the known model blends and unknown commercial blends.

As this project is designed to answer the WSP product in terms of use for ointments, it is important to consider the end use consumer and the suitability of the WSP in terms of long time storage/use. This will be achieved with storage experiments, as well as processing investigations with the purpose of sample destruction, to determine a top end limit of constituent component use within WSP blends. This will ultimately also guide the production of WSP blends for future manufacturing within the pharmaceutical industry.

Chapter 2 Blending Plan and White Soft Paraffin Development

2.1 Introduction

As part of my PhD, the investigation of a commercial pharmaceutical grade white soft paraffin (WSP) was fundamental. However, to understand the role of the main WSP constituent components in the final product, model WSP blends were created. Furthermore, the possibility to produce model WSP blends without the strict control of a pharmaceutical industry process was assessed, using fewer constituent components with a blending ratio. If these blends passed the standard tests for WSP products, then these would be good systems to try and understand the key characteristics of WSP required from suppliers.

It has been previous stated (Freund et al., 1982) that WSP is made of various components including liquid paraffin (oil) (LP), paraffin (macrocrystalline) wax (PW) and microcrystalline wax (MW), all of which are various fractions of crude oil (Freund et al., 1982). Commercial WSP consists of blends of these ingredients in various ratios. The overall physical characteristics of the WSP are believed to depend on the composition of the mixture and the characteristics of

the individual components. Information obtained from one WSP suppliers, Fuchs Lubricants (UK) plc, indicated that the blends and the components used could be quite complex, consisting of numerous waxes and oils, all with different melting/crystallisation points, viscosities and molecular weights.

In designing a simpler blend for laboratory studies, it should be noted the aim was to design a WSP blend for use in ointments, i.e., oleo-continuous mixtures. This is important because the ratio of the constituent components will change depending on the intended product use (Sarker, 2013). Ointments are usually a mixture of high molecular weight hydrocarbons, paraffinic waxes and/or polyethylene glycols, but can also contain beeswax, plant wax, wool fat and vegetable fats (Sarker, 2013). They can include up to 20 % water as a water-in-oil emulsion (Buhse et al., 2005), whereas creams can contain 50 % to 75 % water where the WSP is present as an oil-in-water emulsion (Sarker, 2013). To produce a more understandable model WSP for ointments only oil, paraffin wax and microcrystalline wax were blended, without any other oils, waxes, water, stabilizers or other additives.

The WSP to be used in pharmaceutical products must pass various standardised tests set by pharmacopoeia editions for different consumers on different continents: British Pharmacopoeia (BP), European (EP), United States of America (USP) and Japan (JP), which cover most of the world when testing pharmaceutical products. The pharmacopoeia standards are based on human product use and human health based on the medicinal properties of the product in question. The standardised tests in relation to WSP are congeal point tests and penetration tests. Failure to meet such tests could result in misuse or misapplication of possibly life-saving medicines.

Figure 2.1 shows a matrix of idealised paraffin product characteristics suitable for the WSP blends to be produced in the laboratory.

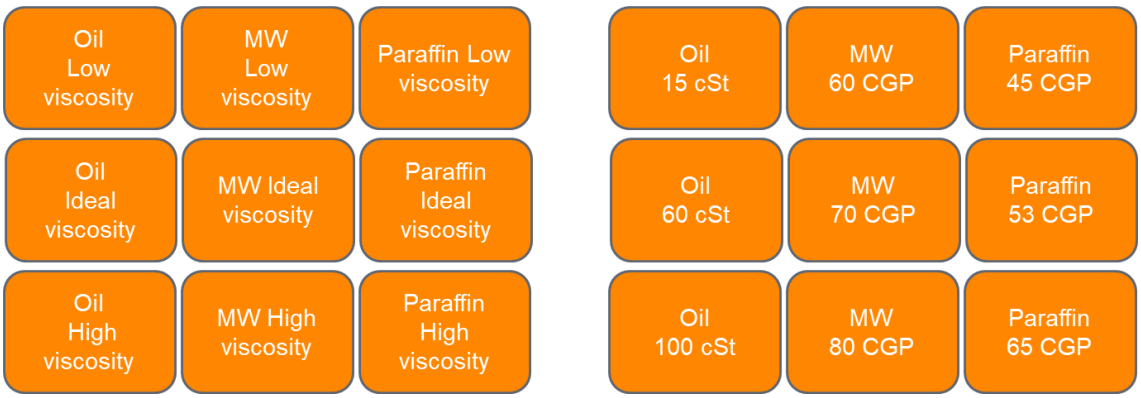

Figure 2.1 – Chart showing the basic matrix of constituent components required to make satisfactory blends of WSP within Leeds. cSt = Centistokes, CGP = Congeal Point.

Information from industry sources suggested that at least 10 % of the WSP blend must be microcrystalline wax (MW) and a maximum 15 %, to allow enough structure forming material to be present to trap liquid paraffin whilst at the same time give rheological properties suitable for product use, i.e., not too viscous or rigid. Bearing this in mind, the % of oil, PW and MW were fixed at 70, 15 and 15 %, respectively, believed to be representative of typical commercial WSPs.

There are many possible ratios that can be made from the 8 materials. To reduce complexity further, a blend of half high viscosity and half low viscosity oil was used as the oil phase, a so-called ‘ideal’ viscosity oil. This was justified on the basis that the oil phase was the component least like to contribute to the structure and rigidity of the blend. Figure 2.2 shows the final matrix of WSP blends that were made up and tested against the commercial blends provided.

1	OIL	MW	PW	2	OIL	MW	PW	3	OIL	MW	PW
LOW		x		LOW				LOW			
MED	x		x	MED	x	x	x	MED	x		x
HIGH				HIGH				HIGH		x	
4	OIL	MW	PW	**5**	OIL	MW	PW	**6**	OIL	MW	PW
LOW		x	x	LOW			x	LOW			x
MED	x			MED	x	x		MED	x		
HIGH				HIGH				HIGH		x	
7	OIL	MW	PW	**8**	OIL	MW	PW	**9**	OIL	MW	PW
LOW		x		LOW				LOW			
MED	x			MED	x	x		MED	x		
HIGH			x	HIGH			x	HIGH		x	x

Figure 2.2 – Matrix of Leeds produced WSP blends, based on extreme variations of theoretical blends.

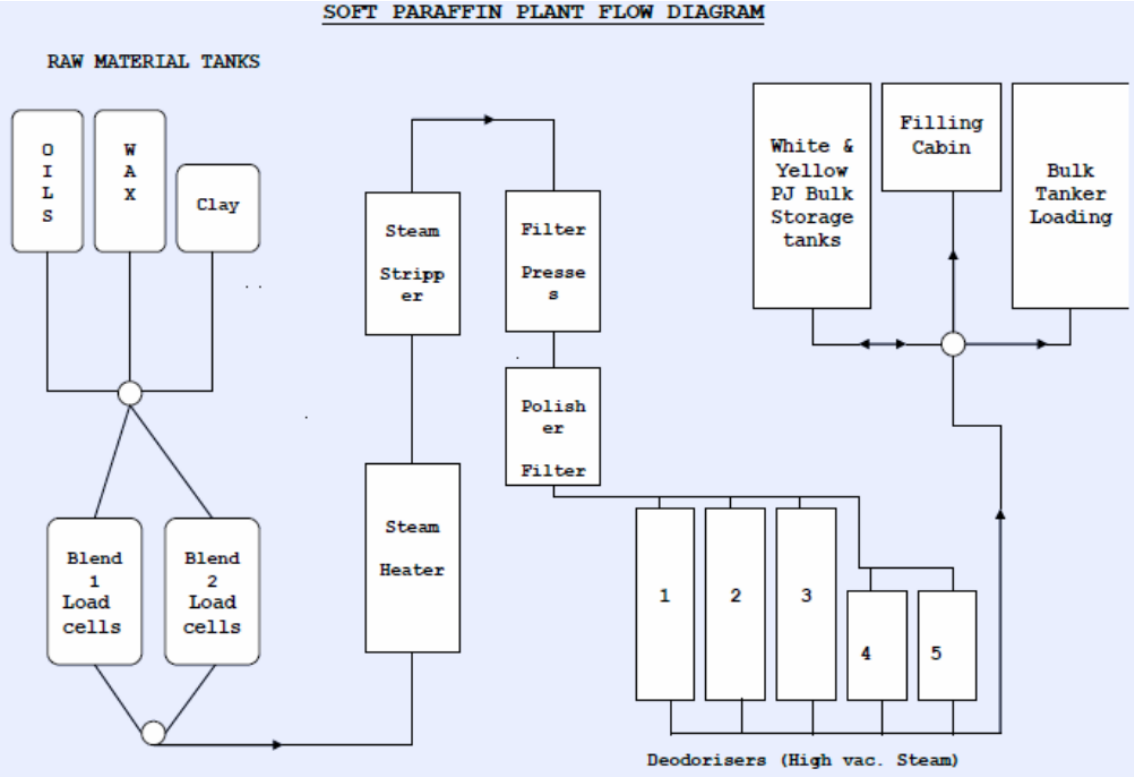

Figure 2.3 – Flow Diagram of the production of soft paraffin in a Fuchs production plant.

Figure 2.3 shows an outline of the soft paraffin factory production by Fuchs. As can be seen, there are many steps involved including some intensive processes that would have been difficult to replicate accurately in the laboratory, including the final bleaching process to make white soft paraffin. The WSP Leeds blends (WSP1-9) were produced by a much simpler process, outlined below.

The aim of blending constituent components is to produce model WSP blends that would closely mimic commercial WSP blends used by the pharmaceutical industry. Commercial WSP must pass strict testing regulations set in place by multiple Pharmacopoeia and regulatory bodies, depending on the

destination of the WSP based product. However, with multiple components being used it was theorised that a model WSP blend could be made to pass these tests but lack the stability and homogeneity characteristics of those of commercial blends that would be existent in long term storage and usage. It is believed that blending paraffin products of known Mw, those of lower and higher Mw, it would be possible to produce a WSP blend with required characteristics suitable for a consumer end use product. As such, based on materials available and paraffin component supplier's information a variety of WSP blend would be producible based on extremes of wax physical, thermal and chemical properties.

2.2 Materials and Method

Samples of microcrystalline wax, paraffin wax and paraffin oils were provided by Kerax Limited, Cowling Road, Chorley, Lancashire, PR6 9DR. Keratech 15 is a light paraffin oil with an average viscosity of 15 cSt ($1.5x10^{-2}$ Pa s) at 40 °C, Keratech 68 is an oil with an average viscosity of 70 cSt ($7x10^{-2}$ Pa s) at 40 °C, Kerawax 2245 is a paraffin wax of a congeal point average of 42 °C, Kerawax 482 is a paraffin wax with an average congeal point of 53 °C, Kerawax 1301 is a paraffin wax with an average congeal point of 65 °C, Techniwax P9805 is a microcrystalline wax with an average congeal point of 70 °C, Techniwax P9820 is a microcrystalline wax with an average congeal point of 77 °C and Techniwax P9830 is a microcrystalline wax with an average congeal point of 85 °C.

Table 2.1 – Table of constituent components used to make WSP(lab) blend.

Sample	Description	Acronym
Keratech 15	Low viscosity oil	LO
Keratech 68	High viscosity oil	HO
Kerawax 2245	Low congeal point paraffin wax	PWL
Kerawax 482	Medium congeal point paraffin wax	PWM
Kerawax 1301	High congeal point paraffin wax	PWH
Techniwax P9805	Low congeal point microcrystalline wax	MWL
Techniwax P9820	Medium congeal point microcrystalline wax	MWM
Techniwax P9830	High congeal point microcrystalline wax	MWH

WSP1-9 blends were made from a 70 % by mass mix of the two oils (LO, HO) blended in a ratio of 1:1 to give a target viscosity ≈ 45 cSt, 15 % by mass of a paraffin wax (PW) and 15 % by mass of microcrystalline wax (MW). The components were first weighed out into screw-top glass bottles, before heating in an oven to 110 °C. The oven was fitted with four thermocouples logged to a Datatracker to ensure uniformity of heating. The components were then mixed in the 300 ml glass bottles, manually stirred to ensure good homogeneity and then cooled for 24 h at ambient temperature before use. Each WSP blend made was placed in a separate container and fully labelled for identification. This process was carried out twice, where one set of WSP1-9 was stored in ambient conditions, where a second set of WSP was stored in an oven at 100 °C over a period of 12 months with intermittent testing as described later.

2.3 Summary

Table 2.2 shows the full blends available for testing, and their acronyms used throughout the remainder of this thesis.

Table 2.2 – Table of total model blends corresponding to figure 2.2, with included commercial blends.

Sample/Acronym	Description	Constituent Component Ratio 70:15:15
WSP1	Leeds white soft paraffin blend 1	OIL:PWM:MWL
WSP2	Leeds white soft paraffin blend 2	OIL:PWM:MWM
WSP3	Leeds white soft paraffin blend 3	OIL:PWM:MWH
WSP4	Leeds white soft paraffin blend 4	OIL:PWL:MWL
WSP5	Leeds white soft paraffin blend 5	OIL:PWL:MWM
WSP6	Leeds white soft paraffin blend 6	OIL:PWL:MWH
WSP7	Leeds white soft paraffin blend 7	OIL:PWH:MWL
WSP8	Leeds white soft paraffin blend 8	OIL:PWH:MWM
WSP9	Leeds white soft paraffin blend 9	OIL:PWH:MWH
WSP10	Typical commercial sample of relevance to pharmaceuticals in general.	UNKNOWN
WSP11	Same as WSP10 but after significant storage at variable temperatures for extreme lengths of time	UNKNOWN

All samples were prepared together from the same stock materials. Samples of WSP tested at 0 months are intended to give baseline, standard sample results. Other samples were tested monthly over 12 months via techniques described later.

Chapter 3 Rheological Characterisation

3.1 Large Deformation: Cone Penetration Tests

3.1.1 Introduction

Large deformation rheological measurement of materials allows detection of large inhomogeneities in the material as well as the testing force needed to break or penetrate a sample. Penetration by a cone is an empirical method that breaks the surface of the WSP (Barry and Grace, 1971c). It is commonly used in the pharmaceutical industry to test white soft paraffin (WSP) and is part of standardised quality testing for WSP (Pharmacopoeia, 2005). Despite its widespread practice, up to date information about cone penetration results in WSP is scarce.

This chapter will investigate the large deformation rheology of WSP and the constituent components of the model blends. Testing was based on standardised quality testing used in industry but adapted using texture analyser equipment (figure 3.1) to make the test more reproducible and the results more quantitative. For example, with the texture analyser, it is possible to control the probe with speed, penetration depth and maximum force applied. Use of standardised equipment has been altered and a 60 ° Perspex cone has replaced the penetration cone described in pharmacopoeia (Pharmacopoeia, 2005), the cone lacks a pointed tip found in standard tests, and as such will measure the force of surface deformation, instead of the direct penetration.

It has been hypothesised that when testing penetration forces, constituent components will increase in penetration force recorded as congeal points increase. When testing model WSP blends this theory is believed to also occur, however, there may be possible inhomogeneities experienced when mixing constituent wax components of extreme congeal point values, due to their stark difference in chemical and thermal characteristics, such as mixing PWL and MWH.

3.1.2 Materials and Methods

Penetration force tests were carried out using a TA-XT plus texture analyser (Stable Micro Systems, UK) with a 60 ° Perspex cone (Pharmacopoeia, 2005) (figure 3.1).

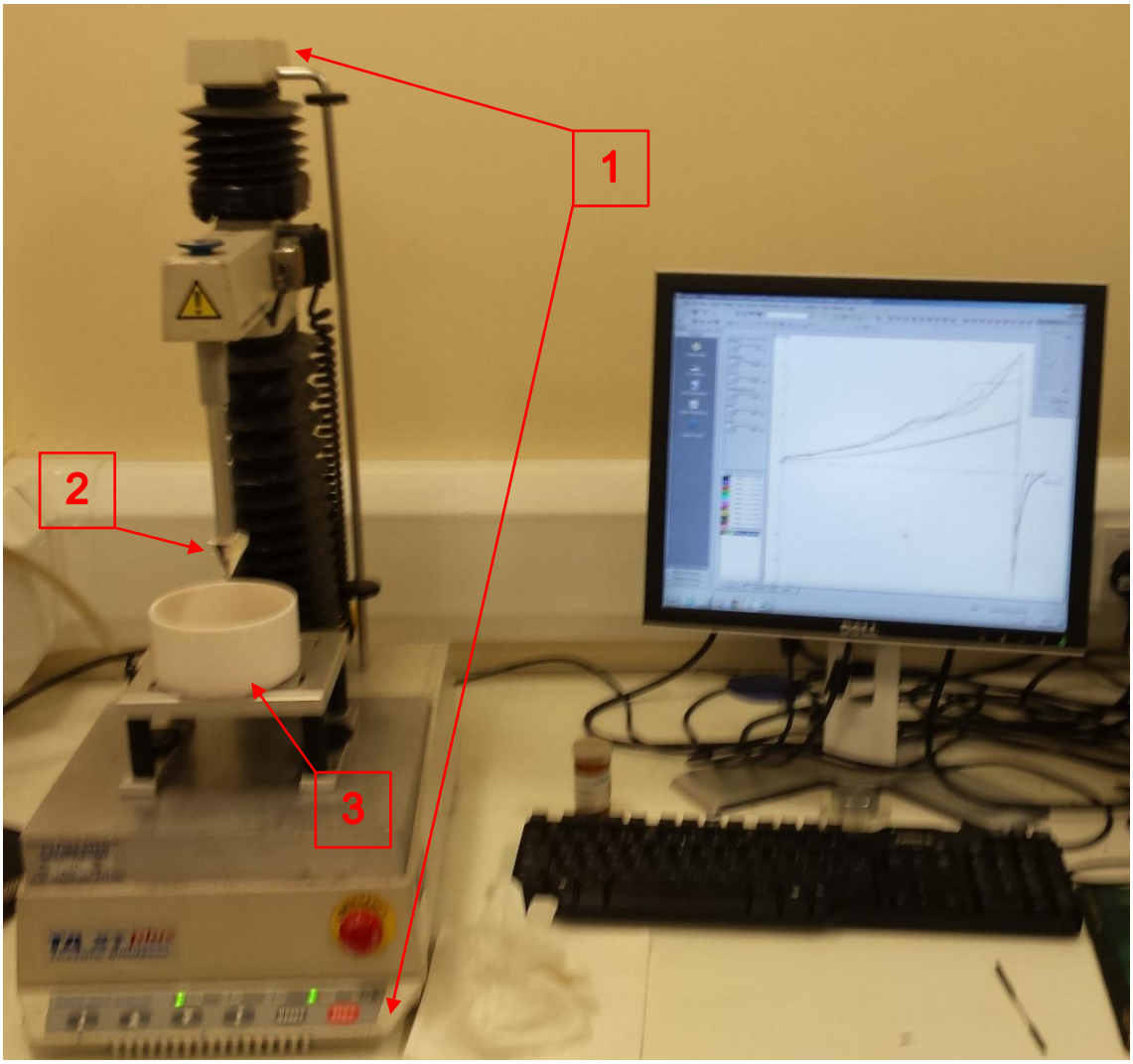

Figure 3.1 – (1) TA-XT Plus texture analyser, (2) 60 ° Perspex cone, (3) PTFE container; All used for penetration testing of all constituent wax and white soft paraffin products.

Exponent software and Microsoft Excel were used for analysing the resulting data. PTFE (polytetrafluoroethylene) containers of diameter 100 mm and depth of 50 mm were chosen to hold the WSP sample while testing to allow repeats within the same container and to minimise interference from the wall. The depth of the sample was at least 30 mm.

Samples were first melted in an oven at 100 °C and left until transparent. The sample was then transferred to the PTFE container. The testing container

was cooled to 25 °C in ambient conditions. The European Pharmacopoeia standard for penetration testing (Pharmacopoeia, 2005) was used as a guide to derive the test protocol. After positioning the tip approximately 25 mm from the edge of the container and 1 mm from the surface, the tip was driven into the sample at a constant speed of 1 mm s^{-1} to a depth of 5 mm. The sample was deemed under test once the force was greater than 0.01 N. After the test, the cone was withdrawn at 5 mm s^{-1}. The sample container was rotated 45 º. To obtain a reasonably small standard deviation, six replicates were taken at least for each sample. The temperature was controlled for all experiments that were performed at 25 °C according to standard testing (Pharmacopoeia, 2005). The maximum force at penetration (N) was recorded as a measure of sample 'hardness'.

3.1.3 Results

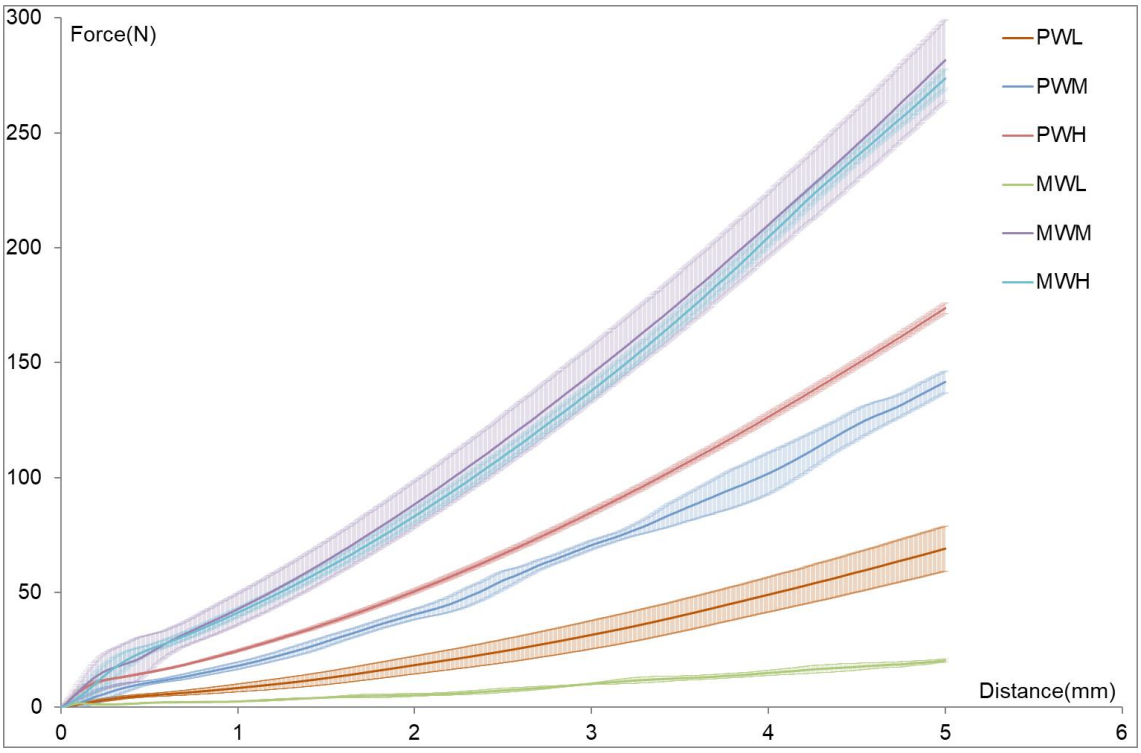

Figure 3.2 – Force versus distance penetration curve. Effect of constituent components' penetration force at month 0.

Typical results of penetration force versus penetration into the individual components of the constituent components are shown in figure 3.2. MWM and MWH have the greatest penetration maximum forces (281.62 and 273.67 N respectively). MWL has the lowest penetration force overall (20.40 N). PWL (69.12 N), PWM (141.64 N) and PWH (173.77 N) fall between the other two sets

of data. For figure 3.2 for all samples, there is a change in gradient after 0.2 mm of penetration. This change is more obvious in the harder samples (MWH, MWM, and PWH). Thereafter, all samples show a slight increase of gradient over the remaining penetration. This is more obvious for PWL, PWM and PWH samples. There is greater variability in recorded values for PWL and MWM, where lowest variability is recorded for samples MWL and PWH.

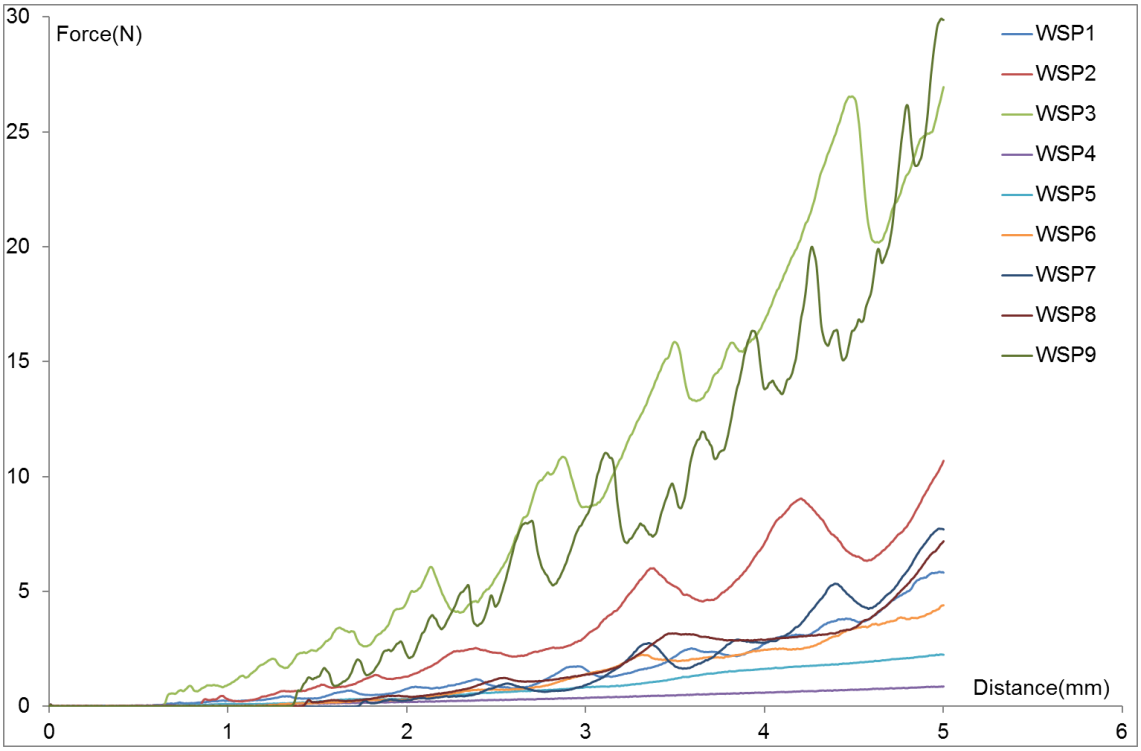

Figure 3.3 – Force versus distance penetration curve. Model blend WSP penetration forces at month 0.

Figure 3.3 shows the penetration curves for the model WSP blends made in the laboratory in Leeds. Unlike in figure 3.2, there are distinct differences in each of the curves. For all samples except WSP4 and WSP5, there is a degree in jaggedness in the curves, most prominent in WSP3 and WSP9. There are still large fluctuations in the force versus penetration curves for other WSP samples: WSP1, WSP2, WSP6, WSP7, WSP8. However, overall the penetration forces for model WSP blends are lower than the constituent components, since the largest penetration force recorded is WSP9 with a maximum force of 29.92 N. The WSP blend with the lowest penetration force is WSP4 with a maximum force of 0.87 N. It should be noted that, as this set of samples are so soft, they did not pass the initial texture analyser threshold of 0.01 N, therefore penetration of the samples is not recorded at first contact with the probe and WSP. WSP1 starts at 0.60 mm, WSP2 starts at 0.85 mm, WSP3 starts at 0.65 mm, WSP4 starts at 0.8

mm, WSP5 starts at 0.71 mm, WSP6 starts at 1.24 mm, WSP7 starts at 1.74 mm, WSP8 starts at 1.43 mm and WSP9 starts at 1.37 mm.

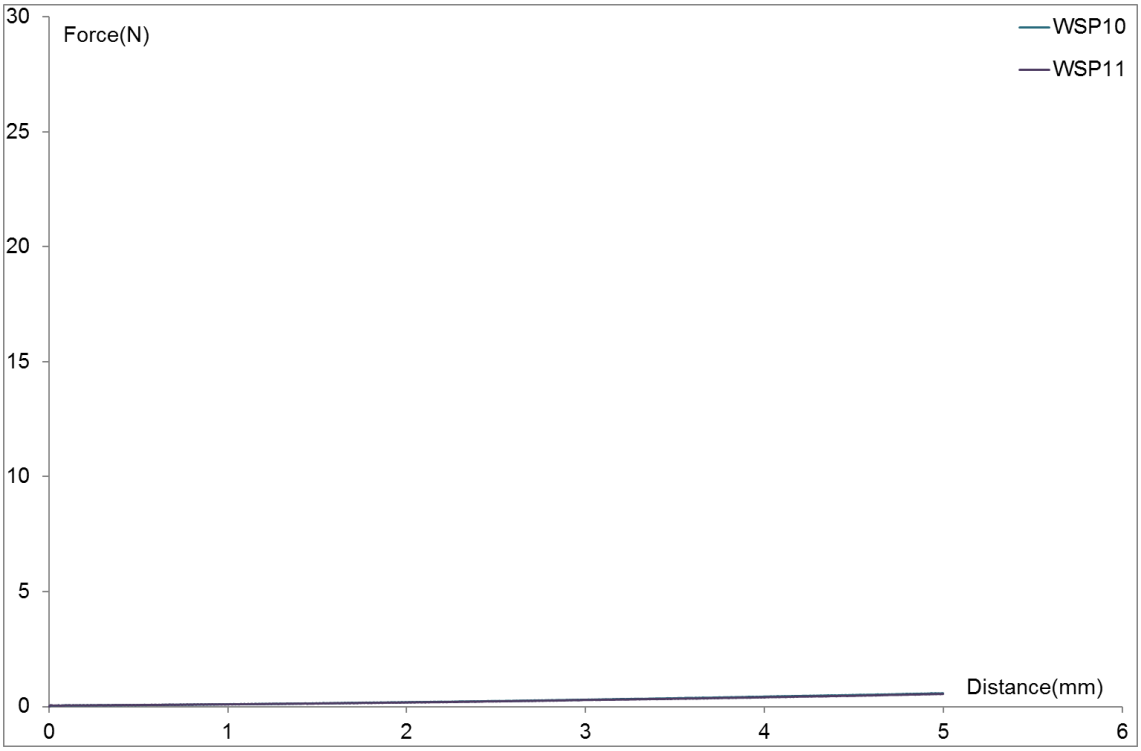

Figure 3.4 – Force versus distance penetration curve. WSP blends at month 0 (0 N – 30 N scale).

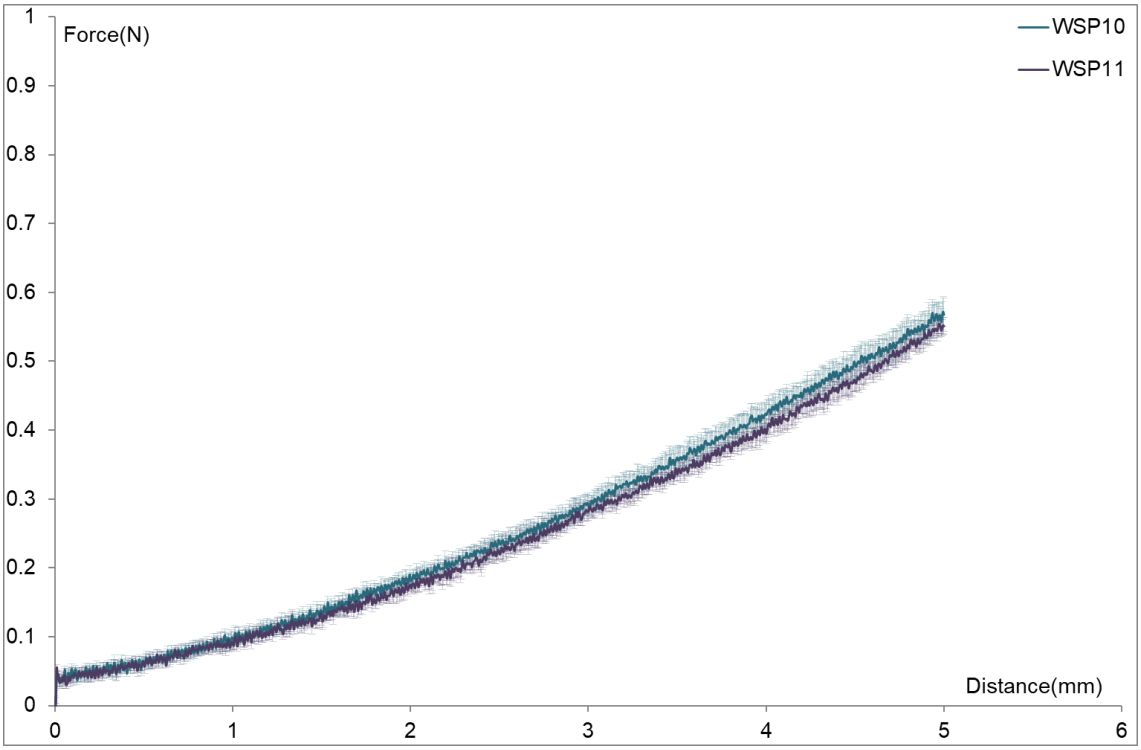

Figure 3.5 – Force versus distance penetration curve. WSP blends at month 0 (0 N – 1 N scale).

Figure 3.4 and figure 3.5 show the results from WSP10 and WSP11, these being commercial pharmaceutical grade WSP blends. As shown in table 2.2 WSP10 and WSP11 are white soft paraffin taken from stock before manufacture temperature profile experience and white soft paraffin taken from stock after

manufacture temperature profile experience, respectively. Figure 3.4 shows the penetration force of the WSP blends and commercial samples on the same scale for comparison. However, some of the differences are hard to discern, and so figure 3.5 also shows results on a smaller scale. As it can be seen the maximum penetration for WSP10 is 1.41 N and for WSP11 is 0.97 N.

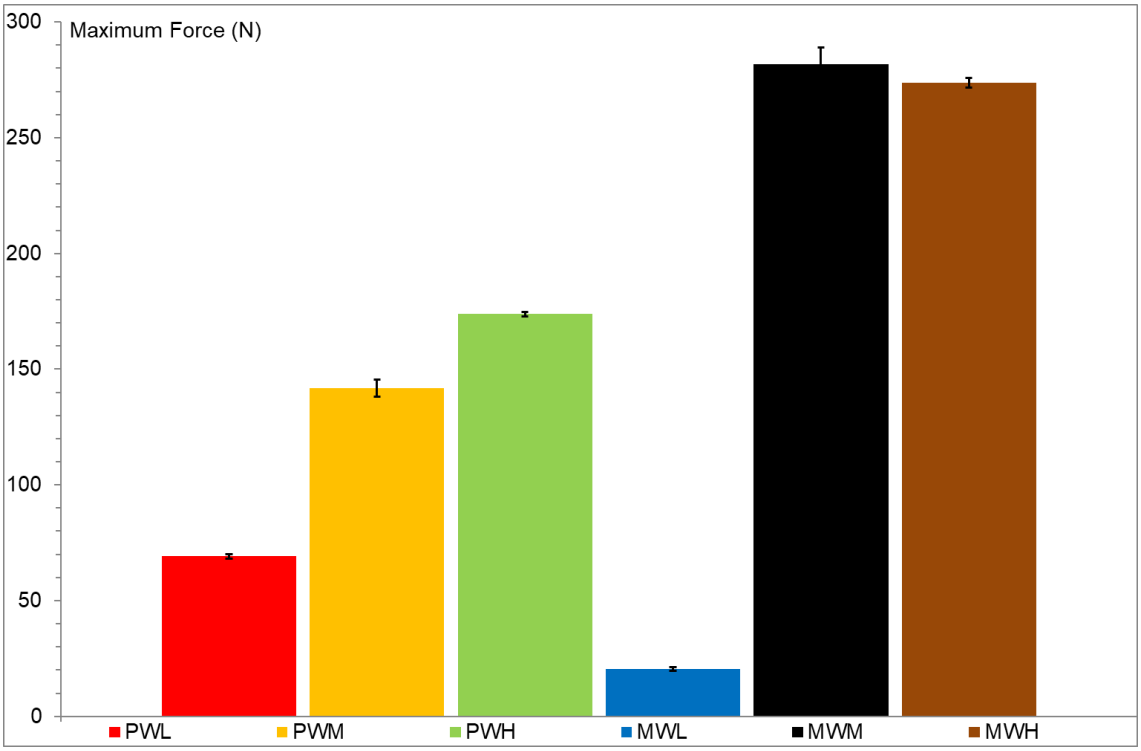

Figure 3.6 – Maximum peak penetration forces (N) for all constituent components.

Figure 3.6 shows a comparison of maximum penetration forces for constituent components, MWM shows the largest penetration for, while MWL shows the overall lowest penetration force.

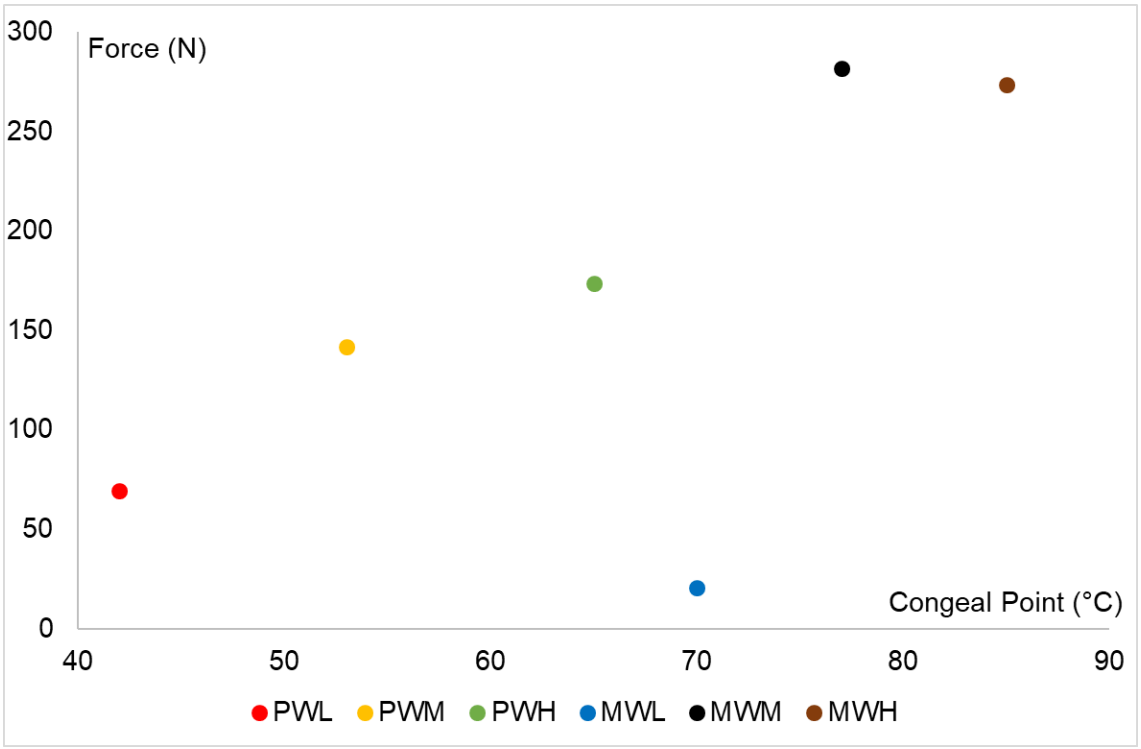

Figure 3.7 – Plot of maximum penetration force versus the congeal point for constituent components.

Figure 3.7 shows that in general as congeal point increases with constituent components, so does the penetration force. There is one obvious exception for MWL where congeal point is 70 °C but penetration force is only 20.40 N, giving the lowest force of all constituent components.

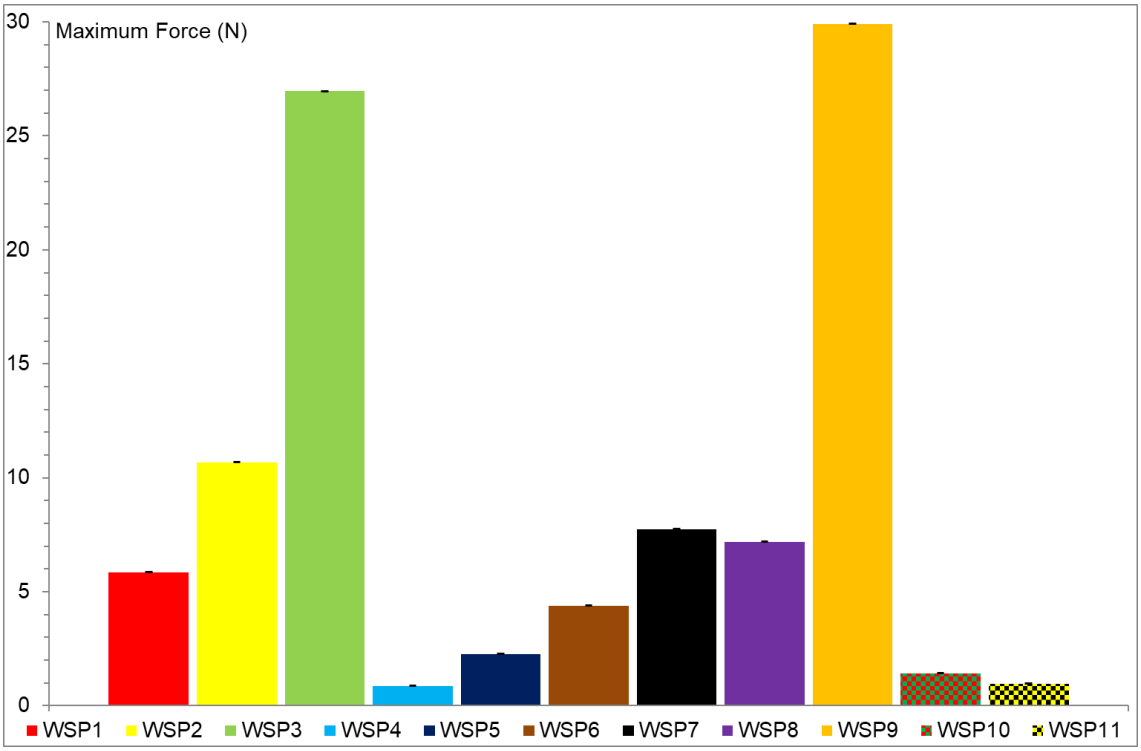

Figure 3.8 – Maximum peak penetration forces (N) for all WSP blends.

It can be seen in figure 3.8 that WSP4 and WSP5 are closest in maximum penetration force to the commercial pharmaceutical grade blends of WSP10 and WSP11. WSP9 as previously stated has the highest penetration force and WSP3 is only slightly less than that, but these are far stiffer samples than the remaining WSP model blends and commercial pharmaceutical grade blends.

3.1.4 Discussion

Figures 3.6 and 3.8 shows a summary of all maximum penetration forces of the white soft paraffin (WSP) and the constituent components. The larger resistance to penetration was for samples, MWM and MWH, along with WSP3 and WSP9. This occurrence is to be expected as both WSP3 and WSP9 contain MWH. WSP6 is the third blend to contain MWH, however as it also contains PWL (figure 2.2) the penetration force drops.

MWM, which has the largest penetration force, is contained in samples WSP2, WSP5 and WSP8. The difference in microcrystalline wax, therefore, seems to be the main determinant of the maximum force. Thus, WSP2 shows a maximum force of ≈ 10.5 N and contains PWM, WSP5 has a maximum force of ≈ 2 N and contains PWL. Interestingly, WSP8 contains PWH and only has a penetration force ≈ 7.5 N, a relatively small value compared to the high forces experienced by PWH and MWM.

WSP7 has a higher maximum force of ≈ 8 N, slightly higher than WSP8 containing MWM. The higher force for WSP7 is likely due to PWH, which has a very high maximum penetration force of ≈ 175 N.

In summary, the maximum penetration force seems to be largely determined by the hardness of the constituent waxes: the penetration force of the WSP blends is in the order, WSP4 < WSP1 < WSP7 (containing MWL); WSP5 < WSP8 < WSP2 (containing MWM); WSP6 < WSP3 < WSP9 (containing MWH). The only sample which does not seem to fit in with this trend is WSP8, where from the results of the other samples one might have expected a penetration force of ≈ 15 - 20 N. From figure 2.2 it can be seen the WSP7 has the same oil content and PW content, but contains MWL, whereas WSP8 contains MWM and thus would be expected to result in higher penetration forces.

One other cause of the low penetration force for WSP8 could be due to the microstructure of the blend. It is seen in figure 3.3 that for some of the samples there is a lot of variability in the gradient and the onset and persistence of force is variable. This indicates that the surface of the WSP is not as stiff as the bulk material, i.e., it could be collapsing under the first part of the test and as such, the trigger point of the texture analyser failed to recognise full contact with the material. Cooling of the WSP blend after placing in the test dish will be more rapid at the surface than that of the bulk material, especially possible for WSP due to their thermal retentive properties, which is why they are used as phase change materials (Luyt et al., 2010; Sánchez et al., 2010; Hawlader et al., 2003). If a WSP blend is cooled too rapidly there will be a promotion of growth of different crystal shapes and habits at the surface compared to the bulk. Rapidly cooling WSP produces crystals that are not conducive to forming a stable lattice network, causing surface softness. Slower cooling rates will promote large plate and needle shaped crystals, and this will allow the growth of a stable lattice, while also allowing time for the full formation of the interlaced network to trap oil within cavities leading to a fully developed WSP blend. It is possible that when the rapid cooling occurs high melting components crystallise as small plate crystal, ones that may even transfer into mal crystals if also in contact with a molten bulk WSP, as in the case of cooling here, without agitation. When WSP cools with greater amounts of mal crystals, lattice networks do not form, or very few will form as some plate and needle crystal will still manage to form lattice networks.

The zig-zag variations in the curves in Figure 3.3, especially in the samples that have a greater stiffness such as WSP3 and WSP9, is also evident in softer samples like WSP2, WSP7, WSP8 and to some extent WSP1. On the other hand, WSP4, WSP5 and WSP6 all give relatively smooth curves, indicative of a more uniform structure from the surface the bulk. The zig-zag pattern could also arise due to the cone used in this penetration test, the use of a cone without a tip will cause the sample to simply displace. Due to the chemical nature of the paraffin waxes, on a microscopic level, the wax could fracture in larger group motions at extended times, rather than small individual small movements, overall causing the variation and the jumps in penetration force recorded. Unfortunately, errors cannot be plotted in figure 3.3 as the data was not available, and would have to be repeated in the future to show true repeatable results.

Figure 3.4 and figure 3.5 show that, compared to other lab WSP blends, the commercial pharmaceutical grade blends are softer samples comparable to lab samples WSP4 and WSP5. The WSP10 and WSP11 curves are smooth and show no signs of oscillation on the curve, indicating the samples are homogenous, a key factor to be expected from factory manufactured samples, that will have passed through quality assurance to be consumer ready.

3.1.5 Conclusions

- MW plays a leading role in structure formation, increase in MW congeal point = increase in stiffness
- PW plays secondary role, in general, increase PW = increase in stiffness, but change is less than MW
- Cooling process/rates could influence crystal habit and effect overall structure of WSP
- Surfaces appear softer than bulk WSP, probably because they were not agitated during cooling.
- Crystals layers may laminate, possibly in plate layers with some needles and mal shaped crystals will interrupt the lattice structure, making it weaker and causing disjointed layer systems in the WSP blends.
- Factory produced WSP is homogenous
- Classic penetrometer tests deform the surface of the paraffin wax as well as the underlying layers but such tests do not actually record any force-

distance data. As such the tests will only give a qualitative result of hardness of the white soft paraffin, whereas the simple procedure adopted here gives far more information on the overall 'strength' and uniformity of the material.

3.2 Small Deformation Rheology

3.2.1 Introduction

Within this investigation, only the dynamic elastic modulus (G') is to be reported in detail (see Chapter 1), due to the nature of the product in its normal mode of use, where the 'solidity' of the material is key to its functional properties. G' is a measure of the stiffness of a material this is more important when considering the viscoelastic nature of the WSP rather than the viscosity of the WSP at high temperatures when 'fully' melted. The choice to concentrate on G' was also made because molten WSP is only utilized during storage and pumping in the factory, whereas in all other stages of manufacture WSP is within a viscoelastic region. From initial tests, it was also seen trends in G' were simply mirrored in G'', i.e., if G' went down, e.g., due to an increase in temperature, G'' concomitantly became more dominant over G', as expected. The exact cross-over points of G' and G'' in terms of temperature were not as important as the absolute values of G' above these points.

Although in this chapter the focus was on oscillatory testing, some measurements of viscosity at a constant shear rate as a function of temperature (20 °C to 100 °C) were also made, to mimic testing standards for viscosity performed by the petrochemical companies that supply WSP and its constituent components.

When testing viscosity, it was hypothesised that wax constituent components of higher congeal point and Mw would also have greater viscosity values, the greater Mw and molecular contained within the constituent components would generate more interactions between molecules, therefore, affecting the increase in viscosity.

Considering the G' oscillatory values, it is believed that those blends made of higher Mw constituent components and will show to have higher G' values and record these values at higher temperatures. It is also believed that as the

temperature is altered in carrying out the experiment, the G' value will decrease as temperature increases.

By carrying out oscillatory testing it is the belief that the information can be related to large penetration data, as well as viscosity data, to be able to carry out a quick simple test on constituent components and relate those results to hypothesis WSP and wax constituent component behaviour, based on the small molecular deformation observed in the rheological oscillatory testing.

3.2.2 Materials and Methods

All rheological measurements were carried out using a Kinexus ultra+ (Malvern Instruments Ltd.). The analysis was carried out using a cone and plate geometry, CP2/60 : PL65 (with the inbuilt Peltier plate used to heat the sample) and the rSpace software and Microsoft Excel to analyse data.

Testing the viscosity of waxes was carried out by following the rSpace software standard test for viscosity. A sample was applied to the plate, already set to 100 °C (this is so the sample becomes fully molten to achieve 'bright and clear' to remove any stored history), the viscosity protocol was applied and followed on rSpace. For oil samples shear rate was set to start at 0.1 s^{-1} and finish at 100 s^{-1}; for waxes to start at 0.01 s^{-1} and finish at 100 s^{-1}.

Preliminary measurements suggested the most useful testing protocol for WSPs would be to monitor G' and G'' from 80 °C to 20 °C and back to 80 °C (in 10 °C intervals) and for 3 cycles to assess any thermal history effects, which might also mimic typical temperatures during ointment manufacture. Prior to routine testing, the linear viscoelastic region (LVER) was established to ensure that measurements were made in a region independent of strain up to a critical strain level. Beyond this critical strain level, the material behaviour was non-linear and G' decreased. Measurements over a wide range of conditions established a frequency range of 0.1 – 10 Hz and a strain of 0.04 % was within the LVER, and consequently, these conditions were used for all routine data collection. Of course, WSP materials may be subjected to stresses and strains far outside the LVER in product manufacture, but the objective here was to obtain reproducible measurements that might explain the fundamentals of how composition and temperature cycling affects WSP rheology. Measurements of

these complex materials in the LVER are therefore required as the first step towards this understanding.

As mentioned above, viscosity as a function of shear rate was also measured using the test protocol Viscosity Shear Rate Table template in the rSpace software between 0.01 and 100 s^{-1} at 100 °C. All samples were loaded into the rheometer at 100 °C prior to carrying out rheological testing.

3.2.3 Results

3.2.3.1 Viscosity Measurements

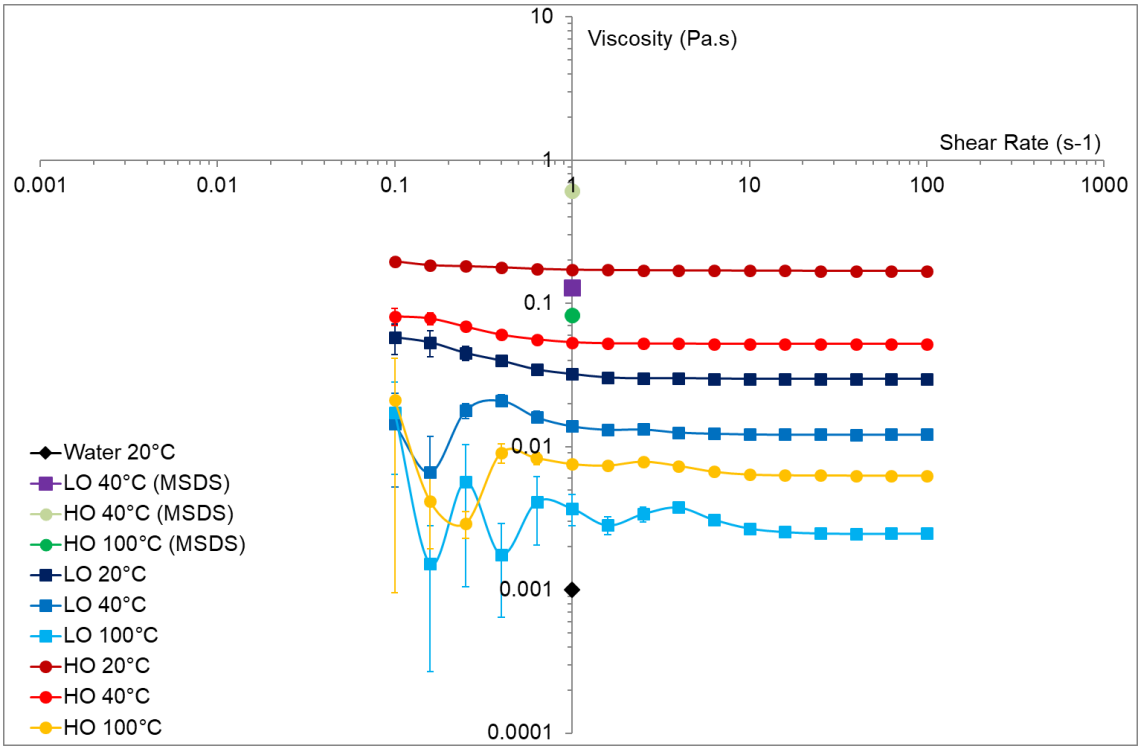

Figure 3.9 – Viscosity versus shear rate at various temperatures for oil components. Line values indicate results obtained from Kinexus rheometer. Single markers indicate data obtained from supplier MSDS.

Figure 3.9 shows viscosity values obtained for the oil samples supplied by Kerax Ltd. Data supplied on the MSDS by Kerax Ltd. only shows one data point per sample, as it is likely they would use a single point measurement device such as a viscometer, not a rheometer. HO 40 °C (MSDS) shows the greatest viscosity of all samples (0.61 Pa s), independent of shear rate. For HO at 100 °C (MSDS), the viscosity is 0.08 Pa s, a reduction in 0.53 Pa s. LO 40 °C (MSDS) is close to the high temperature HO viscosity giving a value of 0.13 Pa s. For all oil samples above 0.01 Pa s results were mostly independent of shear rate. Measurements below 0.01 Pa s had increasing noise as viscosity decreased and

the noise decreased as the shear rate increased, as expected due to limits in instrument sensitivity and accuracy. Water viscosity at 20 °C has been added to figure 3.9 as a point of reference of a Newtonian fluid, it should be noted that as oil values at 100 °C contain large amounts of noise, these are close to Newtonian fluid values.

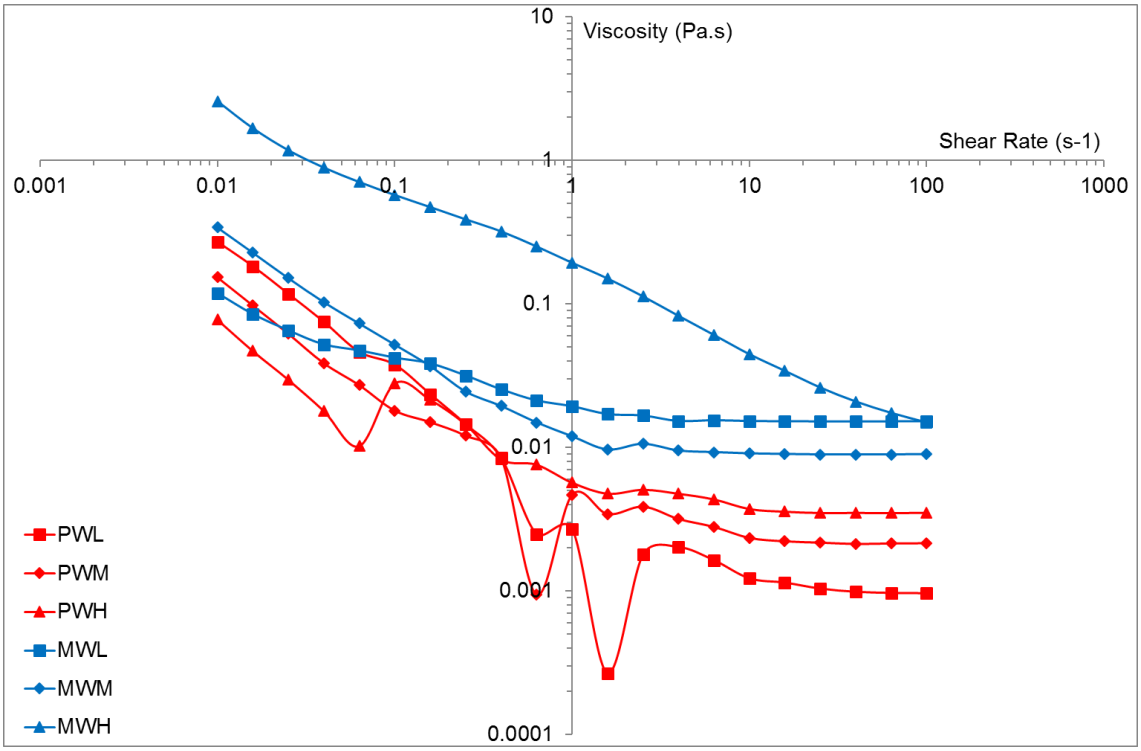

Figure 3.10 – Viscosity versus the shear rate of constituent wax components at 100 °C.

Figure 3.10 shows viscosity results for the constituent PW and MW components supplied by Kerax Ltd. All samples were tested just at 100 °C because all these samples were too viscous or completely solid at 20 °C to room temperature. In contrast to the oils, all samples showed shear thinning, indicative of persistent internal structure even at this high temperature.

Table 3.1 – Table showing viscosity values and differences at extreme values of shear rate measurements, relating the figure 3.8.

Sample	Viscosity at 0.01 s^{-1}	Viscosity at 100 s^{-1}	Difference	Difference (%)
PWL	0.27	0.001	0.27	99.63
PWM	0.15	0.002	0.15	98.67
PWH	0.08	0.004	0.08	95.00
MWL	0.12	0.015	0.10	87.50
MWM	0.34	0.009	0.33	97.35
MWH	2.59	0.015	2.57	99.42

Table 3.1 helps to show the differences in viscosity changes when increasing shear rate. The greatest change is experienced by MWH and least by PWH. It is also noted that PWL, the sample with the lowest viscosity at almost all shear rates, also shows the largest amount of noise in the data, particularly between 0.5 s^{-1} and 5 s^{-1}. It can be seen in figure 3.10 that for all samples apart from MWH, after shear rate values of 5 s^{-1} the values of viscosity reach a plateau and there is a slight change in the viscosity as the shear rate is increased. This plateau could be extended to 1 s^{-1} for samples of MWL and MWM.

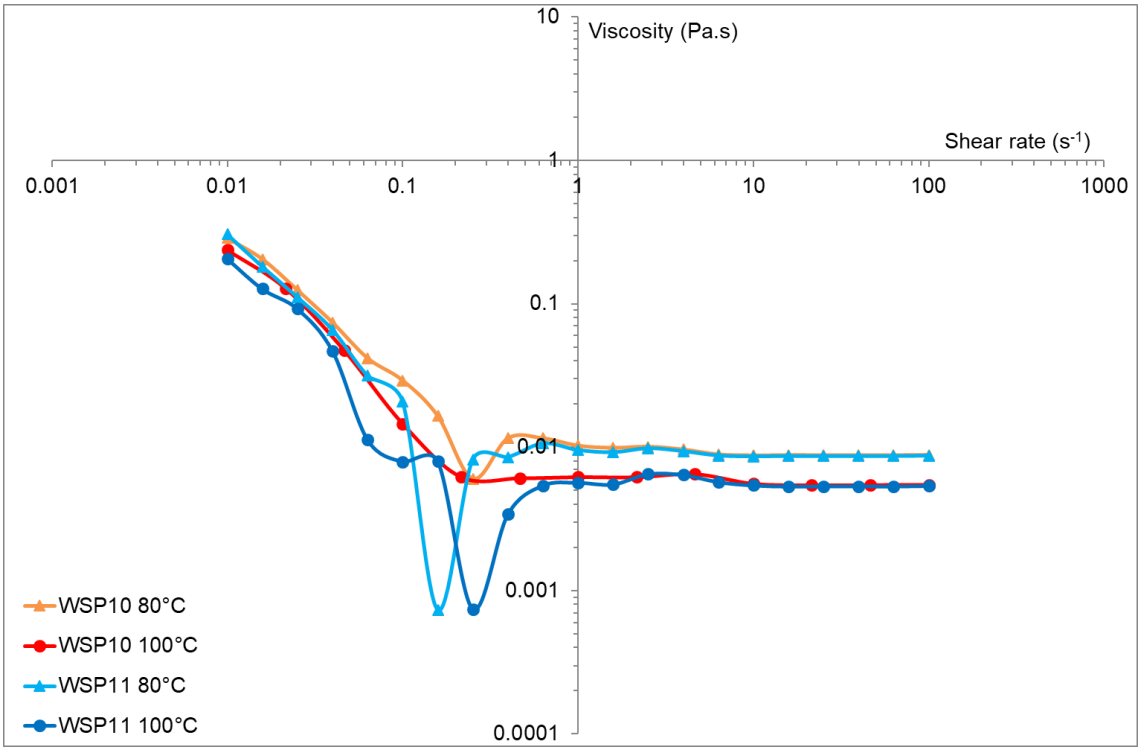

Figure 3.11 – Viscosity versus shear rate of commercial pharmaceutical grade samples at various temperatures.

Figure 3.11 shows the viscosity versus to shear rate for WSP10 and WSP11 at 80 °C and 100 °C. At 80 °C and 100 °C WSP10 show very similar curves, with values of 0.29 Pa s and 0.24 Pa s at 0.01 s^{-1}, respectively, starting the curve and reaching a plateau of 0.01 Pa s at 1 s^{-1} at 80 °C. For the 100 °C curve, a plateau of 0.006 Pa s is achieved at 0.22 s^{-1}. For WSP11 the results again are like WSP10 at both 80 °C and 100 °C. At 80 °C the plateau is achieved at a value of 0.008 Pa s at 0.25 s^{-1} and at 100 °C a viscosity value of 0.006 Pa s is achieved at 1 s^{-1}. These values are subtly different, but when looking at figure 3.11 the plateaus are achieved at similar times.

3.2.3.2 Oscillation Measurements

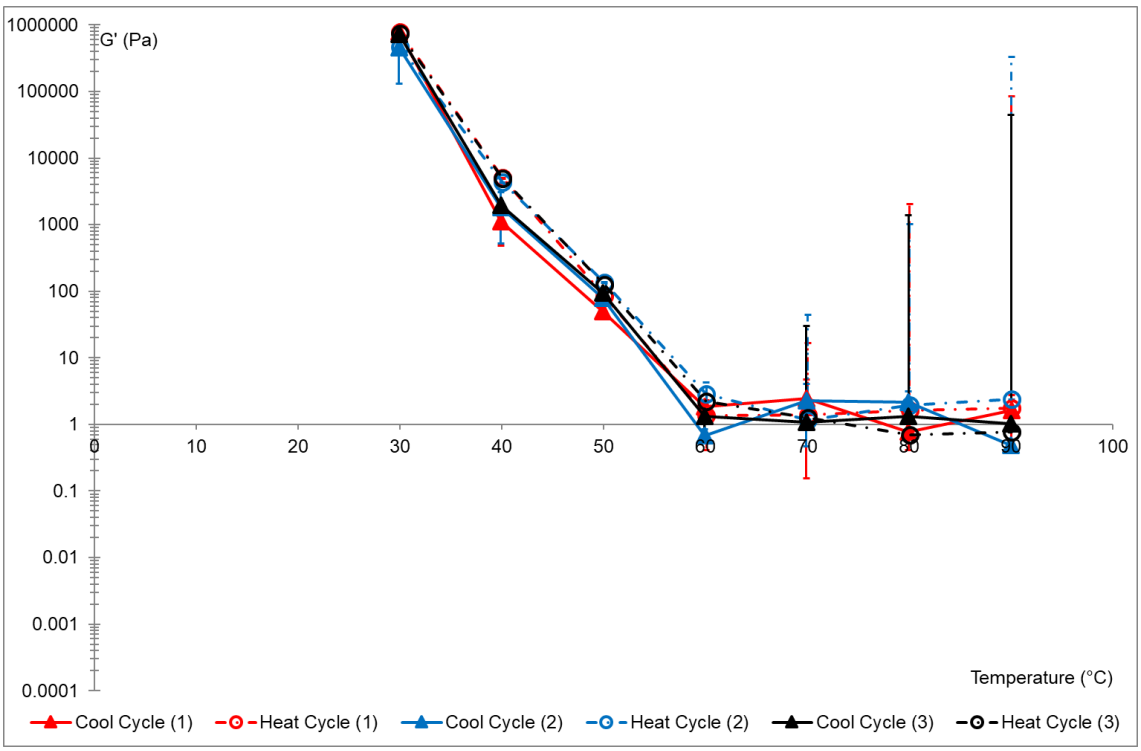

Figure 3.12 – G' values for WSP1 at 5 Hz frequency with three temperature cycle completions.

Figure 3.12 shows G' values when ramping temperature between 30 °C and 90 °C for WSP1. The temperature cycle had to be altered from the standard method due to errors of the rheometer when recording data at 20 °C. Figure 3.12 shows that at 30 °C the sample is solid, with G' values of ≈ 1000000 Pa, as temperature increases to 40 °C, G' decreases by a magnitude of three with a value of ≈ 1000 Pa, this will mean the sample is semi-solid and will contain part of the material in a liquid phase. As the temperature continues to increase, G' decreases with the same linearity reaching a fully molten stage at 60 °C where G' has a value of ≈ 1 Pa. it should also be noted that between the three temperature cycles used with this sample there is good repetition between cycles, with only a slight variation in G' values at 40 °C between the heat and cooling cycles. Cool cycles show values of ≈ 1000 Pa, while heat cycles have values ≈ 5000 Pa.

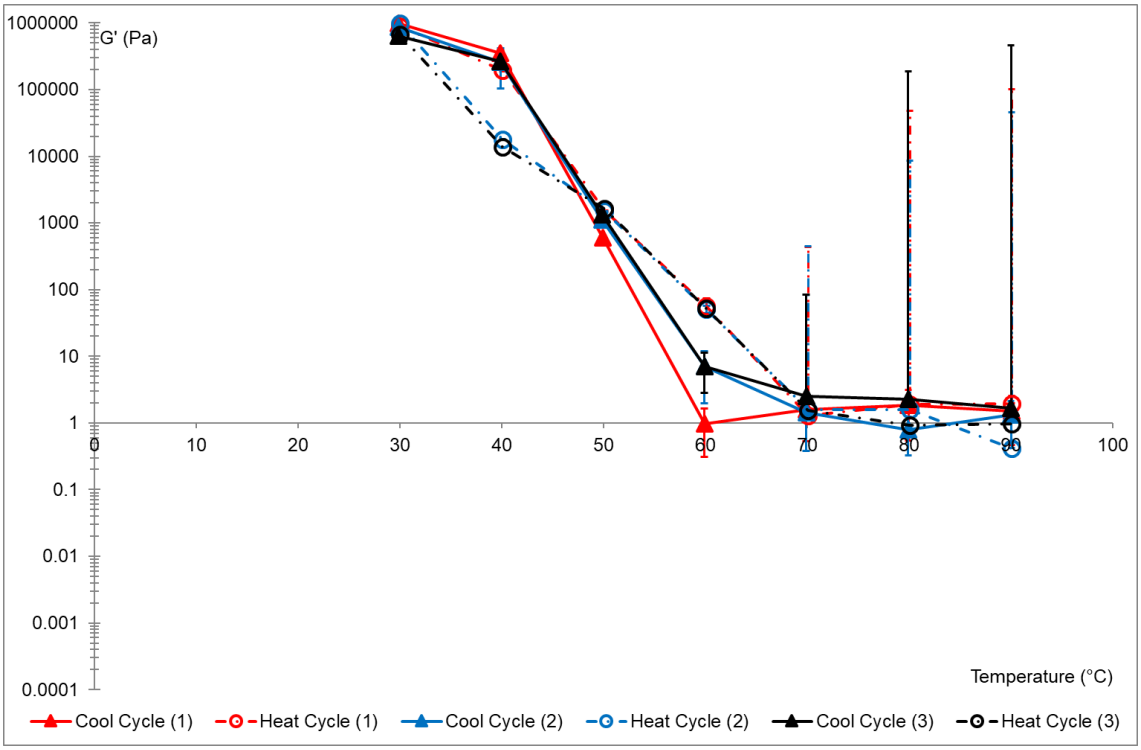

Figure 3.13 – G’ values for WSP2 at 5 Hz frequency with three temperature cycle completions.

Figure 3.13 shows G’ values when ramping temperature between 30 °C and 90 °C for WSP2. WSP2 at 30 °C is very stiff with a G’ values of ≈ 1000000 Pa, at 40 °C the sample is still relatively stiff with G’ value of ≈ 500000 Pa while cooling, but ≈ 100000 Pa while heating, indicating a more liquid phase affinity while heating at this temperature. At 50 °C the sample shows good homogeneity as both heating and cooling cycles have a G’ value of ≈ 1000 Pa. At 60 °C the sample is molten with cooling cycle G’ values being ≈ 1 – 10 Pa.

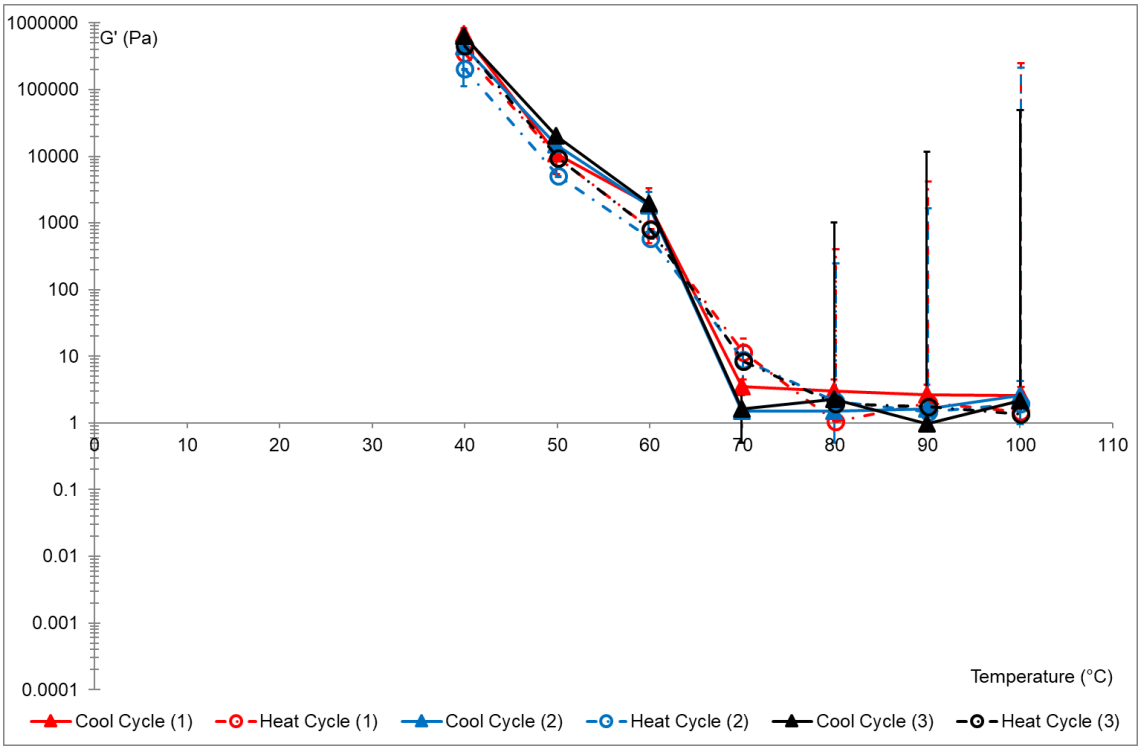

Figure 3.14 – G’ values for WSP3 at 5 Hz frequency with three temperature cycle completions.

Figure 3.14 shows G’ values when ramping temperature between 40 °C and 100 °C for WSP3. The temperature had to be increased once again for this sample as it was not possible to run rheology testing below 40 °C. We see that WSP3 is a stiff sample, at 40 °C G’ is ≈ 1000000 Pa and achieves liquid phase at 70 °C where G’ for cooling is ≈ 1 Pa and while heating is ≈ 10 Pa. WSP3 shows good homogeneity until 70 °C where there is a slight difference in G’ values while heating and cooling the sample.

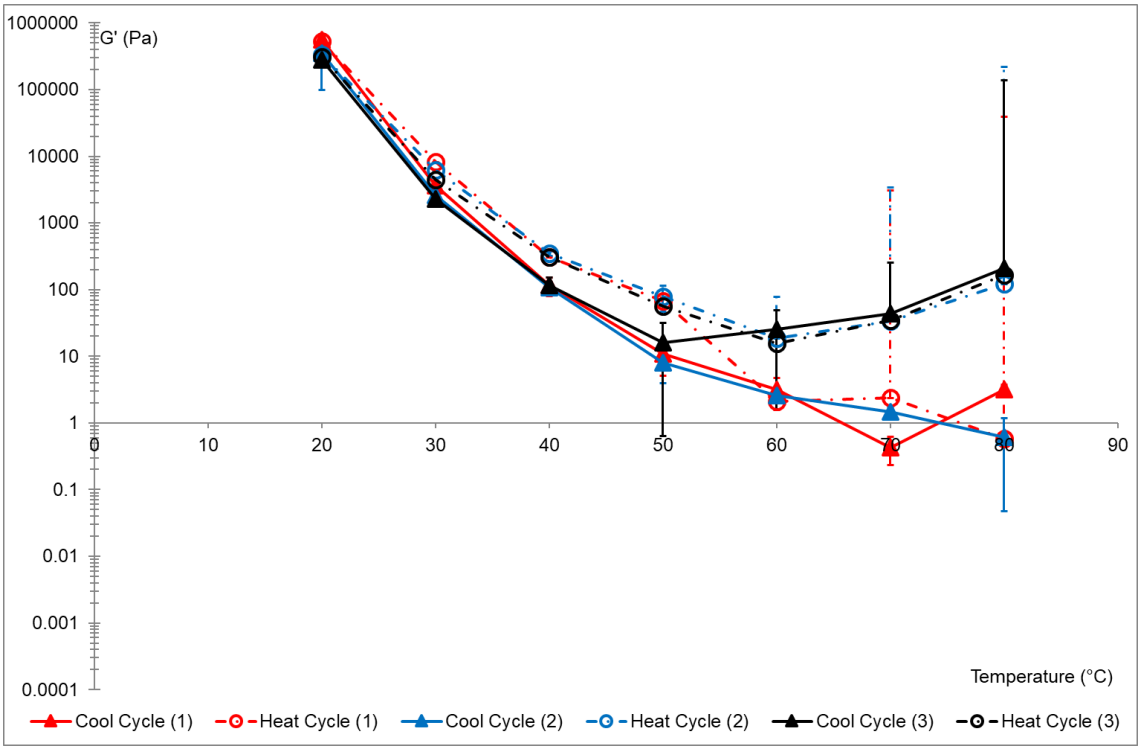

Figure 3.15 – G’ values for WSP4 at 5 Hz frequency with three temperature cycle completions.

Figure 3.15 shows G’ values when ramping temperature between 20 °C and 80 °C for WSP4. This sample has a G’ value of ≈ 500000 Pa at 20 °C and ≈ 5 Pa at 60 °C. WSP4 shows a more gradual change in G’ values with increasing temperature compared to other samples. Figure 3.15 also shows that after the third cycle there is an increase of G’, achieving 100 Pa at 80 °C.

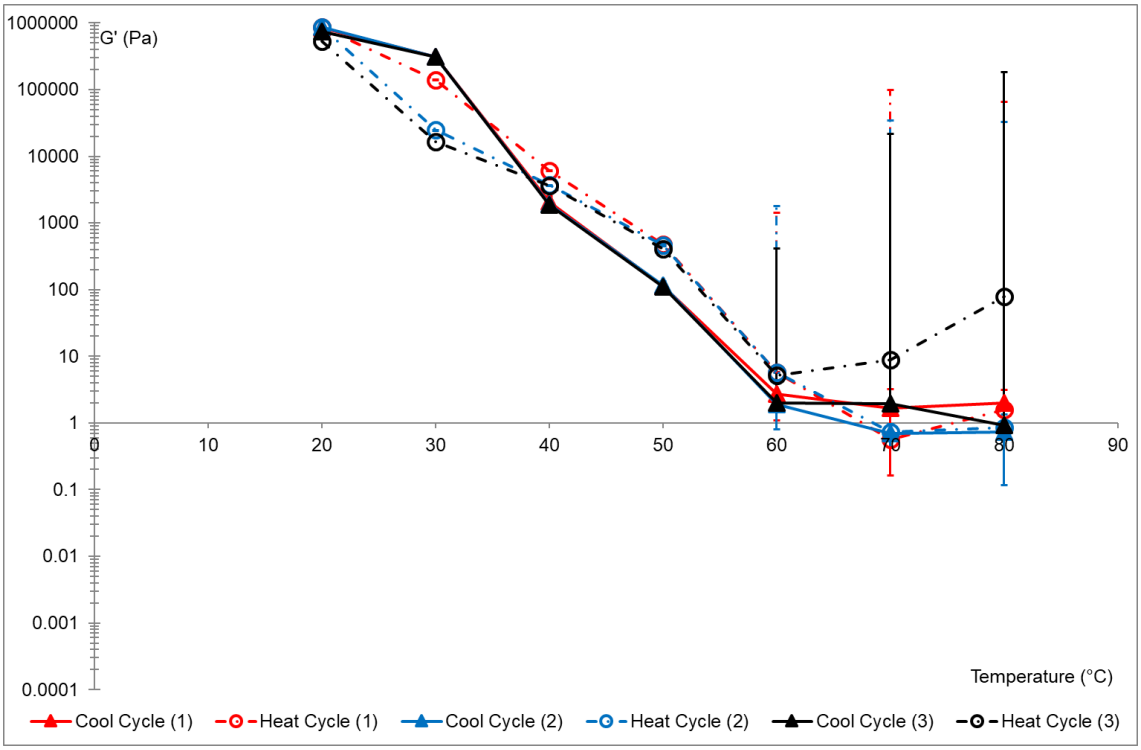

Figure 3.16 – G’ values for WSP5 at 5 Hz frequency with three temperature cycle completions.

Figure 3.16 shows G’ values when ramping temperature between 20 °C and 80 °C for WSP5. WSP5 shows a G’ value of ≈ 1000000 Pa at 20 °C and shifts to fully molten at 60 °C with a G’ of only ≈ 2 Pa. It can be seen at 30 °C there is a large difference in G’ values between the heating and cooling cycles, whilst at other temperatures, there is good agreement between the cooling and heating values of approximately 500000 Pa and 20000 Pa, respectively, except for heat cycle 1. It can also be seen that there is an increase in G’ for WSP on heat cycle 3, rising from ≈ 6 Pa at 60 °C to ≈ 10 Pa at 70 °C and finally ≈ 100 Pa at 80 °C.

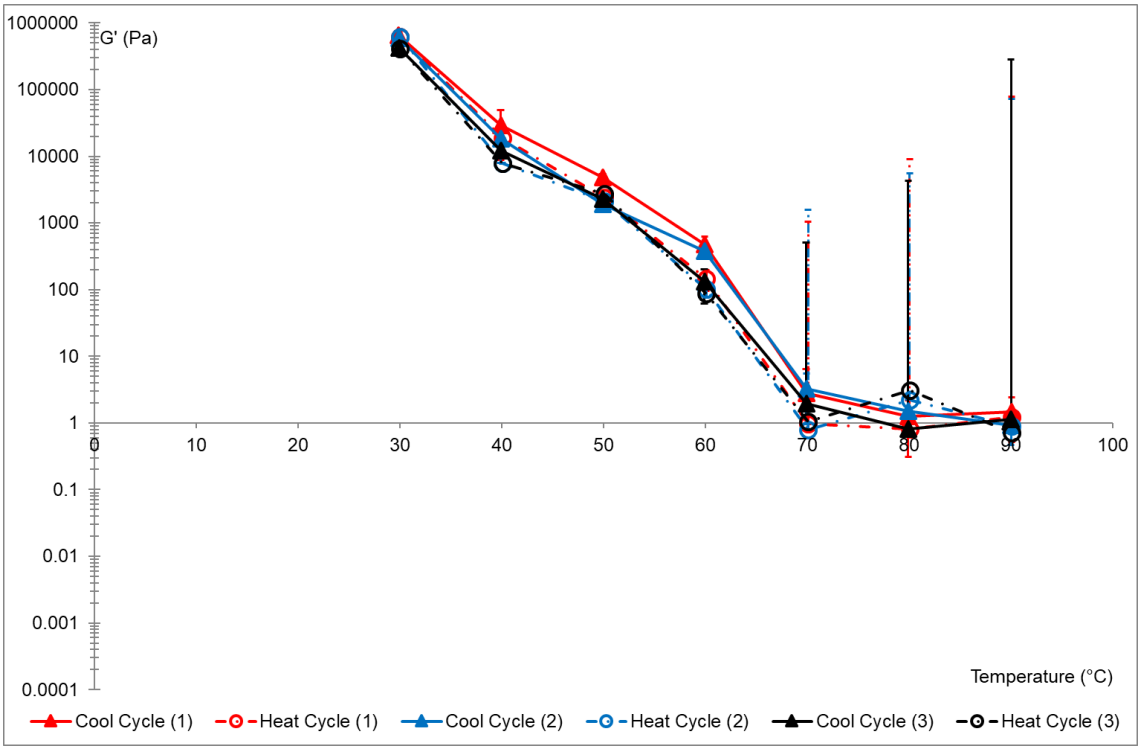

Figure 3.17 – G’ values for WSP6 at 5 Hz frequency with three temperature cycle completions.

Figure 3.17 shows G’ values when ramping temperature between 30 °C and 90 °C for WSP6. WSP6 has minor difference in heating and cooling cycles, the starting temperature of 30 °C shows a G’ of ≈ 800000 Pa and then fully molten at 70 °C with a G’ value of 1 Pa. (It was not possible to go below 30 °C due to the very high rigidity of the samples below this temperature).

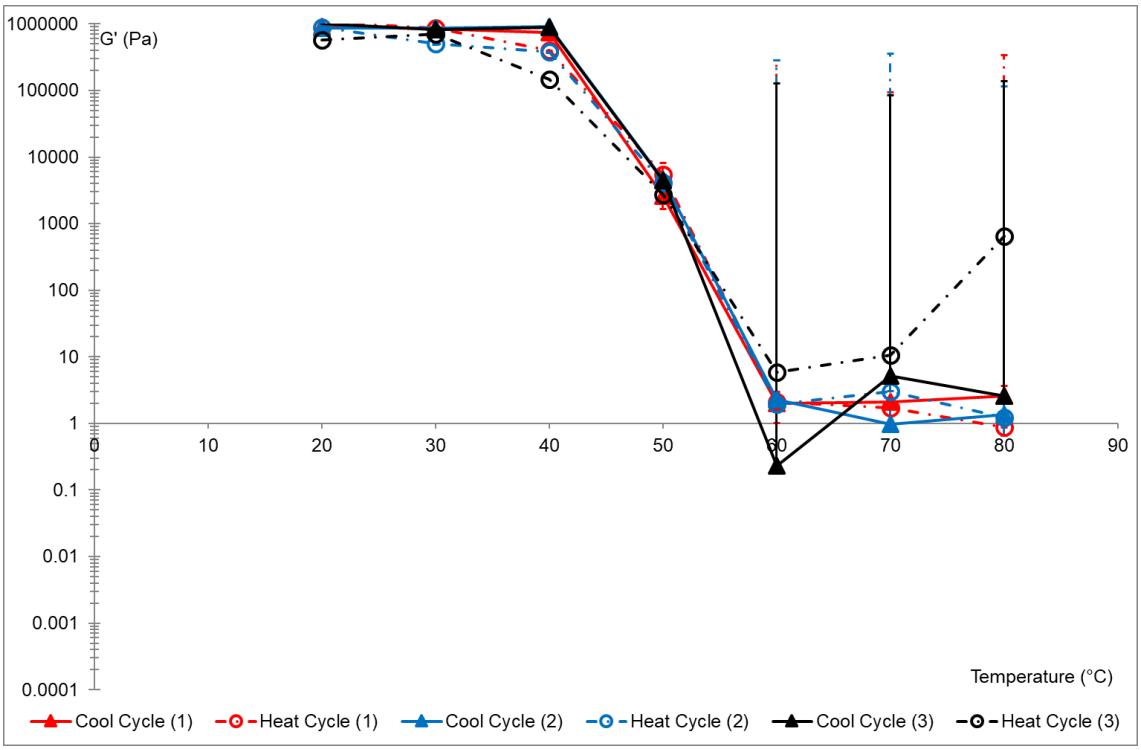

Figure 3.18 – G' values for WSP7 at 5 Hz frequency with three temperature cycle completions.

Figure 3.18 shows G' values when ramping temperature between 20 °C and 80 °C for WSP7. For WSP7 the sample is very stiff with a G' value of 1000000 Pa up to 40 °C where heating starts to decrease G' value to ≈ 200000 Pa. There is a dramatic drop in G' between 40 and 60 °C, where values reach ≈ 1 Pa. Heating/cooling cycle three shows some differences with G' increasing to 1000 Pa in the final stages of heating and then jumping back down between 0.1 Pa to 10 Pa on cooling.

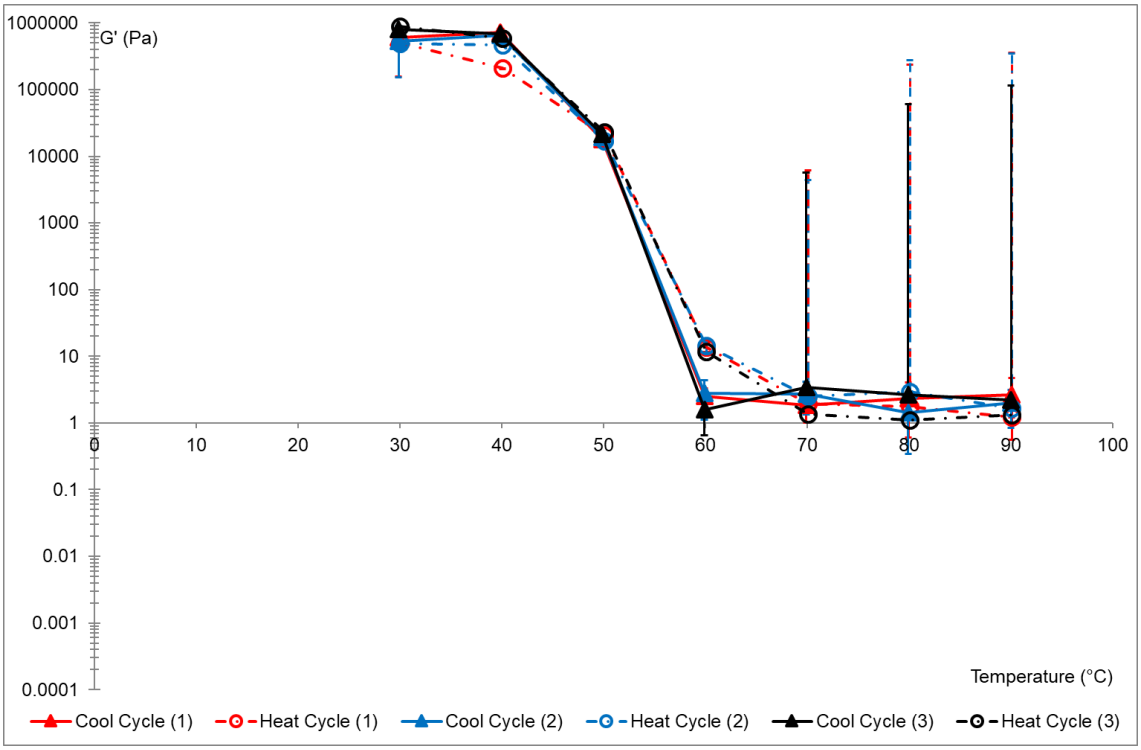

Figure 3.19 – G’ values for WSP8 at 5 Hz frequency with three temperature cycle completions.

Figure 3.19 shows G’ values when ramping temperature between 30 °C and 90 °C for WSP8. In general, there is good agreement between the values on heating and cooling for all 3 cycles. There is a steep drop in G’ between 40 and 60 °C, though not as steep as for some of the other samples.

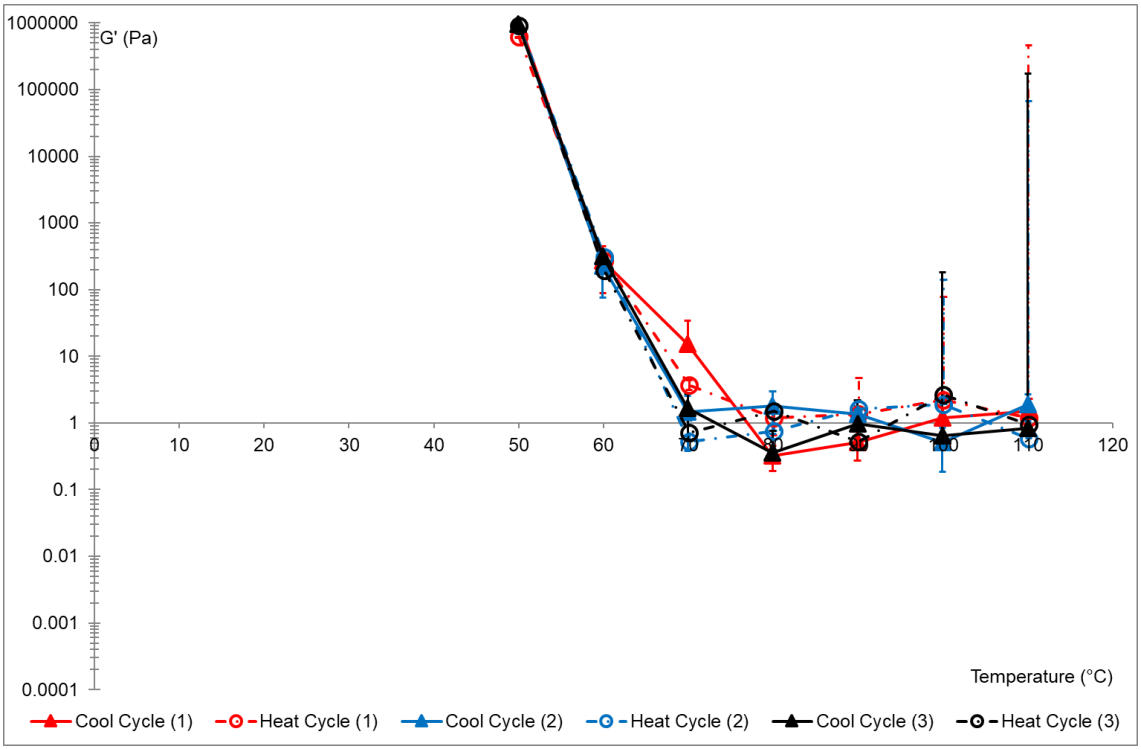

Figure 3.20 – G’ values for WSP9 at 5 Hz frequency with three temperature cycle completions.

Figure 3.20 shows G’ values when ramping temperature between 50 °C and 110 °C for WSP9. WSP9 is a very stiff sample, the first temperature able to record a G’ value was 50 °C where G’ was 1000000 Pa, dropping to 100 Pa at 60 °C and the sample apparently finally molten at 70 °C, with G’ values of ≈ 1 Pa to the end of recording.

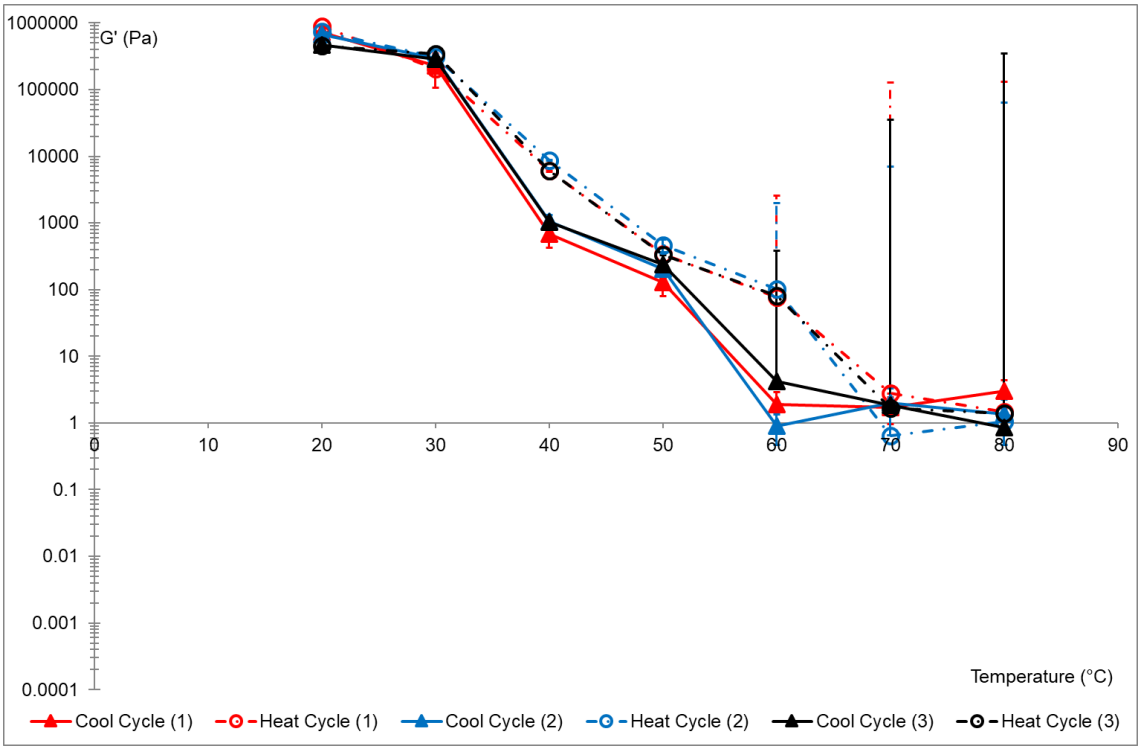

Figure 3.21 – G' values for WSP10 at 5 Hz frequency with three temperature cycle completions.

Figure 3.21 shows G' values when ramping temperature between 20 °C and 80 °C for WSP10. Between the two cycles, there is a good agreement but the heating and cooling cycles do differ at 40 °C and 60 °C. At 20 °C G' values are ≈ 1000000 Pa and remain high at 30 °C; at 40 °C heating cycles show G' values of ≈ 10000 Pa, while cooling cycles show G' values of ≈ 1000 Pa. 50 °C shows similarity in G' values but at 60 °C again there is a large difference. G' values for heating cycles are ≈ 100 Pa while for cooling cycles they are ≈ 2 Pa and the sample is apparently fully molten at 70 °C.

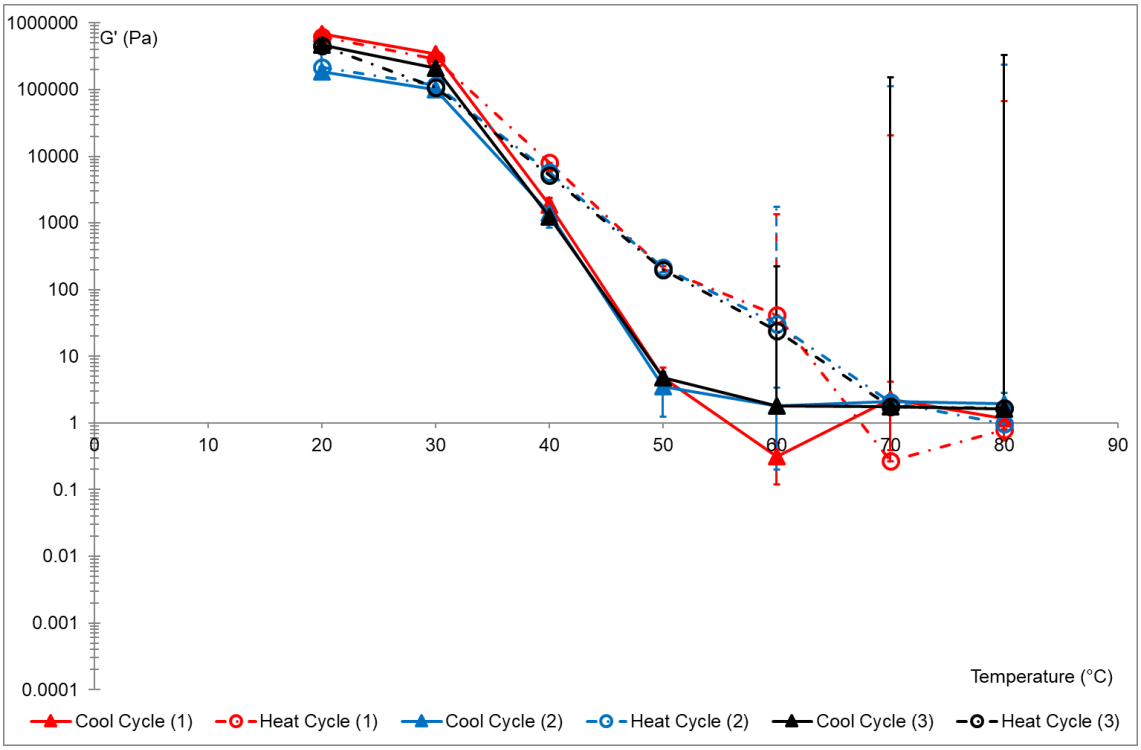

Figure 3.22 – G' values for WSP11 at 5 Hz frequency with three temperature cycle completions.

Figure 3.22 shows G' values when ramping temperature between 20 °C and 80 °C for WSP11. As stated in previous chapters WSP11 is the same sample as WSP10, but taken after undergoing temperature storage and cycling treatments that would be expected in a manufacturing process. We see that figure 3.21 and figure 3.22 are alike, but with a variation at 50 °C, for WSP11 G' at 50 °C is ≈ 5 Pa on the cooling cycle, while on the heating cycle G' remains ≈ 500 Pa. At 60 °C there is variation in heating and cooling cycles, with G' values of ≈ 50 Pa and ≈ 1 Pa respectively. At 70 °C and above the sample is fully molten.

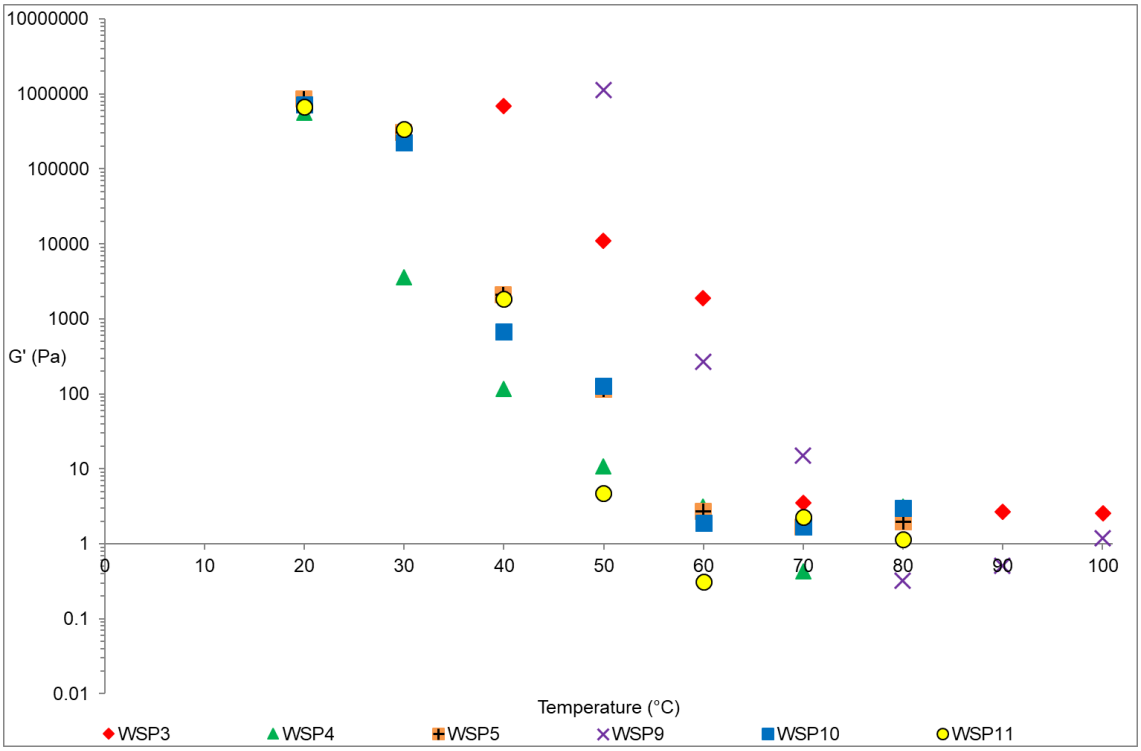

Figure 3.23 – G' values for WSP3, WSP4, WSP5, WSP9, WSP10 and WSP11 (0.04 % Shear Strain, 5 Hz Frequency,): G' vs. Temperature

To try and summarize all the different rheological behaviour of the samples as seen in figures 3.12 to 3.22, in figure 3.23 the maximum G' values at 5 Hz and 0.04% strain amplitude for WSP3, WSP4, WSP5, WSP9, WSP10 and WSP11 have been plotted. Both WSP3 and WSP9 have high G' values across the temperature range. WSP3 shows similar values to WSP4, WSP5, WSP10 and WSP11 at 70 °C with a G' value of ≈ 3 Pa while WSP9 still has a value of ≈ 20 Pa. At 80 °C all samples have become fully molten with G' value lower than 1 Pa but for samples WSP4, WSP5, WSP10 and WSP11 G' drops to ≈ 1 Pa at 60 °C. WSP4 has the lowest G' values of all samples at all temperatures when the samples are solid, however, at 50 °C and 60 °C, WSP11 shows a lower G' values. The sudden drop in G' values for WSP11 is experienced between 40 °C and 50 °C, unlike WSP10 which is the same sample as WSP11 (without going through a manufacturing temperature cycle). It is interesting that WSP5 shows a similar drop, whilst for WSP4 a sharp drop occurs between 30 °C and 40 °C, of ≈ 500000 Pa, like the values for WSP5, WSP10 and WSP11 between 40 °C and 50 °C.

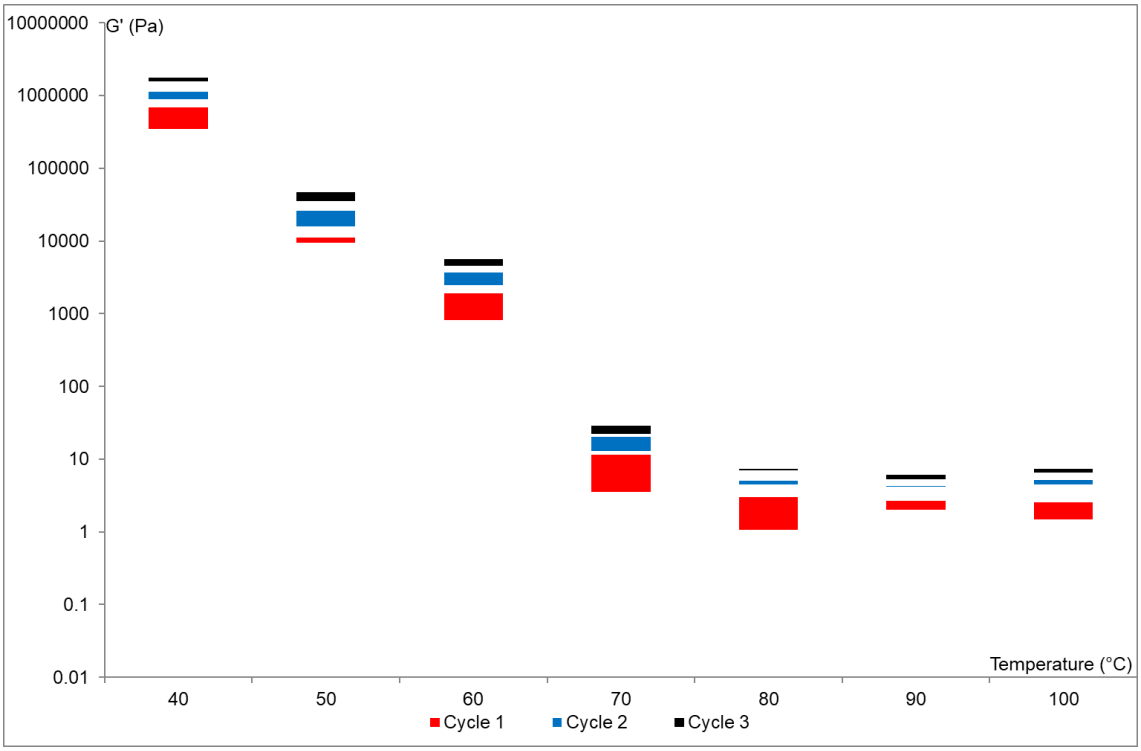

Figure 3.24 – Difference of G' in heating and cooling cycles for WSP3.

Figure 3.24 shows there is little hysteresis experienced by WSP3, the greatest difference in heating a cooling is experienced at 70 °C. Between the three cycles, the first cycle also contains the greatest hysteresis at each temperature point for WSP3.

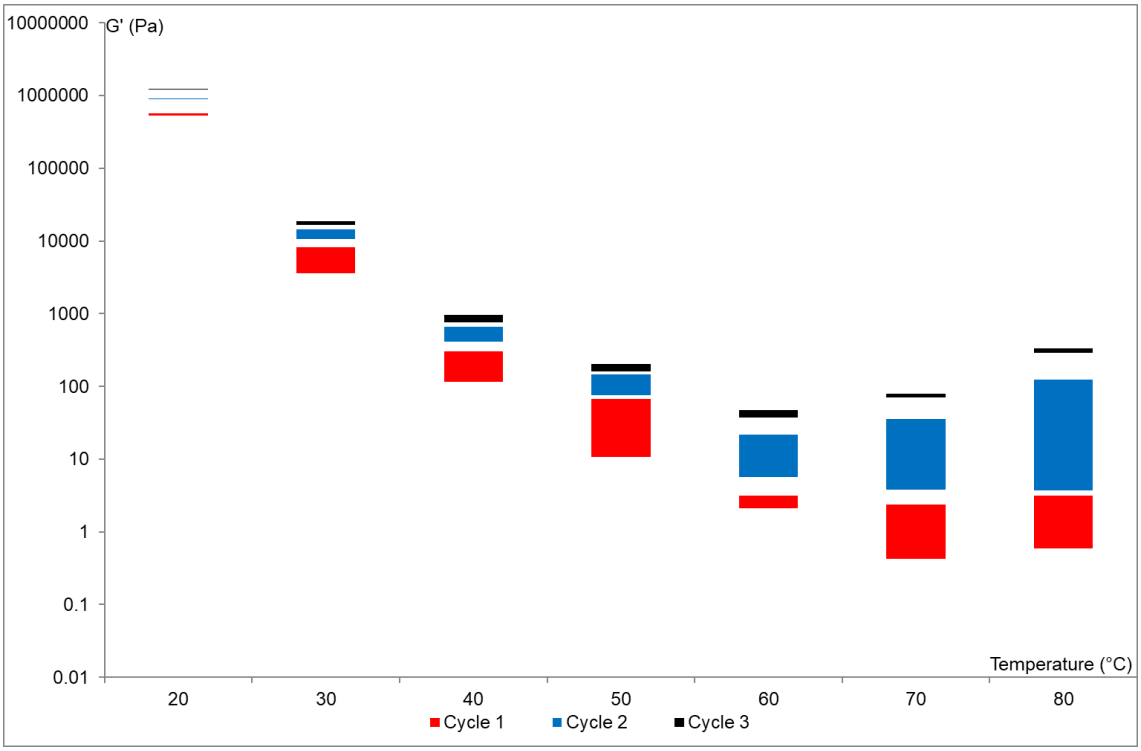

Figure 3.25 – Difference of G' in heating and cooling cycles for WSP4.

Figure 3.25 shows that WSP4 contains much hysteresis, in this samples the difference in heating a cooling is evident in cycle 1, with the greatest difference occurring at 50 °C. However, in cycle 2 there are greater differences of G' values, especially prevalent at higher temperatures.

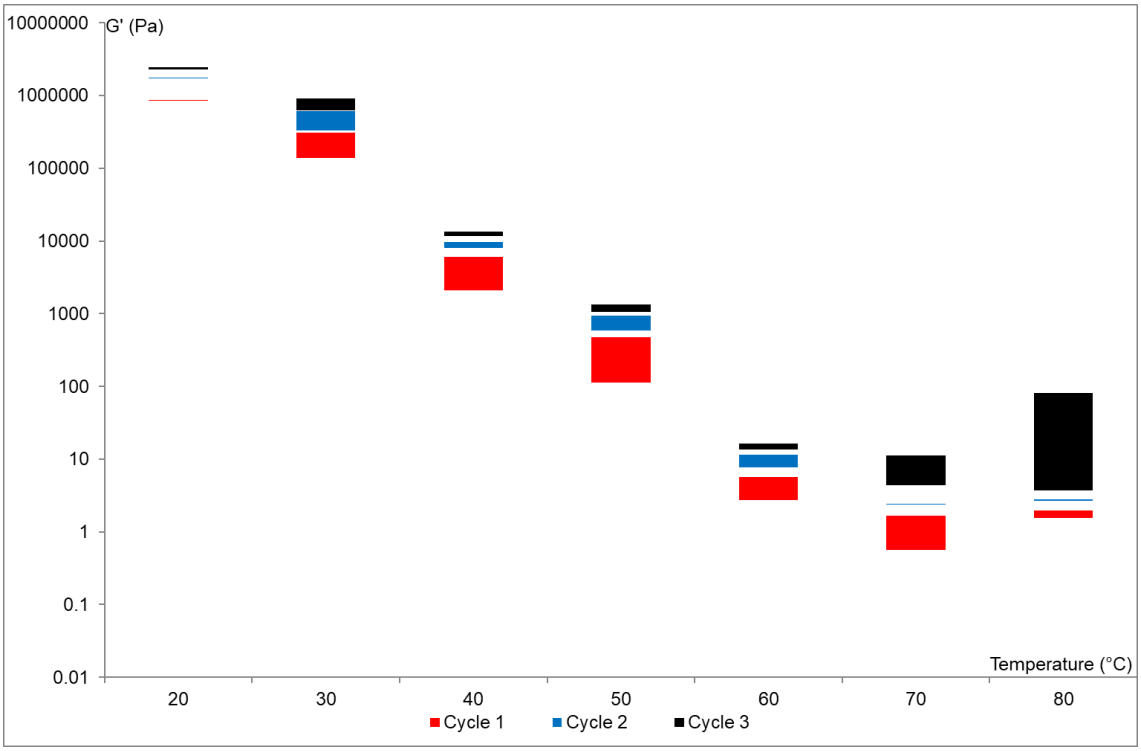

Figure 3.26 – Difference of G' in heating and cooling cycles for WSP5.

Figure 3.26 shows that WSP5 again has more hysteresis on the first cycle, with the great differences in G' values at 40 °C and 50 °C. At 80 °C, a large difference in G' values is obvious on the third temperature cycle.

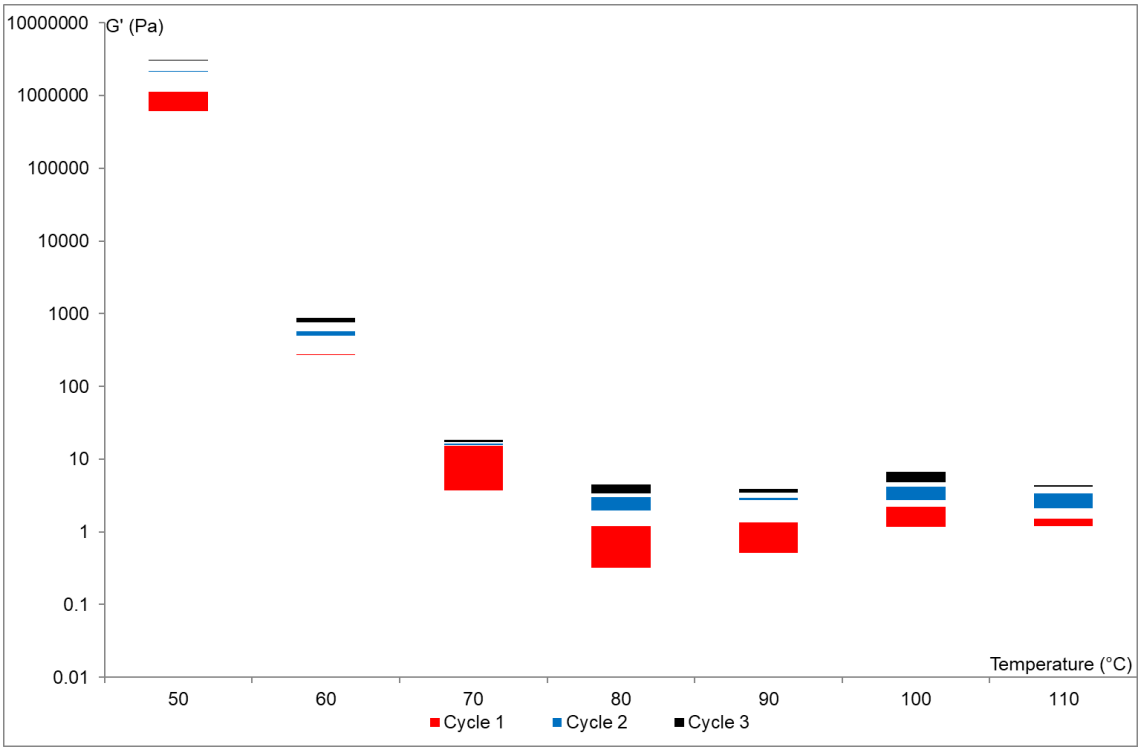

Figure 3.27 – Difference of G' in heating and cooling cycles for WSP9.

Figure 3.27 shows that WSP9 experiences little hysteresis, but still has some contained in the first temperature cycle, especially at 70 °C and 80 °C.

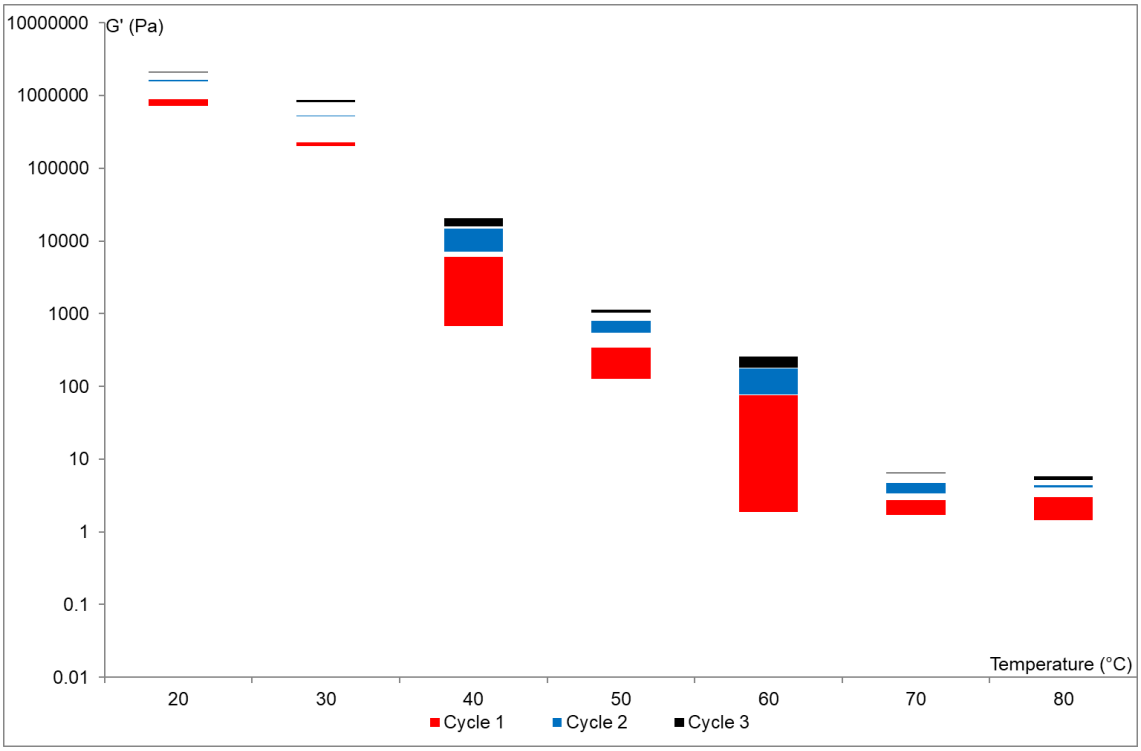

Figure 3.28 – Difference of G' in heating and cooling cycles for WSP10.

Figure 3.28 shows that WSP10 experiences great hysteresis in cycle 1, as does WSP11 in figure 3.29. For WSP10 there is greater hysteresis at 40 °C, however, for WSP11 there is greater hysteresis experienced at 50 °C, 60 °C and 70 °C. for cycles 2 and 3 the differences in G' values are alike.

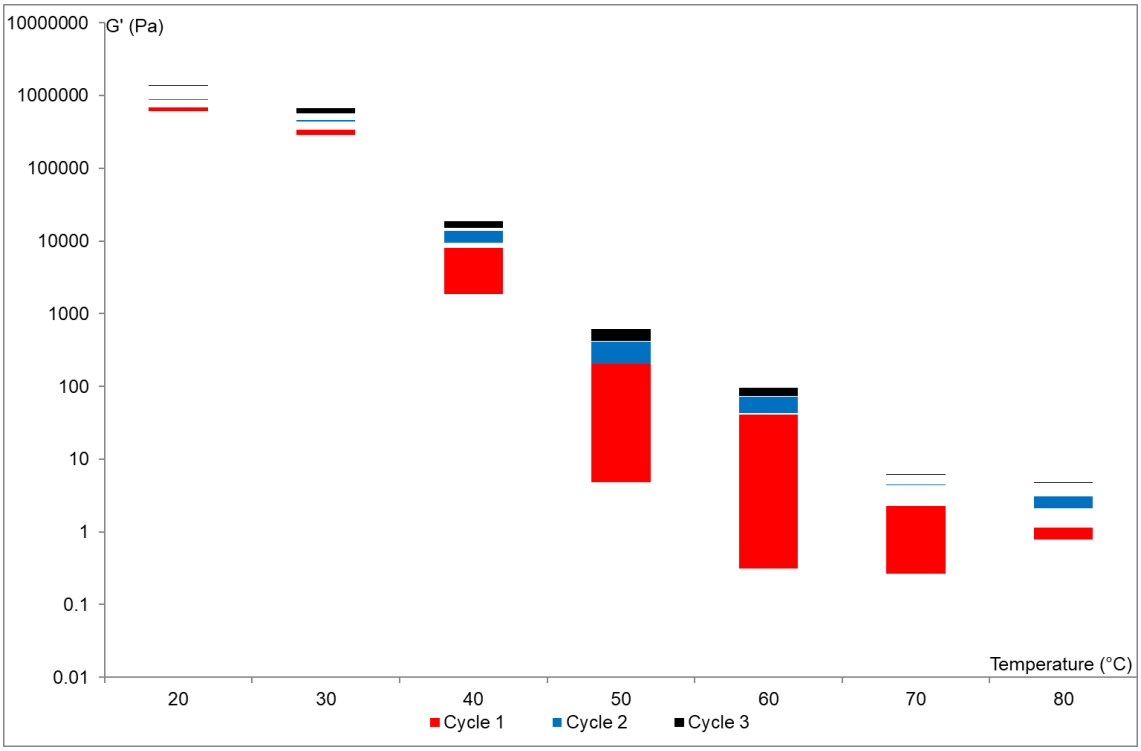

Figure 3.29 – Difference of G' in heating and cooling cycles for WSP11.

3.2.4 Discussion

3.2.4.1 Viscosity Measurements

In chapter 3 the physical characteristics of white soft paraffin and their constituent components have been studied. Figure 3.9 shows the results of measuring the viscosity of the oil components used for making WSP blends, the two oil grades supplied were tested at 20 °C, 40 °C and 100 °C and these results were plotted against supplied MSDS information from the supplier, Kerax Ltd., which were assumed to be measured at 1 s^{-1}.

It can be seen in figure 3.9 that measured values for LO and HO at 40 °C do not correspond to the MSDS information. At 1 s^{-1} the measured LO at 40 °C is 0.015 Pa s, while the MSDS states that the viscosity is 0.13 Pa s, almost a difference of 0.1 Pa s. The difference for the HO at 40 °C is ≈ 0.6 Pa s. This suggests that the testing method/conditions were most likely different.

As expected HO is shown to have the highest viscosity values, with larger viscosities at lower temperatures. HO at 20 °C and 40 °C show constant and Newtonian behaviour, with a slightly increased viscosity at 0.1 s^{-1}. As the temperature is increased to 100 °C there is a large drop in viscosity, to around 0.01 Pa s. Below 1 s^{-1} the data is noisy, no doubt due to instrument sensitivity and temperature control limitations at low shear rate values.

LO follows a similar trend to HO, with a small decrease in viscosity from 20 °C to 40 °C, then a large decrease in viscosity at 100 °C. At 20 °C, the data is very stable, with a slightly higher viscosity value recorded at 0.1 s^{-1}. As the temperature increases and viscosity decreases, more data noise is for HO, except that for LO at 100 °C this noise extends to higher shear rate values, e.g., 5 s^{-1}. Another reason for data noise in this range may be a slip between the cone and plate at these low viscosities for such 'lubricating' materials.

In figure 3.9 a value for water viscosity has been given as a reference, for LO, especially, and partially HO at 100 °C the viscosities are like water. As such this could explain why values are noisy at low shear rates for the oils. At such low viscosity values, the use of a cone and plate rheometer is not ideal as the liquid being tested could be forced out of the testing area when interfacial energies are too low to keep the liquid on the flat plate geometry. It would be of greater use to use a capillary viscometer, that could be used with the known values of density of the oil and pressure implemented for the use of the viscometer.

Figure 3.11 shows the viscosities recorded for constituent component waxes obtained from Kerax Ltd. All tests for the paraffin wax (PW) and microcrystalline wax (MW) were carried out at 100 °C due to the solid nature of the waxes at lower temperatures of 40 °C or 20 °C.

Figure 3.11 shows that there is a reduction in viscosity for all samples as the shear rate increases. In general, PW has lower viscosities than MW, and MWH has the highest viscosity of all samples. Table 3.1 shows the differences between low shear and high shear.

MWH has a continuous decrease in viscosity as shear rate increases, whilst all other samples experience a large drop in viscosity between 0.01 s^{-1} and 1 s^{-1} after which the viscosity remains relatively stable. The high congeal point of the MWH suggests a greater crystal content and probably explains the continuous shear thinning nature of this sample across the wide range of shear rates, even at this high temperature, whereas as the other samples probably have very limited amounts of solid (wax) structuring agents. Any weak network present in the other samples is thus more easily completely broken down at low shear rates.

It is likely that the first measured values (at the lowest shear rate) for PWM and PWH are not accurate, due to the noise in the data. It might be expected that the viscosities would decrease in the order as PWH > PWM > PWL but as can be seen, the trend is the opposite.

Figure 3.11 shows the viscosities of commercial pharmaceutical grade samples WSP10 and WSP11. As expected the viscosities at 80 °C are slightly higher than at 100 °C, even though all the recorded plots start very low at ≈ 0.3 Pa s. At 80 °C the samples plateau at 0.01 Pa s, while at 100 °C they plateau at 0.006 Pa s. As might be expected, being the same sample, the curves are very alike, with almost the same values of data. Higher temperatures for both samples give lower measured viscosities, no doubt due to more residual solid crystalline elements being melted. Below 1 s^{-1} there is a lot of noise for the sample WSP11 at both 80 °C and 100 °C. Again, such large drops may be indicative of slip occurring.

3.2.4.2 Oscillatory Measurements

Figures 3.12 – 3.20 show oscillation plots or WSP blends 1-9; figures 3.21 and 3.22 show commercial pharmaceutical grade samples WSP10 and WSP11 respectively. There are differences in most of the samples, with various maximum melting temperatures, melting force gradients, solid material components and hysteresis in samples, seen in figures 3.24 – 3.29.

Figures 3.15, 3.16 and 3.17 (WSP4, WSP5 and WSP6) are all samples that contain PWL and the results indicate that these samples are ‘softer’, since the gradient of the G’ versus temperature curves are gradual and do not shift dramatically like other samples, such as WSP9 (figure 3.20), which contains PWH and MWH. Considering model blends WSP1, WSP2 and WSP3 containing PWM (see figures 3.12, 3.13 and 3.14, respectively), the gradient is higher, i.e., the phase change (solid to liquid) occurs over a more narrow and specific temperature range. In the same vein, considering model blends WSP7, WSP8 and WSP9 containing PWH (see figures 3.18, 3.19 and 3.20, respectively) the gradient of change in G’ with temperature is even steeper. In these samples at no temperature below 40 °C is the sample liquid or semi-solid, and it became increasingly difficult to measure G’ due to high sample stiffness.

In summary, the PW component seemed to have a large controlling effect on the temperature range of transition between a stiff sold and liquid molten sample.

As stated previously MW also influences the overall stiffness and melting range of the WSP blends. Figures 3.12, 3.15 and 3.18 (WSP1, WSP4, WSP7) show samples that contain MWL. Figures 3.13, 3.16 and 3.19 (WSP2, WSP5, WSP8) show samples that contain MWM. Figures 3.14, 3.17 and 3.20 (WSP3, WSP6, WSP9) show WSP blends that contain MWH. There is a definite trend for MW to increase G' more at the higher temperature end of the tests compared to PW. WSP7 shown in figure 3.18 contains MWL and PWH and indicates that there is a rapid change in rheology from high to low G' values within 20 °C between 40 °C and 60 °C. Figures 3.14 and 3.20 show WSP3 and WSP9, and contain MWH along with PWM and PWH, respectively. Both WSP3 and WSP9 have high G' values as well as higher melting temperatures. Figure 3.17 (WSP6) contains MWH and PWL, in this plot the G' values have slightly decreased over the whole temperature range, however, the melting points have increased to a range between 30 °C and 90 °C. WSP6 implies that a combination of high congeal point and low congeal point of alternative waxes has a cancelling out effect on the WSP blend, imparting characteristics of both singular waxes within the blend. This makes sense in terms of the accepted chemical differences between PW and MW, the latter thought of as consisting of higher molecular weight and higher melting point components. The high melting components might, therefore, be expected to persist as solid crystals at the higher temperatures and maintain a network with some residual elasticity. Although it was not possible to know if there is a presence of crystalline network within the WSP, as the currently used testing methods (seen following) were not carried out. Possible methods of testing wax crystalline material, to be able to measure the concentration of wax present within the WSP have been shown by previous authors, and have shown that it is possible to change concentration of wax present within oil mixtures, as such, the wax appearance temperature (WAT) was measured giving standard curves of temperatures vs wax concentration (Ijeomah et al., 2008)(Jiang et al., 2001)(Kok et al., 1996)(Neto and Neto, 2009). Following the known quantity of wax with WSP blends 1-9 it could also be possible to measure the wax concentration against measured G' values if a WAT had been completed within

this body of work. Although theoretically, this could be possible, it would be a very difficult multi-step process to be able to identify the wax presence and wax types present, in order to detail the quality and structure of the crystalline network.

It can also be observed that in some WSP blends there are synergistic effects on G'. For example, WSP5 (see figure 3.16) includes MWM, a wax that might be expected to induce a very stiff WSP blend with a high melting point range. However, there is also PWL present in this sample, and this apparently helps to reduce the melting temperature whilst an extended viscoelastic region occurs (on heating) between 30 °C to 60 °C. This behaviour on heating would be desirable in terms of consumer application to the skin (from a cooler spot of sample) and aid incorporation of active pharmaceutical ingredients during mixing and manufacture, whilst a lower temperature generally gives improved shelf life, appearance, acceptability and uniformity of product efficacy. The interactions between the different wax components will be discussed later, but clearly, it may be related to the mutual solubility (or not) of the different WSP components in each other, which is expected to be complicated.

Clearly, some data is lacking on the actual stiffness of the samples at room temperature (below 30 °C say) due to limitations on the instrument and some samples containing MWM and MWH maybe unacceptably stiff at these temperatures.

Figure 3.21 shows WSP10 and figure 3.22 shows WSP11, these two plots show the results for commercial pharmaceutical grade samples, these samples contain constituent components that are unknown but when comparing with WSP blends made in laboratory WSP10 and WSP11 are like WSP5. When on heating cycles there is greater stiffness in the WSP10 and WSP11 especially at 60 °C, however, WSP10 and WSP5 when considering cooling, cycles are very alike.

In figures 3.15, 3.16 and 3.18 (WSP4, WSP5 and WSP7) there is the presence of erroneous values in G' at temperatures ≥ 60 °C, especially after a third temperature cycle. This increased error seen in the figures is not seen in first and second temperature cycles, indicating that after extended testing there is a change to the WSP under testing. Due to the small sample size in use

through one test cycle (≈ 2 ml), it is possible that evaporation has become an issue. As these samples are particularly ‘soft’ samples with lower congeal point waxes present within the WSP blend ratio, the evaporation of the molten WSP phase at high temperatures is an added factor. Another possible cause of these high error value is, as the testing cycle is increased the molten WSP contained on the testing plate of the rheometer could be expelled from the testing plate area due to the relatively high shear oscillation implemented in the testing protocol. At these higher temperatures, the WSP is mostly molten and liquid-like, as such, the testing method using a plate-plate rheometer may not be the most suitable in this exact, liquid, state. With the WSP being in a liquid state the rheometer records large values of ‘noise’ within the sample due to the testing geometry’s inability to gain sufficient friction on the WSP surfaces.

Figure 3.23 shows the maximum G’ values at 5 Hz of frequency and 0.04% strain when running oscillation rheology tests for the WSP blends, blends chosen based on extremes of sample data recorded, such as for WSP3 and WSP9, the two stiffest samples, and WSP4 and WSP5 as the two softest samples. WSP10 and WSP11 were the commercial pharmaceutical grade samples used to compare laboratory made samples for future possible consumer quality assurance. In figure 3.23 WSP4 is shown to be the softest and reaches G’ ≈ 1000 Pa at 30 °C whereas WSP5, WSP10 and WSP11 reach this region at 40 °C and WSP3 and WSP9 reach this region at 60 °C. At 50 °C, there is a drop of G’ for WSP11 compared to WSP10 and WSP5 that could indicate some hysteresis in the commercial pharmaceutical grade sample due to temperature cycling it may have experienced in the manufacturing process, plus the additional temperature cycling within the experiment. It is possible that WSP10 may contain a similar (unknown) mixture of an MWM and a PWL wax as to WSP5, although manufacturers (e.g., Fuchs) often maintain that commercial products are blends of several different MWs and PWs, rather than just one of each.

Figures 3.24 to 3.29 show difference in G’ values between the three cycles completed for each tested WSP. All the WSP blends shown, show that in the first temperature cycle the blends contain hysteresis, as the differences are greater on average than other cycles. There are exceptions to the differences, seen in figures 3.25 (WSP4) and at higher temperatures in figure 3.26 (WSP5). In figure 3.25 there is evidence of greater G’ difference above 60 °C on the second

temperature cycle, this is possibly still some remaining hysteresis within the blend, however it is more likely, due to the softness of the blend, the G' values recorded show greater variation when the WSP blend is in a molten state. This molten factor creating variability in G' value data is also seen within WSP5 seen in figure 3.26 in cycle 3, where it would be expected that any hysteresis would now have been removed from the WSP blend.

Figure 3.24 and 3.27 show WSP3 and WSP9 respectively, both blends show little hysteresis apart for the first temperature cycle, this is to be expected of the first cycle as the processing method used to make this blend did not contain a homogenisation stage, enough mixing was done to ensure turbidity was not visible but there was not time dependent high shear mixing to ensure homogenisation.

Figure 3.28 and 3.29 show plots for WSP10 and WSP11, both plots are similar, with a slight difference in the first temperature cycle at 50 °C, that being there is greater G' difference for WSP11. At 60 °C and 70 °C there is also greater difference in G' value for WSP11 in figure 3.29, indicating the repeat temperature cycling can induce crystal memory in a WSP blend when the sample is stored for prolonged periods, as is the case with WSP11, a commercial blend that has been through a manufacturing temperature profile.

3.2.5 Conclusions

3.2.5.1 Viscosity Measurements

- As temperature increases, the viscosity of samples decreases.
- After 1 s^{-1} (shear rate) most samples reach a plateau in viscosity that does not change as the shear rate is increased, indicating that there is no further solid structure to break down.
- Some samples, notably MWH, show viscosity decrease with increased shear rate up to high temperatures and therefore probably still contain solid crystal material that heavily influences the viscosity.

3.2.5.2 Oscillatory Measurements

- Paraffin wax (PW) influences the viscoelastic region of the model WSP blends as a function of temperature: the higher the melting point of the PW,

the narrower the temperature transition from solid- to liquid-like viscoelastic behaviour.

- Microcrystalline wax (MW) has a greater effect on the structure and overall stiffness of the model blends, particularly in the higher temperature regions.
- The three temperature cycle oscillatory tests developed is probably a better indicator of WSP performance during manufacture and usage than simple congeal point and penetrometer data.
- Hysteresis is prevalent in most WSP blends on temperature cycles directly after blends have been stored.
    - Hysteresis is seen in 1st temperature cycles.
- Softer WSP blends show greater potential for hysteresis after sample storage and repeat temperature cycling.

Chapter 4 Differential Scanning Calorimetry Characterisation

4.1 Introduction

Differential scanning calorimetry is a method of thermal analysis with the ability to link energy requirements changes in a materials thermal properties including change of temperature and phases. This technique is well suited to materials incorporating divergent phases and has found application in industries such as food (chocolate, margarine, etc.) or the pharmaceutical sector (white soft paraffin (WSP)). These phase changes, indicate crystal melting, crystallisation temperature points of WSP and will also show the total energy of the WSP system to effect a complete change in phase.

Following previous work (Matthäi et al., 2001), using DSC to test WSP characteristics is often implemented and is used to correlate with other testing methods such as rheology and chemical analysis techniques, some of these techniques can be seen in chapter 3, and chapter 5.

Preliminary testing was carried out with WSP samples and from these previous conclusions, a testing method was developed and used for all further tests. Sampling is problematic with viscous substances such as waxes

(Gallagher et al., 1998), including WSP and as such, the use of large sample pans (40 µl) and a heating rate of 5 °C per minute was used to simulate the best temperature change used in manufacture. The method adopted for use also included a 6-step cycling method allowing for removal of hysteresis in the sample and taking one recording of endo- and exothermic reactions in the WSP.

Chapter 3, details of the differences between samples the WSP1-9 were clear to see. From this work, WSP5 is selected as having similar rheological properties as compared to plant grade material (WSP10). There is a vast difference between samples when considering the rheology of the WSP blend and the constituent components. It was proposed to use DSC to help characterise the constituent components and the corresponding WSP blends made of those components, it is theorised that the combination of the constituent components could be used to determine the thermal characteristics of the WSP blends.

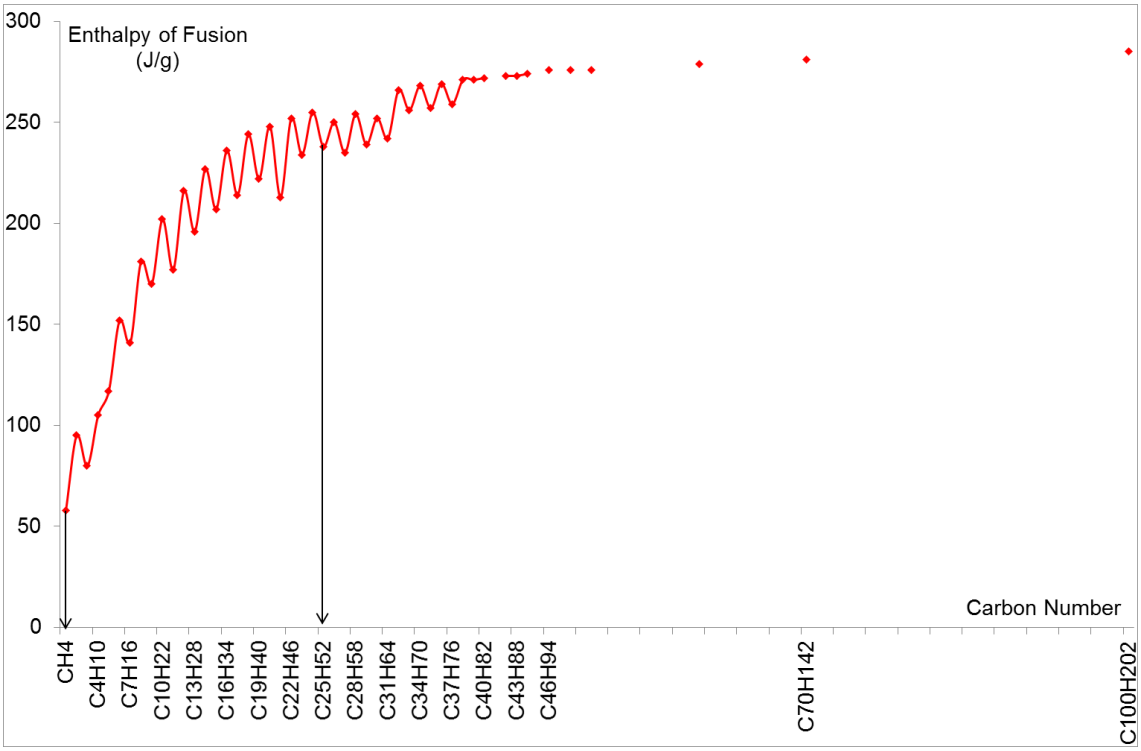

Figure 4.1 – Graph showing the enthalpy of fusion for hydrocarbon standards (HIMRAN et al., 1994).

Figure 4.1 gives the enthalpy of fusion required for increasing carbon length hydrocarbons, the chart starts with methane (CH_4), ending with hectane ($C_{100}H_{202}$). Pentacosane ($C_{25}H_{52}$) represents the average hydrocarbon and carbon length suitable to indicate ‘paraffin wax’. Figure 4.1 shows that the enthalpy energy has a generally increasing trend, however, there is an oscillation

of energy, increasing, and decreasing through each addition of carbon to the hydrocarbon length. The increasing energy points represent even carbon numbers, while energy points that show a slight decrease in energy transition represent odd carbon length numbers. This fluctuation in enthalpy is due to the steric effect within the hydrocarbon chain. As these are alkanes they contain no double bonds and groups can rotate about the carbon backbone. It is also possible that isomers of hydrocarbons can occur, this can cause the steric effect, as a repulsion force between isomeric groups contained on the hydrocarbon chain that line up along the hydrocarbon backbone.

With the use of DSC, it may be possible to calculate the enthalpy of wax materials and corresponding WSP blends since the constituent components of WSP5 are available it is possible to assess the unformulated parts and the formulated WSP5. A key question is to relate the behaviour of the individual elements to the final blend of WSP.

4.2 Materials and Method

Differential scanning calorimetry was carried out using an ‘Excellence DSC1 Differential Scanning Calorimeter’ with HSS8 Sensor for Ultra Low Noise and Ultra High Sensitivity (Mettler Toledo), with a robotic arm autosampler. The DSC1 uses a power compensating method of analysis using a sample and reference thermograph to provide accurate results. Sample pans had a 40 µl capacity. A Mettler Toledo crucible sealing press was used to seal the sample pans. Results were analysed using the STARe evaluation software (Mettler Toledo).

Samples of paraffin wax, microcrystalline wax were provided by Kerax Limited, Cowling Road, Chorley, Lancashire, PR6 9DR. Kerawax 2245 is a paraffin wax of a congeal point average of 42 °C, Kerawax 482 is a paraffin wax with an average congeal point of 53 °C, Kerawax 1301 is a paraffin wax with an average congeal point of 65 °C, Techniwax P9805 is a microcrystalline wax with an average congeal point of 70 °C, Techniwax P9820 is a microcrystalline wax with an average congeal point of 77 °C and Techniwax P9830 is a microcrystalline wax with an average congeal point of 85 °C. These waxes were then used to produce WSP blends, WSP(1-9) (see Chapter 2), also to be tested

by DSC was WSP10 and WSP11, commercial pharmaceutical grade plant grade WSP blends.

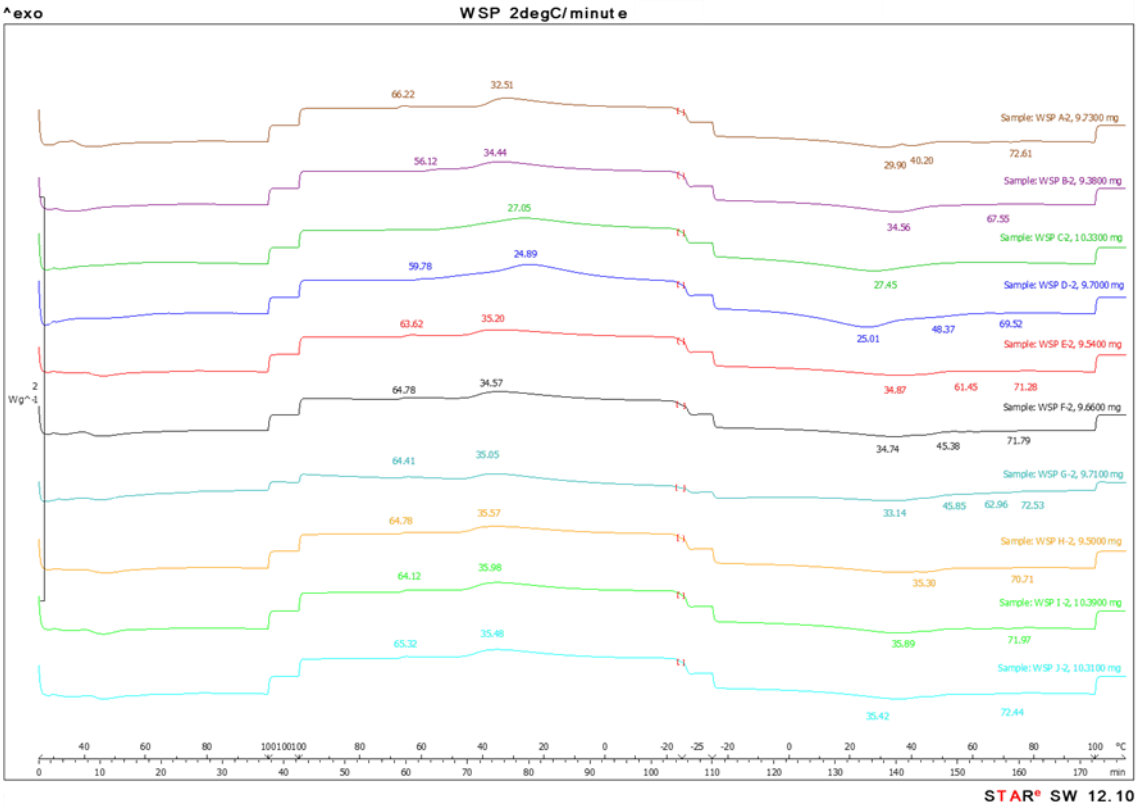

Figure 4.2 – Plot of commercial pharmaceutical grade plant grade WSP tested at 2 °C min^{-1}.

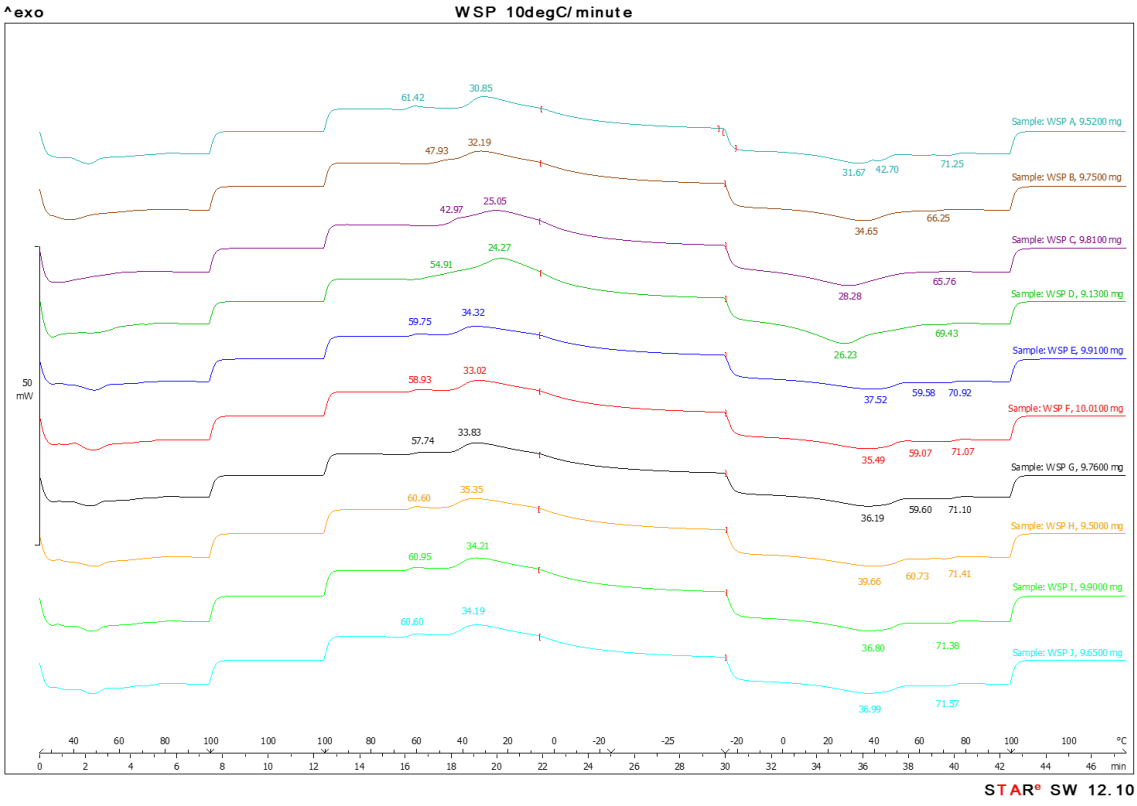

Figure 4.3 – Plot of commercial pharmaceutical grade plant grade WSP tested at 10 °C min^{-1}.

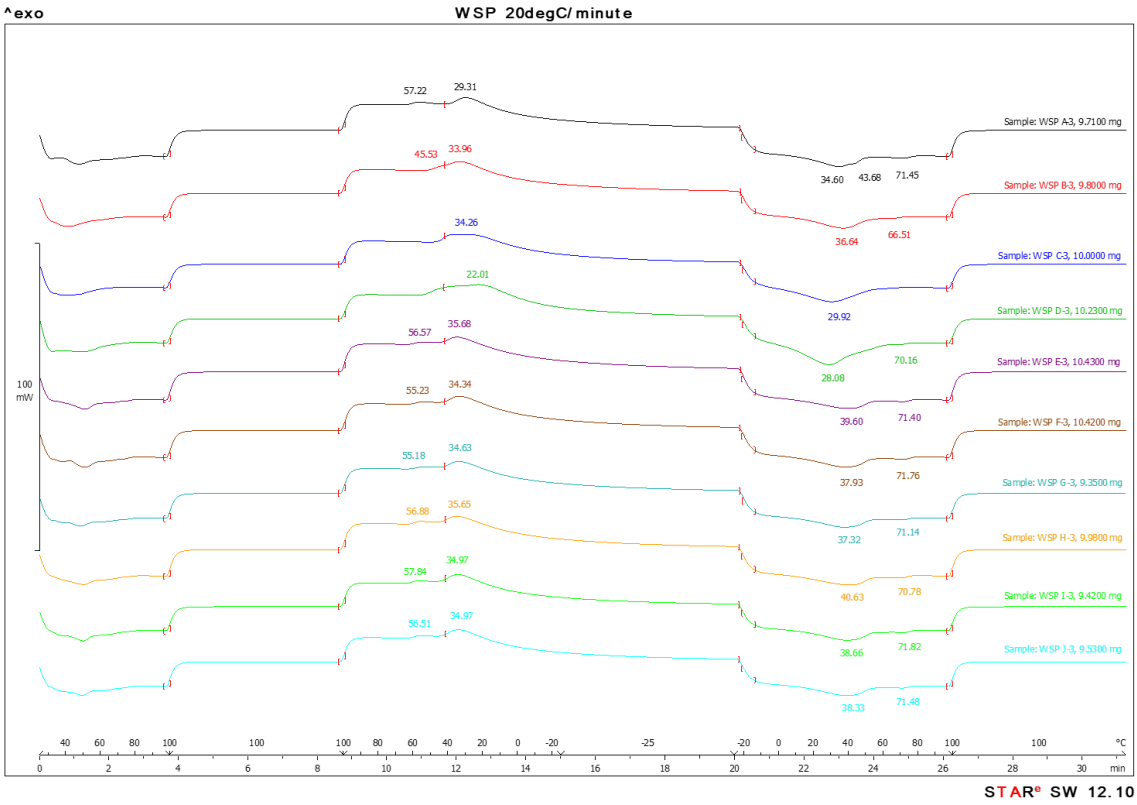

Figure 4.4 – Plot of commercial pharmaceutical grade plant grade WSP tested at 20 °C min^{-1}.

Through preliminary testing, seen in figures 4.2, 4.3 and 4.4, where higher temperature rates caused peak merging and loss of information, and lower temperature rates did not impart enough energy to observe suitable peaks heights for important phase changes in materials. The following protocol was therefore adopted using 5 °C min^{-1} based on criteria speed of analysis and repeatability of results:

1. Increase the temperature from 25 °C to 100 °C at a rate of 5 °C per minute.
2. Hold the temperature at 100 °C for 5 minutes.
3. Decrease the temperature from 100 °C to -25 °C at a rate of 5 °C per minute.
4. Hold the temperature at -25 °C for 5 minutes.
5. Increase the temperature from -25 °C to 100 °C at a rate of 5 °C per minute.
6. Hold the temperature at 100 °C for 5 minutes.

This protocol allowed distinct peak observation, as well as closely mimicking the approximate temperature changes experienced in manufacturing

of WSP materials within a pharmaceutical production process. Both WSPs and the paraffin and microcrystalline wax components of WSP(1-9). It was not possible to test oils samples due to sealing within the pans however significant phase changes were not expected for the oils over the temperature ranges investigated, where they appeared as clear liquids throughout. The reference pan used was with air, both pans were crimp sealed to ensure that the soft WSP samples were not extruded, pans were also without a pinhole to allow for a fully sealed environment.

It was decided that the use of industry standard protocol was best for the use of DSC, this means the temperature was reduced to -25 °C. Protocol for chapters generally keeps low range temperatures to 20 °C. as such it should be noted that as the temperature is reduced to supercritical temperatures there is high chance that there is greater crystal presence within the WSP blend being tested. Also, any liquid paraffin oil present will remain trapped within the crystal lattice and movement of the crystals due to oil presence will be at a minimum as the crystals are too rigid. This process is carried out within the industry to ensure that all hysteresis is removed from a sample upon testing, as previously stated the supercritical temperatures will ensure crystal growth in the entirety of the sample, instead of the growth from crystal within the wax melt at higher temperatures.

4.3 Results & Discussion

4.3.1 DSC of Paraffin Wax Components

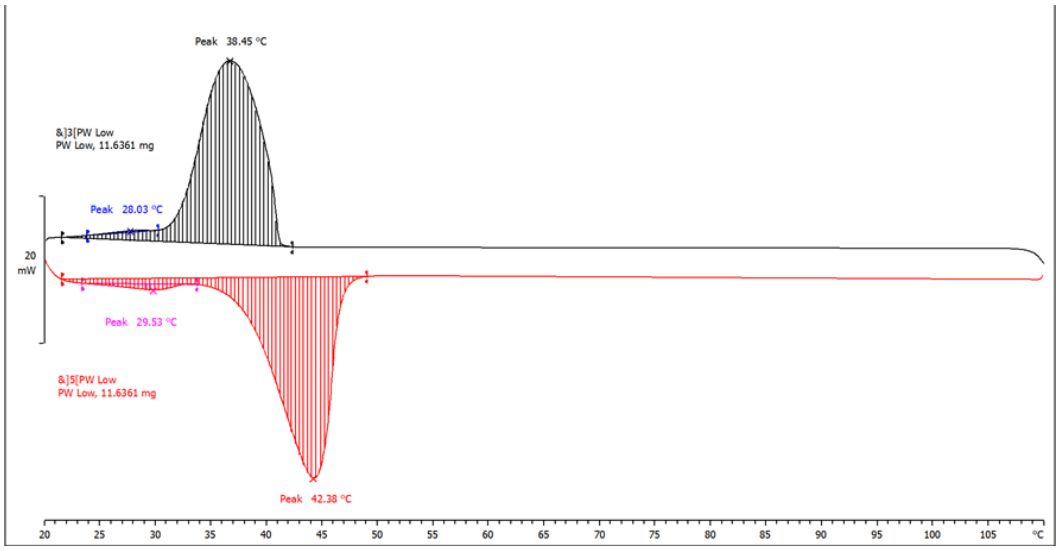

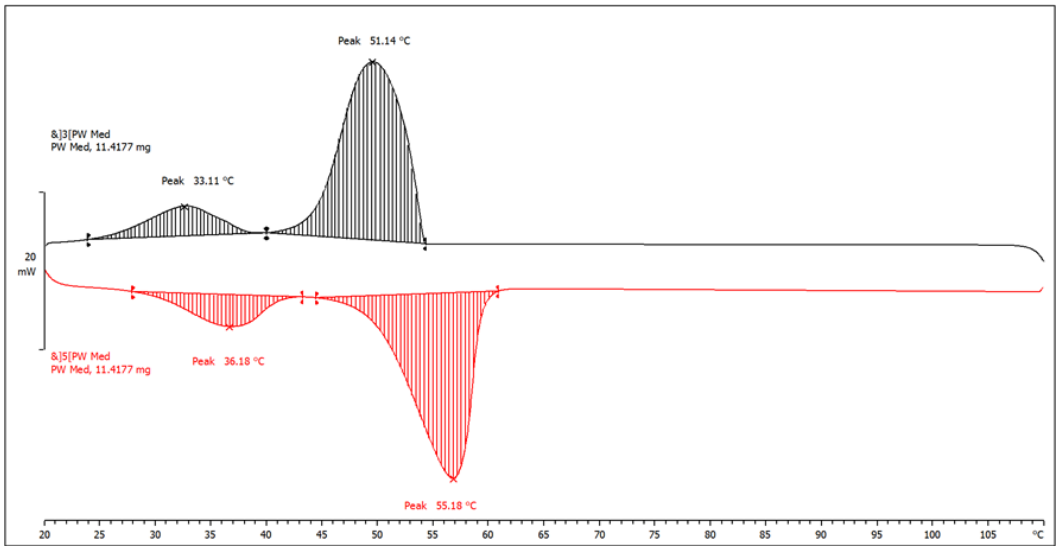

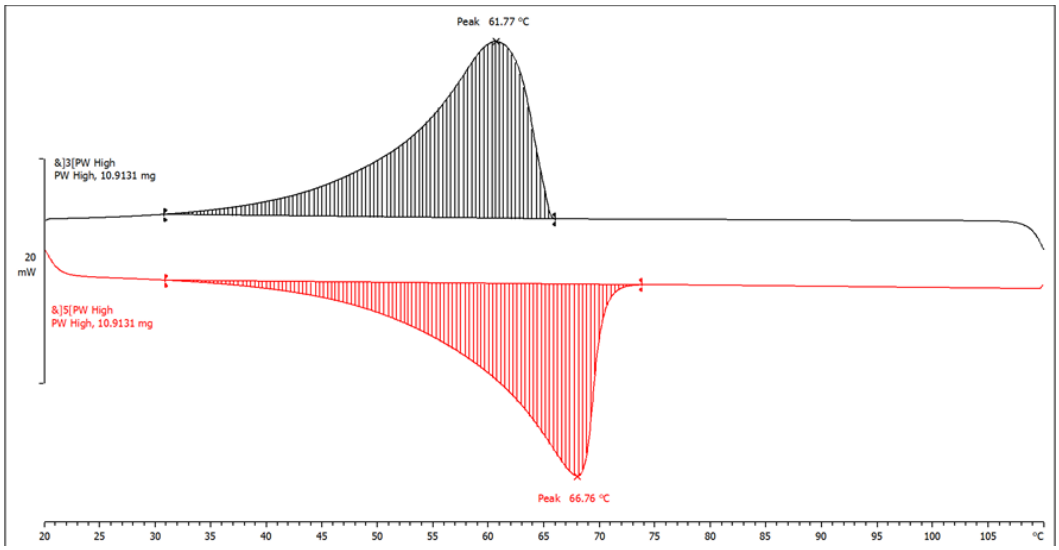

Figure 4.5 – Graph showing DSC thermograph of (a) PWL, (b) PWM and (c) PWH. Black peaks (exothermic) denote the crystallisation peaks, and red peaks (endothermic) denote the melting peaks.

Figure 4.5a and table 4.1 show that there are distinct peaks for melting at 42.38 °C and crystallisation at 38.45 °C for PWL. there are also secondary peaks at 29.53 °C for melting and 28.03 °C for crystallisation. Although these secondary peaks are combined with the larger primary peak.

Figure 4.5b shows that there are two sets of two distinct peaks and table 4.1 shows the corresponding temperatures for PWM. The two melting peaks appear at 36.18 °C and 55.18 °C and for crystallisation peaks appear at 33.11 °C and 51.14 °C.

Figure 4.5c shows that there is one large peak observed when measuring PWH with the DSC. The peak temperature obtained for melting is 66.76 °C and peak temperature for crystallisation is 61.77 °C. It can be seen though, these peak temperatures are misrepresentative as the area (equating to total energy) under the graphs is large and these peaks could be hiding smaller conformational changes for the crystals within the constituent component.

Table 4.1 – Table showing melting and crystallisation temperature peaks for PW samples tested using DSC, and the weights of those samples.

Sample	Melting Temperature Peaks (°C)			Crystallisation Temperature Peaks (°C)			Weight (mg)
PWL	29.53	42.38	n/a	n/a	38.45	28.03	11.64
PWM	36.18	55.18	n/a	n/a	51.14	33.11	11.42
PWH	n/a	n/a	66.76	61.77	n/a	n/a	10.91

When considering the paraffin wax (PW) that the increasing congealing point of the grade (PWL < PWM < PWH) shows a change in the thermograph plots. Figure 4.5a shows a large peak at a low melting range and low crystallisation range, 42.38 °C and 38.45 °C respectively, for PWL there can also be seen a small initial peak, however, these are likely solid-solid phase changes within the PWL (Luyt and Krupa, 2007). This is followed by a large enthalpy peak

which would represent the solid-liquid melting phase and liquid-solid phase upon crystallisation.

PWM in figure 4.5b shows the same pattern seen in figure 4.5a, there is an initial enthalpy peak with a melting peak of 55.18 °C and a crystallisation peak of 51.14 °C. Here the temperature lag that was seen in PWL (3.93 °C) is also evident here with a difference of 4.04 °C. What should be noted is that both curves in figure 4.5b have more defined solid-solid phase orientation peaks, these are likely due to the greater molecular weight of components within PWM compared to PWL.

Figure 4.5c shows the thermograph for PWH, we see that the peaks of both melting and crystallisation curves, seen in figure 4.5a and figure 4.5b have combined. The melting curve has a temperature peak of 66.76 °C and the crystallisation curve has a peak temperature of 61.77 °C. These curves again show that there is a thermal lag between the melting and crystallisation of PWH, with a difference of 4.99 °C, greater lag is due to the increased molecular weight of the PWH compared to the other PW samples.

4.3.2 DSC of Microcrystalline Wax

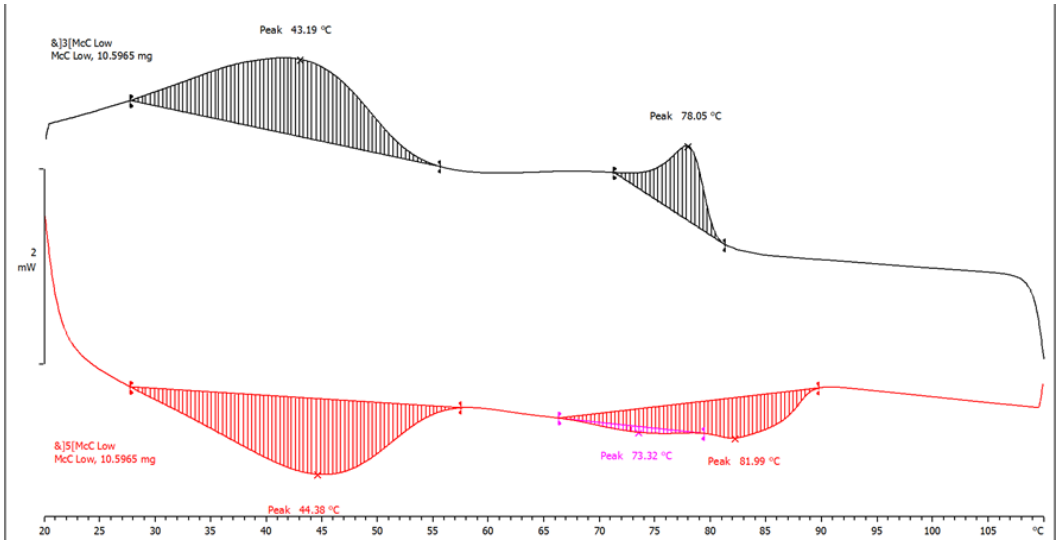

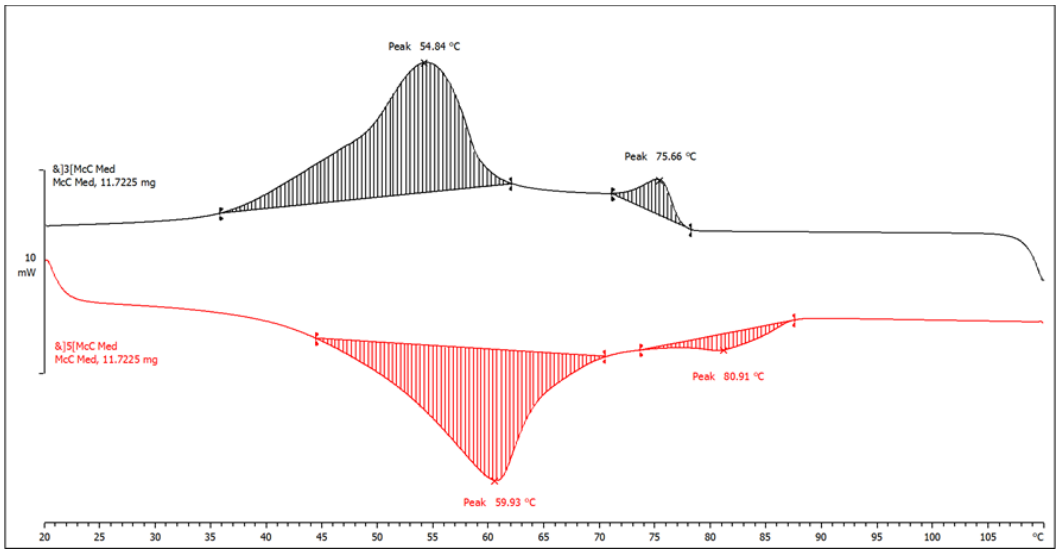

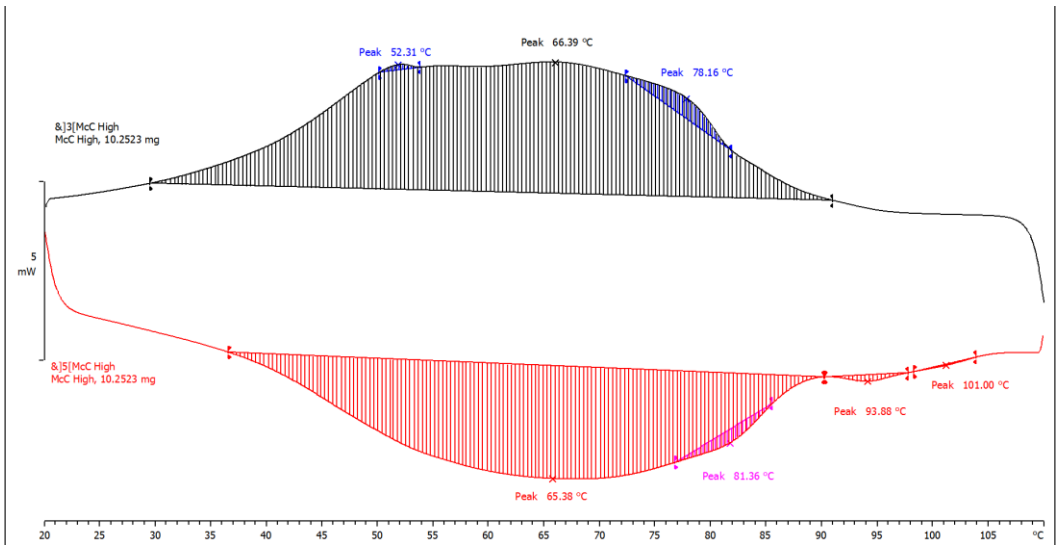

Figure 4.6 – Graph showing DSC thermograph of (a) MWL, (b) MWM and (c) MWH. Black peaks (exothermic) denote the crystallisation peaks, and red peaks (endothermic) denote the melting peaks.

Figure 4.6a shows that there are two distinct peaks observed for the melting curve, at 44.38 °C and secondly at 81.99 °C, however, there is a small peak contained within the higher temperature peak area which is observed at 73.32 °C. For the crystallisation curve temperature peaks, it can be observed at 43.19 °C and 78.05 °C.

Figure 4.6b shows that there are two sets of distinct peaks observed for both melting and crystallisation curves. For the melting curve, there is a large primary peak observed at 59.93 °C and a smaller secondary peak at 80.91 °C. for the crystallisation curve there is a large primary peak observed at 54.84 °C and a smaller but pronounce peak at 75.66 °C.

Figure 4.6c shows the curve obtained for MWH, these curves are pronounced but are not very distinctive. There are singular large peaks observed for both melting and crystallisation curves. Using the STARe software, it was calculated that the peak temperatures obtained were 65.38 °C for the melting curve and 66.39 °C for the crystallisation curve. Within the melting curve there are three other smaller peaks observed, one within the larger peak at 81.36 °C, and two others outside the larger peak at 93.88 °C and 101.00 °C. for the crystallisation curve there are two other smaller peaks observed within the larger singular peak, these are found at 52.31 °C and 78.16 °C.

Table 4.2 – Table showing melting and crystallisation temperature peaks for MW samples tested using DSC, and the weights of those samples.

Sample	Melting Temperature Peaks (°C)			Crystallisation Temperature Peaks (°C)			Weight (mg)
MWL	44.38	73.32	81.99	78.05	n/a	43.19	10.60
MWM	n/a	59.93	80.91	75.66	54.84	n/a	11.72
MWH	65.38	81.36	93.88	78.16	66.39	52.31	10.25

MW follows a similar trend to that of the PW and the temperature increases can be seen in figure 4.6a, figure 4.6b and figure 4.6c for MWL, MWM and MWH, respectively. What should be noted is that for MWL and MWM the thermograph curves show a different shape to that of the PWL and PWM. Figure 4.6a and figure 4.6b (MWL and MWM) show that there are two defined peaks of enthalpy for both melting and crystallisation curves.

Figure 4.6a, MWL, shows temperature peaks experienced are slightly higher compared to PWL, with initial peaks of 44.38 °C (melting) and 43.19 °C (crystallisation) giving a thermal lag of 1.19 °C. When considering the melting curve for figure 4.6a there is also a secondary enthalpy peak containing two temperature peaks of 73.32 °C and 81.99 °C, these temperature peaks are likely due to phase transition shifts in crystals and the melting of the high melting point crystals contained within the microcrystalline wax. Microcrystalline wax is made of a combination of n-alkanes, naphthalic hydrocarbons and branched hydrocarbons, and while comparing PWH and MWL, molecular weight may be similar, it is likely the chemistry is different. Within the melting curve, it is likely the first enthalpy peak is due to melting of low melting point crystals and straight chain hydrocarbons, while the second enthalpy peak will show the energy and the melting points of branched hydrocarbons (Luyt and Krupa, 2007). The crystallisation curve shows two peaks of enthalpy with peak temperatures, an initial small peak at 78.05 °C, this is likely to be crystallisation of high melting point wax crystals, while the second smaller enthalpy peak is the further full crystallisation of wax crystals and the main structure formation, with a peak temperature of 43.19 °C. The increasing trend in the crystallisation curve indicates that the heating capacity of MWL is increasing also, this is a property expected in MW as when used as a phase change material within thermal insulation.

Figure 4.6b shows that on melting and crystallisation curves there are two distinct enthalpy peaks, melting has one large enthalpy peak of peak temperature 59.93 °C and a second small peak at 80.91 °C, like MWL this is likely high melting point crystals transitioning to liquid oil. On the crystallisation curve, there are two distinct enthalpy peaks with peak temperatures of 75.66 °C and 54.84 °C. Between these curves, we see that there was a thermal lag of 5.09 °C for melting and crystallisation of wax crystals, an increase from MWL.

However, one difference in MWL and MWM is that the enthalpy peaks appear to be beginning to merge, moving closer together possible indicating an increased similarity of chemistry in the molecules with increasing molecular weight. The two distinct enthalpy peaks can be an indication of distillation of the MW sample, as the temperature is increased lower fractions of the wax could be separating from the bulk leaving higher melting point materials still unaffected.

Figure 4.6c, the MWH thermograph shows that enthalpy peaks have merged and there is one large peak enthalpy for both melting and crystallisation curves. There are slight changes on the melting curve occurring near the end of the peak, the peak temperature of the enthalpy peak is 65.38 °C, at 81.36 °C there is a small transition peak within the larger enthalpy curve, likely wax crystals of greater melting point and high Mw transitioning into a liquid phase. Finally, at 93.88 °C, there is a small enthalpy peak, which could indicate the final melting of high melting point crystals. The crystallisation curve shows that there is one large enthalpy curve with two other small transition peaks contained within, first at 78.16 °C and secondly at 52.31 °C, with the main peak temperature of 66.39 °C. Here it is calculated, that there is a thermal lag of -1.01 °C, indicating that when crystallising the peak effect would occur at a temperature higher than the melting peak, this is obviously not possible and as such these curves cannot be considered truly accurate and that multiple repeats would be required to obtain a true result. The other peaks mentioned are good examples of transition temperatures for higher melting point crystals at 78.16 °C and lower melting crystals at 52.31 °C.

4.3.3 DSC of White Soft Paraffin Blends

4.3.3.1 WSP1, WSP2, WSP3

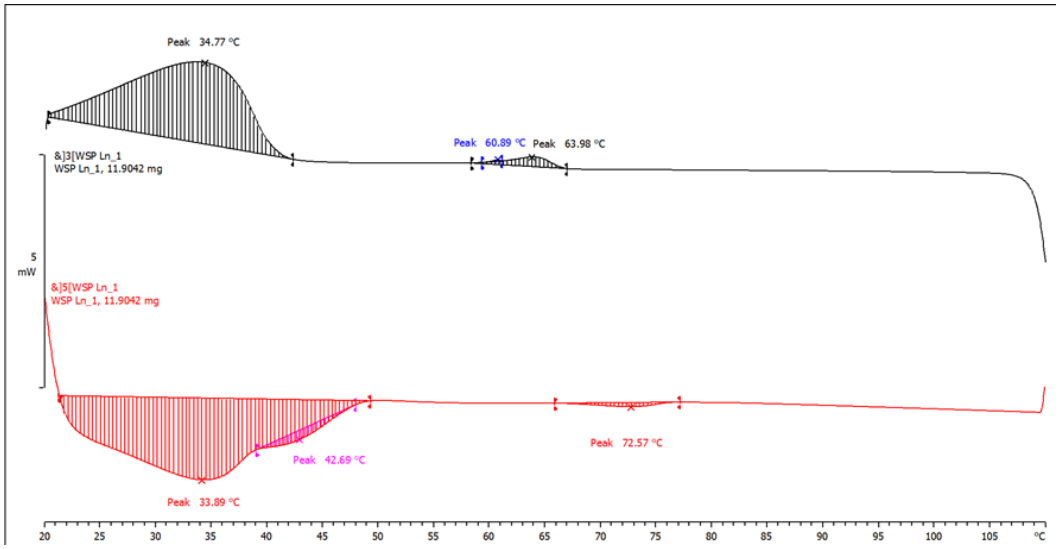

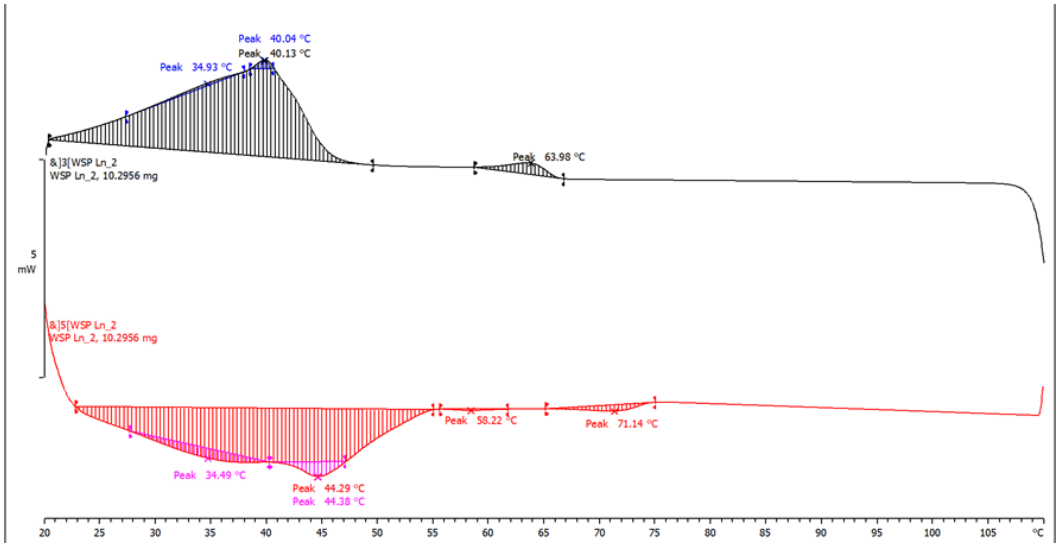

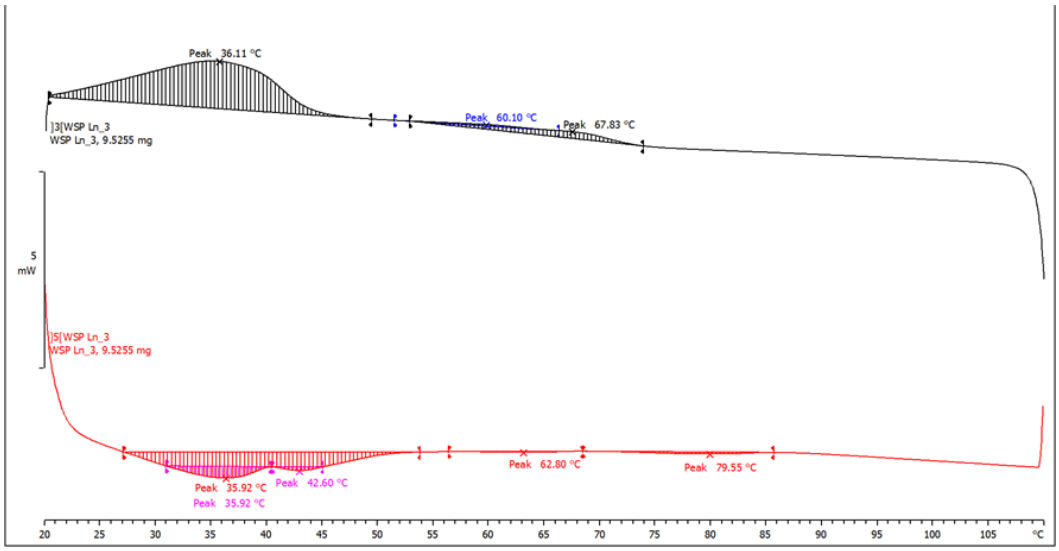

Figure 4.7 – Graph showing DSC thermograph of (a) WSP1, (b) WSP2 and (c) WSP3. Black peaks (exothermic) denote the crystallisation peaks, and red peaks (endothermic) denote the melting peaks.

Figure 4.7a shows that there are early set primary peaks observed for both melting and crystallisation curves, the melting curve has a primary peak at 33.89 °C, containing a small step peak at 42.69 °C. There is also a small secondary peak observed at 72.57 °C. for the crystallisation curve there are two peaks observed, a large peak with temperature 34.77 °C and a secondary peak with a temperature of 63.98 °C.

Figure 4.7b shows that there are multiple peaks observed for both curves like figure 4.6a. the primary temperature peak on the melting curve is a little more elongated in range, there is a singular peak observed at 44.29 °C, however, there is a smaller peak contained within this large peak range, at 34.49 °C. There are then also two smaller peaks observed at 58.22 °C and 71.14 °C. on the crystallisation curves the peaks are more defined, there is a large primary peak with a temperature peak at 40.13 °C and a smaller secondary peak at 63.98 °C.

Figure 4.7c shows that there are large peaks observed on both curves, however, are smaller than the previous one observed in other figures within this chapter. On the melting curve, there is a primary peak observed with a temperature of 35.92 °C, but also contains smaller temperature peak at 42.60 °C, there is also a smaller peak observed at 79.55 °C, however, this is very small and could be a sampling error. On the crystallisation curve, there are two peaks observed, a primary peak at 36.11 °C and a secondary peak at 67.83 °C.

Table 4.3 – Table showing melting and crystallisation temperature peaks for WSP1, WSP2 and WSP3 tested using DSC, and the weights of those samples.

Sample	Melting Temperature Peaks (°C)			Crystallisation Temperature Peaks (°C)			Weight (mg)
WSP1	33.89	42.69	72.57	63.98	60.89	34.77	11.90
WSP2	34.49	44.38	71.14	63.98	40.13	34.93	10.30
WSP3	35.92	n/a	79.55	67.83	n/a	36.11	9.53

WSP1 and WSP2 show great likeness within the thermograph curves and the melting and crystallisation peaks being within ± 1 °C, WSP3 shows slightly similar thermographs, however, enthalpy peaks are not as defined as in WSP1 and WSP2, as well as the melting and crystallisation peaks being slightly shifted, as seen in table 4.3, by up to 6 °C difference on the secondary melting peak. Within all plots, there are small transition states, mostly within the larger enthalpy peaks. These transitions are evidence of crystal morphology and phase change within a melting and crystallisation region.

When considering the contribution from PW, as seen in figure 4.5b, PWM for these three WSP blends, it appears that there is little similarity in thermograph shape and melting/crystallisation peaks. There are two peaks observed in PWM which could add a small contribution to the thermographs as they all experience two main melting and crystallisation peaks.

When considering the MW contribution (figure 4.6) of MWL, MWM and MWH for WSP1, WSP2 and WSP3 respectively, there is a distinct correlation in the thermographs of MW and WSP blends. For WSP1 there is an apparent shift of melting and crystallisation peaks to lower points of both PWM and MWL. For MWM there is a slight increase in melting and crystallisation peaks observed in synergy in WSP2. However, WSP3 shows little or no correlation with MWH and PWM, with the apparent loss of a large amount of enthalpy from the constituent components.

Overall WSP1 and WSP2 show similarities where peaks from WSP1 begin to move closer together in WSP2, much like that of the enthalpies of MW. In WSP3 there are distinct large peaks at low melting and crystallisation temperatures but with the presence of elongated, small enthalpies. MWH contributes a region of elongated enthalpy, however, there is a loss of energy from MWH to the results WSP3 blend.

4.3.3.2 WSP4, WSP5, WSP6

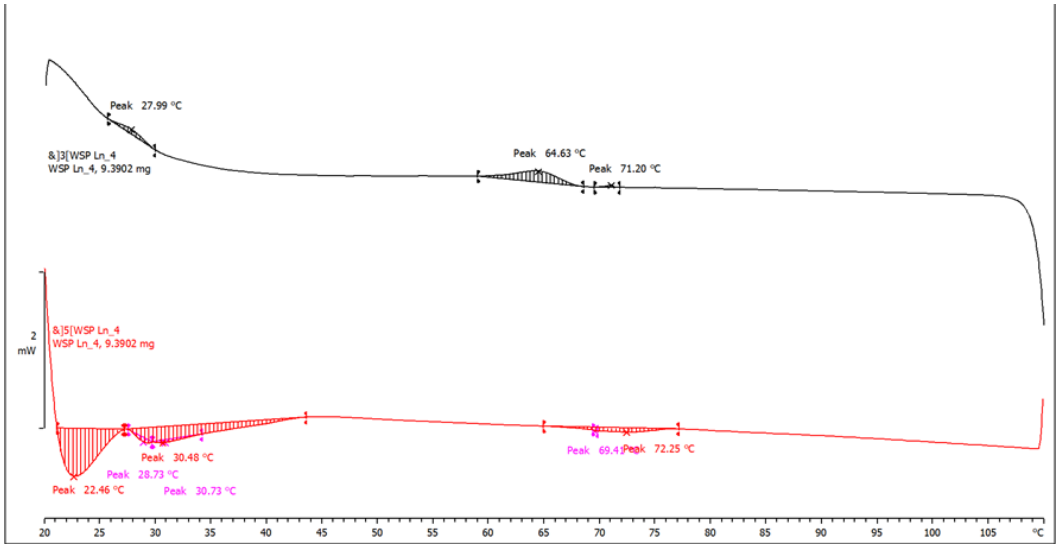

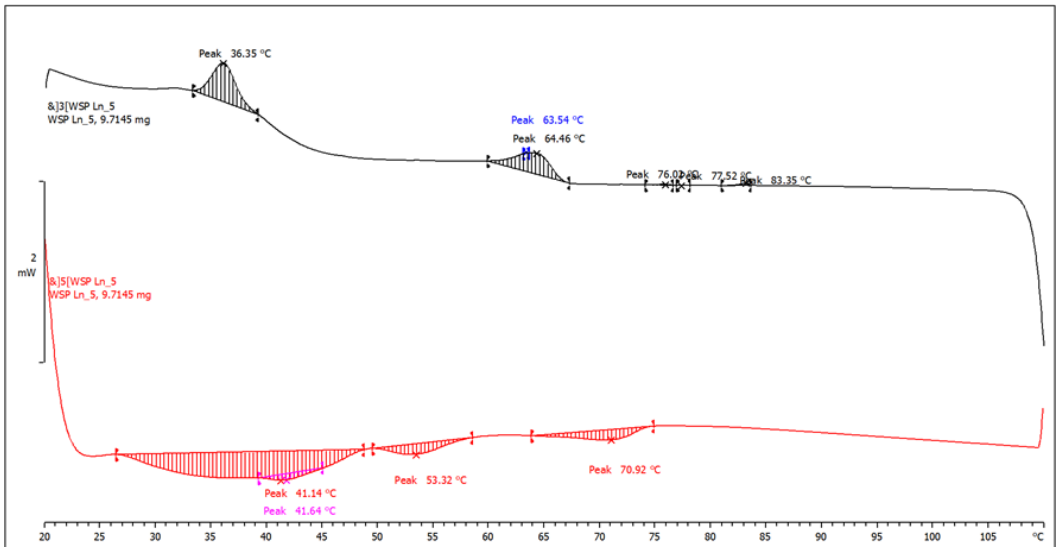

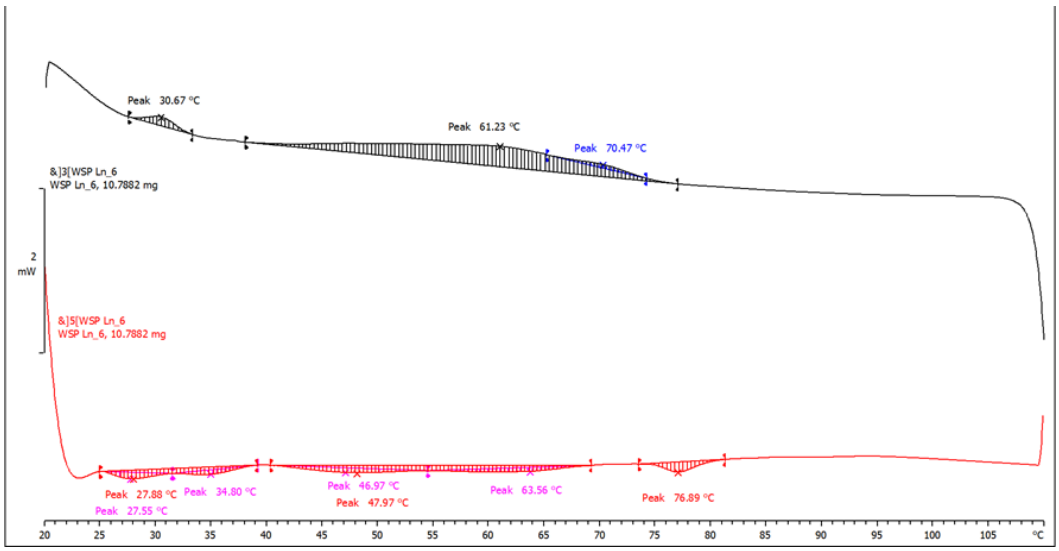

Figure 4.8 – Graph showing DSC thermograph of (a) WSP4, (b) WSP5 and (c) WSP6. Black peaks (exothermic) denote the crystallisation peaks, and red peaks (endothermic) denote the melting peaks.

Figure 4.8a shows peaks are observed for both curves however these are very small indicating little energy use in DSC experiment. On the melting curve, there is a primary peak observed at 22.46 °C with a closely connected secondary peak with a temperature of 30.48 °C. There is also a smaller tertiary peak observed at 72.25 °C. On the crystallisation curve, the peaks observed are small with the largest peak being observed at 64.63 °C and a very small peak observed at 27.99 °C. It is possible that at 27.99 °C this small peak is part of a larger peak that is not observable on this scale due to the limitation of the experimental protocol used for these DSC thermographs.

Figure 4.8b shows that on the melting and crystallisation curves there are multiple peaks observed. On the melting curve, a broad range primary peak is observed with a peak temperature of 41.14 °C, then secondary and tertiary peaks observed at 52.32 °C and 70.92 °C. On the crystallisation peak, there are two main peaks observed, a primary peak at 36.35 °C and a secondary peak at 64.46 °C. On the crystallisation peak, there are also multiple small artefacts observed on the curve between temperatures 76.02 °C and 83.35 °C.

Figure 4.8c shows the thermograph for WSP6 and shows that there is a definite peak observed on the crystallisation curve, however on the melting curve it is difficult to define an absolute peak. Using the STARe software, three peaks were observed, at 27.08 °C, 47.97 °C and 76.89 °C but all these peaks contain smaller peaks within the range of energy change recorded. On the crystallisation curve, there are two defined peaks, a broad range primary peak with a peak temperature of 61.23 °C and a small secondary peak at 30.67 °C.

Table 4.4 – Table showing melting and crystallisation temperature peaks for WSP4, WSP5 and WSP6 tested using DSC, and the weights of those samples.

Sample	Melting Temperature Peaks (°C)			Crystallisation Temperature Peaks (°C)			Weight (mg)
WSP4	30.48	69.41	72.25	71.20	64.63	27.99	9.39
WSP5	41.14	53.32	70.92	83.35	64.46	36.35	9.71
WSP6	34.80	63.56	76.89	70.47	61.23	30.67	10.79

Once again there is a likeness between the first two blends of this family, in WSP4 and WSP5, with WSP6 showing different thermograph curves. In WSP4 and WSP5 there are distinct curves for melting and crystallisation, with WSP4 exhibiting peaks with lower enthalpies than those of WSP5. The peaks of WSP5 are also showing the slight merging of peaks seen in WSP2 in figure 4.7b. WSP6 shows a small elongated peak while crystallising and many small enthalpies very closely linked with an onset of 25.28 °C to an end set of 79.73 °C.

In the WSP blends, there is little correlation between them and the constituent components of PWL and MWL, MWM and MWH for WSP4, WSP5 and WSP6, respectively. The only small likeness that exists is that the WSP blends show similar peak trends to those of the MW but no melting or crystallisation peaks of the waxes match those of WSP blends.

For WSP4, WSP5 and WSP6 there is a great loss of enthalpy from the wax components to the WSP blends, the minor differences that exist in the WSP appear to be contributed from MW. The inclusion of PWL within these blends appears to affect the loss of enthalpy in the WSP blends, much more than that experienced by WSP1, WSP2 and WSP3, which included PWM.

4.3.3.3 WSP7, WSP8, WSP9

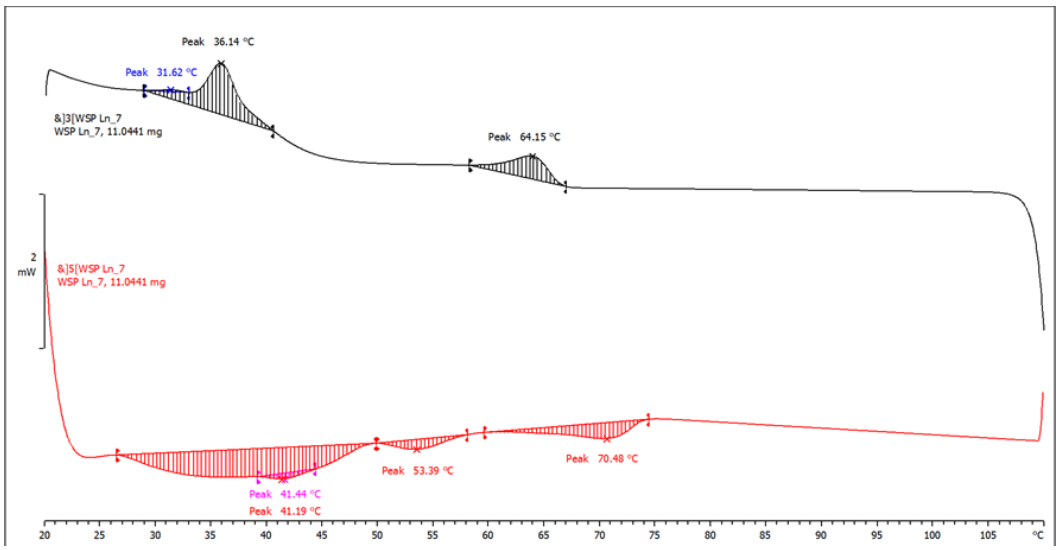

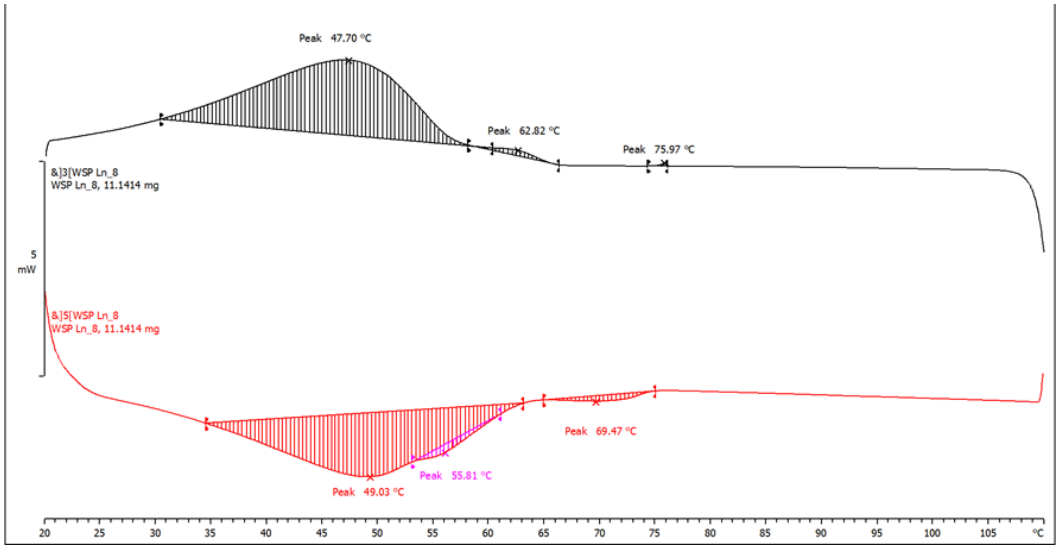

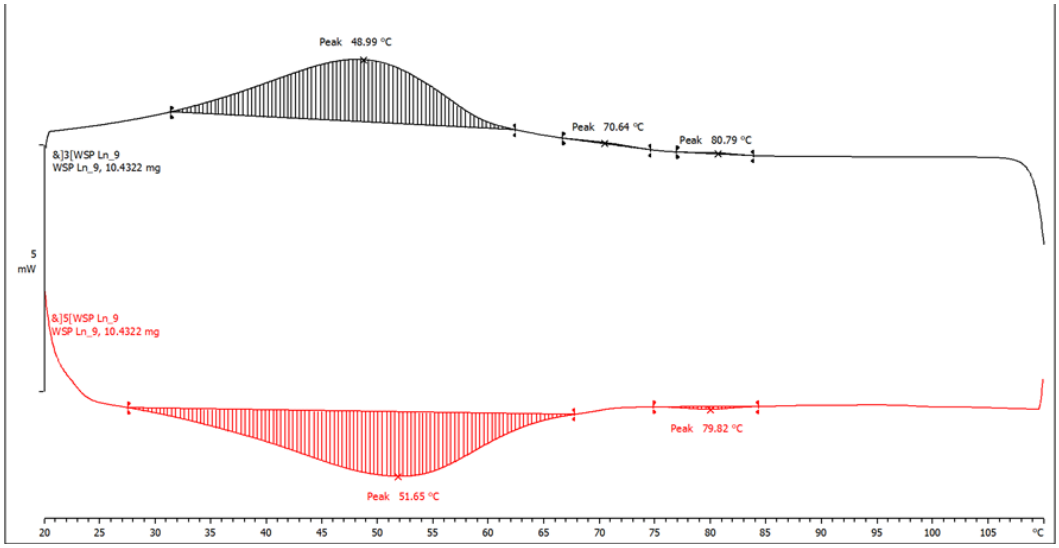

Figure 4.9 – Graph showing DSC thermograph of (a) WSP7, (b) WSP8 and (c) WSP9. Black peaks (exothermic) denote the crystallisation peaks, and red peaks (endothermic) denote the melting peaks.

Figure 4.9a shows that there are three peaks observed on the melting curve, one broad range peak with a temperature of 41.19 °C then a following secondary and tertiary peak with temperatures observed at 53.39 °C and 70.48 °C respectively. On the crystallisation curve, two peaks are observed, one primary peak at 36.14 °C and a secondary peak at 64.15 °C

Figure 4.9b shows that on the melting curve there are two main peaks observed, a primary one with a temperature of 49.03 °C and a secondary peak at 69.47 °C. The primary peak does, however, contain a small temperature peak at 55.81 °C. On the crystallisation curve, there are two temperature peaks observed at 47.70 °C and 62.82 °C.

Figure 4.9c shows that there are singular peaks observed on both melting and crystallisation curves, on the melting curve there is a large peak range with a temperature of 51.65 °C and on the crystallisation curve there is a broad range with a temperature peak at 48.99 °C. There are other smaller peaks observed on both curves, however, these are very small and may be errors with the experimental run, or software analysis.

Table 4.5 – Table showing melting and crystallisation temperature peaks for WSP7, WSP8 and WSP9 tested using DSC, and the weights of those samples.

Sample	Melting Temperature Peaks (°C)			Crystallisation Temperature Peaks (°C)			Weight (mg)
WSP7	41.19	53.39	70.48	64.15	36.14	31.62	11.04
WSP8	49.03	55.81	69.47	75.97	62.82	47.70	11.14
WSP9	51.65	n/a	79.82	80.79	70.64	48.99	10.43

In figure 4.9a, WSP7 demonstrates different behaviour to those of WSP8 and WSP9 in figures 4.9b and 4.9c, respectively. WSP7 shows that similar trends to previous WSP blends are observed where there are distinct peaks with smaller enthalpies compared to its constituent components. WSP7 contains PWH and MWL and in figure 4.9a there is a strong correlation in peaks placement with that

of MWL while the WSP blend is melting when crystallising there is a slight decrease in peak placement in the blend, however, the contribution of PWH could allow that change to occur. PWH appears to also contribute to the increased enthalpy peaks seen in WSP7 compared to previous WSP blends, where loss of enthalpy occurred. There is still a great loss of enthalpy values in WSP7 compared to the constituent components.

In figure 4.9b and 4.9c, WSP8 and WSP9 respectively, there are strong similarities in the blends, both exhibiting one large enthalpy peak in melting and crystallisation curves, with small phase transition peaks following the larger peaks. In WSP8 there are still two enthalpy peaks for both curves, a contribution from MWM with two distinct peaks, while here PWH contributes to the increased overall enthalpy experienced by WSP8. In WSP9 the contribution from both PWH and MWH are evident in both the single large enthalpy peak on both curves for WSP9.

4.3.4 Commercial Plant Grades

4.3.4.1 WSP10, WSP11

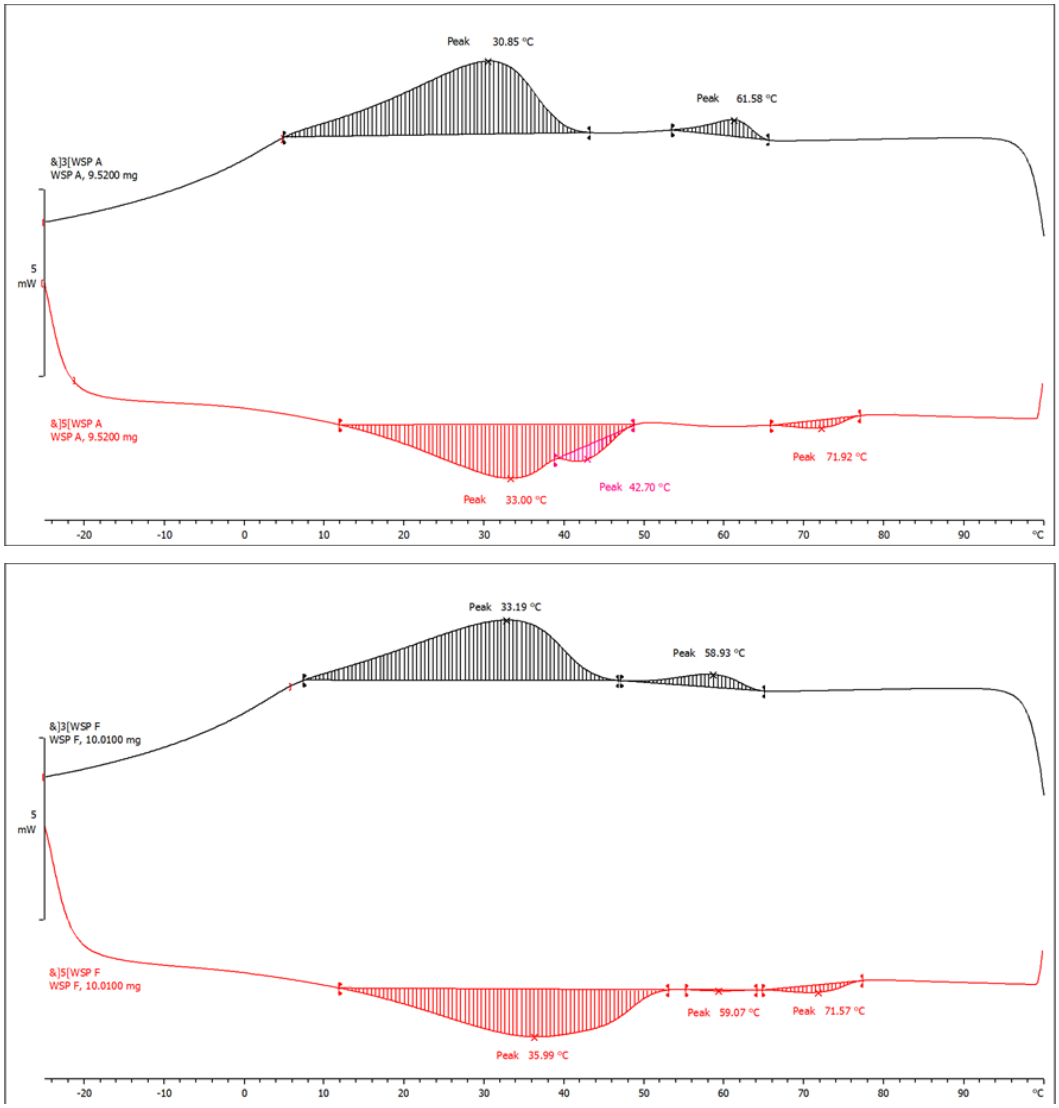

Figure 4.10 – Graph showing the DSC thermograph of (a) WSP10 and (b) WSP11. Black peaks (exothermic) denote the crystallisation peaks, and red peaks (endothermic) denote the melting peaks.

Figure 4.10a shows that there are main temperature peaks on both curves, also with small secondary peaks. On the Melting curve, there is a one large primary peak at 33.00 °C and a smaller secondary peak at 72.92 °C, there is also a small peak step contained within the primary peak with a temperature of 42.70 °C. on the crystallisation curve there are two peaks present only, one primary large peak at 30.85 °C and a smaller secondary peak at 61.58 °C.

Figure 4.10b indicates that on the melting curve there are two distinct peaks, one large peak at 35.99 °C and a second smaller peak at 71.57 °C, using the STARe software there was recognised a small peak at 59.07 °C, however,

this is possibly just an artefact in the experiment and not dependent on the sample. On the crystallisation curve, there are only two distinctive peaks, one large primary peak at 33.19 °C and a second smaller peak at 58.93 °C.

Table 4.6 – Table showing melting and crystallisation temperature peaks for WSP10 and WSP11 tested using DSC, and the weights of those samples.

Sample	Melting Temperature Peaks (°C)			Crystallisation Temperature Peaks (°C)			Weight (mg)
WSP10	31.67	42.70	71.25	61.42	n/a	30.85	9.52
WSP11	35.49	59.07	71.07	58.93	n/a	33.02	10.01

When comparing WSP blends with the two plant grade samples (WSP10 and WSP11), WSP1, WSP3 and WSP8 show similarities. When looking at the thermographs for these samples, in figures 4.7a, 4.7c and 4.9b there are differences in the temperature peak heights and energy peaks for both melting and crystallisation curves.

However, when comparing data on figure 4.12 we see that for enthalpy of formation values for WSP3 and WSP9 are like WSP10, while WSP1 is like WSP11. When considering the enthalpy of fusion WSP10 and WSP11 are alike, but the closest blends to them are WSP1 with 30.02 J g^{-1} or WSP3 with a value of 11.94 J g^{-1}.

The large differences in the enthalpy value to the industry samples may well be due to the few constituent components used to produce the laboratory made WSP blends, and that WSP made within the industry are likely to contain a greater amount of waxes with better homogenisation methods used to produce these blends.

4.3.5 Enthalpy of Fusion Comparison

Table 4.7 – Table of Melting and crystallisation energy peaks for samples tested using DSC, and the weights of those samples.

Sample	Melting Energy Peaks (mJ)			Crystallisation Energy Peaks (mJ)			Weight (mg)
PWL	0	-2006.53	0	0	1959.25	7.97	11.64
PWM	0	-2405.17	0	0	1799.18	333.98	11.42
PWH	0	-2331.55	0	2289.38	0	0	10.91
MWL	0	-389.13	0	39.08	0	145.72	10.60
MWM	0	-1732.58	0	66.78	830.41	0	11.72
MWH	0	-1698.09	0	38.26	1623.91	3.88	10.25
WSP1	-351.60	0	-5.76	10.90	0	257.23	11.90
WSP2	-338.93	0	-8.63	12.31	0	332.83	10.30
WSP3	-108.59	0	-5.16	25.27	0	205.72	9.53
WSP4	-25.13	-19.65	-4.18	0.25	7.74	1.58	9.39
WSP5	-54.82	-6.58	-7.73	10.21	0	13.21	9.71
WSP6	-11.04	-21.89	-4.72	62.30	0	3.54	10.79
WSP7	-69.85	-6.67	-16.35	14.45	31.60	0.54	11.04
WSP8	-491.47	-287.80	-9.79	0	5.65	317.70	11.14
WSP9	-375.47	-317.19	-2.75	0.81	1.20	251.03	10.43
WSP10	-175.09	0	-7.78	16.10	0	223.86	9.52
WSP11	-184.72	-0.99	-8.41	18.11	0	208.17	10.01

Table 4.7 shows the energies required for WSP samples and constituent components to achieve a full phase change, we see that the energy increases with increasing congeal point of samples. This is due to the increased molecular weight of the constituent components. The increase of Mw corresponds to the increasing length of hydrocarbon and the greater number of bonds between all molecules within the wax products, as these bonds are broken, as the heat increases to melt the product, greater energy is required overall.

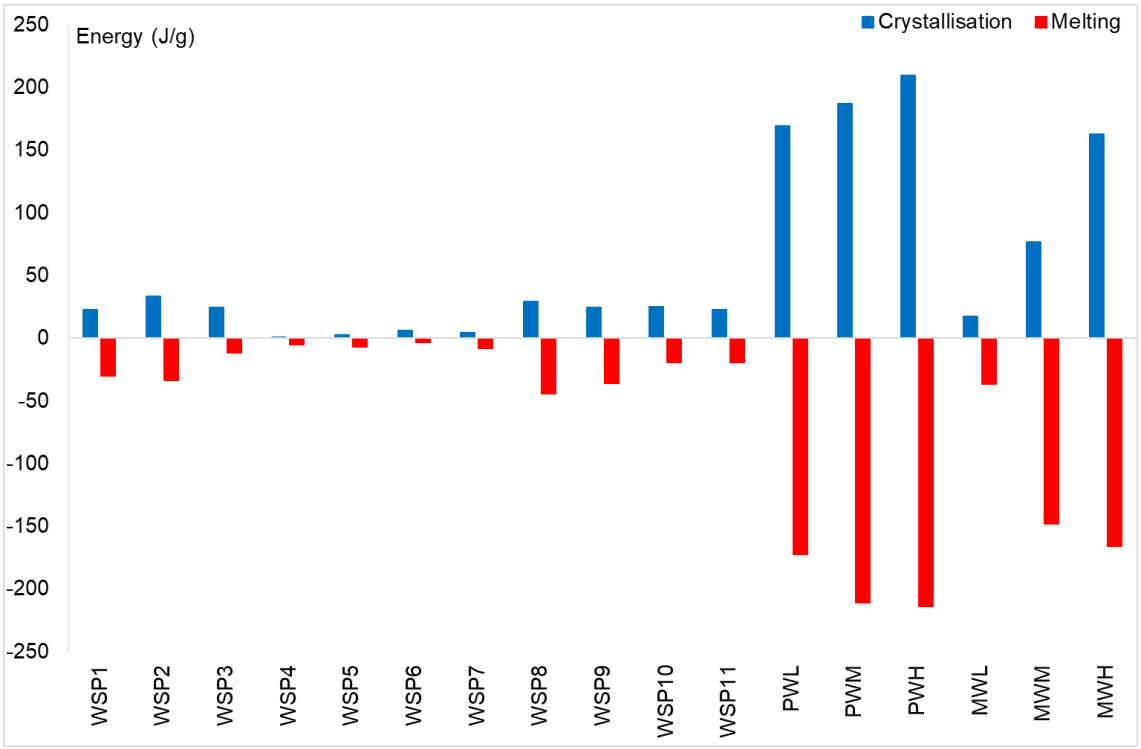

Figure 4.11 – Graph showing the change in total energy per gram experienced for samples WSP1, WSP2, WSP3, WSP4, WSP5, WSP6, WSP7, WSP8, WSP9, PWL, PWM, PWH, MWL, MWM and MWH using the DSC protocol.

Figure 4.11 shows the difference in energy levels experienced by WSP samples and constituent components, these figures represent the data shown also shown in table 4.7, in the figure representation of energies was given as the energy per gram for each sample. Figure 4.11 shows that WSP4, WSP5, WSP6 and WSP7 have the lowest energy requirements when both melting and crystallising the samples. PW has the greatest energy needs within the DSC, when crystallising samples, increasing the order of sample energy shows PWL < PWM < PWH, and for melting PWL < PWH < PWM. MW follows a similar trend to PW, however, requires less energy overall to affect a change in phase of the samples. In order from lowest to highest, crystallisation energy MWL < MWM < MWH and melting energy PWL < PWH < PWM. For all samples, more melting energy is required rather than that required for crystallisation.

In table 4.7 and figure 4.11 we see the energy required for PW and MW, when considering melting curves, both PW and MW follow an interesting pattern, where energy transitions from PWL < PWM > PWH, this also occurs for MW, where MWL < MWM > MWH however for MW there is a much greater jump in energy from MWL to MWM with a difference of 1343.45 mJ. This difference between PW and MW could indicate that paraffin waxes are in general very

similar in chemistry, shape and molecular weight across different congeal point ranges.

For microcrystalline waxes, there is a big difference between low congeal point wax compared with medium and high congeal point waxes. Previously it has been stated that *"energy associated with solid-liquid phase change is much higher in case of pure microcrystalline wax compared to paraffin wax and wax blends"* (Kumar et al., 2004), however within this investigation this was not true and in fact the opposite is true, with MWL having the lowest energy requirements of all samples. The same samples were not used in this investigation as with the previous author and it is possible there is a difference in specification causing different in results.

When considering the crystallisation peaks shown in figure 4.11 we see that for both PW and MW follow the trend that would be expected, increasing energy with increased Mw, is true. The increase for PW is less compared to MW, where the increase in energy for PW goes from 1965.22 mJ to 2133.16 mJ to 2289.38 mJ and for MW the energy increases from 184.80 mJ to 897.19 mJ to 1666.05 mJ according to table 4.7. Crystallisation is an easier energy process, as bonds are forming in the hydrocarbon releasing energy from the surroundings, this is likely the reason for the uniform change in energy levels compared to the melting process that is requiring energy to break bonds. As PW has a greater content of n-alkane, energy requirements for melting increases linearly with increasing mW, the same is true for MW, however, the chemistry of MW has a greater component of branched hydrocarbons and as such could be easier to break down compared to the larger more stable straight chain hydrocarbons in PW.

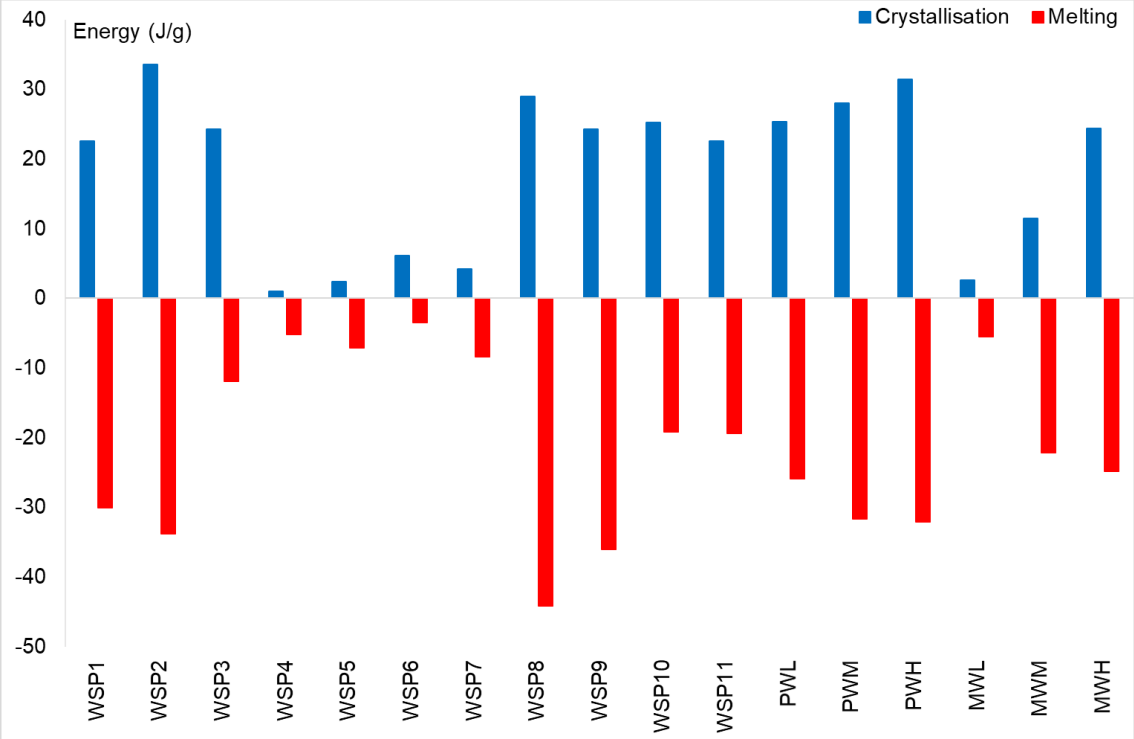

Figure 4.12 – Graph showing the change in total energy experienced for samples using the DSC protocol with a 15% calculated correction for constituent components, considering the ratio makeup of the WSP blends.

Figure 4.12 and Table 4.7 give the same data as figure 4.11 however for the constituent components the overall energy has been reduced to represent 15 % of the data from figure 4.11, this has been done to help represent the possible contribution of energy for the constituent component as the WSP blends are made of 15 % of the two waxes PW and MW plus 70 % of oil, not tested under DSC due to technical difficulties. We see that the PW and MW in figure 4.12 follow the same trend as figure 4.11 however with less energy contribution.

It should be noted that the wax components now show great similarity with the WSP blend contribution. However, even when combining the two wax components to equal the WSP contribution, the WSP would be expected to be greater than the wax parts but in figure 4.12 this is shown not to be true.

Table 4.8 – Table of melting and crystallisation energy peaks for constituent components tested using DSC, also including a calculated 15 % of the total energy recorded, to correspond with WSP blend ratio contribution.

Sample	Melting Energy Peaks (mJ)		Crystallisation Energy Peaks (mJ)	
	100 %	**15 %**	**100 %**	**15 %**
PWL	-2006.53	-300.98	1965.22	295.08
PWM	-2405.17	-360.78	2133.16	319.97
PWH	-2331.55	-349.73	2289.38	343.41
MWL	-389.13	-58.37	184.80	27.72
MWM	-1732.58	-259.89	897.19	134.58
MWH	-1698.09	-254.71	1666.05	249.91

Previous authors have stated the use of DSC for the characteristic analysis of waxes and their WSP blends they can make (Flaherty, 1971), however greater detail and additional study may be required when dealing with certain samples, for example high congeal point microcrystalline waxes as seen in figure 4.6c within this study. This is also true of the blends made from the constituent components of paraffin and microcrystalline waxes. Figures 4.7 – 4.9 show the blends made from the combination of constituent components using the blending chart figure 2.3 within Chapter 2.

We see that when blending constituent components, the ideal energy output calculated from the thermal analysis of the constituent components does not equal the thermal analysis of the individual blends, as seen in figure 4.13.

To be able to represent figures 4.11, 4.12 and 4.13 data of energy values from table 4.7 were all combined to give a total energy (mJ) for enthalpy curves for specific samples1. The total energy was then divided by 1000 to give the value in joules (J). Next, the weight (mg) of the samples measured in the DSC was divided by 1000, to give the weight by grams (g). The energy in joules was then divided by the weight of the sample that was measured in grams giving the enthalpy of fusion measured in J g^{-1}. As this value will only give energy in joules per the whole sample weighed, each value was divided by the recorded mass for each sample to give an energy value of joules per one gram of sample.

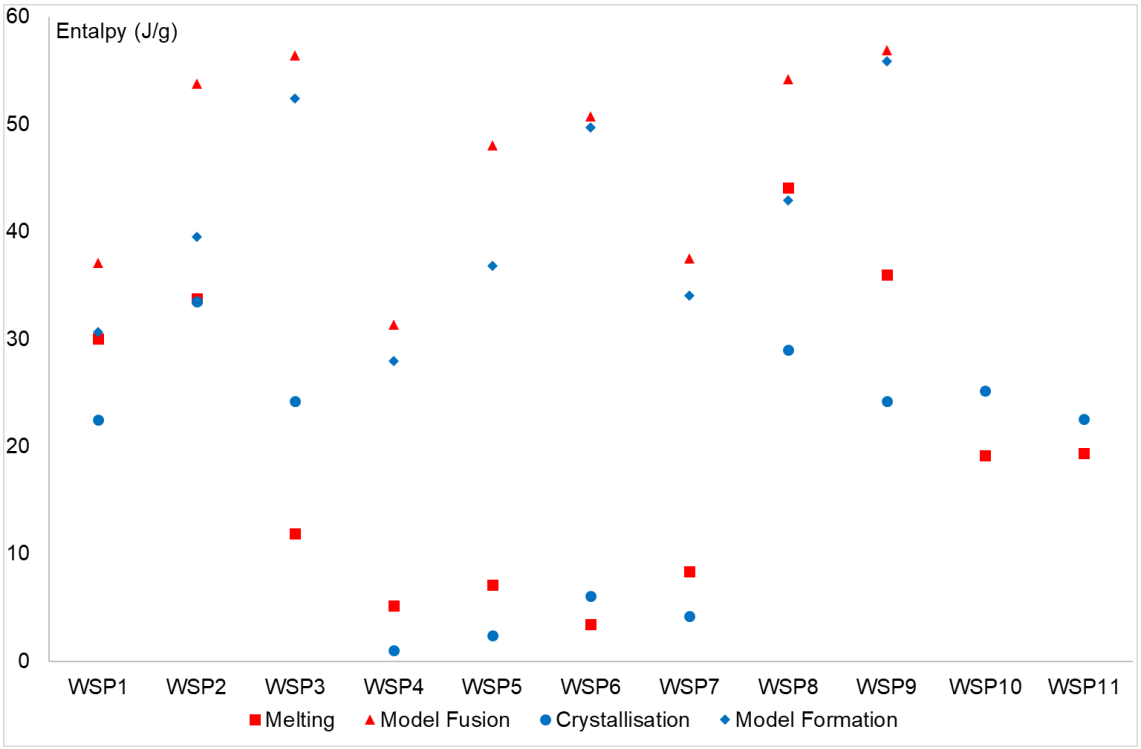

Figure 4.13 – Graph showing enthalpy of fusion and formation for, WSP blends and modelled enthalpies of WSP blend (based on constituent component results) corresponding to the left Y-axis.

Figure 4.13 shows the results of enthalpy of fusion and formation required for WSP blends and the model of blends, based on enthalpies of constituent components. Modelled enthalpies for WSP samples have been calculated based on previous DSC thermograms seen in figure 4.5 – 4.6 of the individual constituent components, the enthalpies have been calculated basing 15 % of two constituent components' enthalpies added together to give the enthalpy of the model. Ultimately, we can see that the modelled values do not show the true values of WSP taken from the DSC results, only WSP1, WSP2 and WSP8 have values like the modelled system.

In figure 4.13 we see that WSP1, WSP2 and WSP8 show the closest correlation with the modelled WSP results in terms of enthalpy of fusion, these blends also require the greatest amount of energy to become fully molten within the DSC, seen in figure 4.11. Curiously the melting points of WSP1 and WSP2 are not as high as the energy required would suggest, while WSP8 has the lowest melting point of all the WSP blends tested.

The relative closeness of enthalpy values of modelled values and recorded data for WSP1, WSP2 and WSP8 could be indicated by the similarities

in chemical components within the wax components. Theoretically, it is possible that chemically the waxes are similar and based on ideas of solubility these like materials could be dissolving into each other causing enthalpies to be similar as the mixture is much more likely to achieve a homogeneous phase compared to other samples that may require greater energy to cause a phase change of multiple system blends.

The belief that material is being ‘lost’ in the mixture within DSC scans is implied by the results shown for blends made with PWL, WSP4, WSP5 and WSP6. It is believed that PWL is most like an oil phase when in a fully molten state, considering carbon chain length and molecular weight, as such it is proposed that the crystals contained within the blend are dissolving within the oil phase, which then upon crystallisation remain, and reform within the oil phase (Freund et al., 1982). This ‘loss’ of crystals reduces the crystal content to produce lattice structures within the WSP blend, causing the sample to lose structure in rheological tests, and to require/store less energy in thermal testing.

4.4 Summary

In this section, differences in thermodynamics caused by WSP and their constituent components have been studied. As previously expressed in Chapter 2, the purpose of WSP1-9 was introduced, to try and mimic the blends that are manufactured by the pharmaceutical industry, such as WSP10 and WSP11.

Following initial testing of various temperature rates, 2 °C, 10 °C and 20 °C per minute, it was found that the best rate was 5 °C per minute, based on manufacturing conditions and finding the best enthalpy peaks on the resulting thermographs.

Paraffin wax showed a trend of increasing melting and crystallisation points as congeal point of the wax increased from PWL, PWM, PWH. Microcrystalline wax showed that at low congeal point two peaks of melting and crystallisation were observed which came closer in MWM and finally merged in MWH.

When combining wax components to produce the WSP blends, in general, the melting and crystallisation point ranges appeared to be controlled by MW, while enthalpy peaks as the energy contained within the WSP blend

were controlled more by PW. However, there will be some obvious contribution from MW, the most obvious changes appeared in enthalpy and PW congeal point was increased.

When comparing commercial pharmaceutical grade plant grade WSP blends with those made in Leeds from wax components, there was little similarity in peaks of enthalpy and melting/crystallisation point ranges. Plant grade blends showed like values for WSP blends' enthalpy (WSP3) but then appeared like other blends in terms of thermograph appearance (WSP8).

From the analysis of wax WSP thermographs, analysis of the enthalpies of the materials was carried out, it was found that similarities in enthalpies existed for some blends, WSP1, WSP2, WSP9, WSP10 and WSP11. However, there was no collaboration between the wax enthalpies and that of WSP blends made from the specific wax components.

By using enthalpies of wax components calculated modelled WSP blends were assessed and compared with the data for the real WSP blends, it was found though that only few showed similarities (WSP1, WSP2 and WSP8). When comparing the melting point ranges of these blends they were found to have some of the lowest of all the recorded data for melting point ranges.

Following the DSC investigation carried out there is an obvious loss of material when combining wax components to produce blends, the expected enthalpies and thermal characteristics of the waxes were reduced. It is seen though, that there are some similarities in properties of WSP blends, therefore moving forward further testing has been proposed for greater chemical analysis. Raman spectroscopy and investigation of solubility parameters are expected to show the chemical nature of the wax components and their possibility of dissolving into each other depending on their chemical likeness.

4.5 Conclusions

- The energy associated with solid-liquid phase change would be expected to be much higher in microcrystalline wax compared to paraffin wax and wax blends, and while MW generally requires greater energy than WSP blends, in the case of this investigation it does not require more than PW. Therefore, the spectrum of wax products is evident here and that obtaining the same

grade of material is important when trying to replicate testing methods previously used by other authors.

- Primary melting peaks for the low congeal point paraffin wax is due to solid-solid transitions, while secondary melting peaks are due to melting.
- In microcrystalline wax, there were no solid-solid transitions evident, and melting peaks found to the end of a DSC endothermic curve were due to the melting of different molar mass fractions, at the higher molecular weight.
- PW helps to contribute to WSP blends enthalpy increase, as PW congeal point increases.
- MW contributes to melting and crystallisation points of WSP blends, while also partly contributing to the energy content of WSP blends.
- Increasing Mw of materials also leads to a general increase in energy required for melting and increased energy of fusion for crystallisation.
- When combining constituent components to make WSP blends, it was found that the combination of enthalpies or energy requirements did not equal that of a calculated model for the WSP blend.
- It is likely that crystalline material is being dissolved within the oil phase when the WSP blends become molten, where the crystals will remain and reform once the crystallisation process begins on cooling.
    - Crystalline interactions break in the waxes as the energy increases in the system, these individual crystals can later reform when energy is reduced and cooling is occurring.
- Materials of very large Mw do not always give representative results, leading to large energy peaks, and information can be lost without a true definition of thermal properties.
    - Maybe further testing of MS/GCMS is required.
- When comparing to industry standard WSP blends the comparison found in other characteristic tests is not represented here in DSC thermal testing.
    - In rheological testing WSP10 is like WSP5, however, within DSC testing, WSP10 is most like WSP3 in terms of energy and enthalpy results.

Chapter 5 Chemical Analysis; Solubility Parameters and Raman Spectroscopy

5.1 Solubility Testing

5.1.1 Introduction

In the previous chapter, Chapter 4, the differences between theoretical and experimental enthalpies were shown. As such it was proposed that wax hydrocarbons were being 'lost' in the mix as the temperature of the DSC scan was increased. It was uncertain as to the reason of why the enthalpy of the model blends changed so much compared to the theoretical calculations. It was hypothesised that this might be due to the different mutual solubility of the different wax components.

Much previous work has been done on measuring the solubility of compounds in different solvents as a way of characterizing their overall physicochemical properties (Ruoff et al., 1993; Carvalho et al., 2013; Hansen and Smith, 2004; Freund et al., 1982; Jennings and Weispfennig, 2005). For hydrocarbons the theory of 'like dissolves like' was first proposed by Hildebrand (Hildebrand, 1916; Hildebrand and Scott, 1979). Based on this well-known theory and on the work of previous authors (Carvalho et al., 2013), a series of experiments were proposed with the aim of investigating the solubility of the model WSP blends, their constituent components and commercial pharmaceutical grade supplied WSPs in solvents possessing a range of chemical structures and polarity, as a way of understanding their different chemical profiles and mutual solubility. This also required measurement of the solubility of various pure standard compounds of known chemical structure in the same solvents.

It is believed that by testing the solubility of components and WSP blends there should be similarities in soluble components seen in solvents between the components and the blends they make. Such as seen similarities in solubility between PWL, MWL and WSP4.

5.1.2 Materials and Method

Components were dissolved in a range of solvents and solubility was determined by measuring UV/Vis absorbance with the pure solvent as the blank, via a JENWAY 6715 UV/Vis. spectrophotometer (Bibby Scientific Limited, Stone, UK) using two calibrated quartz cuvettes.

Due to the large number of samples available only a certain number were selected for testing. All constituent components PWL, PWM, PWH, MWL, MWM, MWH, LO, and HO were tested and WSP blends WSP5, WSP9, WSP10 and WSP11 as blends most like commercial samples, also the 'extreme' blends. Pure hydrocarbons were also tested as reference materials of 'known' solubility parameter (Carvalho et al., 2013). These included hexadecane ($C_{16}H_{34}$), isocetane (2,2,4,4,6,8,8-heptamethylnonane) ($C_{16}H_{34}$), octadecane ($C_{18}H_{38}$), eicosane ($C_{20}H_{42}$), and toluene (C_7H_8). Solvents included heptane, toluene, carbon disulphide, 1-chloronaphthalene, decahydronaphthalene, acetonitrile, nitromethane, diethyl ether, ethyl L(-)-lactate, propylene carbonate, formamide, glycerol, ethanol, methanol, propylene glycol, and 1-butanol.

To prepare samples for measuring absorbance, 5 mg of sample were placed into a 20 ml volumetric flask which was then filled to the calibrated line with one of the selected testing solvents, this gave an overall concentration of 0.25 g per 1 L sample in tested solvent. Glass stoppers were placed in the neck of the flask to give a hermetic seal and then the flask was shaken to ensure the sample was fully mixed with the solvent. The sample/solvent mixture was then left at room temperature for 24 h to ensure a standard time of solvation for all mixtures. All sample preparations were carried out within a fume cupboard for safety reasons regarding the evaporation of solvents into the atmosphere. After 24 h, a cuvette was filled with the mixture to its marker line and a blank cuvette with pure solvent. Both cuvettes were sealed with a lid comprised of a layer of aluminium foil, Parafilm and a PTFE cuvette lid, to prevent solvent evaporation.

The order of cuvettes was kept the same for all measurements and the difference between them was considered by filling both cuvettes with pure water and recording the difference between them and taking this into account when calculating the true absorbance of the mixtures. All scans for calibration, baseline and sample measurement scans were carried out between 200 nm – 800 nm.

To measure the samples the blank solvent standard was first scanned then the cuvette containing the mixture was scanned. Data was saved via the JENWAY software and then later downloaded and analysed with Microsoft Excel.

5.1.3 Results

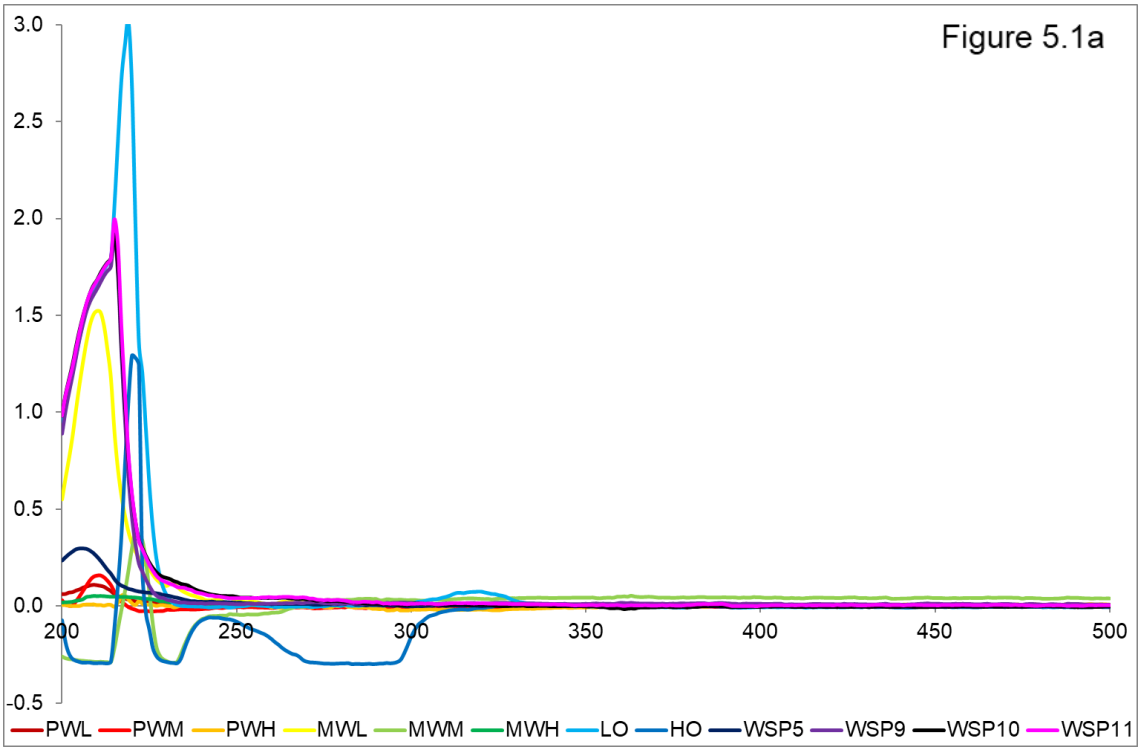

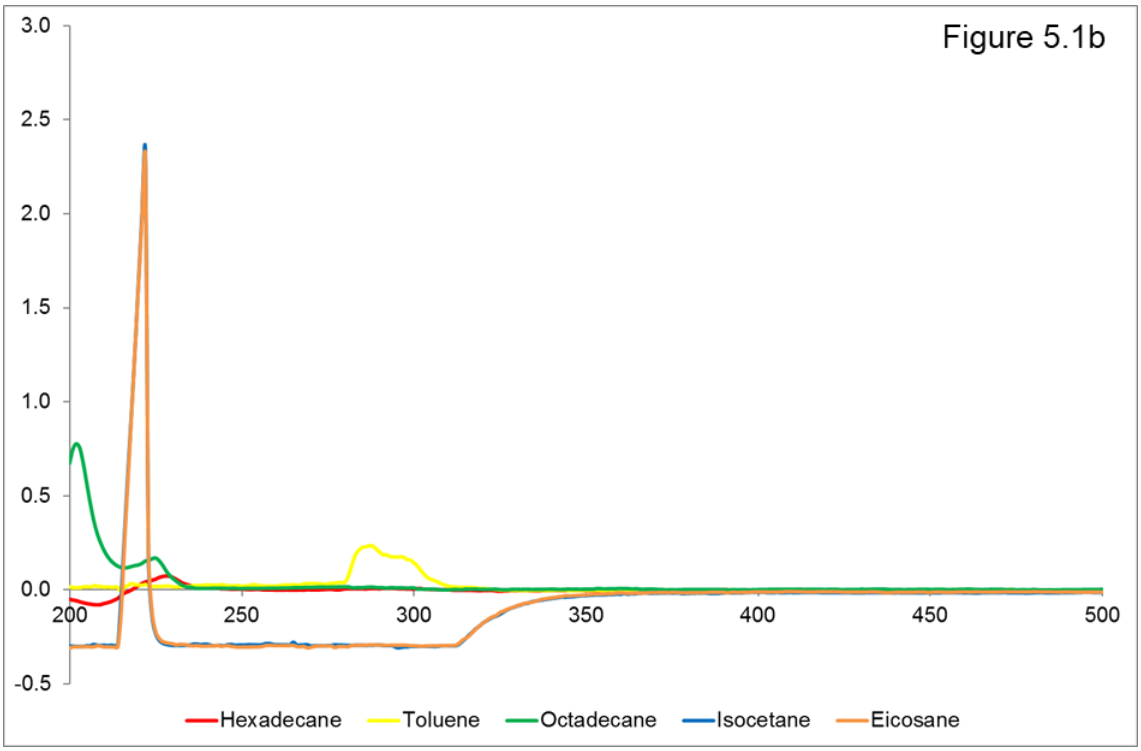

Figure 5.1a – Graph showing the spectroscopic scan of constituent components and WSP blends within solvent heptane. **Figure 5.1b** – Graph showing the spectroscopic scan of pure hydrocarbons within solvent heptane.

Figure 5.1a shows the solubility of constituent components and WSP blends within heptane, figure 5.1b shows pure hydrocarbon materials in heptane. In figure 5.1a LO has the largest peak absorbance around 225 nm, also the largest area under the curve. Other samples showing peaks and areas are WSP10 and WSP11, which have curves that are alike. WSP9 also has an absorbance like WSP10 and WSP11; MWL has a large area with a medium sized peak of 1.5 around 210 nm; finally, HO also shows absorbance at 225 nm of 1.4.

In figure 5.1b eicosane and isocetane have the highest peaks at 225 nm of 2.4. The start of the curve also shows that octadecane has a large area, but small peak. There is also a small peak of absorbance around 275 nm for toluene.

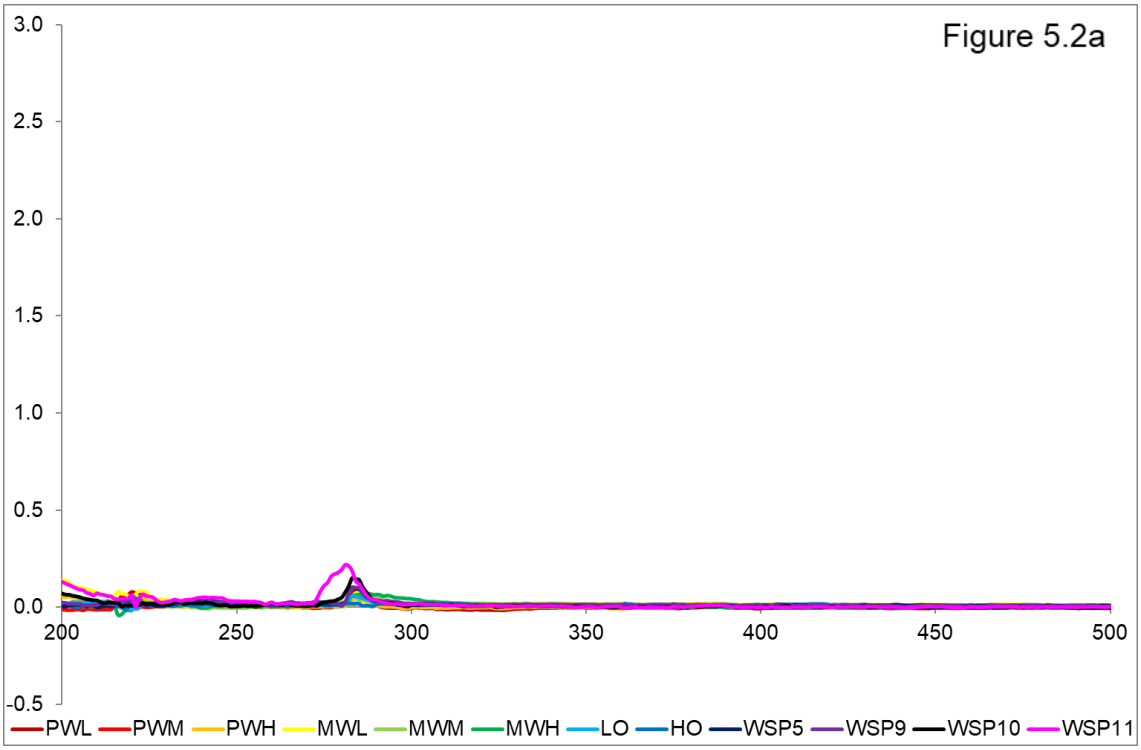

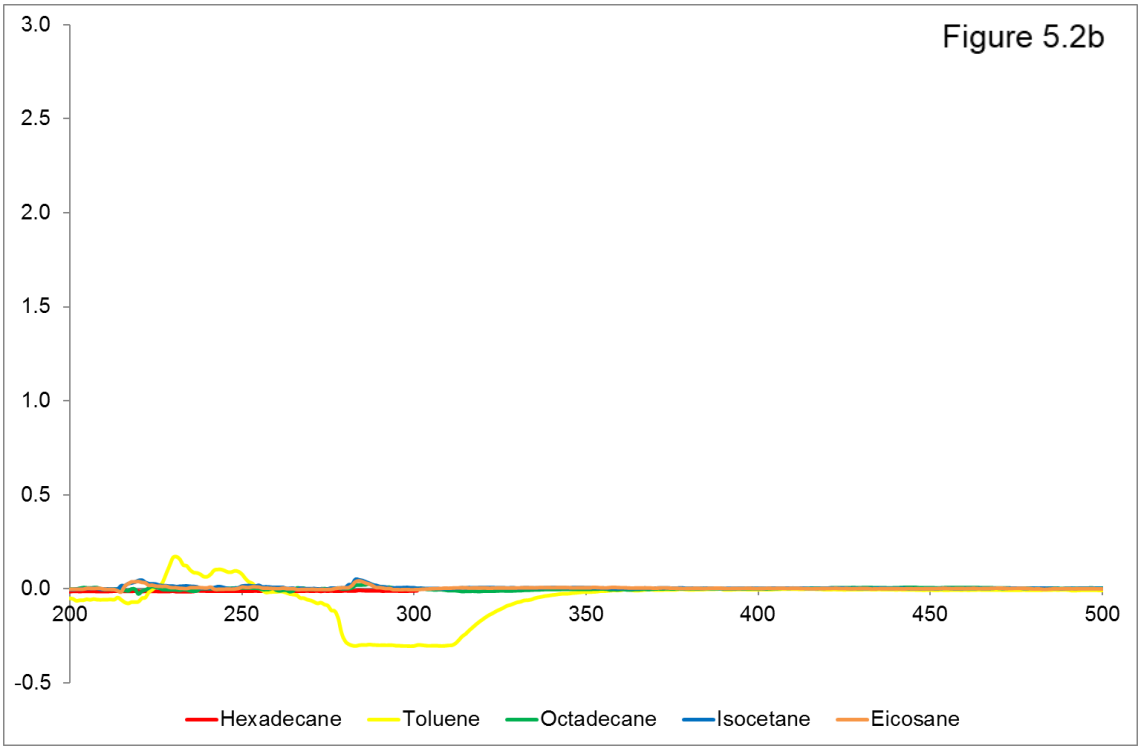

Figure 5.2a – Graph showing the spectroscopic scan of constituent components and WSP blends within solvent toluene. **Figure 5.2b** – Graph showing the spectroscopic scan of pure hydrocarbons within solvent toluene.

Figure 5.2a shows that all samples have little absorbance in toluene. The most soluble in toluene is WSP11 around 280 nm, with other samples showing low absorbance at 285 nm, of which WSP10 shows the next highest peak, of

around 0.2. Figure 5.2b shows that there is no solubility of any pure hydrocarbon in toluene.

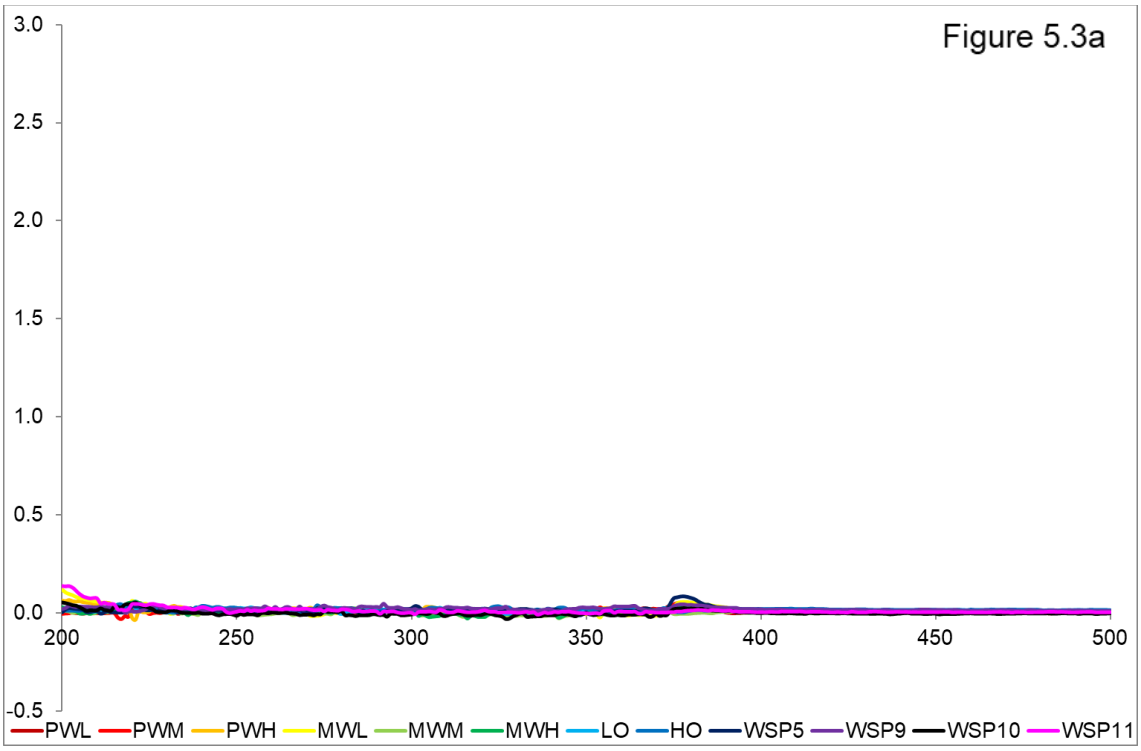

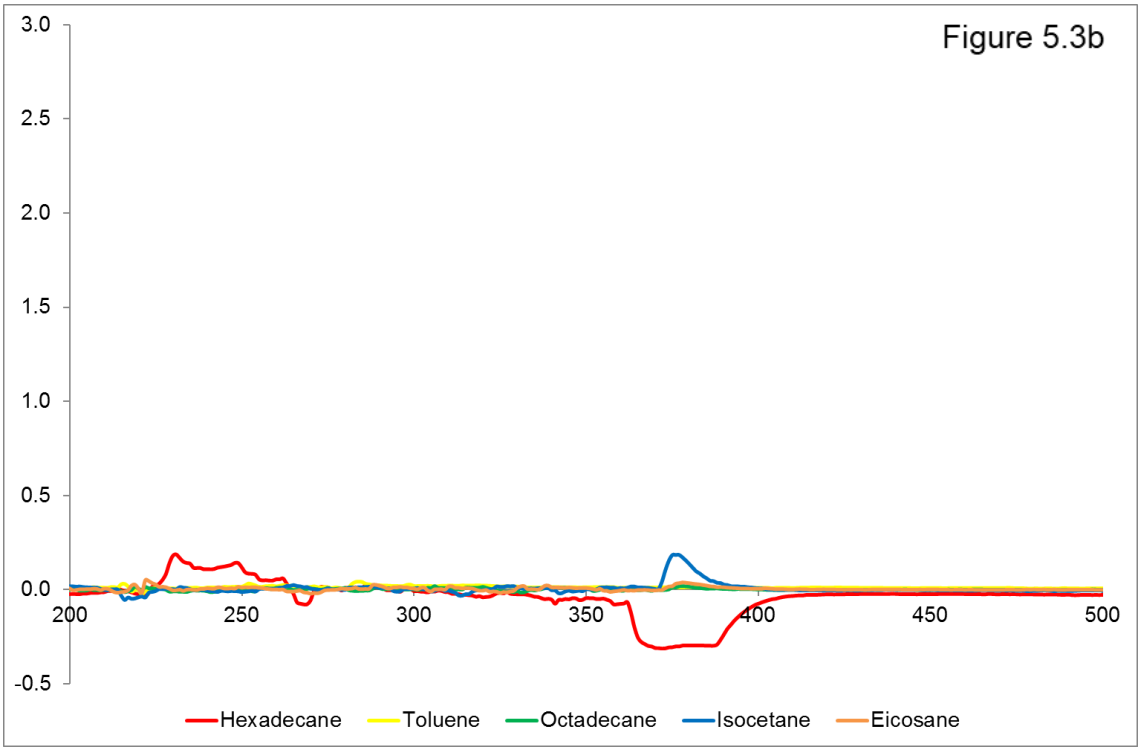

Figure 5.3a – Graph showing the spectroscopic scan of constituent components and WSP blends within solvent carbon disulphide. **Figure 5.3b** – Graph showing the spectroscopic scan of pure hydrocarbons within solvent carbon disulphide.

Figure 5.3a shows that no sample gives absorbance and therefore they have no solubility in carbon disulphide. In figure 5.3b there is a small area peak between 225 nm and 260 nm, also a small absorbance peak at 375 nm for isocetane.

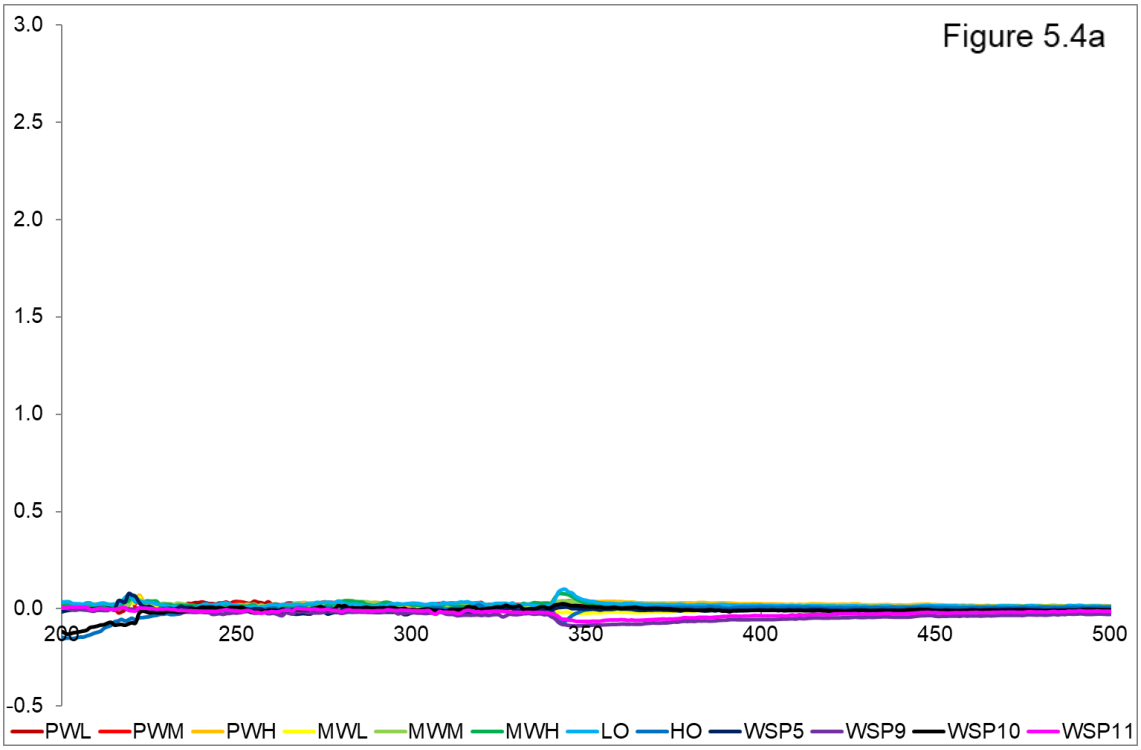

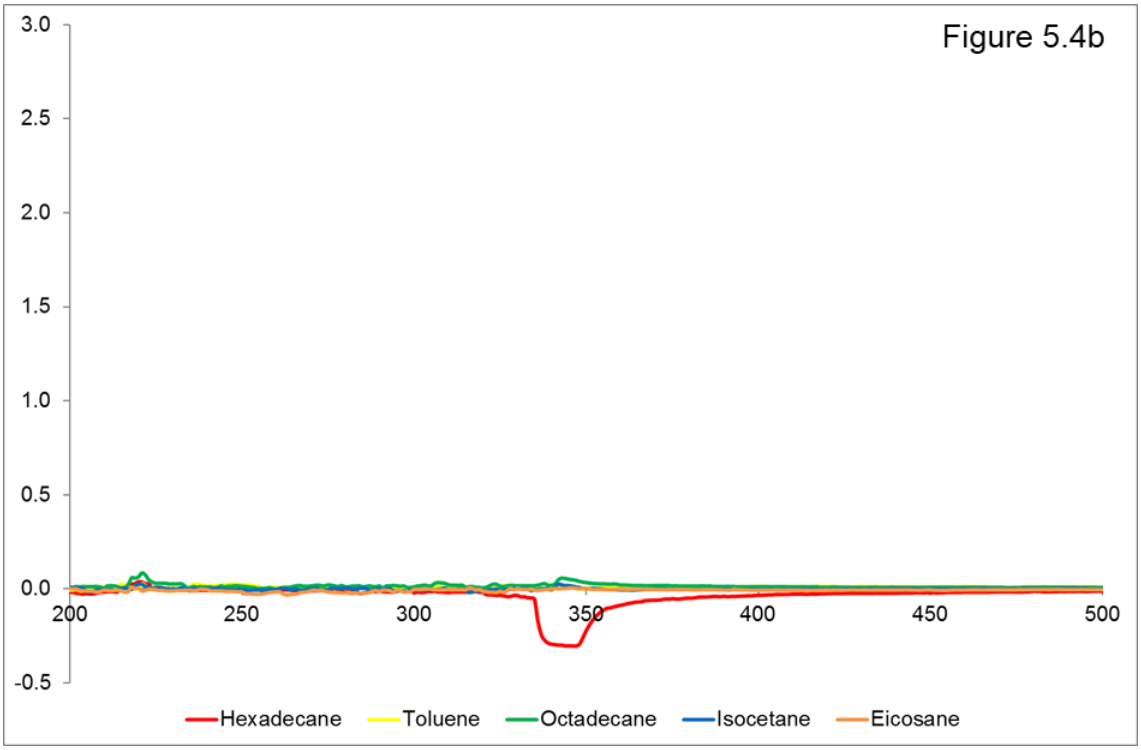

Figure 5.4a – Graph showing the spectroscopic scan of constituent components and WSP blends within solvent 1-chloronapthalene. **Figure 5.4b** – Graph showing the spectroscopic scan of pure hydrocarbons within solvent 1-chloronapthalene.

Figures 5.4a and 5.4b show that there is no absorbance/solubility for WSP blends, constituent components or pure hydrocarbon standards within 1-chloronapthalene.

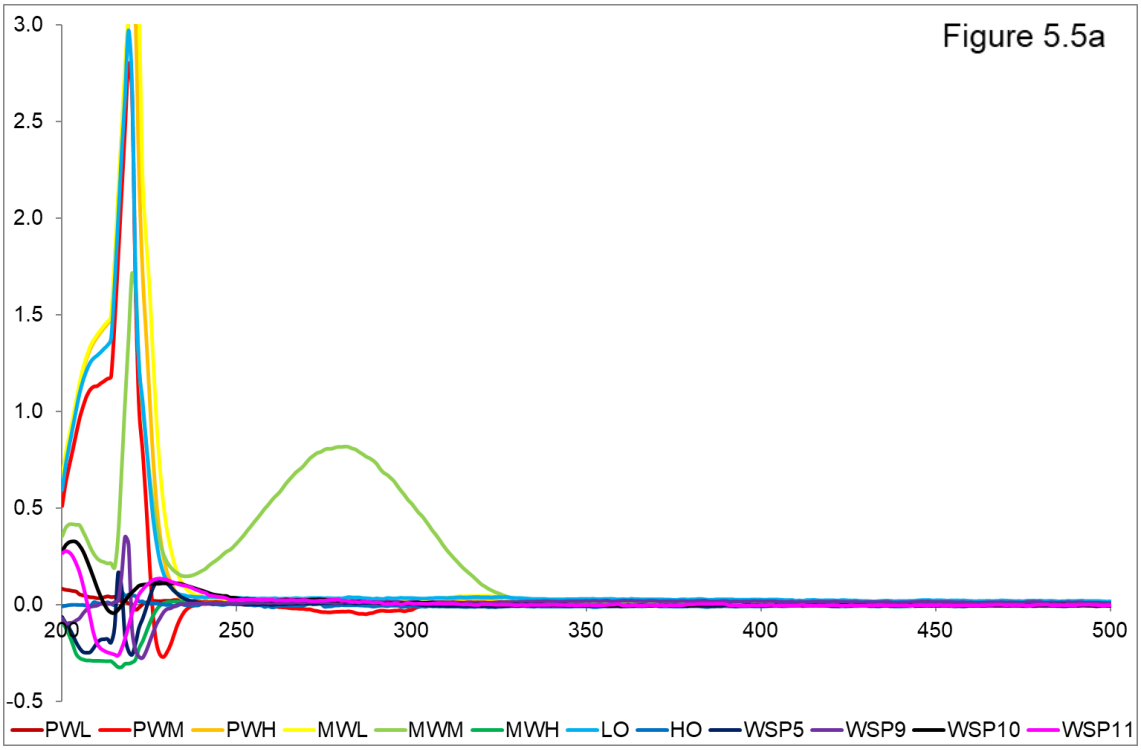

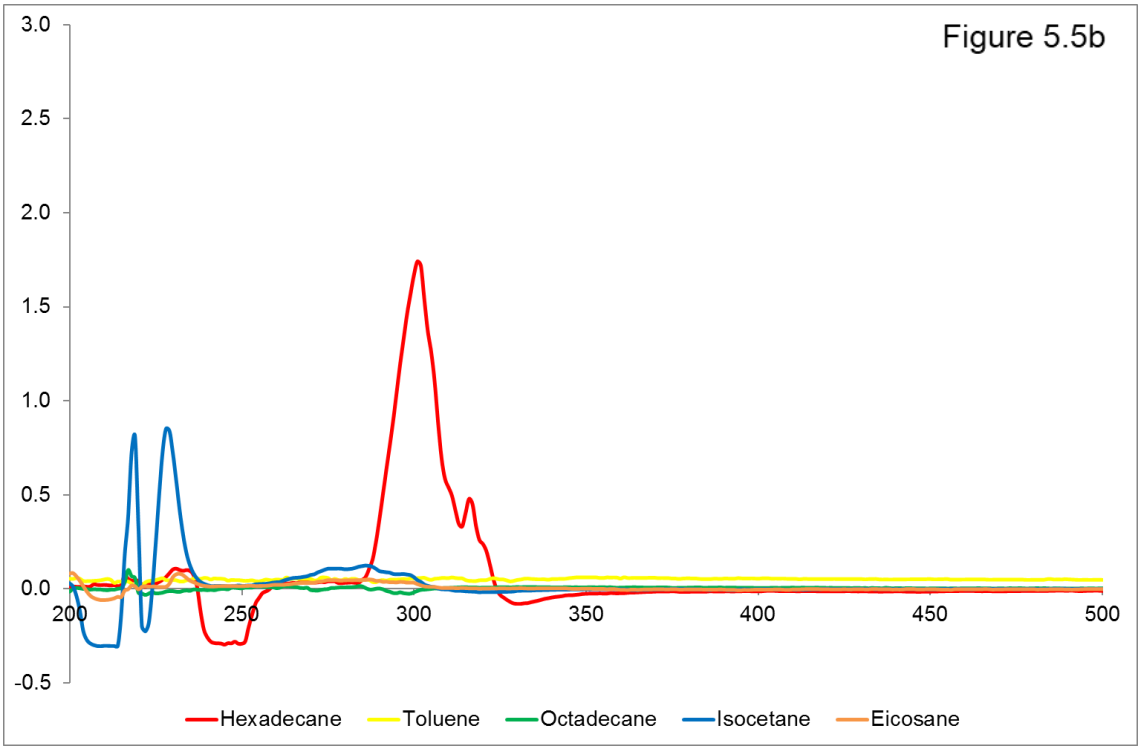

Figure 5.5a – Graph showing the spectroscopic scan of constituent components and WSP blends within solvent decahydronaphthalene. **Figure 5.5b** – Graph showing the spectroscopic scan of pure hydrocarbons within solvent decahydronaphthalene.

Figure 5.5a shows that many samples are soluble in decahydronaphthalene, the highest peak is experienced by MWL, while also

PWH, LO and PWM have high absorbance peaks, MWM also has an absorbance peak at 225 nm, but also has a large second area peak from 230 nm to 325 nm.

Figure 5.5b shows that there is absorbance for isocetane at about 220 nm and 240 nm, there is also a large absorbance peak for hexadecane at 300 nm.

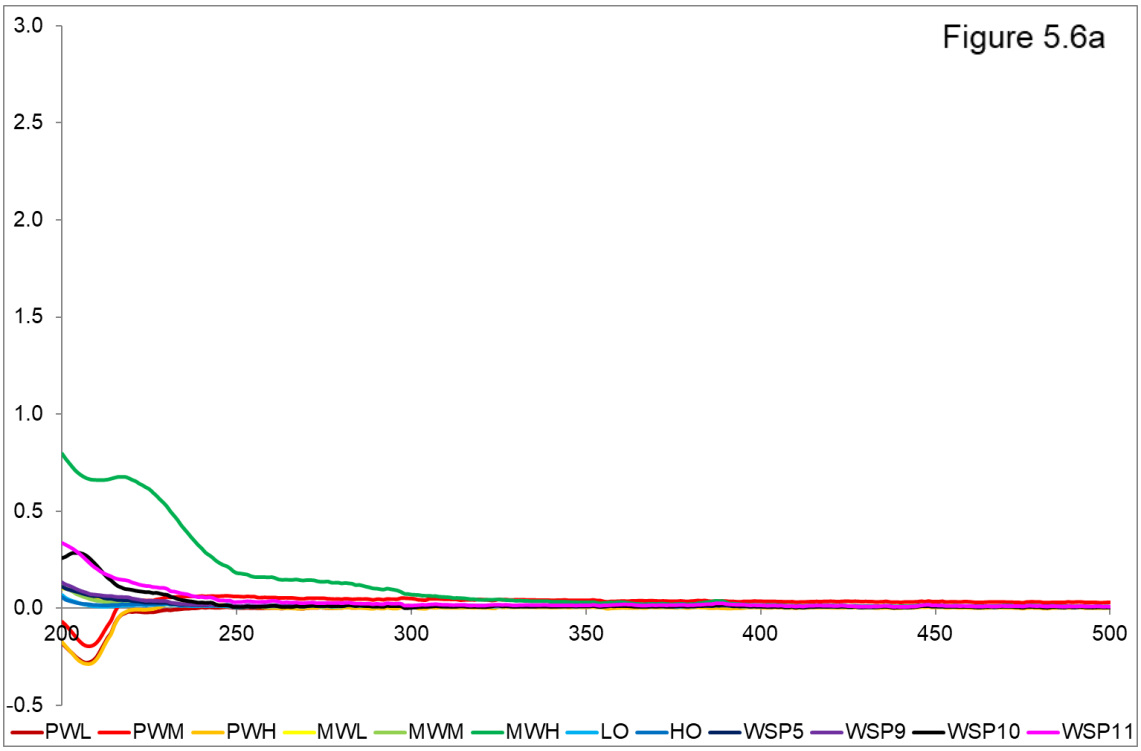

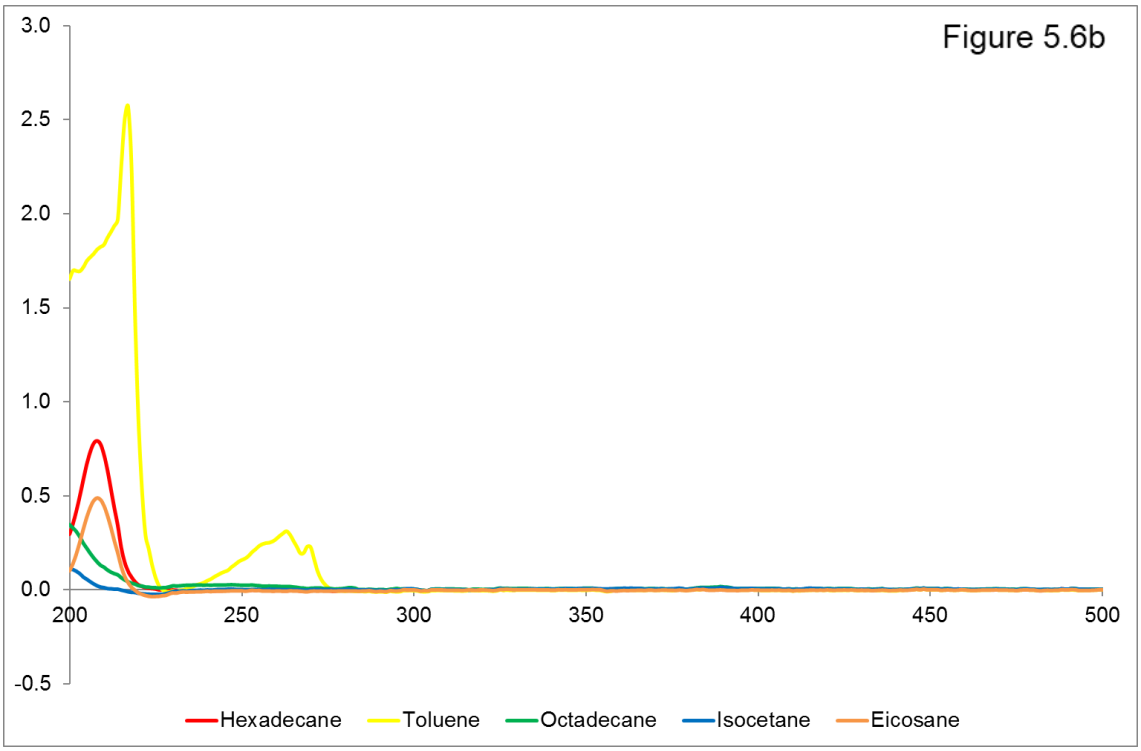

Figure 5.6a – Graph showing the spectroscopic scan of constituent components and WSP blends within solvent acetonitrile. **Figure 5.6b** – Graph showing the spectroscopic scan of pure hydrocarbons within solvent acetonitrile.

Figure 5.6a shows that MWH has the greatest absorbance in acetonitrile, but this is experienced by a wide area peak ranging from before 200 nm to 300 nm. There is also a small peak at the start of the curve for WSP10 and WSP11.

In figure 5.6b there is a large peak experienced by toluene from the start of the curve, peaking at 225 nm with an absorbance of 2.5, then a small secondary peak around 260 nm. There are also smaller peaks experienced by hexadecane and eicosane for solvent acetonitrile.

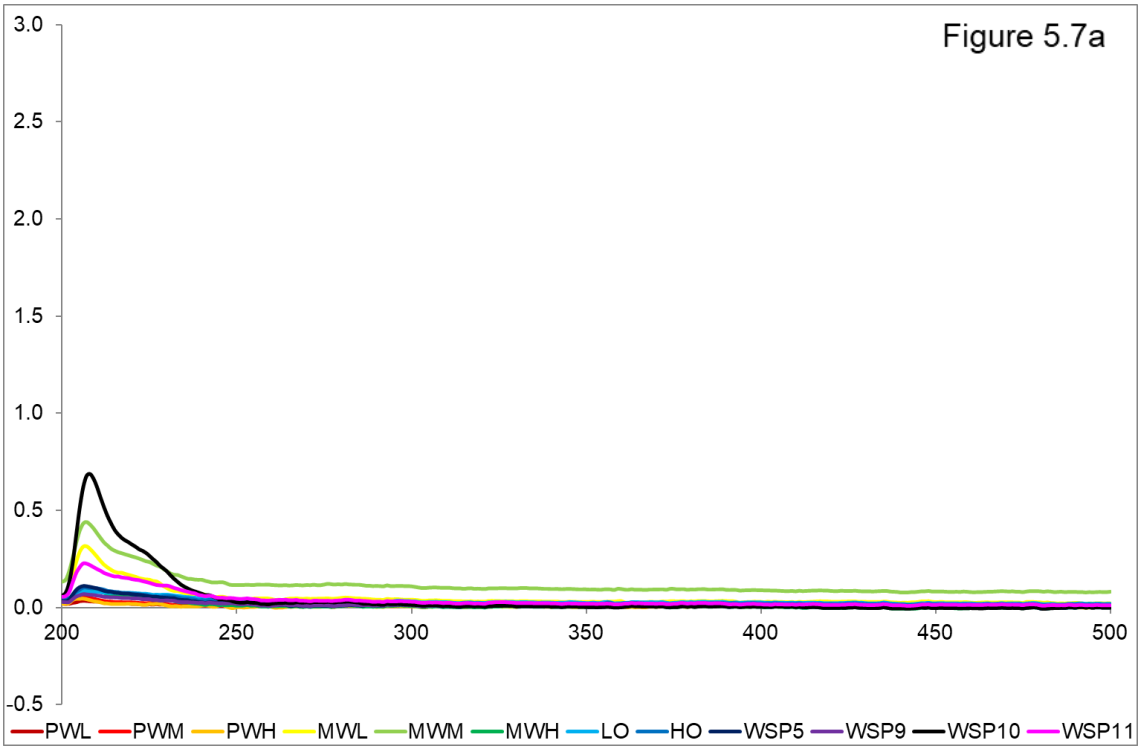

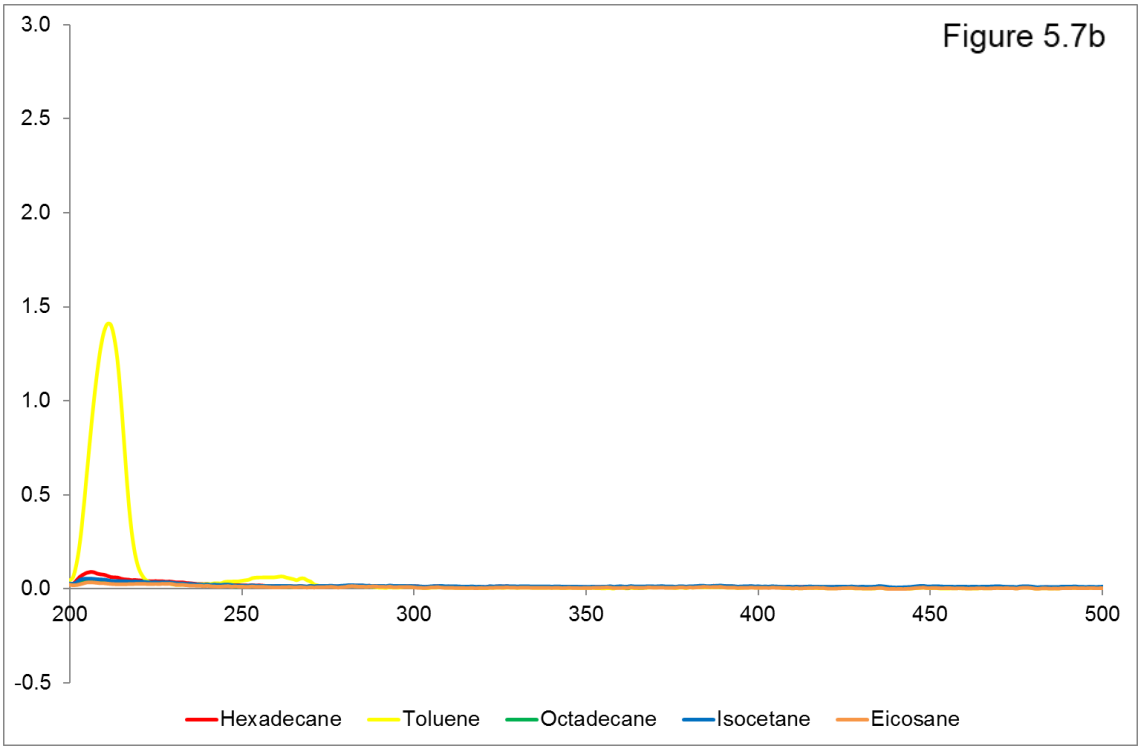

Figure 5.7a – Graph showing the spectroscopic scan of constituent components and WSP blends within solvent diethyl ether. **Figure 5.7b** – Graph showing the spectroscopic scan of pure hydrocarbons within solvent diethyl ether.

Figure 5.7a shows a small peak for WSP10 at 210 nm, with other samples also showing small peaks at 210 nm, those being, MWM, MWL and WSP11.

Figure 5.7b shows one large absorbance peak of 1.5 for toluene at 210 nm but no other peak is soluble in diethyl ether.

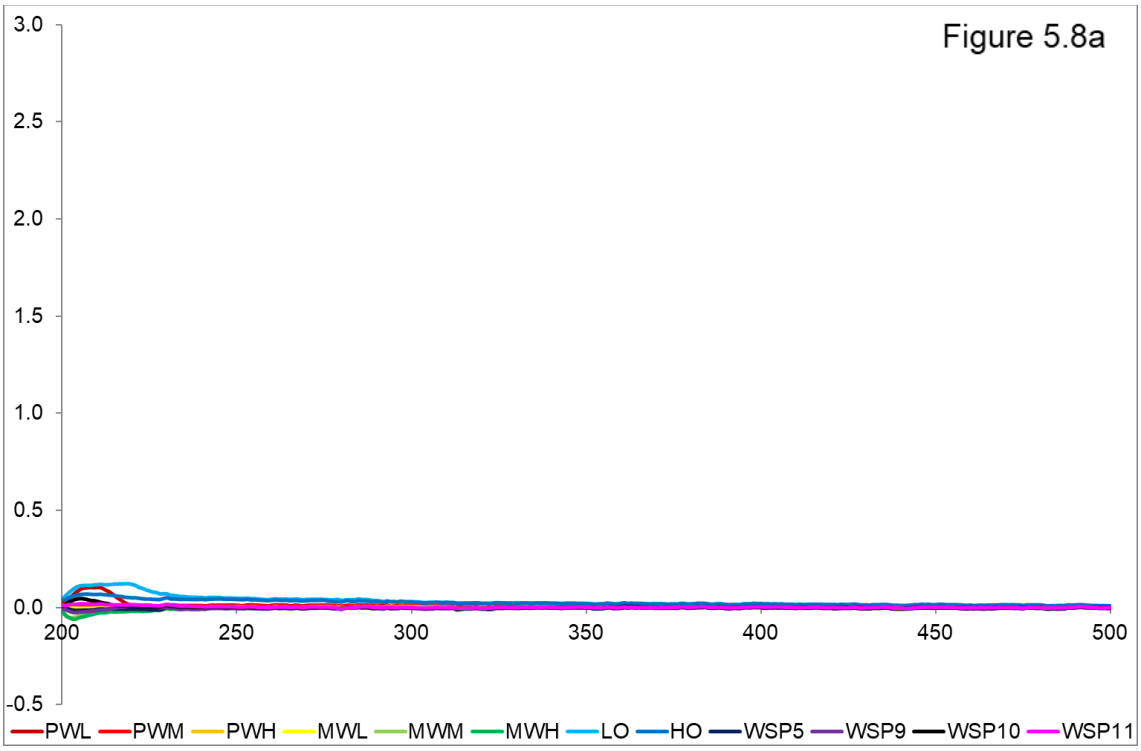

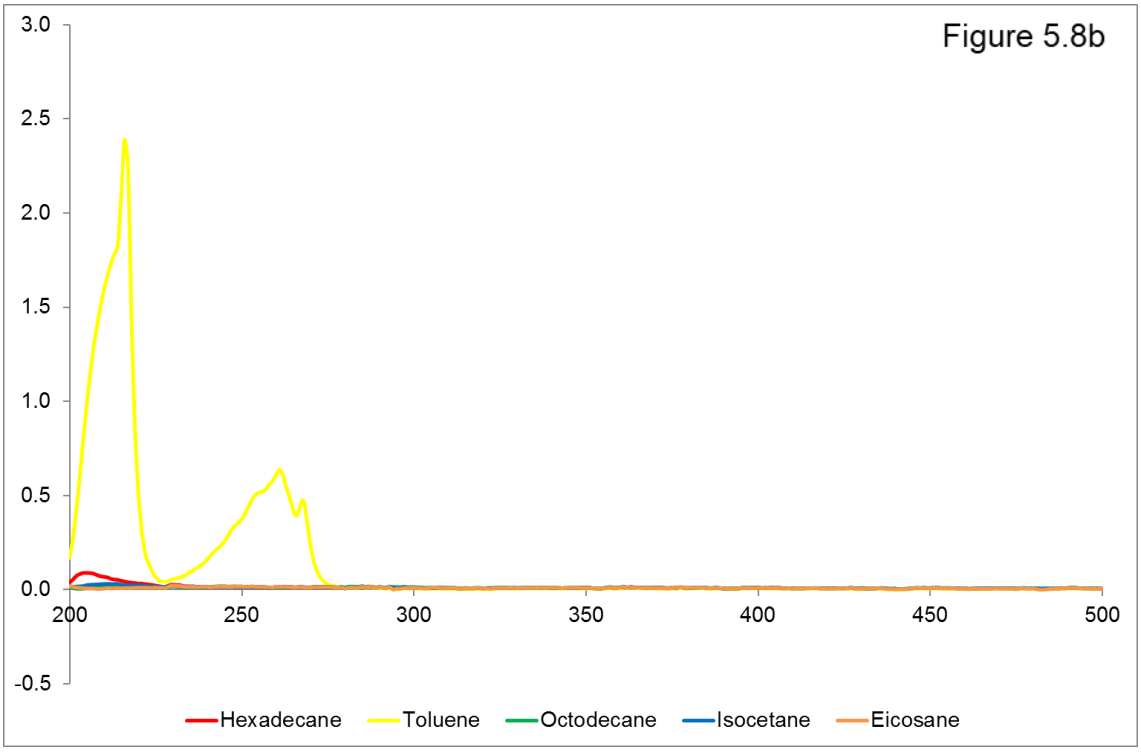

Figure 5.8a – Graph showing the spectroscopic scan of constituent components and WSP blends within solvent methanol. **Figure 5.8b** – Graph showing the spectroscopic scan of pure hydrocarbons within solvent methanol.

Figure 5.8a shows that there is no solubility for WSP blends and constituent components in methanol.

Figure 5.8b shows that toluene experiences large absorbance, with one large peak at 220 nm of 2.5, and a second wider peak between 225 nm and 275 nm.

Taking all these solubility results together, figure 5.9 shows the solubility peaks of WSP blends/waxes/standards as a ratio of the sum of WSP blends/waxes/standards solubility in all tested solvents (equation below).

$$Ratio\ of\ solubility = \frac{Solubility\ absorbance}{\sum solubility\ absorbance\ in\ all\ solvents}$$

PWM, PWH, MWL, MWM, LO, hexadecane and isocetane all have good solubility in decahydronaphthalene. PWL, toluene and eicosane have a small amount of solubility in decahydronaphthalene.

Another notable solvent is heptane, WSP9, WSP10, WSP11, LO, octadecane, isocetane and eicosane all show great solubility in heptane. MWL, HO and WSP5 show good solubility in heptane. PWL and MWM have lesser amounts of components soluble in heptane.

MWH has a very good solubility in acetonitrile, while toluene also shows good solubility in acetonitrile, most samples do not solubilise in acetonitrile.

Another solvent common in all samples is diethyl ether, although solubility is limited for almost all samples, MWM, HO and WSP11 show some signs of solubility, the majority only have small components that dissolve in diethyl ether.

Carbon disulphide and toluene have a common solubility in all samples, however, the solubility is very limited.

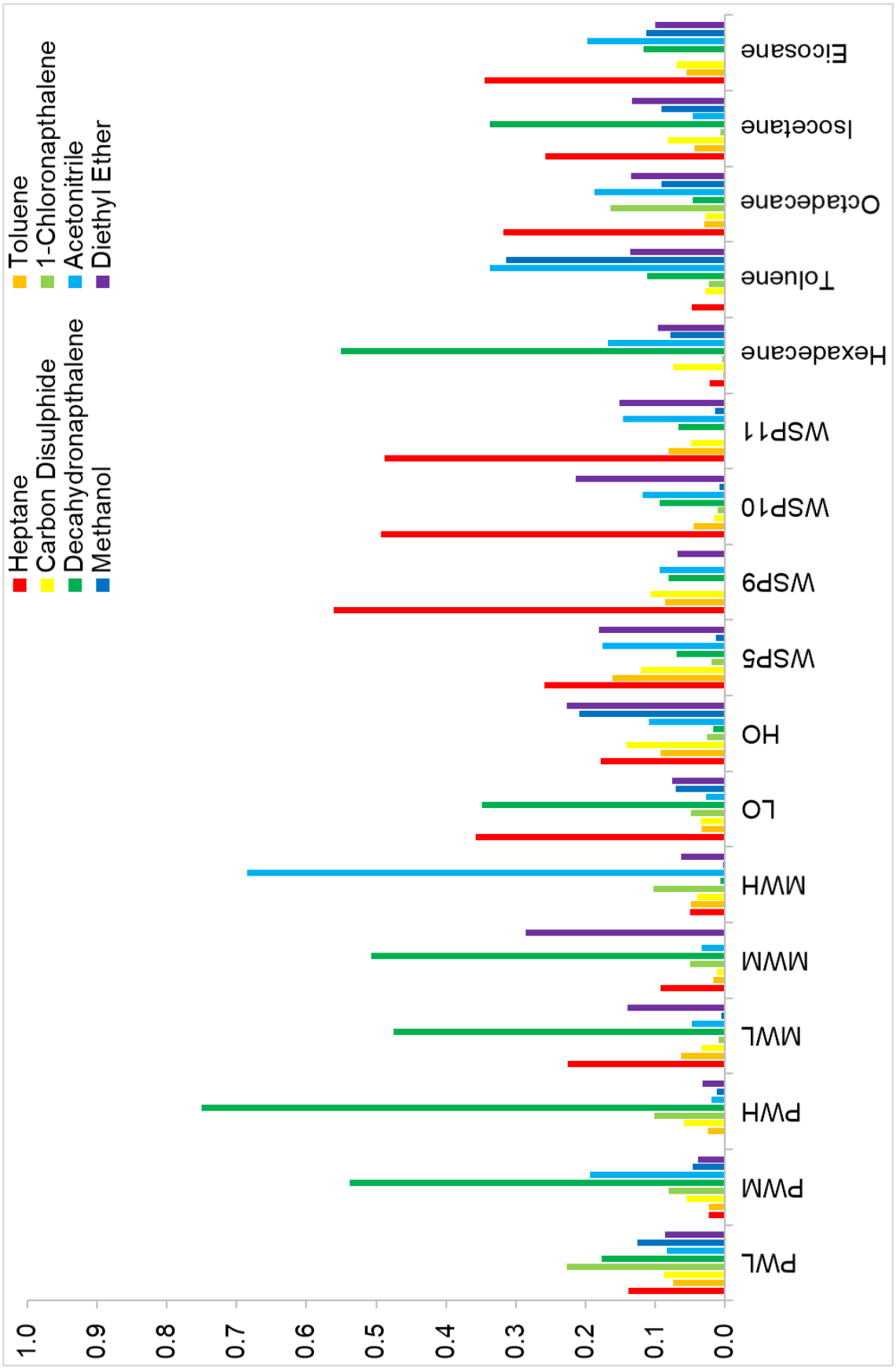

Figure 5.9 – Solubility of constituent components, WSP blends and pure hydrocarbons as a relative ratio of solubility in various solvents for each sample.

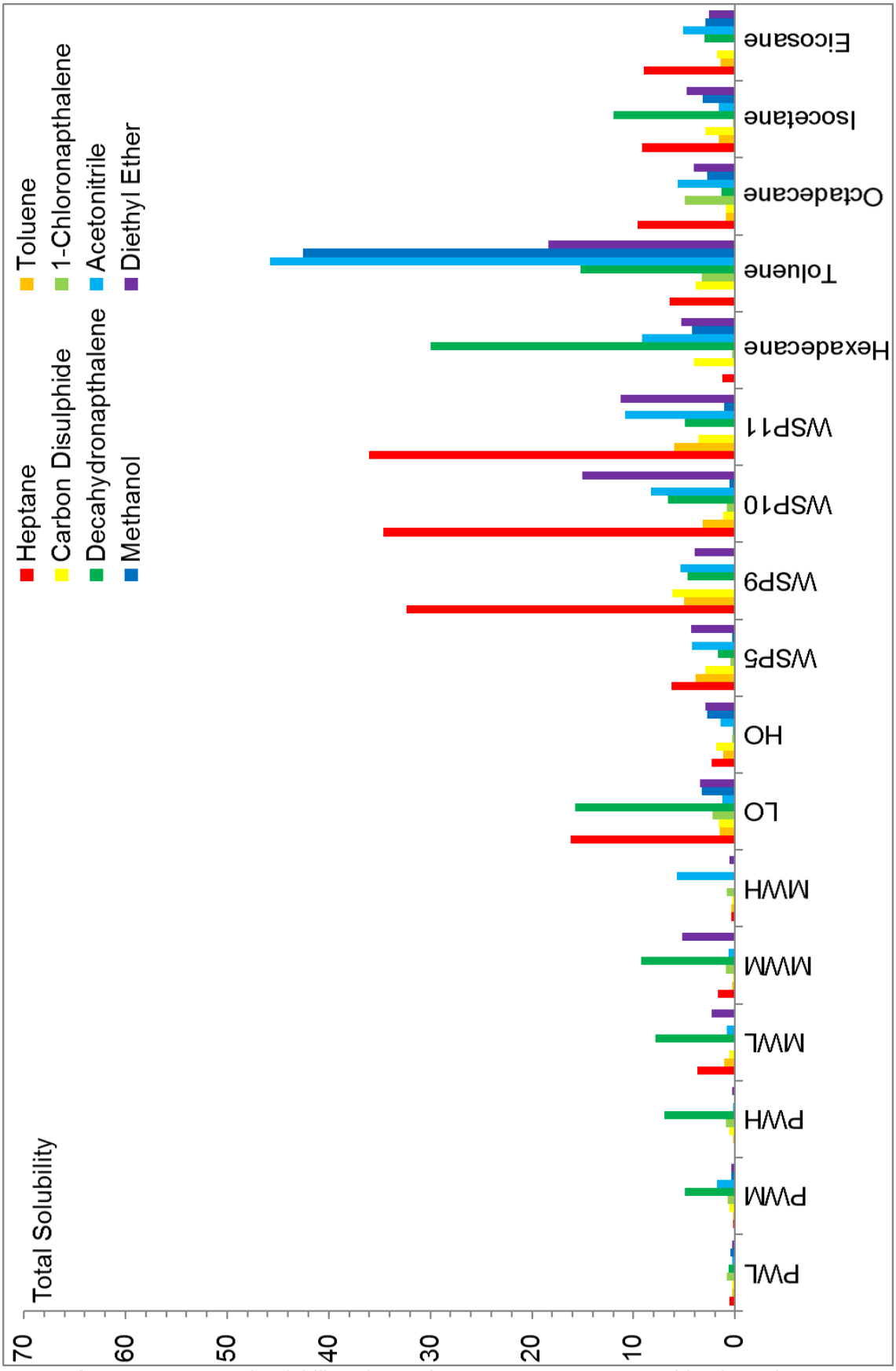

Figure 5.10 – Total solubility of constituent components, WSP blends and pure hydrocarbons. Constituent components have been calculated to show 15 % of the maximum value, as they would contribute to the WSP blends.

Figure 5.10 shows the total solubility of tested samples with the various solvents but re-calculated to represent of their concentrations in the model WSP blends, i.e., 15 % PW, 15 % MW and 35 % of the two oils LO and HO.

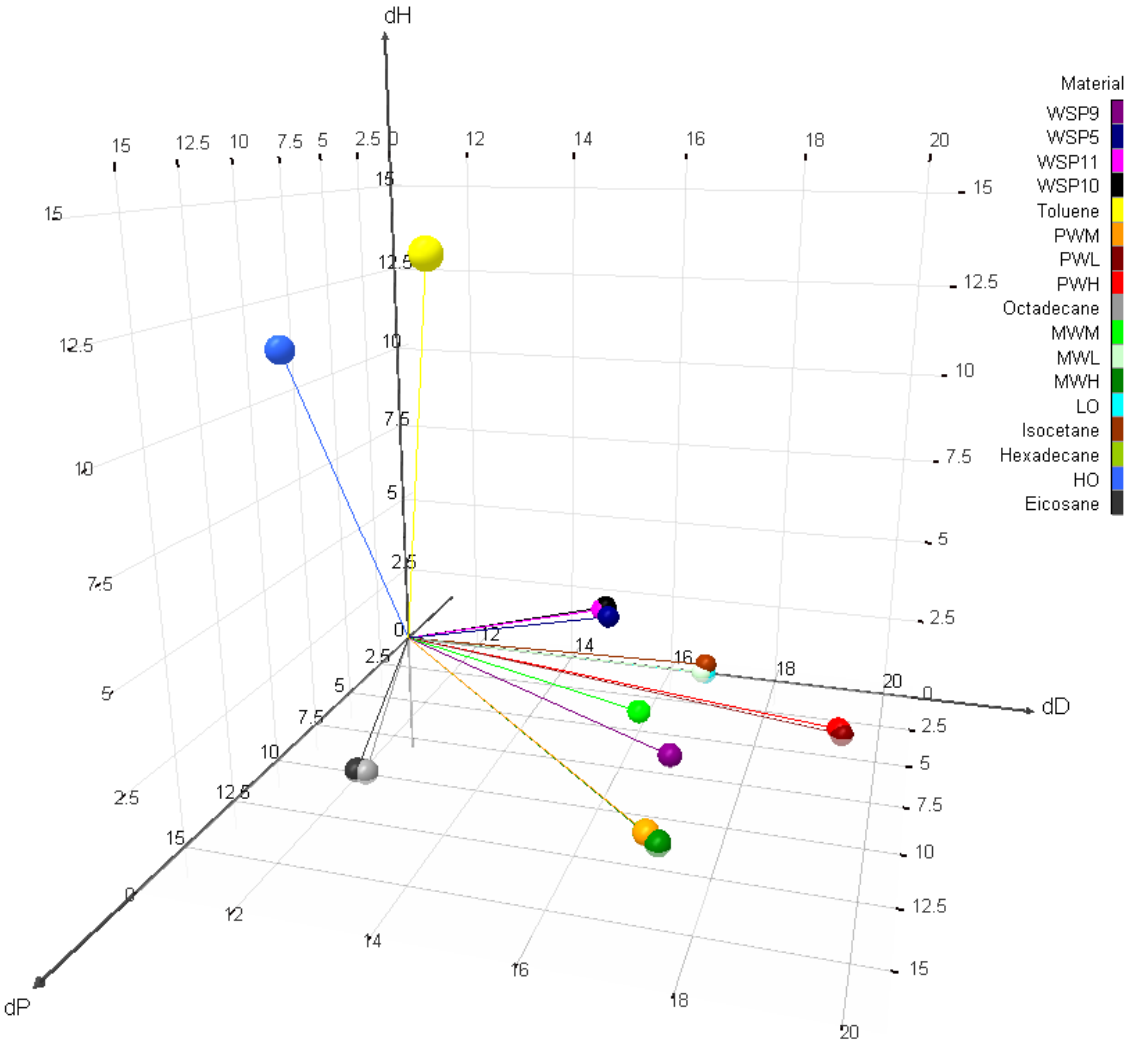

Figure 5.11 – Plot of results of HSP for constituent components, WSP blends and pure hydrocarbons.

Figure 5.11 shows that there are two outlying materials, toluene and HO, while other materials are spread across the plot, there are some groups formed by samples. Eicosane and octadecane group together, PWM, MWH and hexadecane group together, PWL and PWH group together, WSP9, MWL and isocetane group together and WSP11, WSP10 and WSP5 group together.

5.1.4 Discussion

In chapter 4 it was observed that the DSC thermographs of the WSP blends showed little rational similarity to the thermographs of the individual components considering their concentrations in the blends. This was supposed as being due to the components dissolving in each other, which radically affected

the temperature and energies of the phase transitions. Consequently, this also made it impossible to interpret the thermograms of the commercial blends and make any firm conclusions about their probable composition. For this reason, it was therefore of interest to try and quantify the solubility of these varied materials, as described above.

Figures 5.1 – 5.8 show the absorbance in various solvents and figure 5.9 shows the ratio of the peak heights for individual solvents to the total peak heights for all solvents for that said sample. Figure 5.10 scales down peak heights in proportion to the 15 % concentration of the wax components and 35 % of the oil components in the model blends.

Despite the wide range of solvents used, few showed solubilizing power for the constituent components of the WSP blends and pure hydrocarbons. For the constituent components, decahydronaphthalene was the best solvent, seen in figure 5.4a, PWM, PWH, MWL, MWM and LO show the greatest solubility in decahydronaphthalene. Of these samples, the λMAX is ≈ 220 nm, MWM also has a secondary absorbance peak with a λMAX ≈ 280 nm. Considering figure 5.9 the peak absorbance of MWM in decahydronaphthalene is misleading as here MWM has the highest solubility of material, however, λMAX is ≈ 220 nm but has the largest absorbance of material up to ≈ 325 nm. Decahydronaphthalene is a double ringed cyclic hydrocarbon ($C_{10}H_{18}$) and it is likely that there are similar cyclic components within the waxes, especially those from the MW family, as MW contains greater branched and naphthalene components. Decahydronaphthalene is also a solvent of high dispersion force (δd = 18), is a hydrocarbon similar in chemical nature to those samples being tested and as previously stated like materials are generally better at dissolving like materials. Decahydronaphthalene is also a compound of relatively high molecular density allowing for greater energy forces for the size of the actual compound, compared to other hydrocarbon compounds such as heptane a short straight chain hydrocarbon.

Other solvents that dissolve constituent components are acetonitrile and diethyl ether. Acetonitrile dissolves many components within MWH, seen in figure 5.6a, as the area peak of absorbance reaches 300 nm. Diethyl ether dissolves MWM well for some reason, seen in figure 5.7a, when compared to

other samples tested with diethyl ether, however, compared to other solvents does not perform as well.

According to Hansen, decahydronaphthalene has solubility parameter interaction values δ_d (dispersion forces) of 18.0, and δ_p (intermolecular forces) and δ_h (hydrogen bonds) = 0.0. These values explain how the large component of dispersion interaction will be attracted to hydrocarbon compounds within the waxes of high molecular weight.

For acetonitrile, there is a peak experienced for MWM, with a large area indicating a proportion of MWM being dissolved by acetonitrile. Hansen (Barton, 1975) gives acetonitrile solubility parameters of 15.3 for δ_d, 18.0 for δ_p and 6.1 for δ_h . This shows that a small part of dispersion interaction is occurring with the hydrocarbon content of waxes. However, figure 5.6a shows there is a relatively small absorbance peak height compared with decahydronaphthalene in figure 5.4a and this makes sense when considering polarity forces of the two solvents. Toluene has a strong peak with a λMAX ≈ 220 nm, while hexadecane and eicosane have smaller absorbance peaks, each with λMAX ≈ 215 nm. Acetonitrile's much greater polar force component δ_p and a dispersion force component δ_d explain the high affinity for toluene, due to its aromatic ring plus methyl side-chain. The smaller peaks for hexadecane and eicosane are attributed to the hydrocarbon structure and dispersion force component of the solvent.

For the WSP blends the best solvent observed is heptane which is seen in figure 5.1a and figure 5.9. Considering figure 5.1a WSP9, WSP10 and WSP11 all show the same curve with a λMAX ≈ 220 nm, WSP5 is also soluble in heptane, however, has a much smaller soluble component, with a peak absorbance ≈ 225 nm, this also collaborates in figure 5.9.

There is a component of absorbance recorded for MWL with a peak absorbance of ≈ 215 nm indicating that there is a component of lower molecular weight hydrocarbon contained within MWL, which would be expected due to the lower congeal point of the MW.

The absorbance peaks for WSP blends in figure 5.1a are less pronounced compared to those for the individual waxes, as seen in figure 5.4a, as might be expected due to their lower concentration in the blends.

In figure 5.2a, the absorbance curve of toluene shows that there is a small component of WSP11 soluble in toluene, with a λMAX ≈ 260 nm. There are also many other small peaks for other samples around the same wavelength. This could indicate an error in the measurement of the samples due to the regular appearance of an absorbance peak at the same wavelength for all samples tested when similar trends have not been noticed in other solvents.

The pure hydrocarbons tested show that isocetane and eicosane have large absorbance peaks with λMAX ≈ 220 nm, octadecane has a small absorbance peak, with a λMAX ≈ 205 nm, there is finally a small peak recorded for toluene with λMAX ≈ 290 nm. The data indicate that heptane is a good solvent for dissolving pure hydrocarbons, especially high molecular weight hydrocarbons. Heptane also seems able to dissolve both branched and straight chain hydrocarbons, isocetane and eicosane respectively. Toluene is generally not a good solvent for these compounds.

Carbon disulphide shown in figure 5.3b shows a small absorbance for isocetane with λMAX ≈ 375 nm. Carbon disulphide has solubility parameters of 20.5 for δ_d, 0.0 for δ_p and 0.6 for δ_h and is a poor hydrogen bonding solvent (Barton, 1975), this could explain the small affinity for isocetane which is a highly branched methyl compound.

Figure 5.4b shows that hexadecane and isocetane are soluble in decahydronaphthalene. Isocetane and hexadecane are both $C_{16}H_{34}$ hydrocarbons, isocetane being branched and hexadecane being straight chained. With decahydronaphthalene having a δ_d of 18.0 this will allow for greater interaction such as weak Van der Vaal forces (London dispersion forces) between these hydrocarbons and the solvent.

There are small peaks also experienced by the other samples with λMAX ≈ 220 nm and ≈ 230 nm, however, these peaks are not comparable to the other samples.

In figure 5.7b and 5.8b, diethyl ether and methanol respectively, the only sample to dissolve is toluene. Is diethyl ether and methanol absorbance λMAX ≈ 215 nm, in methanol the absorbance peak is stronger than in diethyl ether, as well as there being a second absorbance peak of λMAX ≈ 260 nm. Methanol is a strong hydrogen bonding solvent with 15.1 for δ_d, 12.3 for δ_p and 22.3 for δ_h but also has other multiple components available to interact with toluene, therefore making it overall a good solvent to interact with toluene based on the multiple chemical interactions that can be made.

For figures 5.1 – 5.8 show that there are not only changes in absorbance based on the different solvents being used but also changes in the peaks of the similar solvents for different samples, even though similar in chemical nature. The reasoning for this can be due to absorption and intensity shifts explained by (Sharma, 2007), based on the interaction of an auxochrome with the tested sample material. An auxochrome is a molecule that does not itself act as a chromophore, influencing energy absorption, however, will interact with the sample causing its chromatic effect to be changed. Shift types include; bathochromic, increasing λMAX; hypsochromic, decreasing λMAX; hypochromic, decreasing absorbance and hyperchromic, increasing absorbance.

Figure 5.9 shows a ratio of solubility for materials based on the total solubility of all solvents used. Notably, for MWH, there is a large soluble component in acetonitrile, small components of PWM are also soluble in acetonitrile. Although present in the component material, there is a small component of material that is also soluble within the WSP blends, both model (WSP5/WSP9) and commercial (WSP10/WSP11). From previous chapters, it has been found that MWH is a material with a high melting point, therefore, it is likely that the component soluble in acetonitrile in MWH is also present in the WSP blends and is contributing to increasing their melting point values.

Another component with strong ability to solubilise materials is decahydronaphthalene, which is found to dissolve PWM, PWM, MWL, MWM and hexadecane, there is also an amount of LO found to be soluble with decahydronaphthalene. The solubility in hexadecane implies that a component of the solvent has an affinity to straight chain hydrocarbon materials, which would

be expected to be found within the waxes of lower melting points and oil materials.

Heptane is also shown to heavily influence the solubility of materials, especially within the WSP model and commercial blends. Within the materials, heptane does not act as a strong solvent. There is a small amount of PWL soluble, as well as MWL, heptane shows most affinity with oil like materials, especially LO. PWL and MWL are most like oil materials due to their lower melting points. The affinity for low melting point materials is also shown in the WSP blends, which also show high affinity for heptane.

Figure 5.11 shows the plot combining δ_d (dispersion forces), δ_p (intermolecular forces) and δ_h (hydrogen bonds) for all the materials, the two materials that show high hydrogen bonding forces are toluene and HO. Theoretically, this should not be the case for toluene, and according to the HSP database toluene has a much lower value than recorded, as such it is most likely the lack of testing solvents has cause errors in this result.

The combination of WSP5, WSP10 and WSP11 is encouraging, as with other results, figure 5.9, there is a great similarity between these samples and indicates that chemically these WSP blends are alike based on soluble components.

Interestingly WSP9 does show as an outlying sample, however, considering the makeup of WSP9, PWH and MWH it could be given that WSP9 does fall between the two waxes in solubility terms from figure 5.11. It can also be seen that there is a correlation in WSP5 and its constituent components, PWL and MWM, where WSP5 appears to fall between these waxes, however, showing slightly increased hydrogen bonding force affinity, but this could be due to the HO content, showing very strong δ_h affinity.

Overall grouping in figure 5.11 is good evidence of solubility in materials, and combinations are what would be expected from previous known chemical knowledge, with toluene being one outlier that was unexpected, it is possible a greater number of solvents would be required, to be able to spread the solvent interactive forces needed for HSP.

5.1.5 Conclusions

- Most of the wax samples tested contain components that are most compatible (i.e., soluble in) decahydronaphthalene, most likely due to the higher molecular weight and double ring structure of this solvent.
    - The double ring structure will increase the dispersion force interaction possibilities, improving solvent interaction with similar type materials.
- WSP blends have better solubility in lower molecular weight solvents with medium dispersion force strength.
    - Likely due to solvents used in this body of work having great efficiency and having a greater and equal spread of solubility parameters between δ_d (dispersion forces), δ_p (intermolecular forces) and δ_h (hydrogen bonds).
- Heptane is a better solvent for WSP blends and pure hydrocarbon materials, suggesting a high content of such materials in the blends (probably due to the oils). The shorter chain solvent will be like components within the WSP blends.
- A wider range of solvents would be needed to pin down 'true' values of compound solubility, especially ones of different hydrogen bonding strength, though it is not clear what solvents these should be.
    - At least six of strong, medium and weak hydrogen bonding solvents are required for a better representation of solubility parameters
    - Solvents with differing intermolecular forces are also required to be able to feed into Hansen solubility models.
- Group combinations of HSP testing show good correlation for WSP model blends, for like materials, WSP5, WSP10 and WSP11.
- Combination of wax materials to equate to WSP model blends also shows good correlation, as WSP fall between the wax components.
- The use of a calibration curve for the solubility absorbance would be advisable in future investigations.
    - Without knowing the molar concentration of unknown substances, the concentration of a substance in solvents can be calculated by measuring the absorbance of increasing sample amounts in solvents.

5.2 Raman Spectroscopy

5.2.1 Introduction

Raman spectroscopy was used to try and gain more information about the specific chemical structures and make-up of the WSP commercial samples and constituent components of the model WSP blends.

Previous authors have used Raman spectroscopy to help characterise paraffin waxes (Mian et al., 2014; Zheng and Du, 2006; Clavell-Grunbaum et al., 1997; O Faolain, 2005; Anghel et al., 2014) and microcrystalline waxes (Edwards and Falk, 1997). As previously described, (Chapter 1), Raman spectroscopy is a method of vibrational spectroscopy allowing identification of molecules and their structure. Methods of Raman spectroscopy have been detailed previously (Larkin, 2011; Lide, 2003) and it has been shown that the use of Raman is best suited for hydrocarbon non-polar molecules such as the paraffin and microcrystalline waxes studied here. Furthermore, according to previous work (Zheng and Du, 2006), the identification of multi-component paraffin waxes is possible, with the identification of phase behaviour being apparent within Raman spectroscopy scans. Raman spectroscopy is often used as a fingerprint method for chemical analysis as it gives the information of vibrational patterns for molecules. Since the pattern for each molecule is unique, it is possible to single out the molecules, and their group contributions within certain materials, such as within the WSP blends and those supplied as a commercial pharmaceutical grade.

It has been proposed, with the use of Raman spectroscopy, molecular compounds would be identified and could show differences in macrocrystalline wax and microcrystalline waxes. If these differences could be identified it could also be possible to identify these compounds within the WSP blends. If these compounds could be identified in the WSP then a fingerprint method of detection can be proposed to identify quality issues within WSP blends of required characteristic.

5.2.2 Materials and Method

Raman spectroscopy was carried by the SSPC group in Ireland, School of Chemistry, National University of Ireland, Galway, University Road, Galway,

Ireland. To carry out the experiment a Renishaw InVia Raman Microscope was used, with a 785 nm laser, taking 4 acquisitions, with 10 s exposure time, and at an x20 zoom, scans were carried out between 100 – 3600 cm^{-1}. The following techniques were implemented with this equipment. To determine molecular and crystal vibrations a µ-RS (Micro-Raman Spectroscopy) technique was used with a solid, liquid (1 µm – 1 cm) samples preparation, a line in of liquid laser beam, e.g. Ar-line to determine a Raman spectra observation, with a depth of 0.5 µm and a lateral resolution of 0.5µm (Long, 1977; Brame and Graselli, 1976; Turrell, 1972). Also carried out was a CARS (Coherent Anti-Stokes Spectroscopy) technique to be able to obtain data of high resolution Raman spectra, sample preparation was for a solid, liquid (50 µm – 3 cm) sample, with a line in of a pump beam (ω 0) + and a probe beam (ω 5), the resulting data gave an Anti-Stokes spectrum (Turrell, 1972).

5.2.3 Results

Raman spectra were produced for samples PWL, PWM, PWH, MWL, MWM and MWH. Figure 5.12 shows a spectrum of all samples over the total Raman shift spectra, while further figures show a breakdown of individual identified peaks.

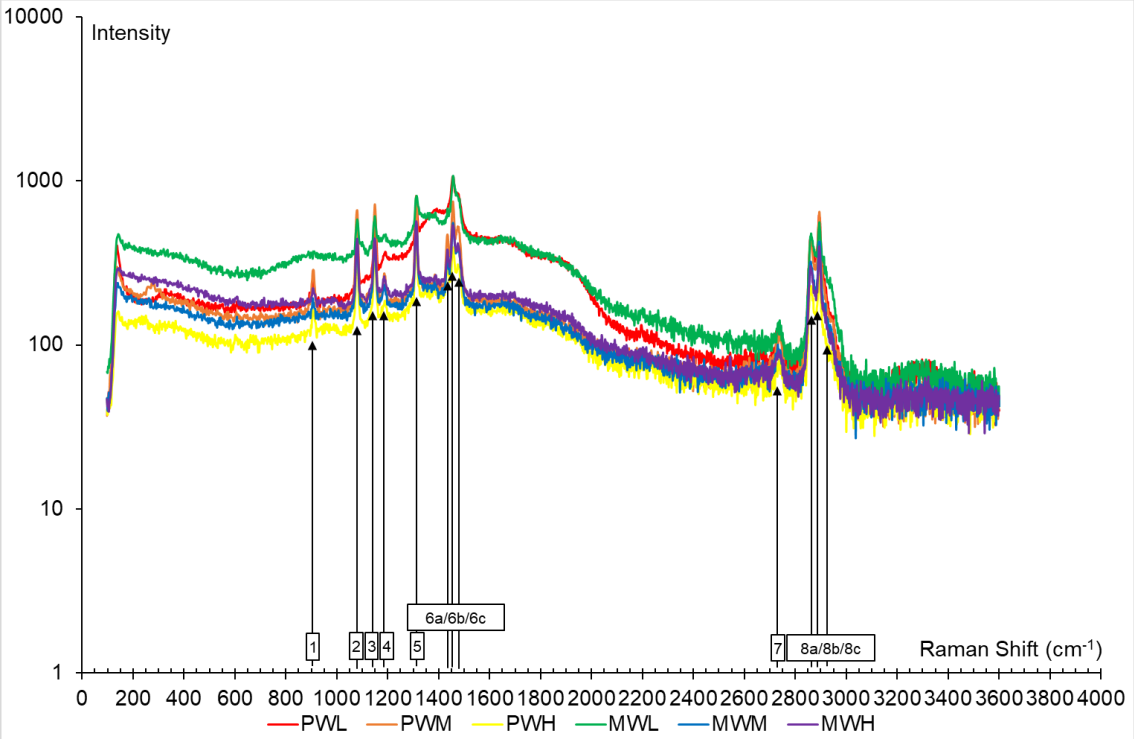

Figure 5.12 – Graph showing the Raman spectra for samples PWL, PWM, PWH, MWL, MWM and MWH.

Figure 5.12 shows the total spectrum for all constituent components contained with the WSP blends produced within the lab. Figure 5.12 shows that there are multiple peaks, some of these peaks are contained within a larger Raman band, as such, the lager Raman band will be denoted 8 and individual peaks contained within will be named Xa, Xb, Xc, etc.

In terms of general observations, overall MWL has a greater intensity up to wavenumber 2800 cm^{-1} and although it gives similar peaks as the other samples these tend to be less distinct. Also, for PWL the intensities begin to increase from 1020 cm^{-1} starting a large peak range that concludes at 2600 cm^{-1}. This peak increase shows the same intensity as MWL. It is seen that at higher wavenumbers (> 2200 cm^{-1}) there is a larger amount of noise for all samples.

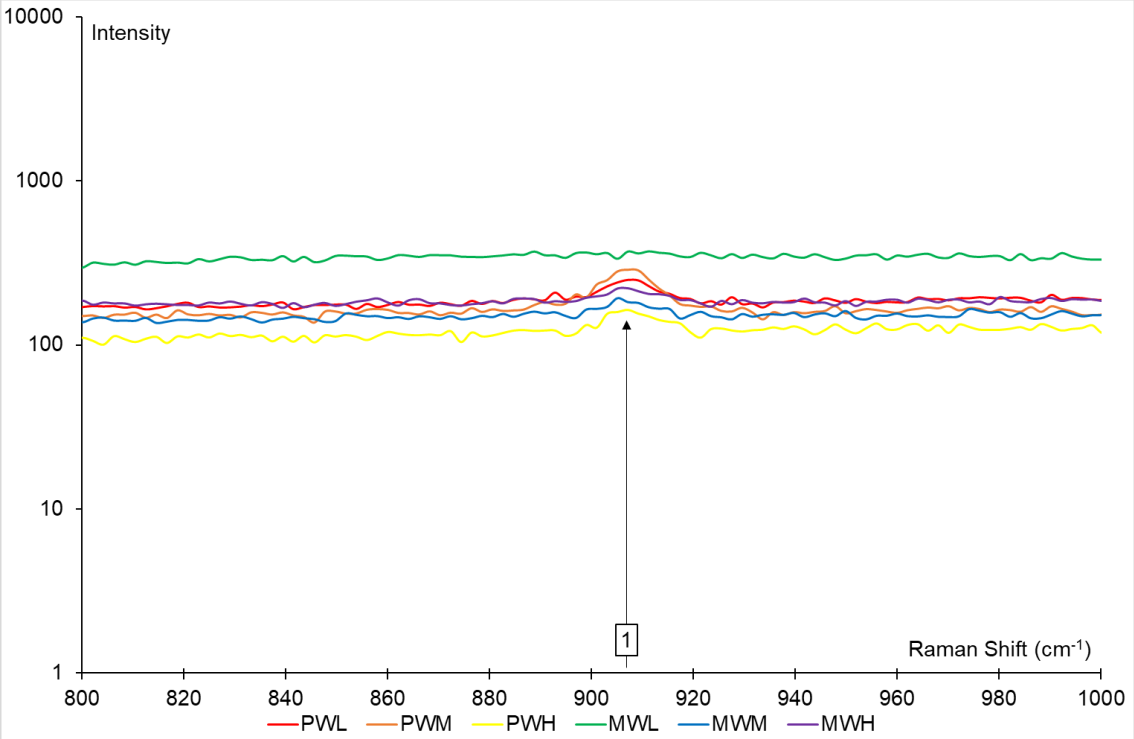

Figure 5.13 – Graph showing the Raman spectra for PWL, PWM, PWH, MWL, MWM and MWH between 800 cm^{-1} – 1000 cm^{-1}.

Figure 5.13 highlights peak 1 between 900 cm^{-1} and 920 cm^{-1}, centred at around 910 cm^{-1}. MWL does not give the same peak definition but does give greater intensity than all other samples present. PWH shows the lowest intensity.

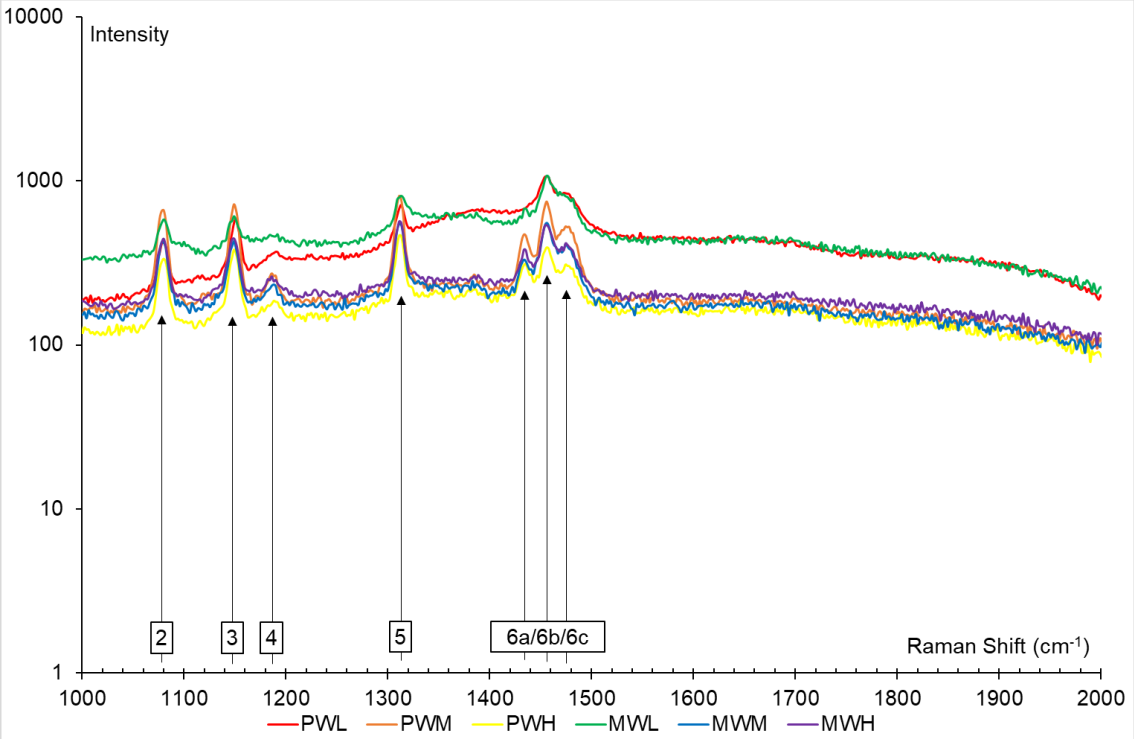

Figure 5.14 – Graph showing the Raman spectra for PWL, PWM, PWH, MWL, MWM and MWH between 1000 cm^{-1} – 2000 cm^{-1}.

Figure 5.14 shows Raman spectra between wavenumber 1000 cm^{-1} and 2000 cm^{-1}. There is one small peak after peak 3 and peak 6 is also made up of three individual peaks in a narrow range of wavenumbers. Intensity for PWL begins to increase from 1000 cm^{-1} and reaches a maximum at 1460 cm^{-1} after that PWL follows a similar trend to the MWL curve. Other samples, PWM, PWH, MWM and MWH all follow similar trends over this wavenumber range.

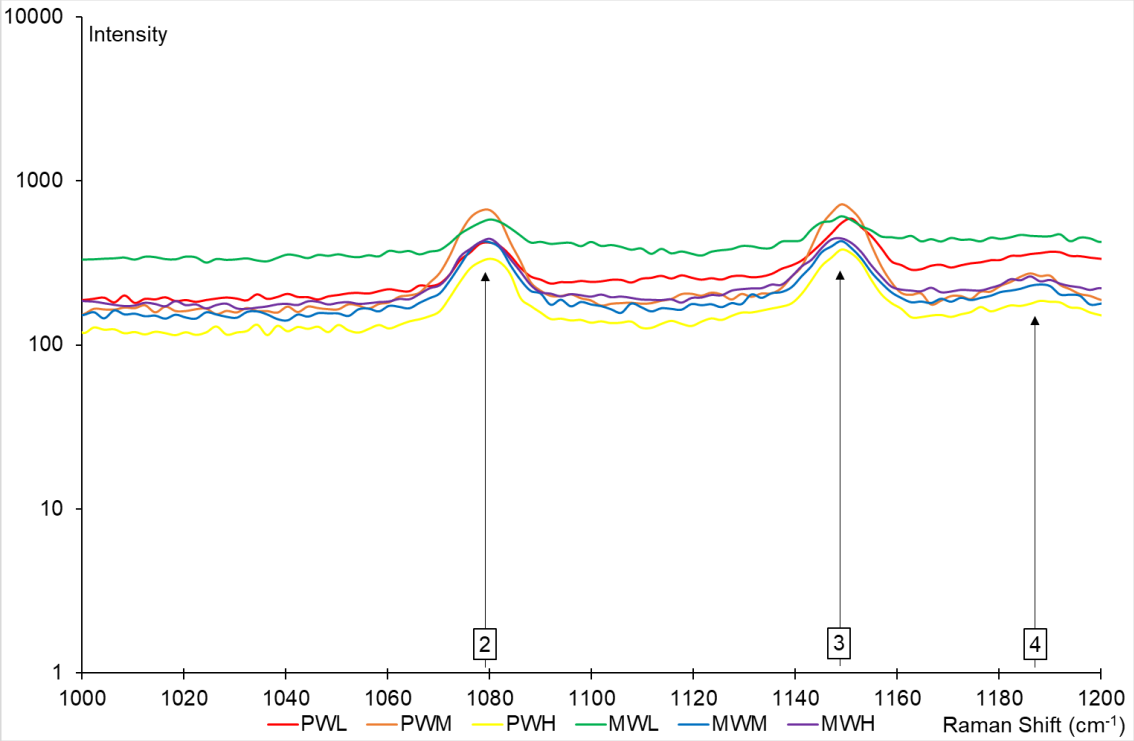

Figure 5.15 – Graph showing the Raman spectra for PWL, PWM, PWH, MWL, MWM and MWH between 1000 cm^{-1} – 1200 cm^{-1}.

Figure 5.15 shows the Raman spectra over wavenumber range 1000 cm^{-1} to 1200 cm^{-1}. This shows the curves and peaks with more definition. The first peak (peak 2) is experienced by all samples with the range falling between 1070 cm^{-1} and 1090 cm^{-1} and on average the peak height experienced is 1080 cm^{-1}. Samples PWM, PWH, MWM and MWH all experience strong peaks, however, PWL on has a medium strength peak, while MWL has a weak peak, at the first peak range PWL can still be considered with the group of samples but is starting to increase intensity to equal MWL, as previously stated. The second peak (peak 3) observed in figure 5.15 is seen at wavenumber range of 1140 cm^{-1} to 1160 cm^{-1} with the peak height experienced by all samples at 1150 cm^{-1}. Peak heights experienced by PWM, PWH, MWM and MWH are like the first peak range, PWL shows an increase in overall intensity, with a peak height equalling that of MWL followed by a greater increase in intensity, breaking away from the other group of samples to be equal with MWL. MWL shows no changes from the first peak range, with the peak experienced being a weak one. The third peak (peak 4) that can be seen in figure 5.12, is only slightly visible on figure 5.15, this third peak occurs between wavenumber range 1175 cm^{-1} and 1195 cm^{-1} with a peak occurring at 1185 cm^{-1}. This weak peak is only experienced by samples PWM, PWH, MWM and MWH, the same grouping that has previously experienced all

large peak changes. PWL does not show any peaks in this third peak range but does continue its increase in overall intensity to become equal with that curve of MWL, while MWL shows no evidence of change at all in this third wavenumber range.

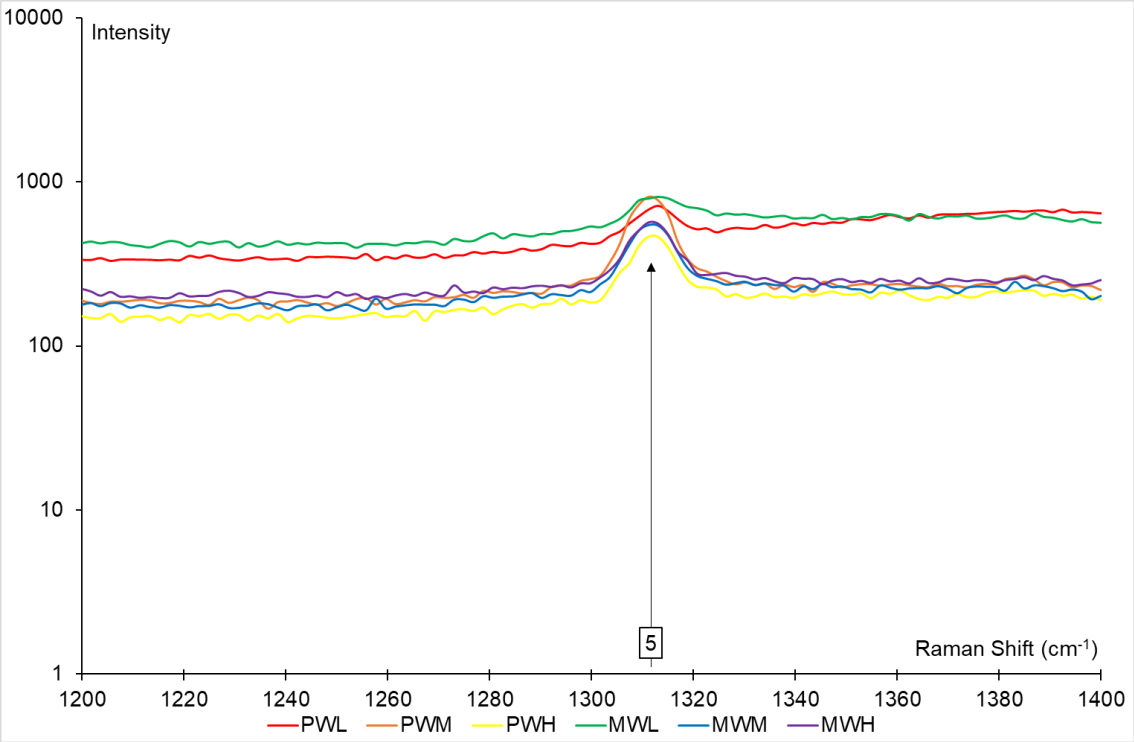

Figure 5.16 – Graph showing the Raman spectra for PWL, PWM, PWH, MWL, MWM and MWH between 1200 cm^{-1} – 1400 cm^{-1}.

Figure 5.16 shows a further break down of the wavenumber range shown in figure 5.14, between 1200 cm^{-1} and 1400 cm^{-1}. In figure 5.16 PWL is almost equal to MWL at the start of the range and by the end of the range surpasses MWL in intensity. Throughout this range PWM, PWH, MWM and MWH all remain equal in their changes and distinct separation in their spectra is observed. Between the range 1300 cm^{-1} and 1320 cm^{-1} there is a peak (peak 5 in figure 5.12) centred on 1310 cm^{-1}, experienced by all samples. For PWM, PWH, MWM, MWH the peaks are strong, while for PWL and MWL peaks are weak.

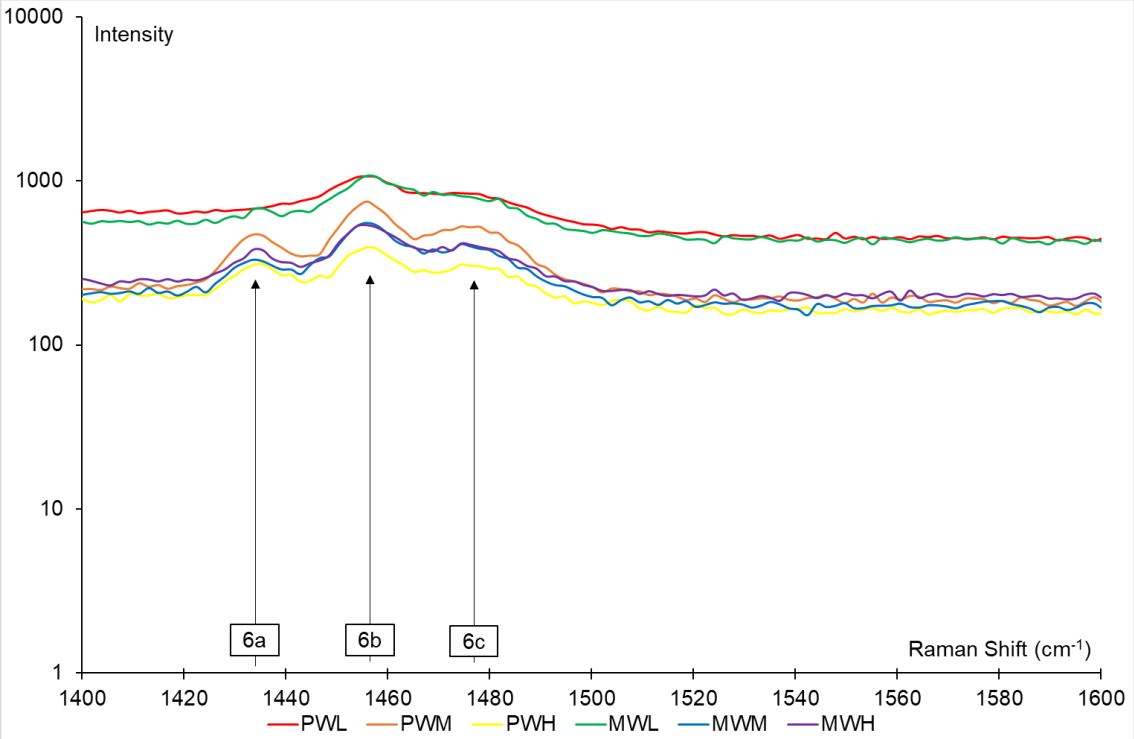

Figure 5.17 – Graph showing the Raman spectra for PWL, PWM, PWH, MWL, MWM and MWH between 1400 cm^{-1} – 1600 cm^{-1}.

Figure 5.17 shows a breakdown of wavenumber range 1400 cm^{-1} and 1600 cm^{-1} and a closer look at peak 6 from figure 5.12. PWL and MWL both show the greatest intensity over the wavenumber range, while the remaining samples all show similarity in intensity. The main peaks are between 1425 cm^{-1} finishing at 1500 cm^{-1}, within this large peak range there are 3 individual peaks experienced by all the samples. With PWM the peaks are more pronounced. If we take the range as peak 6, then from left to right the peaks will be 6a, 6b and 6c. Peak 6a has a range between 1425 cm^{-1} and 1445 cm^{-1} with a peak height of 1435 cm^{-1} PWM, PWH, MWM, MWH all show evidence of medium peaks, while MWL shows a very weak peak and PWL shows no peak at all. Peak 6b has a wavenumber range of 1445 cm^{-1} to 1465 cm^{-1} and a peak height of 1455 cm^{-1}, all samples show evidence of peaks, PWL and MWL both have a weak peak, while the remaining samples show evidence of medium peaks. As part of peak 6b, we see that PWH has the lowest intensity and PWM is starting to break away from the main group of samples, previously grouped together, MWM and MWH are still very similar within the whole of figure 5.17. Peak 6c has a wavenumber range between 1465 cm^{-1} and 1500 cm^{-1} and an average peak height of 1480 cm^{-1}, it should be noted though that this small range is much less

pronounced than previous peaks and all samples should be classified as weak peaks.

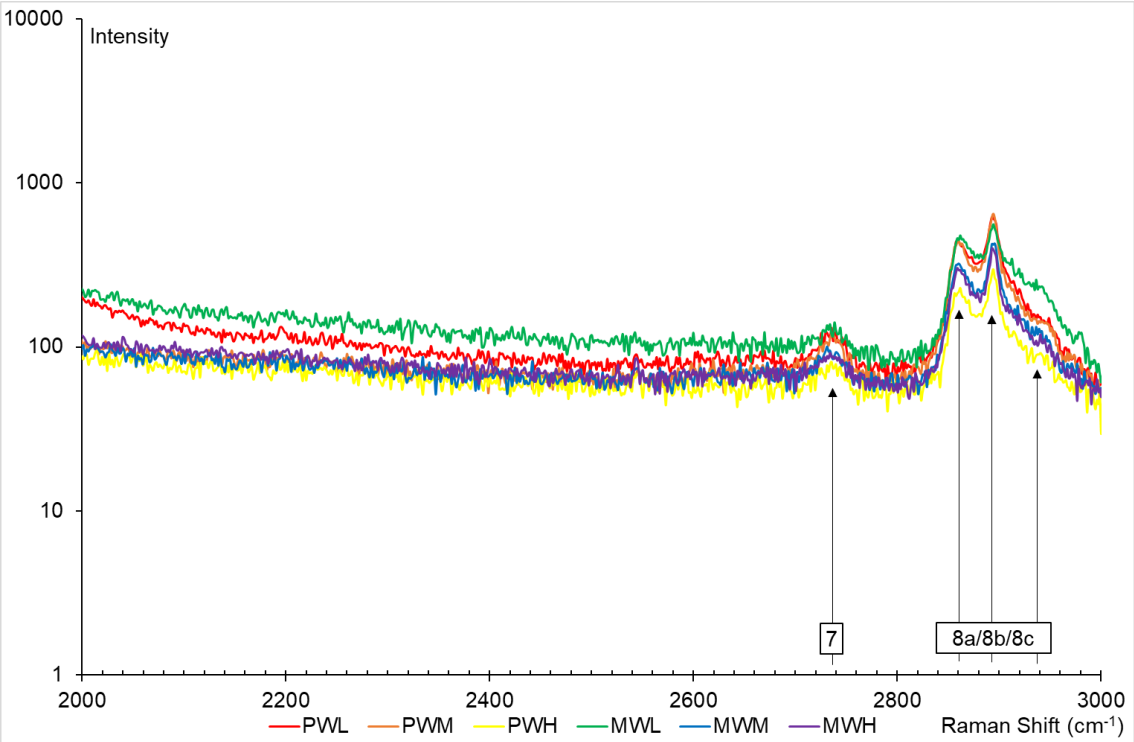

Figure 5.18 – Graph showing the Raman spectra for PWL, PWM, PWH, MWL, MWM and MWH between 2000 cm^{-1} – 3000 cm^{-1}.

Figure 5.18 shows breakdown Raman spectra from figure 5.12, showing the spectra between 2000 cm^{-1} and 3000 cm^{-1}. There are 2 main peaks one smaller peak around 2700 cm^{-1} and a larger peak range (including 2 individual peaks) between 2840 cm^{-1} and 3000 cm^{-1}. From the start of the range at 2000 cm^{-1} we see that the curves for PWL and MWL are beginning to decrease in intensity and by the start of the first observable peak all spectra are similar.

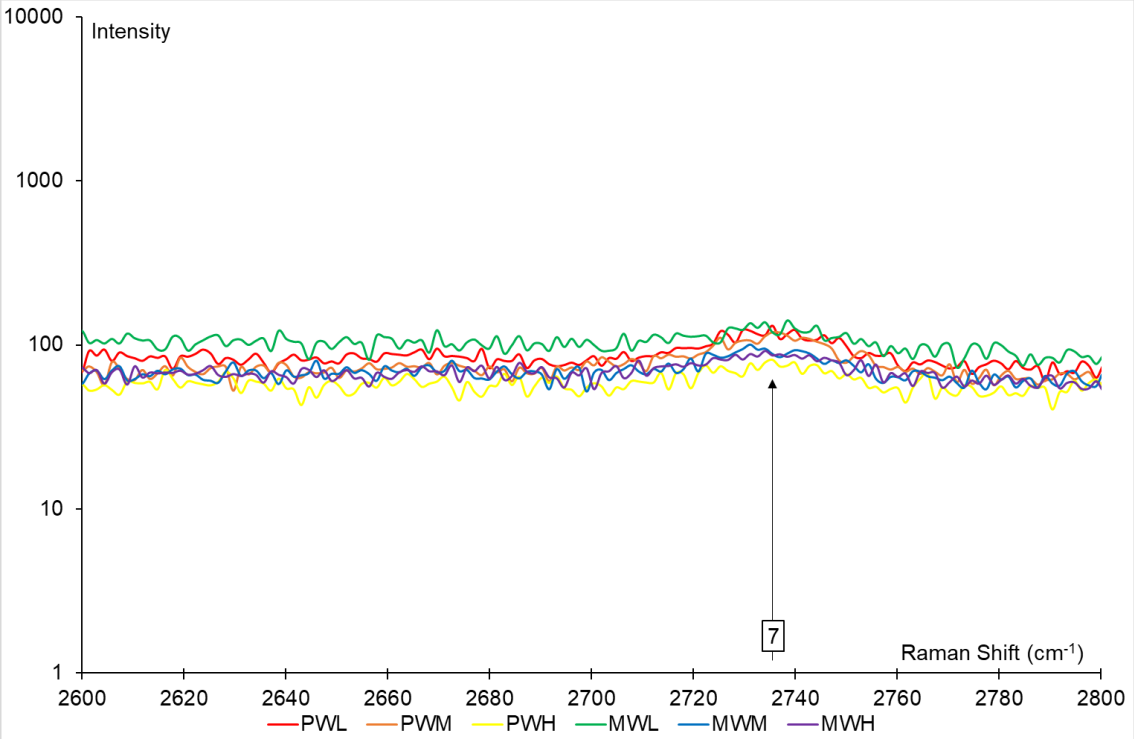

Figure 5.19 – Graph showing the Raman spectra for PWL, PWM, PWH, MWL, MWM and MWH between 2600 cm^{-1} – 2800 cm^{-1}.

Figure 5.19 highlights peak 7 from figure 5.12 between 2600 cm^{-1} and 2800 cm^{-1}, centred on 2735 cm^{-1}. This peak, however, is weak compared to all the others.

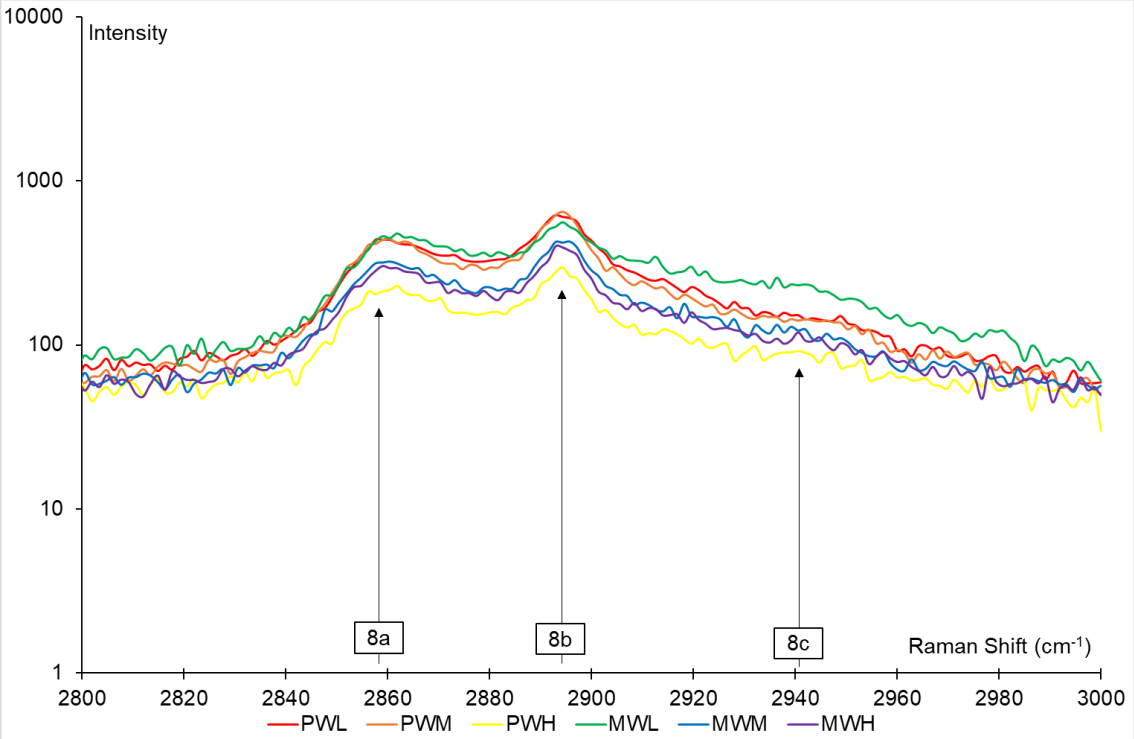

Figure 5.20 – Graph showing the Raman spectra for PWL, PWM, PWH, MWL, MWM and MWH between 2800 cm^{-1} – 3000 cm^{-1}.

Figure 5.20 shows the Raman spectra range between 2800 cm^{-1} and 3000 cm^{-1} highlighting peak 8 from figure 5.12. There are 2 definitive peaks, peak 8a ranges between 2840 cm^{-1} and 2880 cm^{-1} with a peak height evident at 2860 cm^{-1} at this point of the spectra PWL, PWM and MWL have very similar curves and show the greatest intensity over this range, PWH as for all the spectra shows the lowest intensity while MWM and MWH have similar curves. In peak 8a all curves show medium intensity. Peak 8b with the large peak range comes between 2880 cm^{-1} and 2960 cm^{-1} with a peak height of 2895 cm^{-1} for all sample curves. Intensities of samples are all similar in rank to peak 8a but all peaks within for peak 8b should be considered strong definite peaks. There is a final small peak 8c around 2940 cm^{-1}, mainly experienced by MWL.

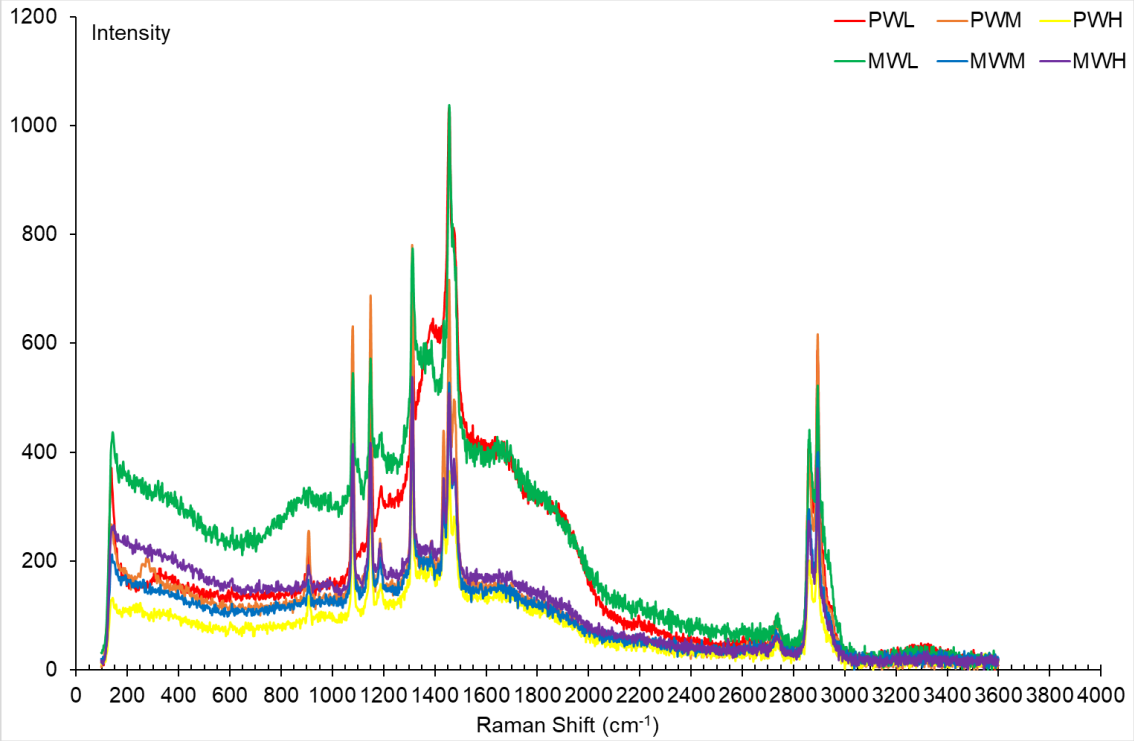

Figure 5.21 – Plot of Raman spectra scan (figure 5.12) without logarithmic Y-scale, with an included minimum baseline removal.

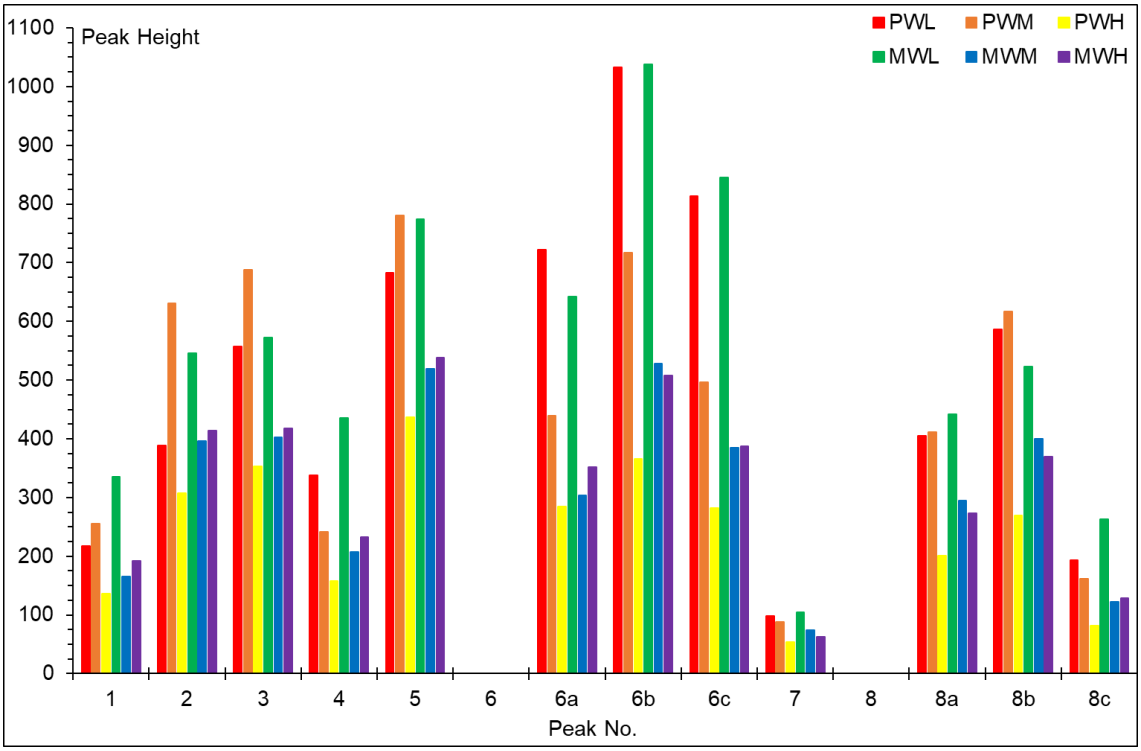

Figure 5.22 – Plot showing maximum peak intensity observed from Raman spectra data, based on figure 5.12.

Figure 5.21 is a plot of Raman spectra, without a logarithmic scale. As with figure 5.12 individual peaks can be noticed, in figure 5.21 MWL is more varied in intensity, as with figure 5.12 MWL appear of greater uniformity between 600 cm^{-1} and 2000 cm^{-1}, apart from the peaks experienced. In figure 5.21 the

same wavelength range shows that there is a change in MWL intensity compare to other samples, a trend not observed in figure 5.12. Peaks at 1500 cm^{-1} and ≈ 2800 cm^{-1} show greater intensity compared to the rest of the “flat” regions of the spectra in figure 5.21, wherein figure 5.12 these peaks appeared to have similar intensity to the remaining spectra.

Peaks previously unrecognised due to the logarithmic scale are not visible in figure 5.21, at 1390 cm^{-1} a small intensity peak is evident for all peaks, even PWL and MWL at higher overall intensities. There are also present small intensity peaks between 1600 cm^{-1} and 1700 cm^{-1}.

Figure 5.22 shows the maximum peak heights experienced by each of the constituent components. PWM has some of the greatest peak heights in the lower wavelength band (900 cm^{-1} to 1200 cm^{-1}), the only peaks with greater height are for MWL. Between 1200 cm^{-1} and 1500 cm^{-1} PWL peak heights begin to equal MWL and PWM following in height. At the final wavelength range (2800 cm^{-1} to 3000 cm^{-1}) peak heights become more grouped, with only slight differences in heights, PWH still maintains the lowest peak height, as it has through the whole Raman spectra.

Table 5.1 – Summary of Raman shift peaks and band intensities. ρ = depolarisation ratio; δ = bond twisting/deformation; v = bond stretching; s = symmetric bond movement; as = asymmetric bond movement; sci = scissoring bond movement.

Peak Number	Raman Shift Peak (cm^{-1})	Raman Shift Band (cm^{-1})	Weak Intensity	Medium Intensity	Strong Intensity	(Faoláin et al., 2005)	(Zheng and Du, 2006)	(Edwards and Falk, 1997)
1	910	900 – 920	PWL/PWM PWH/MWM MWH	MWL	-	-	ρCH2	ρCH2; δ(COC)
2	1080	1070 – 1090	MWL	PWL/PWM PWH MWM/MWH	-	v(CC)	v_s(CC)	v(CO)
3	1150	1140 – 1160	-	PWL/PWM PWH/MWL MWM/MWH	-	v(CC)	v_{as}(CC)	v(CC)
4	1185	1175 – 1195	PWM/PWH MWM/MWH	PWL/MWL	-	v(CC)	-	v(CC)
5	1310	1300 – 1320	-	PWL/PWH MWM/MWH	PWM/MWL	δ(CH2)	δ(CH2)	δ(CH2)
6	-	1425 – 1500	-	-	-	-	-	-
6a	1435	1425 – 1445	MWL	PWM/PWH MWM/MWH	-	δ(CH3)	-	δ(CH2)
6b	1455	1445 – 1465	-	PWH MWM/MWH	PWL/PWM MWL	δ(CH2)	δ_{as}(CH2)	δ_{sci}(CH2)
6c	1480	1465 – 1500	PWH	PWM/MWM MWH	PWL/MWL	δ(CH2)	δ(CH2)	-
7	2735	2710 – 1760	ALL	-	-	-	v(CH3-CH2)	v(CH3-CH2)
8	-	2840 – 2960	-	-	-	-	-	-
8a	2860	2840 – 2880	PWH/MWM MWH	PWL/PWM MWL	-	-	v_{as}(CH2)	v_s(CH2)
8b	2895	2880 – 2900	PWH	PWL/PWM MWL/MWM MWH	-	-	v_s(CH2)	v_{as}(CH2)
8c	2940	2900 – 2960	ALL	-	-	-	v_s(CH3)	v_s(CH3)

Table 5.1 summarises the main results of the previous figures, with the breakdown of the peaks, the Raman shift band and the intensity of the peaks, all to help indicate what functional group of bonding type is present within the material tested.

5.2.4 Discussion

Figure 5.12, figure 5.21 and table 5.1 show the overall results from the Raman spectroscopy on all paraffin waxes and microcrystalline waxes. As seen in figure 5.12 there are multiple peaks recorded, and as such, further figures 5.13 – 5.20 show individual peaks. Figure 5.21 shows the same Raman spectra; however, the plot has had the logarithmic Y-scale removed to distinguish plots and peaks more clearly, between samples. Table 5.1 indicates that the peaks for the paraffin waxes and their blends at wavenumbers around 3000 cm^{-1} indicate aromatic and aliphatic –CH, whilst peaks around 1500 cm^{-1} indicate CH_2 and CH_3 groups. Other sources, (Zheng and Du, 2006; Edwards and Falk, 1997), corroborate that this is what would be expected from the paraffinic samples tested here.

Previous authors (Edwards and Falk, 1997; Zheng and Du, 2006; Faoláin et al., 2005; Socrates, 2004) have found that with hydrocarbon (alkane) -based waxes, the spectra are very similar. For example, figure 5.23 (Zheng and Du, 2006) shows a Raman spectrum of a paraffin wax that correlates strongly with figure 5.12.

If there are any clear distinctions, they are mostly experienced at lower wavenumbers, between 900 cm^{-1} and 1500 cm^{-1} and seem to be between PWL and MWL (see figure 5.21 and 5.22). For MWL for the entire spectrum has an elevated intensity, and while PWL starts its spectrum with similar intensity to other samples it begins to rise at 1200 cm^{-1} wavelength to match the intensity plot of MWL, falling again to match other samples around 2000 cm^{-1}. Overall, although results show differences in the spectra, they do not enable one to make clear conclusions about the chemical make-up of the different samples.

When considering table 5.1 and figure 5.22, it should be noted that at peaks 6a, 6b and 6c, there is an overall increase in intensities for the PW and MW. PWL and MWL have especially high peaks in this region indicating the large presence of bonds such as C-C and CH_2 bonds expected for the type of

hydrocarbons present. Except for PWH, PW have high peak values. This may be due to PW containing a greater component of straight chain hydrocarbons, and MW containing more branched and naphthalic compounds the peaks here are not as intense due to the difficulty to break down these compounds compared to straight chain materials.

Peaks around 2800 cm^{-1} – 2900 cm^{-1} in figures 5.21 and 5.22, these peaks are not as intense as would be expected. In figures 5.12 and 5.21 a great amount of noise is in this region of the Raman spectra, as such some information may have been lost as the sample was not detected by the equipment as it should have been.

Figure 5.21, due to the removal a logarithmic scale shows few more peak definitions compared to other figures. Peaks can be observed at 1390 cm^{-1} as a small intensity peak, also present is small intensity broad peak between 1600 cm^{-1} and 1700 cm^{-1}. (Socrates, 2004) states that at 1390 cm^{-1} methyl bond wagging is to be expected, while in the range of 1600 – 1660 cm^{-1} presence of cyclopropenones is possible, however, it would be expected that the peak observed would be of strong intensity.

Within this investigation, there is much greater volume of material more susceptible to bond bending and manipulation according to other authors (Zheng and Du, 2006; Edwards and Falk, 1997; Faoláin et al., 2005; Socrates, 2004). The levels of C-C bond bending are prevalent in PW and MW as seen in figure 5.23, however, the high level of CH_2 bond bending is not as evident in this investigation as would be expected.

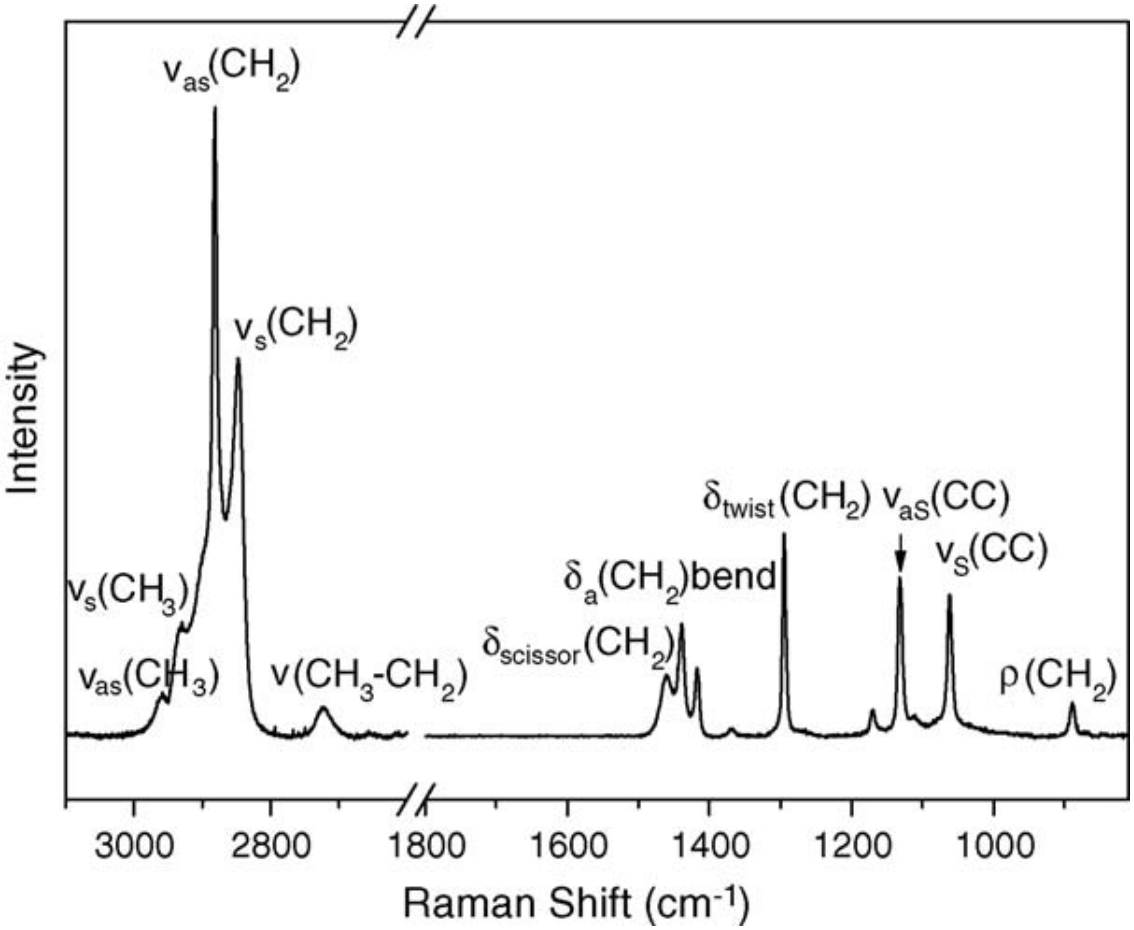

Figure 5.23 – Raman spectrum of paraffin wax (Zheng and Du, 2006).

In figure 5.21 there is evidence of fluorescence in all the wax samples. Between wavelengths of 200 – 2200 cm^{-1} the spectra of all samples are elevated from the baseline, in PWL there is greater fluorescence between 1300 - 2200 cm^{-1} and for MWL that range is expanded to 600 cm^{-1} or possibly from the beginning of the spectral scan. It is possible that with both samples being lower congeal point samples, the lasers incident on the samples were too powerful causing greater excitation of the sample and leading to the absorbance of energy and sample fluorescence of PWL and MWL. This fluorescence appears to alter the true values of the Raman spectra, as elevated peaks are observed at positions of spectra peaks for bonding alteration identification.

5.2.5 Conclusions

Raman spectroscopy can be used as a fingerprint method to identify compound types within WSP and its components. The technique could be used to identify significant errors in samples, in raw material quality assurance testing, for example, identification of impurities. However, identification of the concentration of individual WSP molecular components will need much more

work, due to the complexity of the mixtures (plus variations due to the testing protocol). If individual identification is required, a testing method like GCMS would be more suitable, although this has its difficulties due to the low volatility (high molecular weight) of many of the components.

This investigations' results indicate that the bending of C-C bonds is prevalent and the manipulation of CH_2 bonds ≈ 1450cm^{-1} is strong, however, the bending of CH_2 and CH_3 bonds between 2800 – 3000 cm^{-1} occurs less, compared to those expected from previous authors.

Chapter 6 Factory Processing; Stability with Microscopy

6.1 Factory Processing and Addition of Excess Oil

6.1.1 Introduction

Paraffin wax products (PW, MW) and White Soft Paraffin (WSP) are products widely used within the pharmaceutical industry and while there are many constituent components used, at various grades and with different chemical/physical characteristics, these materials will undergo mixing with various other ingredients and factory processing based on the type of product being made. This has been covered in Chapter 1 and Chapter 2. The first task described in this chapter was to investigate how a simulated factory process might affect targeted model WSP blends. The blends were WSP4, WSP5 and WSP6 since these seemed to behave most closely to the commercial samples in previous tests. Their compositions are shown again in figure 6.1 below and their method of preparation was described earlier in Chapter 2.

1	Oil	McC	Para	2	Oil	McC	Para	3	Oil	McC	Para
low		x		low				low			
med	x		x	med	x	x	x	med	x		x
high				high				high		x	
4	**Oil**	**McC**	**Para**	**5**	**Oil**	**McC**	**Para**	**6**	**Oil**	**McC**	**Para**
low		x	x	low			x	low			x
med	x			med	x	x		med	x		
high				high				high		x	
7	**Oil**	**McC**	**Para**	**8**	**Oil**	**McC**	**Para**	**9**	**Oil**	**McC**	**Para**
low		x		low				low			
med	x			med	x	x		med	x		
high			x	high			x	high		x	x

Figure 6.1 – Matrix of Leeds produced WSP blends, based on extreme variations of theoretical blends.

Within factory processing, it is common practice to blend WSPs with increasing percentages of oil (of similar viscosity to ones used within the ratio mixture) or propylene glycol (Sarker, 2013), in order to tailor the viscosity of the final product according to its end use. Regarding ointments, which have an oily continuous phase, it has been suggested that ointments are most likely fail quality control tests due to such blending, depending on the amount added and the mixing process. These failures may appear on short and long-term storage of the product. Most consumers do not use all the product in a short period but are more likely to store that product for anything up to two years. The standard industry (Pharmacopoeia, 2005; Barry, 1970; Barry and Grace, 1971c), cone penetration was used for testing model WSP blends after incorporation of other oils.

When adding oil to the three WSP blends it should affect the penetration force and viscosities, by lowering both with additional oil. It is unknown the point of failure of a WSP blend, but it is believed that the order of failure will occur from WSP of constituent components with lower congeal points to higher, i.e., WSP4 < WSP5 < WSP6.

6.1.2 Materials and Methods

The source and nature of the WSP wax materials used, was provided in Chapter 2. To be able to alter the viscosity of the WSP blend a 15 cSt oil, Keratech 15, was used, described by the manufacturer as a light paraffin oil with an average viscosity of 15 cSt (i.e., 1.5 x 10^{-2} Pa s) at 40 °C. Three aluminium containers were used to blend and store the WSP. This was done to ensure good heat transfer when blending at elevated temperature. The samples were heated

in a small convection oven (Cookworks, 23 L, Argos), at 100 °C ± 2 °C. Four thermocouples were placed inside the oven at each corner, spaced internally by 5 cm towards the centre of the oven, to check that the oven was maintained at this temperature over the period of the experiment.

A Silverson L4r Series mixer (Silverson Machines Ltd. Waterside, UK) was used to blend oil into the samples as the aluminium containers were submerged close to the rim in a water bath at 90 °C. The blending head (fitted with an Emulsor screen (Silverson Machines Ltd. Waterside, UK)) was submerged 2 cm below the surface of the WSP and run at 5000 rpm for 5 minutes. After this, the blender was turned off, the head raised and the sample allowed to rest for 10 s to allow excess WSP to fall back into the container. The sample was then placed back in the oven for 10 min, then removed from the oven, covered and left to cool to ambient temperature over 24 h, after which cone penetration tests and viscosity measurements were performed at 40 °C. Various additions of oil were tested: 1 %, 2 %, 3 %, 4 %, 5 %, 10 %, 15 % and 25 %.

6.1.3 Results

	WSP4	WSP5	WSP6
0%			
1%			
2%			
3%			
4%			
5%			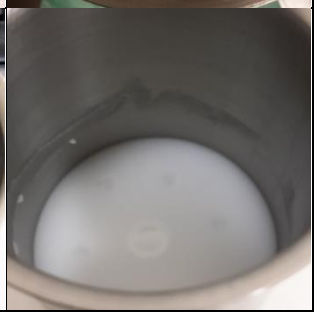

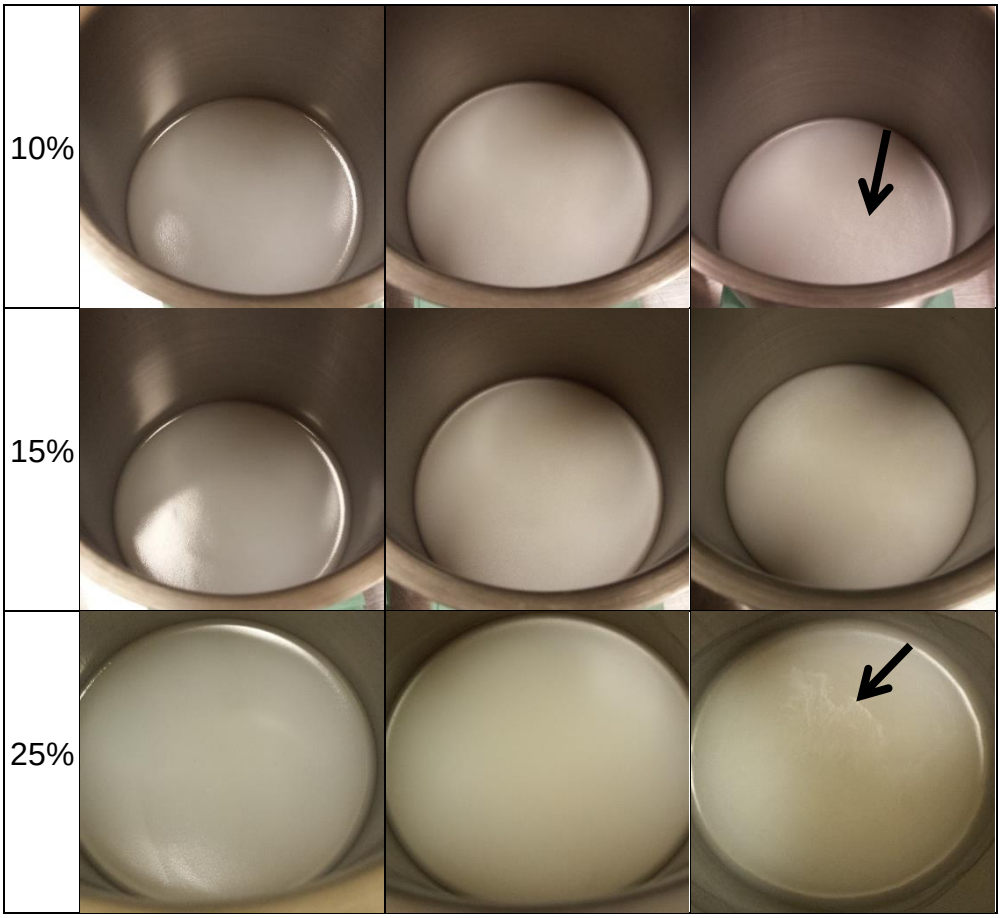

Figure 6.2 – Images of progressive additions of oil to the WSP blends WSP4, WSP5 and WSP6. Images are not to the same scale and were taken at different distances.

As the % of oil added increased, the samples visually changed: the surface became increasingly reflective of light, especially noticeable at 25 % addition, compared with the dull matt reflection before any addition. A degree of crystallisation was visible: for WSP4 at 0 %, 1 %, 2 % and some degree in 3 %, after which free oil was visible on the surface. For WSP5 crystallisation was seen at 0 %, 1 %, 2 %, 3 %, 4 % and to some degree at 5 % addition. Beyond 5 % the surface of WSP5 appeared homogeneous. Although no obvious crystallisation was seen in WSP6 it should be noted that at 10 % and 25 % breaks in the surface of the WSP were seen (marked on the figure), suggesting a possible break down in the crystalline network structure, especially at the surface.

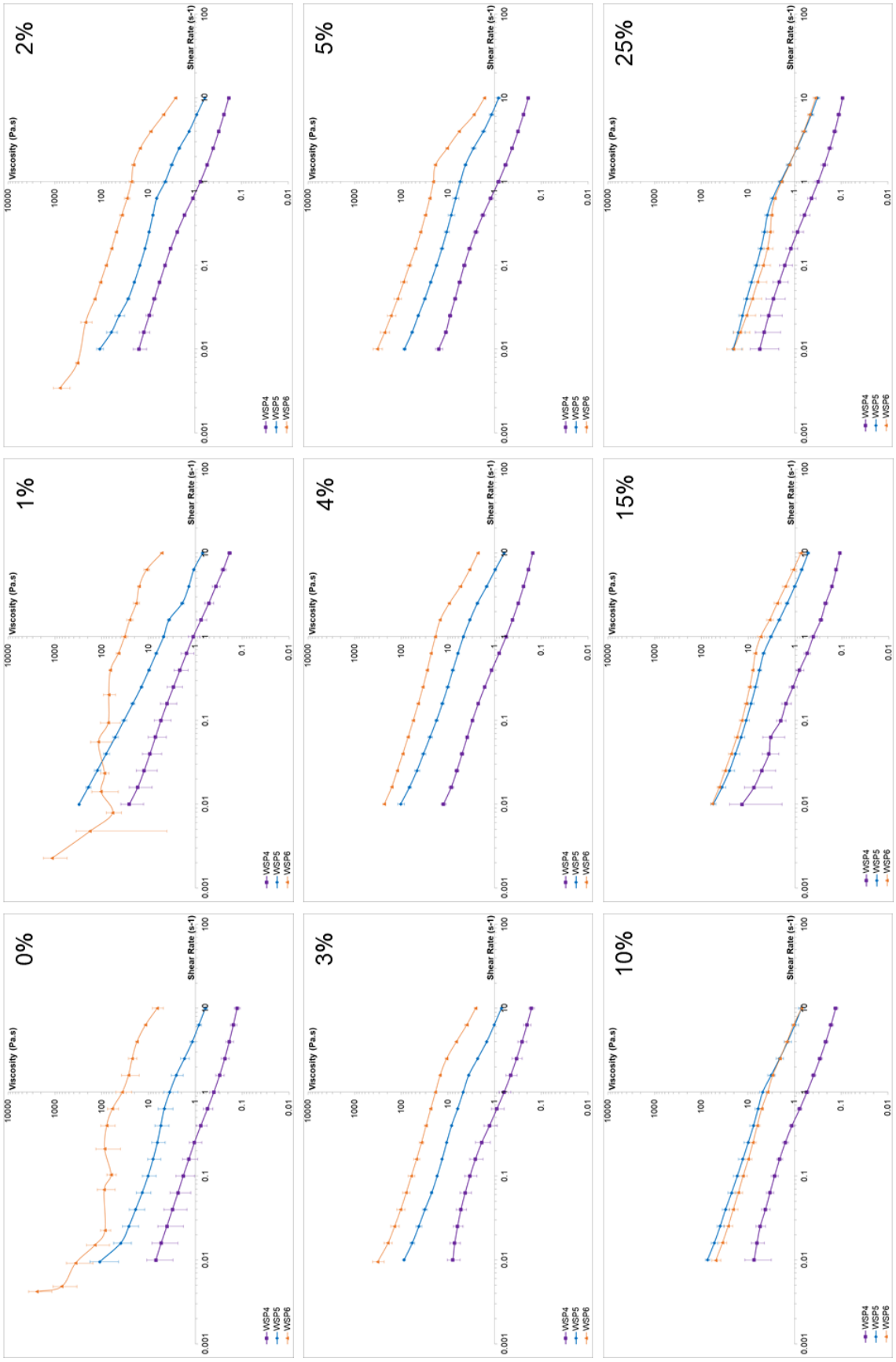

Figure 6.3 – Viscosity plots of WSP4 (■), WSP5 (■) and WSP6 (■) for all oil additions. All measurements were carried out at 100 °C.

Figure 6.3 shows the viscosities of the different blends at 100 °C, for different additions of oil. The viscosity of WSP4 remained undiminished until the addition of ≥ 10 % oil. WSP5 is a stiffer sample that WSP4 and overall the viscosities were higher than for WSP4 at all additions. At 25 % oil addition, there was a big fall in viscosity but this is more noticeable at lower shear rates, i.e., below 0.5 s^{-1}. WSP6 has the most instability, especially below 1 s^{-1} for oil additions of 0 %, 1 % and 2 %. The gradient above 1 s^{-1} is stable for all oil additions. For oil additions, 3 % to 5 %, the gradient below 1 s^{-1} becomes stable and constant, but as shear rate increases the viscosity drops rapidly, especially for 5 % oil addition.

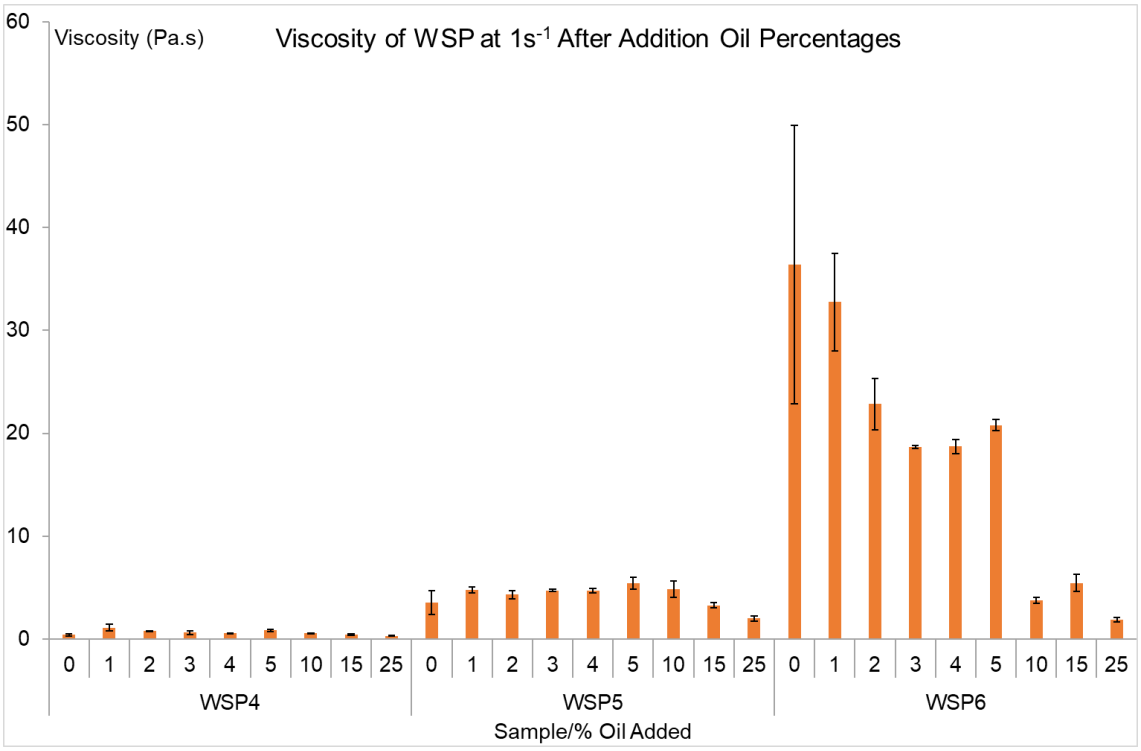

Figure 6.4 – Viscosity of WSP carried out at 100 °C, at 1 s^{-1}, after addition oil percentages.

Figure 6.4 illustrates the main differences between the samples by plotting the viscosities at in the shear rate region where the measurements appear most stable, i.e., 1 s^{-1}. The order of viscosities is clearly WSP6 > WSP5 > WSP4, except at additions beyond approximately 10%, when WSP5 ≈ WSP6.

Figure 6.5 shows the cone penetration results on the corresponding samples. WSP4 has the lowest penetration force of all samples, and WSP6 has the highest penetration force. At 0 % oil addition WSP4 has a force of 0.05 N, this force increases to 0.15 N for oil additions of 3 %, to 5 %. The penetration

force slightly reduces to 0.1 N at 10 %, 15 % and 25 % oil addition. WSP5 shows the same trend as WSP4, at 0 % oil addition WSP5 has a penetration force of 0.3 N, this increases to 0.6 N at 3 % oil addition, reducing to 0.5 N for 4 % and 5 % oil addition and reducing further to 0.4 N for the other higher oil addition percentages. WSP6 shows less sensitivity to 0 % oil addition, except at > 10 %, roughly in accord with trends in the viscosity measurements.

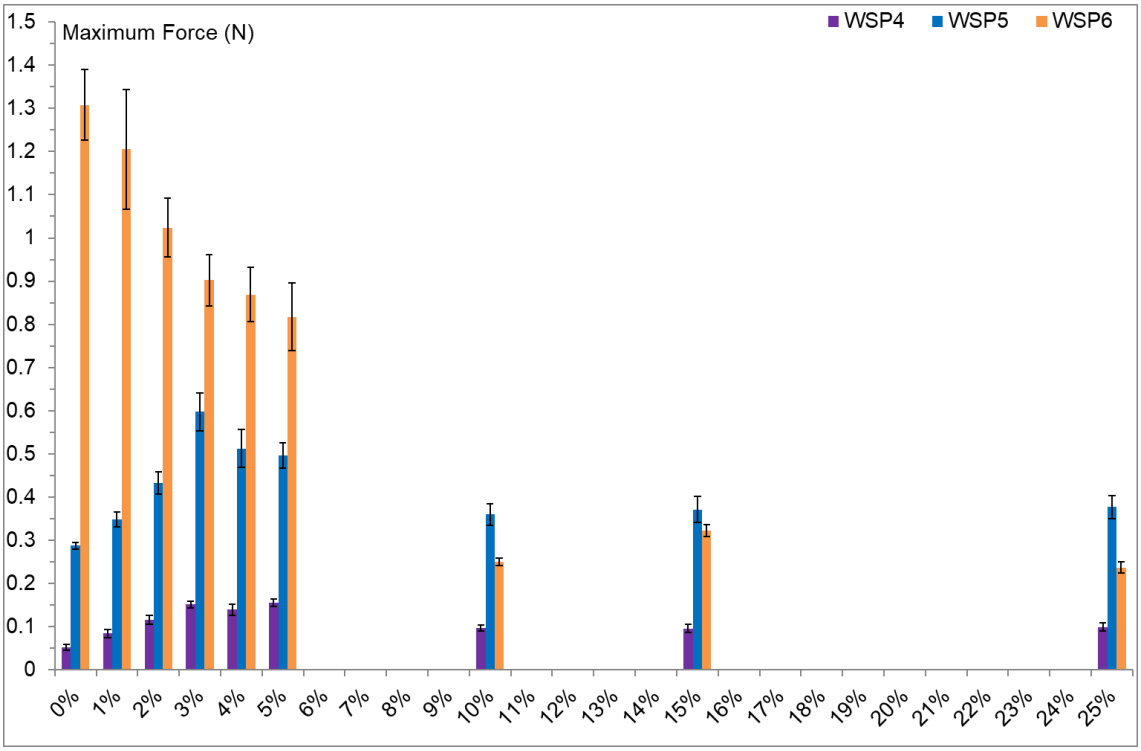

Figure 6.5 – Maximum penetration forces experienced by WSP samples, with addition of oil percentages from 0 % to 25 %.

6.1.4 Discussion

WSP4 is the softest blend with the least structure forming material (i.e., microcrystalline wax) and as such the additional oil causes the surface of the blend to be more reflective at lower oil additions because more oil is not able to be held within the wax crystal lattice of the WSP. WSP5 has been shown to be the most stable sample in other tests and visually this is observed as the blend changes its appearance very little with the addition of oil. At 10 % there is a slight increase in reflection of light. The surface of WSP6 is shown to have a matt finish indicating the lack of oil content on the surface of the blend and that the crystal lattice network is prevalent at lower oil content percentages. At 10 % oil addition, the surface of the WSP begins to reflect light indicating a greater oil presence on the surface.

In figure 6.3 and 6.4, the graphs show that WSP4 undergoes minor changes in viscosity with increasing additional oil percentage. However, the viscosity of WSP4 is already lower than the other blends. The small jump in viscosity experienced by WSP4 at 0.06 s^{-1} is likely due to a slip in the rheometer.

Figure 6.3 and 6.4 indicate that WSP5 is a stable blend, with a slight change in overall viscosity. As previously explained, there is an indication that WSP5 has greater viscosity and higher crystal content at lower oil percentages, as at low shear rates for 0 %, 1 % and 2 %, WSP5 shows greater variation in the viscosity at 0.01 s^{-1}. At 3 %, 4 % and 5 % the curves for WSP5 are most stable, while increasing oil content to 10 %, 15 % and 25 % the viscosity decreases and the blend becomes more Newtonian/less shear thinning. Figure 6.4 also shows that the viscosity at 1 s^{-1} decreases by almost 1/3rd after each addition of oil.

Figure 6.5 shows similar trends for WSP4 and WSP5, in that there are slight increases in penetration force from 0 % to 3 % followed by reductions in maximum force as oil content increases. WSP4 reduces slightly to ≈ 0.1 N, while WSP5 decreases to ≈ 0.35 N. These changes may be due to a slight swelling and strengthening of the crystal lattice at low oil additions, followed by its break-up and or dissolution as more oil is added, leading to greater syneresis of oil.

For WSP6 by adding extra oil into the blend only results in a reduction of maximum penetration force, indicating that the wax network and its trapped oil are already at the optimal level in terms of WSP stiffness. Beyond 10 % addition, there is a collapse and weakening.

In general, for WSP4, WSP5 or WSP6, the addition of > 5 % oil results in the structural failure of the blends.

6.1.5 Conclusions

- Greater oil addition results in syneresis of oil on the surface of the blends.
    - Softer samples show syneresis earlier but this can be misleading as already the crystal lattice is weak in these samples.
- As oil content increases the light reflection and brightness in samples also increases.
    - This could be an indication of sample quality and crystal lattice size, therefore structural content for blend stability.

        - As oil is not able to be blended with the wax due to inhomogeneity.
    - Blends have a greater matt appearance at lower oil content, indicating greater lattice presence, and giving a duller less reflective surface.
- Increasing oil content can benefit some WSP blends by optimising the ratio blend.
    - This can allow crystal lattice structure to swell and strengthen.

6.2 Prolonged High Temperature Stability Testing

6.2.1 Introduction

The previous testing only shows results relevant to the first day. Although this might be useful in terms of screening WSP for possible failures, in practice WSP is stored for much longer times at high temperatures and so this was also investigated.

The model WSP blends shown in figure 6.1 and their constituent components, (shown in table 6.1) two industry samples (WSP10 and WSP11), were examined.

Table 6.1 – Table of constituent components used to make WSP(lab) blend.

Sample	Description	Acronym
Kerawax 2245	Low congeal point paraffin wax	PWL
Kerawax 482	Medium congeal point paraffin wax	PWM
Kerawax 1301	High congeal point paraffin wax	PWH
Techniwax P9805	Low congeal point microcrystalline wax	MWL
Techniwax P9820	Medium congeal point microcrystalline wax	MWM
Techniwax P9830	High congeal point microcrystalline wax	MWH

Within the industry, WSP batches might be stored for up to two years and their characteristics tested systematically over this period. Because of time constraints, samples were stored here for 1 year, at 100 °C and samples periodically (usually every month) removed for testing via the same methods already described earlier, including: large deformation (cone penetration testing) and small deformation (oscillatory) rheology, viscosity at 100 °C plus imaging via polarised microscopy, as suggested by previous authors (Edwards, 1957;

Venkatesan et al., 2005; Hoffmann et al., 2012). Some constituent components were also tested via Raman spectroscopy used at 0 months and 12 months.

Polarised images help to distinguish crystal size, shape and habit. Images were taken under temperature control via a heating plate on the slide, to compare with rheological data and to simulate temperature changes that may occur in WSP when undergoing typical manufacturing processes.

It is hypothesised that WSP blends made from extreme wax constituent components could be susceptible to syneresis due to inhomogeneity in the WSP blend. Chemical stability is believed to remain unaltered, as the storage conditions of the waxes and WSP blends will reduce external catalysts to cause a breakdown in the hydrocarbon chains within the paraffin products.

6.2.2 Materials and Methods

Samples were tested systematically at monthly intervals, every 3 months for constituent components and every month for WSP blends. Two sets of samples were made as described in Chapter 2. One sample set was left at ambient temperature in the dark in airtight glass jars. The second set was stored in the convection oven with heat sensors attached to four corner positions. The heat sensors were connected to a data tracker recording temperature fluctuation over 24 h per day for the 12 month testing period.

The rheological test procedures used have already been described in Chapter 3. For the individual PW and MW components, only viscosity testing was carried out because they were too rigid to be tested via the cone and plate. Raman spectroscopy was described in Chapter 5.

Optical microscopy was carried out using a Nikon SMZ-2T stereo microscope with a Leica MC120 HD camera mounted to the microscope. The microscope was attached with polarising lenses. A hot stage connected to a water pump for temperature control was used to regulate the temperature of the WSP upon the slide used for observation. Light was provided with a Polytec Light source with fibre optic cable. Video capture software from http://www.nchsoftware.com/index.html was used to take time lapse photos for a specific number of photos, the number which had been calculated to cover the complete thermal cycles.

A starting temperature of 110 °C was used, reduced in 20 °C steps between measurements, at a rate of 5 °C per minute in line with other testing methods. The temperature was then cycled once more, increasing the temperature to 110 °C at 5 °C per minute and finally reducing back to 20 °C and a rate of 5 °C per minute.

The slide was prepared by dropping molten WSP (110 °C) onto a preheated slide (100 °C) to prevent initial crystallisation. A coverslip was glued to the glass slide above the sample to ensure the sample was fully sealed to stop any evaporation during subsequent temperature cycling.

6.2.3 Results

6.2.3.1 Large Deformation Rheology (Cone Penetration Testing)

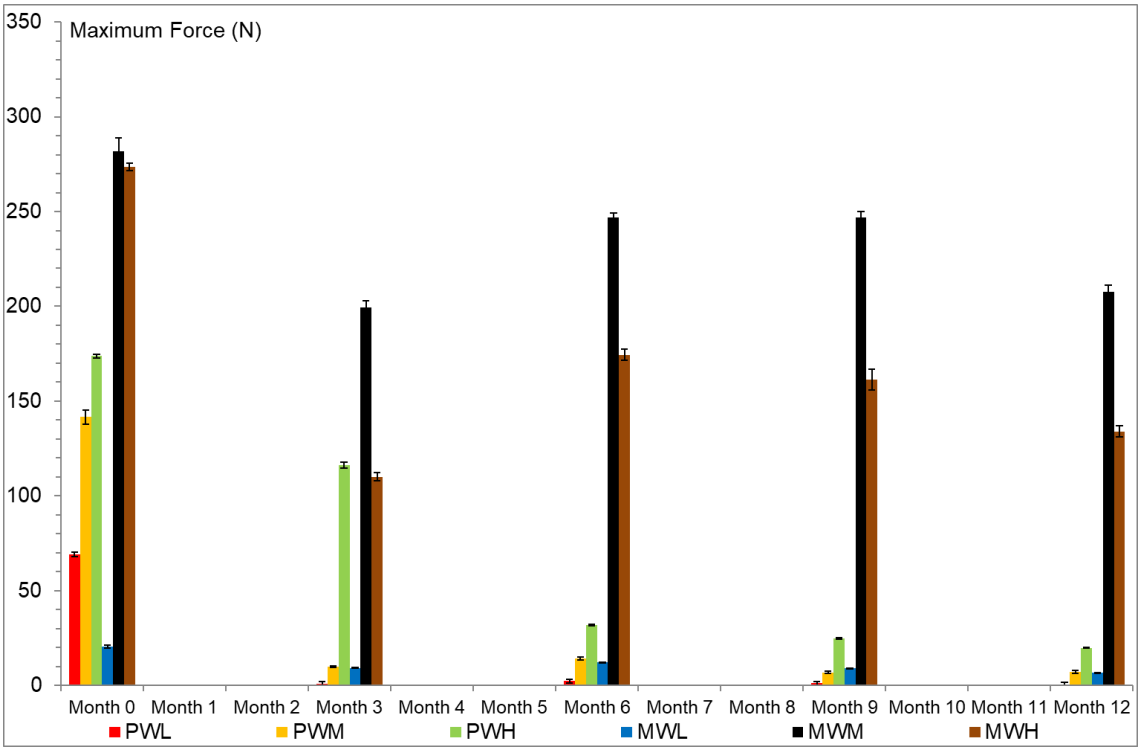

Figure 6.6 – Maximum penetration force of constituent components taken over a 12 month total period, with data recorded every 3 months.

At month 0 there is a large penetration force for all constituent components. MWL of all samples has the lowest recorded value of 20 N followed by the paraffin waxes with increasing congeal point. Finally, MWM has the highest recorded penetration force of 281 N then MWH with 273 N.

PWL and PWM reduce in penetration force after 3 months of storage and but then remain at similar low values at each further 3 month testing point. PWH

does reduce in penetration force after 3 months, but by 57 N, after 6 months storage, PWH drops a further 84 N at which point it only reduces by minor amounts over the next 3 month periods.

MWL, although being the softest sample, loses near half its stiffness after 3 months, and then remains at a lower recorded penetration force ≈ 10 N. There is a slight increase at 6 months but then a further fall in penetration force, though the changes are a relatively minor change compared to other wax samples.

MWM after the first 3 months loses 82 N of penetration force reducing to 199 N, at 6 and 9 months the force increases again to 246 N, reducing again to 207 N after 12 months of storage.

MWH although an initially very stiff component, shows a trend of general decrease in penetration force, with a large exception at 3 months. The loss of penetration force is the greatest of all waxes, after 3 months, with a loss of 163 N of recorded penetration force. The stiffness is then recovered at 6 months but continues to decrease every 3 months, up to 12 months of storage.

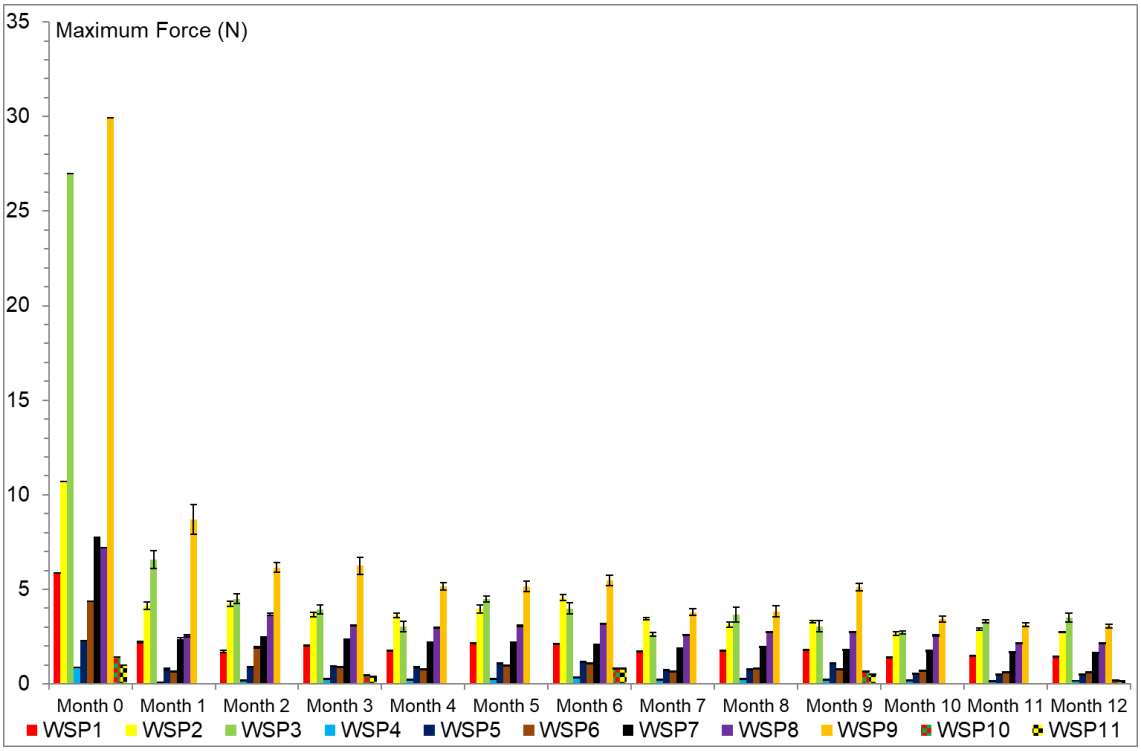

Figure 6.7 – Maximum penetration force of WSP blend taken over a 12 month total period, with data recorded every month.

At month 0 all samples have a higher stiffness than all other months of testing. Figure 6.7 shows that WSP3 and WSP9 lose the most penetration force

after one month of storage with WSP3 losing 20 N of recorded penetration force and WSP9 losing 21 N. Over the 12 months of storage there does appear to be a general trend of reduction in penetration force recorded for WSP3 and WSP9.

Other WSP blend samples also show this reduction in recorded penetration force from month 0 to the other testing months, although the losses do not appear as large as with WSP3 and WSP9. After month 1 there is little variability in the penetration forces recorded for other WSP blends for the other 12 testing months.

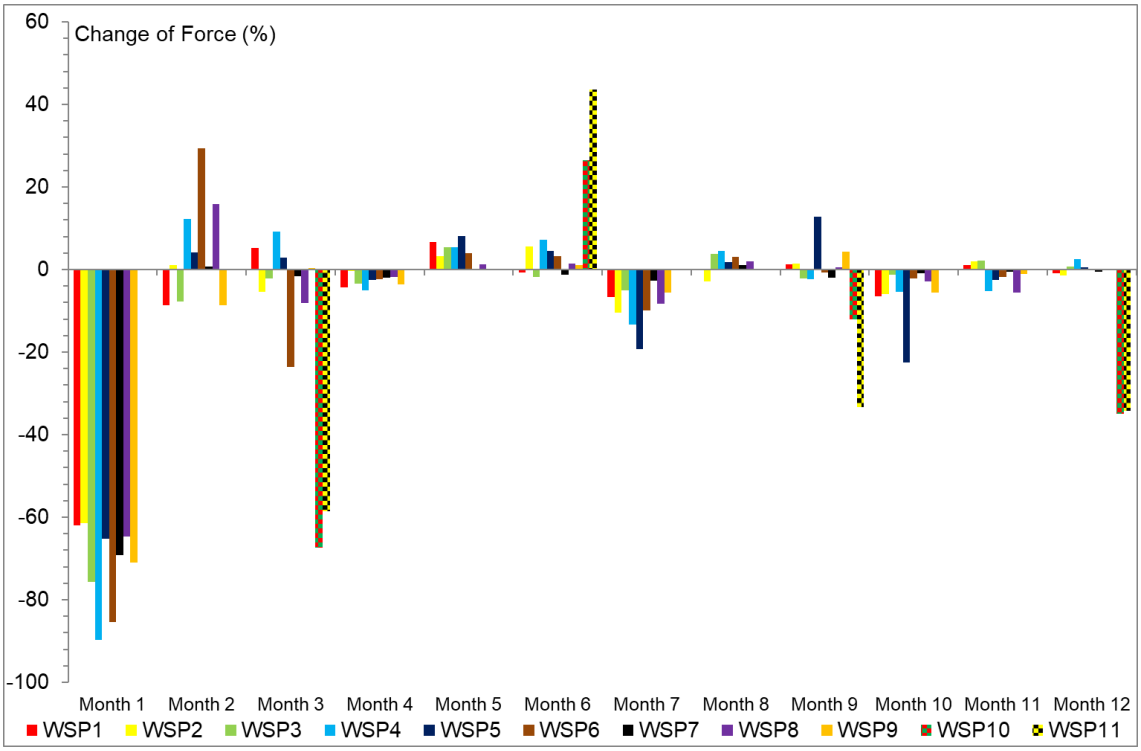

Figure 6.8 – Changes in penetration force recorded as a percentage of the original penetration force recorded for WSP blends.

Figure 6.8 shows the change in penetration force, which perhaps makes the trends with time clearer. Thus, at month 1 all samples lose between 60 % and 80 % of their stiffness as measured by the penetration force. WSP10 and WSP11, the two industry samples, were tested every 3 months unlike every month for other WSP blends. As such figure 6.8 shows that WSP10 and WSP11 also lose 67 % and 59 % respectively after three months of storage.

Figure 6.8 shows that of all the samples WSP10 and WSP11 have the greatest variability over the testing months, with an increase of recorded penetration force of 27 % and 44 % after 6 months' storage, followed by a

reduction of for WSP10 and WSP11 respectively of 12 % and 33 % at 9 months, and reduction of 35 % and 34 % after 12 months' storage.

Figure 6.8 also shows that WSP4, WSP5 and WSP6 exhibit some variability over the months of testing. WSP5 experiences larger fluctuations in penetration force at month 7 with a reduction of 19 % at month 9 with an increase by 13 % and month 10 with a reduction by 23 %. The reasons for this are not entirely clear, but suggest macroscopic inhomogeneities developing in the samples with time that are not visible, e.g., under the surface of the samples.

6.2.3.2 Small Deformation Rheology (Viscosity)

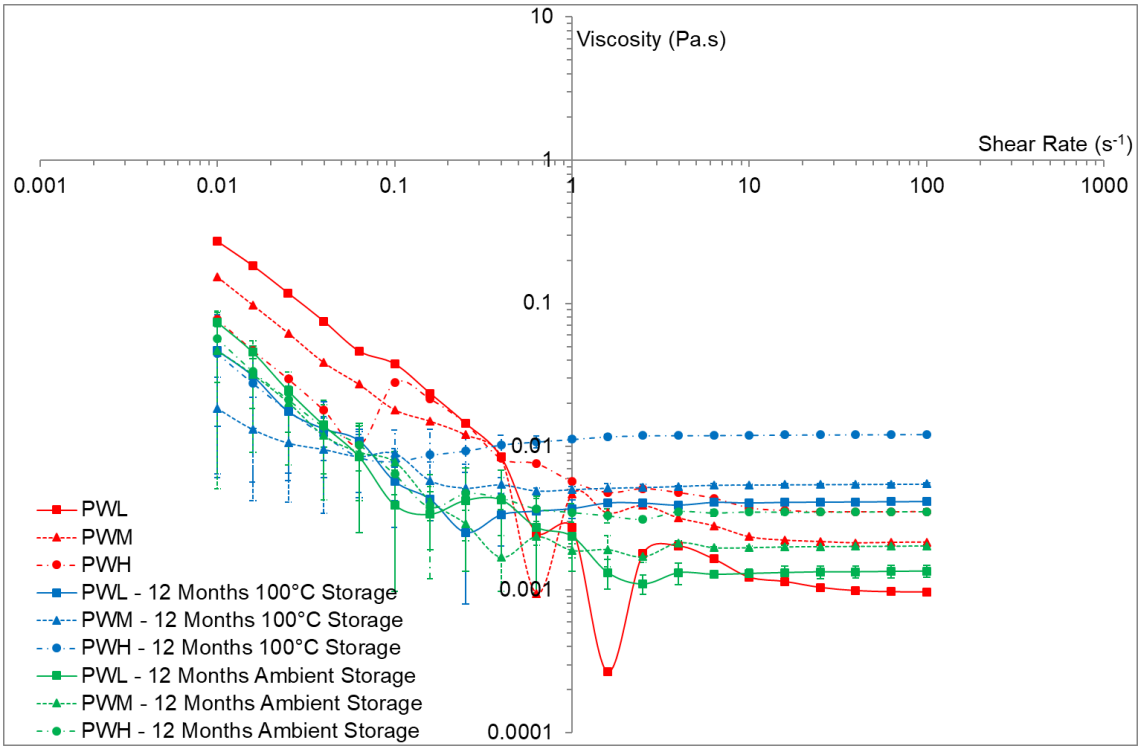

Figure 6.9 – Viscosity of PW after 0 months and 12 months' storage, when stored at ambient temperature and 100 °C.

Figure 6.9 shows PW viscosity at 0 months, and after storage at ambient temperature and 100 °C for 12 months. For each sample, there is a general trend of lowering viscosity as the shear rate increases. Samples at 0 months show higher viscosity at low shear rates but have comparable values to 12 month ambient storage samples when compared at high shear rates. 0 month samples show more noise than other samples, especially below 1 s^{-1} and appear to be more shear thinning. Samples stored for 12 months at 100 °C still show noise in the data but less at the lower shear rates, showing more Newtonian behaviour.

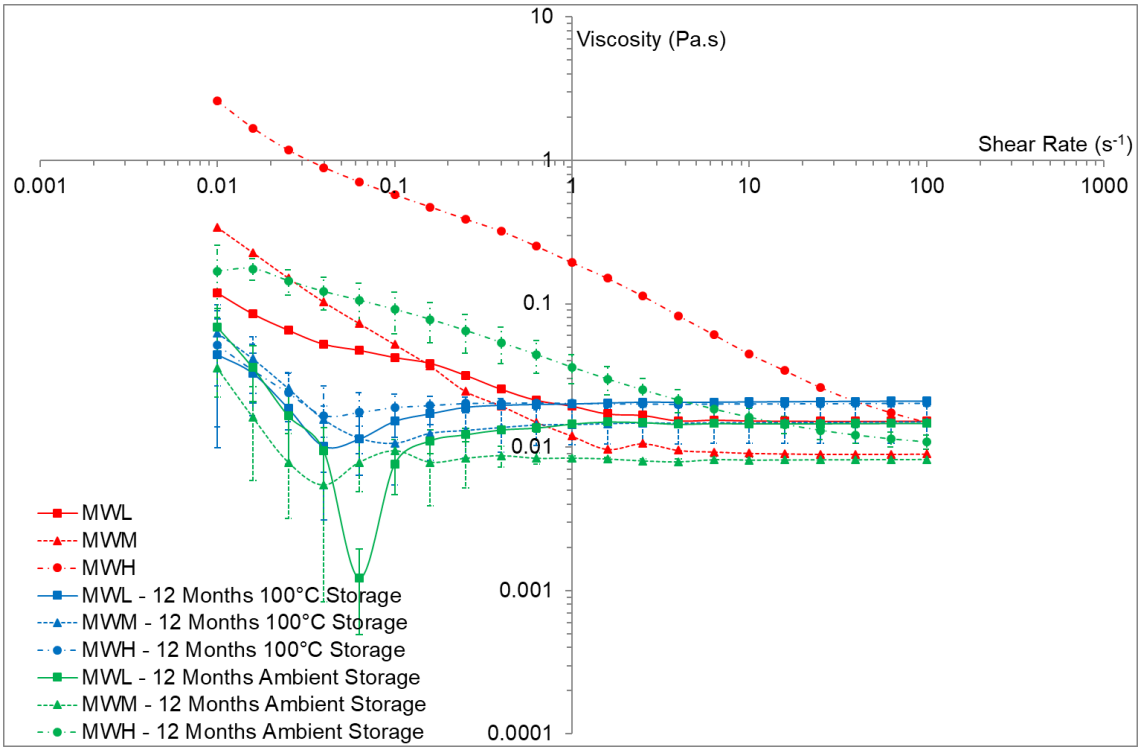

Figure 6.10 – Viscosity of MW after 0 months and 12 months' storage, when stored at ambient temperature and 100 °C.

MW, shown in figure 6.10, is seen to have a higher viscosity than all other samples shown in figure 6.9. When stored for 12 months at ambient temperatures, MWL and MWM reduce in viscosity at low shear rates and are Newtonian viscosity by 0.2 s^{-1} but MWH retains more non-Newtonian behaviour compared to the other MW under the same conditions. MW samples that have been stored for 12 months at 100 °C show similar low viscosity at low shear rates compared to MW at ambient temperatures, however, all MW samples after 100 °C storage have similar low Newtonian viscosities of ≈ 0.02 Pa s at 0.1 s^{-1}.

6.2.3.3 Small Deformation Rheology (Oscillation)

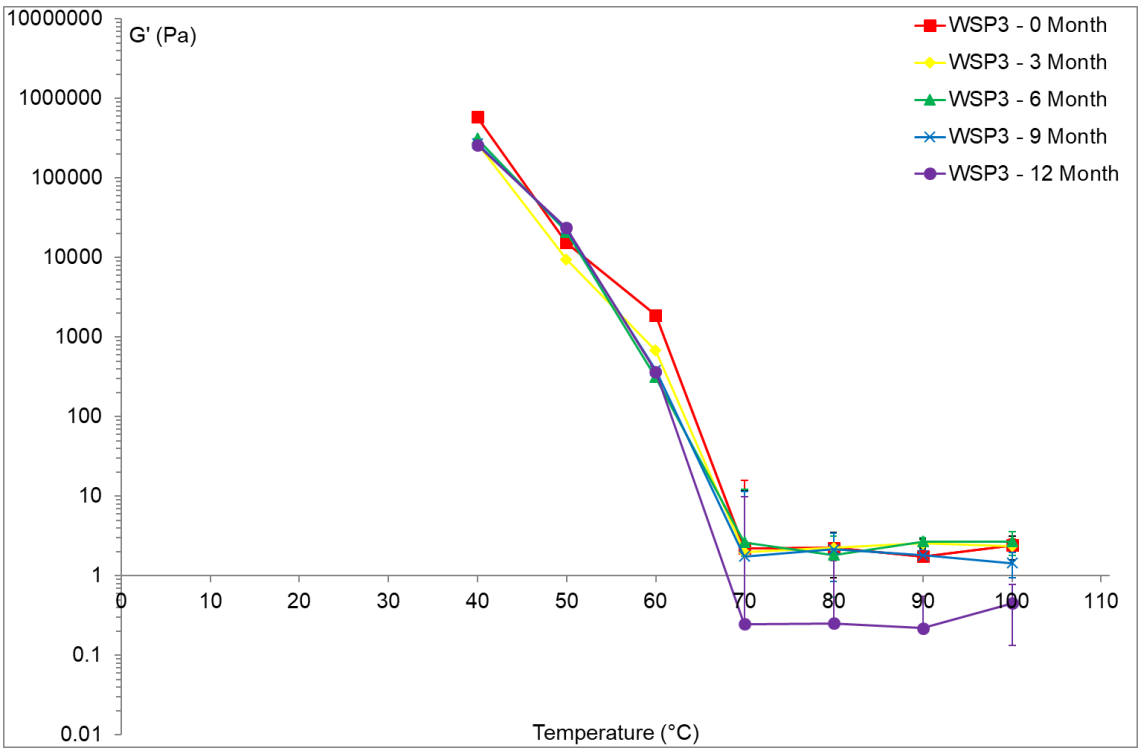

Figure 6.11 – Oscillation plots at 5 Hz frequency and 0.04 % strain, of WSP3 after storage periods of 0, 3, 6, 9, 12 months at 100 °C.

Figure 6.11 shows that there is a minor change in G' plots for WSP3 over the monthly periods of testing, however, at 12 months of storage the final G' values recorded when the WSP blend becomes molten, above 70 °C, are lower than the previous months. At 0 months' storage, the blend is stiffer: at 60 °C G' is 2000 Pa, 3 month storage has G' of 1000 Pa and 6, 9 and 12 months show G' values of 300 Pa.

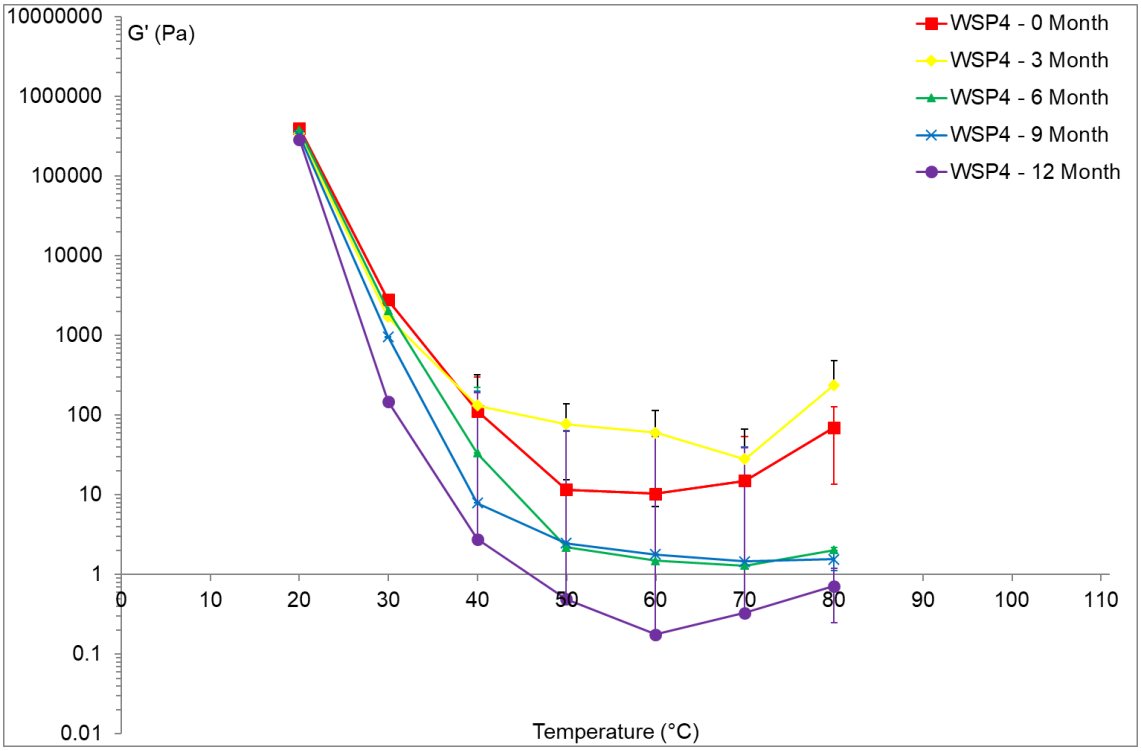

Figure 6.12 – Oscillation plots at 5 Hz frequency and 0.04 % strain, of WSP4 after storage periods of 0, 3, 6, 9, 12 months at 100 °C.

Figure 6.12 shows that as the storage period increases the G' values recorded decrease, in line with the decrease in stiffness of the samples seen in penetrometer tests described earlier. Month 3 shows an apparent increase in G', but this very unusual behaviour is thought to be simply an erroneous result. WSP4 samples have an increased rate of G' loss as temperature increases for all samples, however, the rate of loss increases as the storage temperature period increases. At month 0, G' at 20 °C and 30 °C is 400000 Pa and 3000 Pa, respectively, while for 12 months' storage G' are 300000 Pa and 150 Pa, respectively.

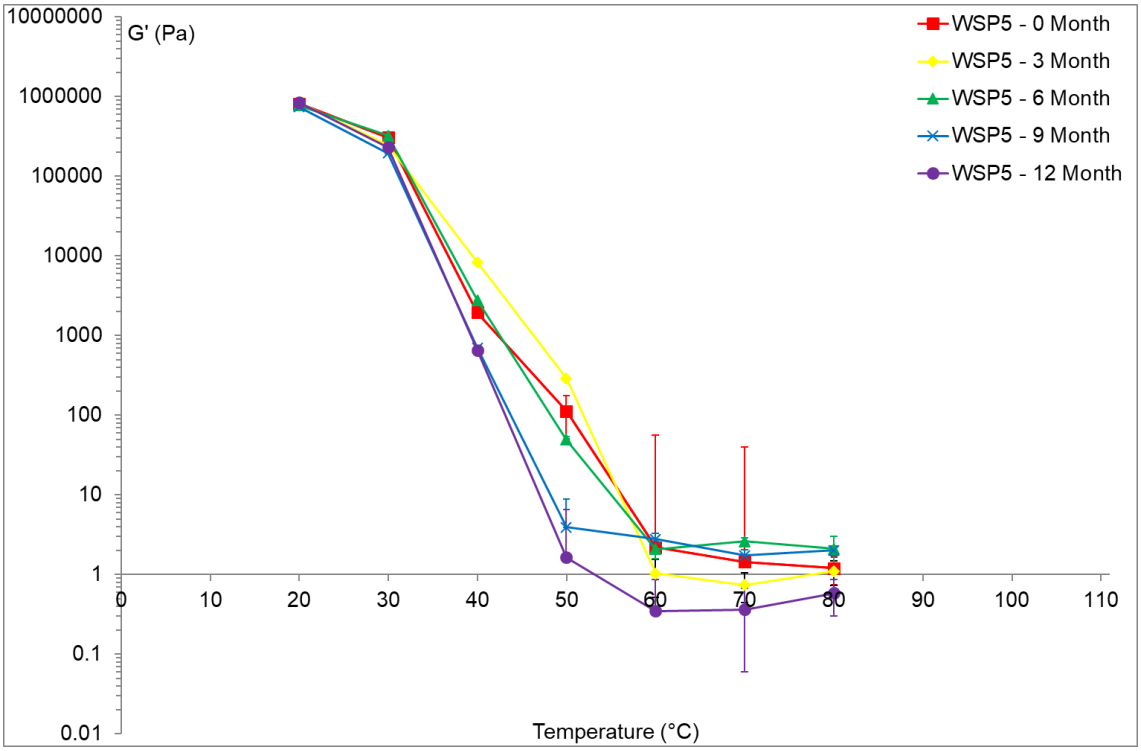

Figure 6.13 – Oscillation plots at 5 Hz frequency and 0.04 % strain, of WSP5 after storage periods of 0, 3, 6, 9, 12 months at 100 °C.

Figure 6.13 shows that WSP5 exhibits greater variation in G' values over the monthly time periods, especially at 50 °C. At 0, 3 and 6 months G' at 50 °C is ≈ 200 Pa, while for 9 and 12 months G' at 50 °C is 3 Pa and 2 Pa respectively. G' for WSP5 at 12 months' storage is generally lower than at all other months of testing.

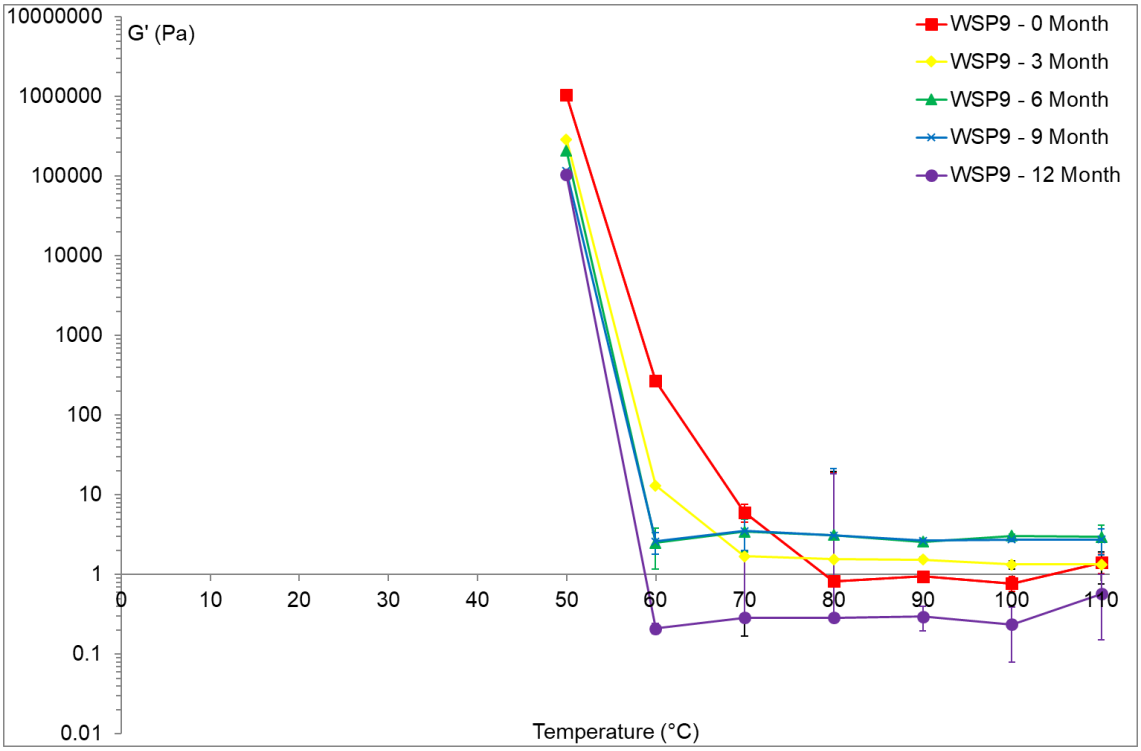

Figure 6.14 – Oscillation plots at 5 Hz frequency and 0.04 % strain, of WSP9 after storage periods of 0, 3, 6, 9, 12 months at 100 °C.

Figure 6.14 shows similar trends to other WSP blends over monthly testing. At month 0 WSP9 shows the greatest G' values, still retaining high values at 70 °C and a G' value of 300 Pa at 60 °C. At 60 °C WSP3 after 3 months' storage G' decreases with a recorded value of 10 Pa. Months 6 and 9 have almost identical plots and indicate loss of solid structure over the testing period since G' falls from 200000 Pa at 50 °C to 2 Pa at 60 °C. At 12 months' storage, there is a further fall: at 60 °C G' = 0.3 Pa.

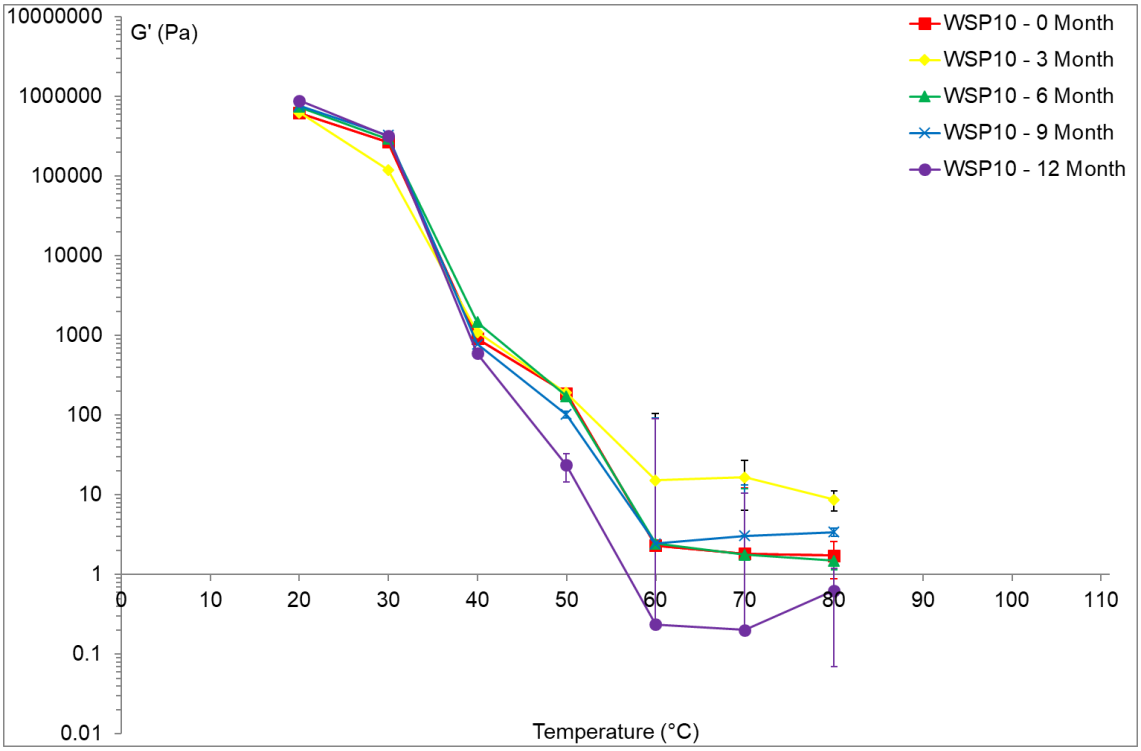

Figure 6.15 – Oscillation plots at 5 Hz frequency and 0.04 % strain, of WSP10 after storage periods of 0, 3, 6, 9, 12 months at 100°C.

Figure 6.15 shows the behaviour of the commercial sample WSP10. There is good uniformity in this sample and little variation as the testing period is increased. Month 3 shows higher G' values after 50 °C, however, this is likely an error. Month 12 shows that there is a loss of stiffness in the WSP blend. At 40 °C G' is like other storage time, with a G' value of 500 Pa. This decreases to 20 Pa at 50 °C whilst at other times G' remains at 200 Pa.

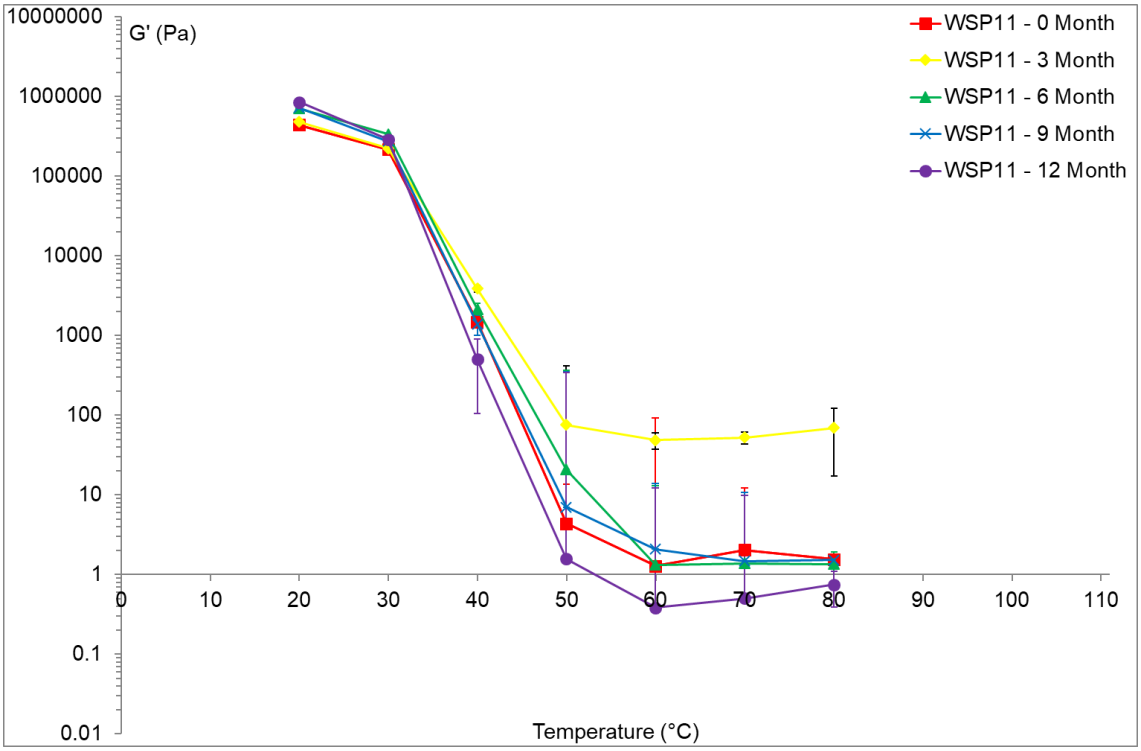

Figure 6.16 – Oscillation plots at 5 Hz frequency and 0.04 % strain, of WSP11 after storage periods of 0, 3, 6, 9, 12 months at 100°C.

Figure 6.16 shows that WSP11 has less stiffness than WSP10 (see figure 6.14) at 50 °C, with G' values falling by ≈ 200 Pa. In figure 6.16 the loss of stiffness is a rapid rate > 30 °C, falling from ≈ 300000 Pa for all sample ages to ≈ 1000 Pa at 40 °C and between 1.5 Pa and 20 Pa at 60 °C. Again, in figure 6.16 the 3 month result seems to be an erroneous plot, with G' ≈ 100 Pa above 50 °C.

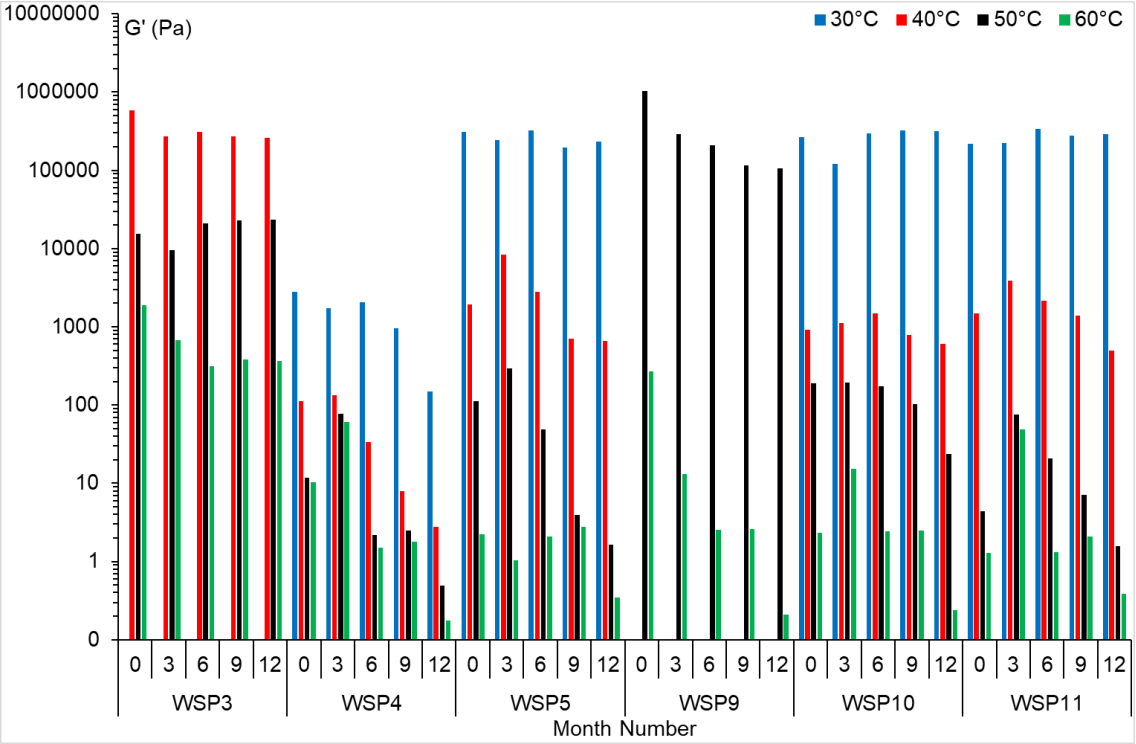

Figure 6.17 – Oscillation data points for WSP blends taken over a range of critical temperatures, viscoelastic region, also seen in figures 6.11 to 6.16.

Figure 6.17 summarizes G' values for all blends for critical viscoelastic temperatures 30 °C, 40 °C, 50 °C and 60 °C, i.e., where samples show (visually and rheologically) the major changes in their solidity/fluidity. For all WSP blends there is a general decrease in G' values as temperatures increase and as the monthly storage period increases.

WSP3 and WSP9 are the stiffest blends and no value could be recorded at < 30 °C, or < 40 °C, respectively. At 50 °C, there is a loss of G' for WSP9 with storage time. For WSP3 there is no change at 50 °C, however at 40 °C there is a slight decrease in G' for ≥ 6 months.

WSP4 is the softest blend, with G' values lower overall at all temperatures and these reduce rapidly with storage time. At month 0 there is some degree of stiffness at higher temperatures, but these values are still low, with G' values of 10 Pa at 50 °C and 60 °C.

WSP5, WSP10 and WSP11 show very similar plots at lower temperatures, 30 °C and 40 °C, with a slight decrease in G' value as storage time increases at 40 °C. At 50 °C WSP10 shows great stability over the 12 month storage period, with only a slight decrease in G' at month 12. At 60 °C, all three

blends again show similar values with G' ≈ 2 Pa, until month 12 where it drops to ≈ 0.2 Pa.

6.2.3.4 Raman Spectroscopy

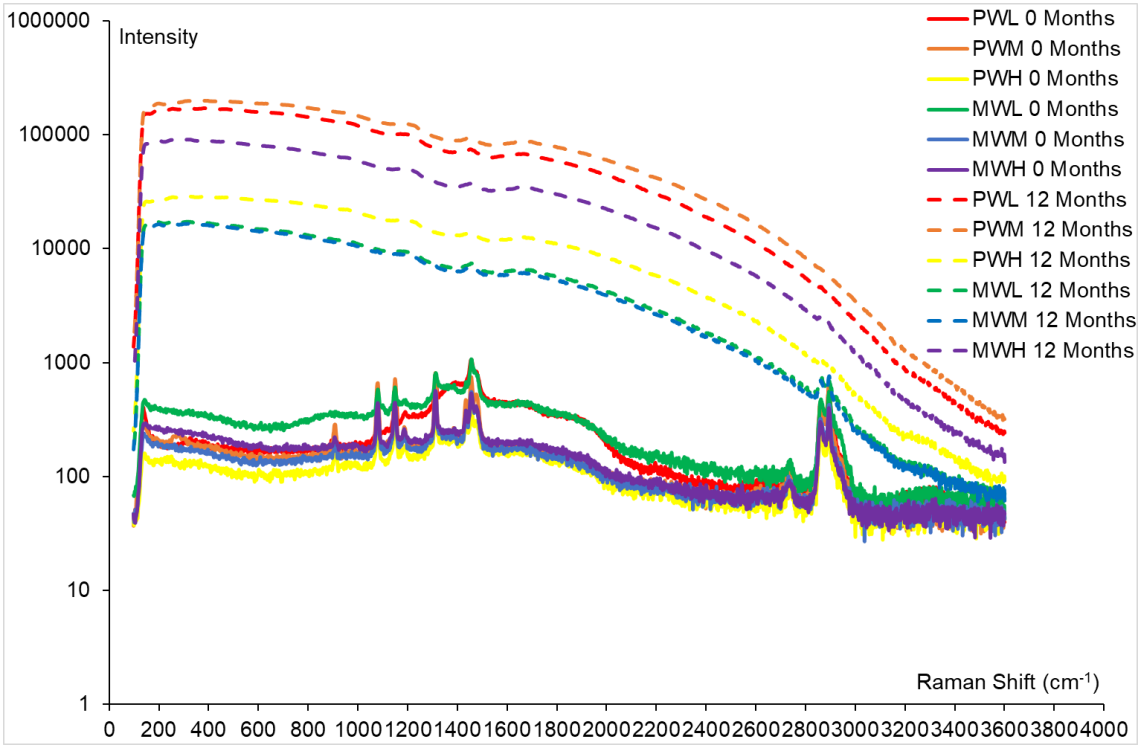

Figure 6.18 – Graph showing the Raman spectra for samples PWL, PWM, PWH, MWL, MWM and MWH at both 0 months' storage and 12 months' storage at 100 °C.

Figure 6.18 shows the spectra at 0 and 12 months. Month 0 has already been discussed at length in chapter 5. The curves in figure 6.18 for the constituent components show very high intensities for all samples compared to the same blends at month 0. PWL and PWM have the greatest intensity of all blends, with MWH next, followed by PWH and MWM and MWL, with almost identical plot curves.

The high intensities for the 12 month samples hide a lot of detail of compounds within the constituent components, however, some peaks are noticeable at bands 1200 cm^{-1}, 1500 cm^{-1} and at 2800 – 3000 cm^{-1} for MWL and MWM and slightly MWH.

6.2.3.5 Optical Microscopy

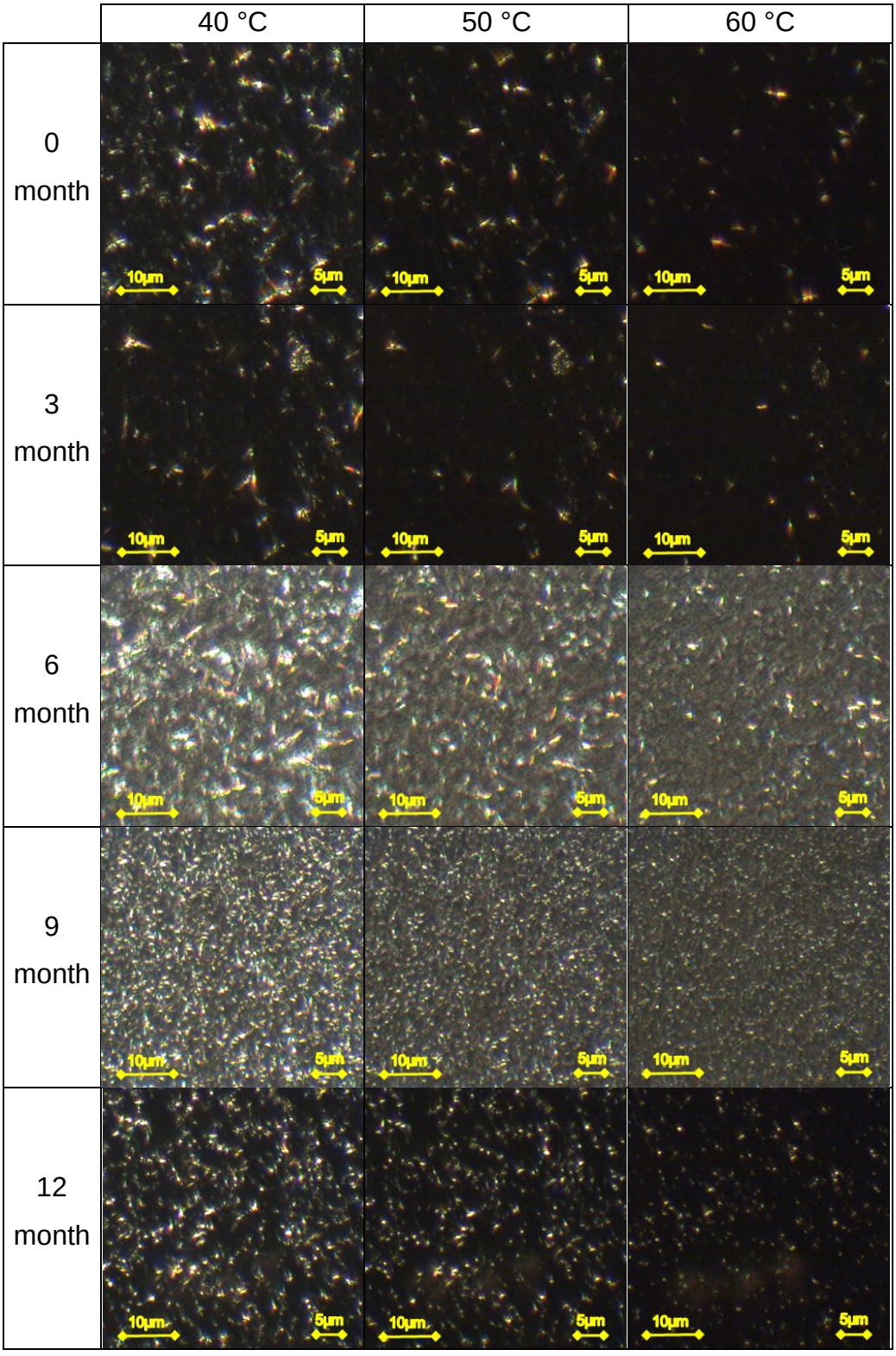

Figure 6.19 – Showing the WSP5 monthly polarized microscope images at critical viscoelastic region temperatures.

Figure 6.19 shows that there is a change in the size of crystals as the storage months increases. The crystal packing is also less dense at lower

temperatures. Between month 6 and month 9 there is a distinct change in the crystal size and packing within the images shown.

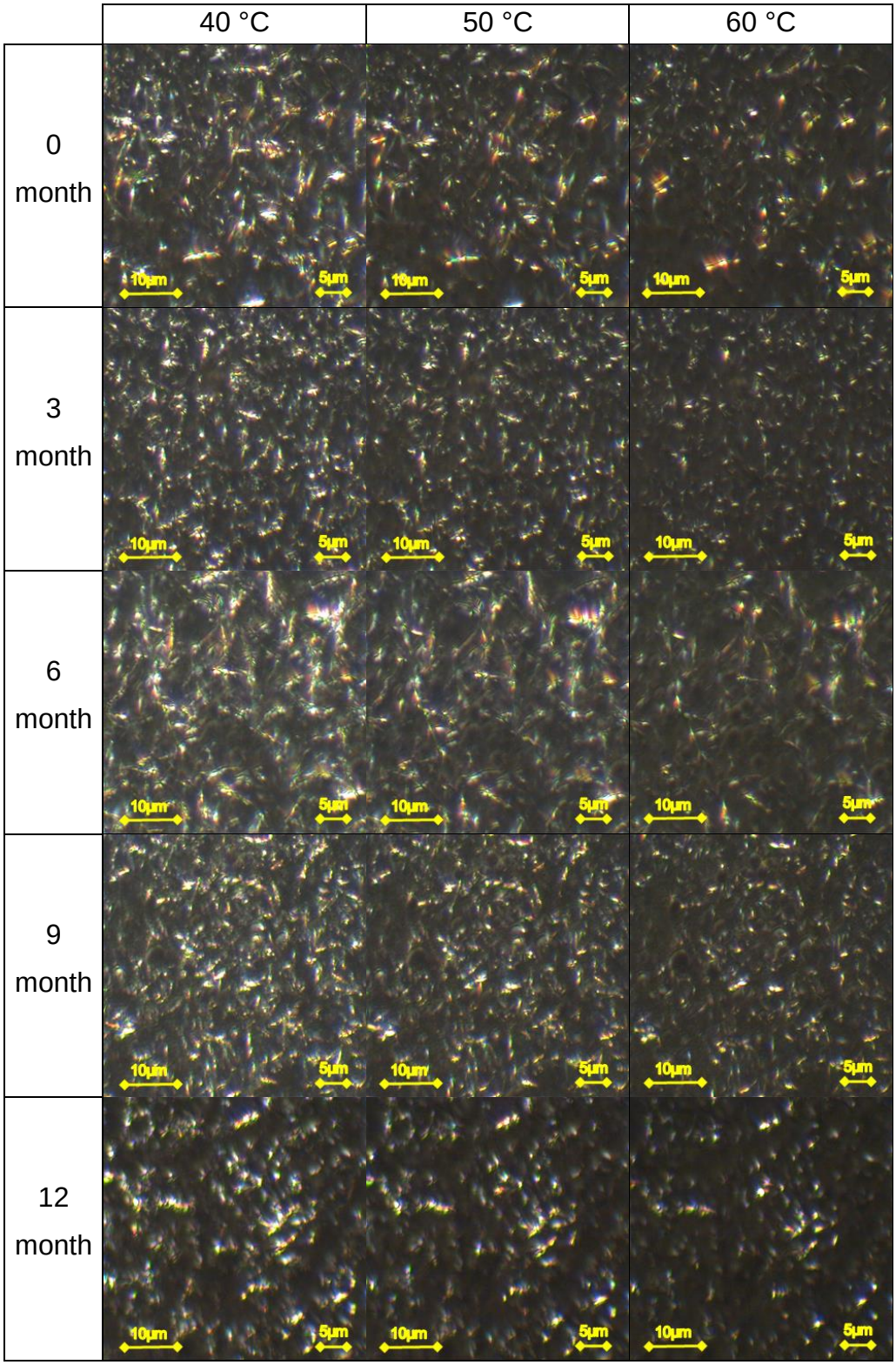

Figure 6.20 – Showing the WSP10 monthly polarized microscope images at critical viscoelastic region temperatures.

In Figure 6.20 there is less variation with increasing storage, crystal sizes remain relatively similar. As temperature increases, the crystal size decreases, but the change compared to WSP5 is less dramatic.

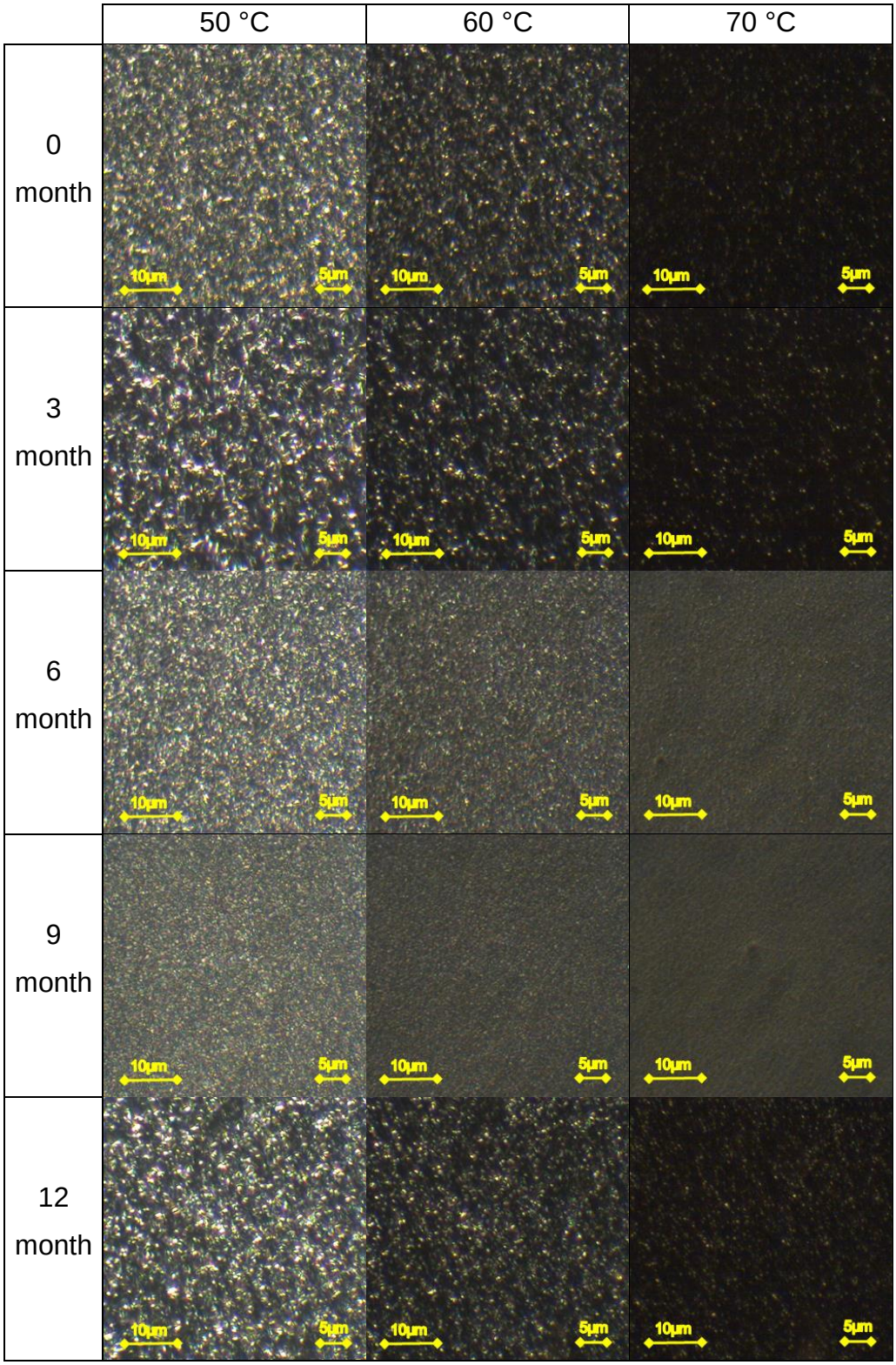

Figure 6.21 – Showing the WSP9 monthly polarized microscope images at critical viscoelastic region temperatures.

Figure 6.21 shows that WSP9 experiences rapid crystal melt over 20 °C change. The crystal density also changes with the months of storage, as the storage increases the crystal density appears to decrease. Crystal size is also much smaller compared to other WSP5 and WSP10.

When taking images, images of PW and MW were also taken using the same temperature profile, however, it was found that due to the 100 % content of wax the melting points and congeal points of the waxes were increased compared to the WSP blends that were made from the individual waxes.

6.2.4 Discussion

6.2.4.1 Large Deformation Rheology (Cone Penetration Testing)

The loss of stiffness experienced by all PW and MWL appears to influence the WSP blends that contain these components, however, the magnitude of the effects of mixing PW with MW does not always match that expected from the proportions in the mix.

PW is a group of hydrocarbons that contain mainly straight chains and the packing ability of the crystals is greater than MW. Their molecular weight is also less than MW, as such these components will be easier to melt, causing the loss of penetration force and formation of a crystal lattice to be weaker. MWL has a low congeal point and although it is classed as MW, it is possible the grade obtained from Kerax ltd. was of lower molecular weight and had more likeness to the PW provided.

MWM is the stiffest of all samples, likely due to the chemical nature of the material, the combination of branched hydrocarbons and small crystal sizes creating a very stable wax crystal network. This is the same for MWH, however, the values recorded for MWH are lower after months of storage, and at month 0. The change over time could be due to a breakdown of the highly-branched nature of the MWH. It is possible the MWH has such a high molecular weight that after storage at 100 °C $\geq$ 6 months chemical breakdown will occur.

The large drop in penetration force at 3 months measured for may be an error. This is most noticeable in MW due to their overall stiffer nature compared with PW. MWL loses 55 % stiffness after the first 3 months, MWM loses 29 % while MWH loses 60 %. All three MW samples then gain stiffness as measured via penetration force before the stiffness again decreases but with a less dramatic change over the remaining storage time.

For WSP blends shown in figure 6.7 and figure 6.8, month 0 shows that there is great stiffness in all the samples, but the losses experienced after 1

month storage are large. This large fall in stiffness is likely due to the production process if homogenisation had been used this might have produced more uniform mixtures. Figures 6.5 and figure 6.6 show that WSP4, WSP5 and WSP6 have much lower initial penetration forces but the samples are relatively unaffected by storage time, i.e., independent of their different compositions.

The larger changes in percentage seen in figure 6.8 can be misleading. For example, WSP4, WSP5 and WSP6 are of the softest of all the WSP blends, with WSP4 recording less than 1 N for an initial penetration force at month 0. Thus a 10 % change represents a very small change in penetration force. More importantly, commercial WSP10 and WSP11, that have been shown to be like model blend WSP5 in previous chapters, all undergo large variations on storage, much larger than those experienced by WSP5. The greater range of components within these commercial samples therefore obviously has more complex effects on structure and texture of the WSP on storage at elevated temperatures.

6.2.4.2 Small Deformation Rheology (Viscosity and Oscillation)

It should first be noted for small deformation rheology, results taken at three months of storage appear to show irregular results. It is believed there was an equipment failure and the results may not be representative of the full set of results obtained. As it can be seen, G' values appear to be elevated compared to the values expected, in trend with following months.

Figures 6.9 and 6.10 show that there is a distinct difference between PW and MW. There is a general trend for the viscosity of both waxes to decrease as the shear rate is increased, but overall PW has a lower viscosity compared to MW. On the other hand, both PW and MW lose viscosity as the storage time is increased, and this loss is even greater when the waxes are stored at 100 °C rather than ambient temperature. This is most obvious for MWH in figure 6.10 when stored at 100 °C, the viscosity becomes very low and Newtonian for shear rates > 0.1 s^{-1}.

A noticeable effect in figures 6.9 and 6.10 is that at shear rates < 0.3 s^{-1} for PW and MW (apart from MWH), the waxes experience higher viscosities, and as the shear rate is increased the viscosity becomes Newtonian. This change would be corresponding to wax crystals possibly present in the wax. Due to the lattice network being present at lower temperatures residual aggregates could

also be present as the temperature of the wax reaches higher temperatures such as 100 °C for the viscosity tests of figures 6.9 and 6.10. At lower shear rates the energy required to break up the aggregates is too low, therefore having a greater effect on the viscosity of the molten wax. As the shear rate increases, the energy in the movement of the molten waxes causes the aggregates to break up, reducing viscosity and showing Newtonian behaviour in the wax.

Figures 6.11 to 6.16 show that there is considerable variation between the model WSP blends depending on their composition. In figure 6.16 the critical viscoelastic regions are shown, with the maximum G’ value recorded over the storage time.

What is most clear is the change that occurs in the rheology between 0 and 12 months storage. Stiffer samples such as WSP3 and WSP9 experience minor changes in G’ values with time. WSP3 contains PWM and MWH, while WSP9 contains PWH and MWH. When considering the viscosities in figure 6.9 and figure 6.10, MWH has a high viscosity at month 0 and but is almost Newtonian after 12 months of storage at 100 °C, correlating with the drop of G’ at 12 months. PWM at month 0, although lower in viscosity, shows greater stability with time. PWH shows less stability and more variability in the measured rheology. This might explain why WSP3 remains stable when increasing storage period, yet WSP9 shows more change when storage period is increased.

WSP4 is the softest of all WSP blends since it contains both PWL and MWL, both of which have low viscosities (see figures 6.9 and 6.10), and although they do not change too much in viscosity over time, the G’ values decrease (see figure 6.12) as storage time increases, G' values are almost half that of the other WSP blends.

WSP5 has been previously described as the closest to the commercial samples, WSP10 and WSP11. Remember WSP10 is a commercial blend before temperature treatment and WSP11 is the same material that has gone through temperature cycles that typically occur in the manufacturing environment. Considering WSP5 between month 6 and month 9 is where the decrease in G’ occurs most. Prior to month 6, WSP5 shows great similarity to WSP10, whereas after month 6 it is more like WSP11, which makes sense since WSP11 is WSP10 that has been stored at unknown but elevated temperatures. This is further

evidence that WSP5 is a good model of this type of commercial material, even though it is probably a much simpler mixture in terms of its composition.

6.2.4.3 Raman Spectroscopy

Figure 6.18 shows that there is a change in the constituent components over 12 months' storage at 100 °C, exhibited as a large increase in intensity for all components. Also, a lot of fine peak detail in the spectrum is lost, although some peaks are still visible at bands 1200 cm^{-1}, 1500 cm^{-1} for PW and MW, and at 2800 – 3000 cm^{-1} for MWL and MWM and slightly MWH. These peaks indicate that it is still possible to identify chemical compounds within the constituent components, as described in Chapter 5. However, this information is largely lost in the spectra for PW and MW after 12 months storage, except for the peaks for carbon-carbon and carbon-hydrogen bonds (as expected for hydrocarbons).

One notable difference is the much lower intensity of the spectrum for MWL and MWM than that of MWH, PWL and PWM after 12 months' storage. Although the reasons for this are not clear, it may be related to different colour changes in the samples on storage.

Previously stated in chapter 5, in figure 5.21 and in figure 6.18, the presence of fluorescence for all samples is evident, especially for samples PWL and MWL for tests taken at 0 months storage. The fluorescence present at 12 months is most likely due to the colour change in the samples that occurred over the 12 months storage period. The wavelength used for the laser in testing and the application of a red filter for the samples is most likely also to contribute towards the overall increase in Raman spectra data, which is hiding the peaks that would be expected.

It would be recommended that upon further testing the use of extended and more accurate equipment should be used, to be able to filter out the fluorescence in the Raman spectra, such as the use of a laser with different energy and alternative filters would be more suitable.

6.2.4.4 Optical Microscopy

Comparing the model blend WSP5 with the commercial sample WSP10, which have been shown to have a strong likeness in rheological terms within the linear viscoelastic region, there is certainly a strong correlation in crystal shape

and size, as well as melting points, as seen in figures 6.19 and 6.20. At 6 months storage, the images in figure 6.19 show crystal sizes of ≈ 5 μm in length, but at 9 months the same crystals have decreased to ≈ 1 μm. In figure 6.20 over the same time period, the crystal size changed from ≈ 7 μm to ≈ 2-3 μm in WSP10. This slightly reduced change in crystal size could be an indication of greater wax ratio optimisation by the manufacturers of the commercial WSP blend WSP10.

Figure 6.21 shows the changes experienced by WSP9, a much stiffer sample than WSP5 and WSP10. The images show that the crystal size is much smaller than those in WSP5 and WSP10, with sizes ≈ 1 μm at 50 °C. When the temperature is increased, there is a slight reduction in crystal size to ≤ 0.5 μm, though it is impossible to give an accurate size in this range due to the resolution limits of the microscope.

For most samples, as the storage period increases up to 9 months the packing density of the crystals decreases due to a reduction in crystal size. However, between 9 and 12 months the crystal size seems to increase back to sizes like that at zero time. However, the behaviour of individual waxes is different. As the wax contribution is diluted in the WSP blends, the specific crystal characteristics of the waxes become less clear. In the WSP blends the crystals are much larger and less densely packed and this dilution could delay the onset of crystal nucleation, and decrease the rate of crystal growth and interaction within the WSP. In the pure wax components, the increased density of nuclei leads to the formation of denser crystal networks.

6.2.5 Conclusions

6.2.5.1 Large Deformation Rheology (Cone Penetration Testing)

- Long term storage of samples at high temperatures causes a breakdown in the physical characteristics of the waxes and WSP blends.
    - There is a general trend of reduction in penetration force over 12 months' storage of molten samples.
- Stiffer blends experience an absolute dramatic drop in penetration force after the first month of storage.
- When percentage changes in penetration force are compared all WSP blends behave similarly.

- Similar percentage changes correspond to the similar composition of WSP blends and therefore probably the commercial samples.
- Percentage changes in very soft samples, such as WSP4, are a bit misleading because absolute values are too low to be measured accurately.
- Similarly, percentage changes for very stiff samples, such as WSP3, are also not very reproducible, possibly due to sample inhomogeneity

6.2.5.2 Small Deformation Rheology (Viscosity and Oscillation)

- The viscosity of waxes does not vary much after storage at high or ambient temperature when samples are compared at high shear rates.
- Storing waxes over prolonged periods and at increased temperatures affects the viscoelasticity.
- Long term storage reduces the G' values within the WSP.

6.2.5.3 Raman Spectroscopy

- It is possible to see similarities in components between 0 and 12 months' storage at 100 °C via Raman spectroscopy.
- Care must be taken with samples and testing methods to ensure consistency of measurements, for example, to take account of colour changes.
- Further analysis could help to filter out results and remove and smooth the Raman spectra plots.

6.2.5.4 Optical Microscopy

- Increasing storage time at elevated temperatures reduces the size of individual crystals.
- Increasing storage time decreases the packing density of WSP blend lattices, due to small crystal sizes.
- Melting points are unaffected by increased storage time of WSP blends and waxes.

Chapter 7 Summary of Conclusions, and Moving Forward

7.1 Summary of Work

White soft paraffin is used as a functional ingredient of ointments. As this thesis has shown it is not a material easy to characterise, being a mixture of complex hydrocarbon waxes of increasing carbon length. However, the pharmaceutical industry requires a consistent product for use.

The aim of the project was to apply a range of characterisation techniques to both white soft paraffin and its constituent components (paraffin wax (PW) and microcrystalline wax (MW)) to define a basis for a functional specification. This was investigated by using a range of techniques. Physical deformation of the material was studied with rheology proving to be a feasible technique to differentiate among WSP. Material's phase changes were studied by DSC and microscopy and showed, not only the thermal behaviour of samples, crucial for handling and material blending but also that the combination of enthalpies. DSC results showed energy requirements did not equal that of calculated values for the model WSP blends, therefore to understand unknown commercial blends, DSC is a crucial step required. To explore the chemical characteristics, solubility and Raman spectroscopy were performed with the expectation of obtaining data about miscibility between samples, and spectra of components and compound identification within the waxes and WSP blends. Finally, investigating the blending process to necessitate the study, of both, underlying components and formulated material (WSP), and relating the findings to key requirements of stability and process changes, needed to be achieved to obtain a suitable end use product.

Initially, the constituent components were combined into a variety of WSP blends. This protocol was followed to simplify the testing of WSP within the confines of this project. It also showed how variations of WSP components changes drastically its properties, exhibiting how difficult it can be to produce WSP consistently, and it is not simply a random mixture of waxes and oils.

Resulting from the blending process penetration tests were carried out in line with standardised cone penetration testing done within the pharmaceutical industry. Both constituent components (PWL, PWM, PWH, MWL, MWM, MWH) and the resulting WSP blends (WSP1-9) were tested, as well as two commercial pharmaceutical grade blends (WSP10 and WSP11). MW was found to be the stiffest of all samples, and with increasing congeal points an increase in stiffness was recorded, both MWM and MWH were found to record values ≈ 275 N of force. PW also showed high force, with PWM and PWH recording values ≈ 150 N of force, both PWL and MWL had lower force value compared to their higher congeal point counterparts.

These constituent components when placed in corresponding WSP blends were found to imitate the higher stiffness values obtained by the individual wax components. WSP3 (combining PWM and MWH) and WSP9 (combining PWH and MWH) showed high stiffness values, recording 26 N and 30 N respectively. After these the next stiffest value was WSP2 with a value of 10 N of force, WSP2 is a combination of PWM and MWM, still highly stiff waxes individually, but when combining the force reduces.

In combined blends of WSP stiffer samples were found to fluctuate in recorded force while under individual test experiments, with blends containing stiffer waxes in their ratio makeup also showing greater fluctuations in penetration under testing. These fluctuations are likely due to crystal layers present in the WSP, with plate layers and needle/mal crystals interrupting the structural lattice network, weakening the WSP blend under testing. Commercial blends were found to be homogenous under testing but as it is unknown the wax types and their ratios, it is unknown how the commercial WSP was produced, but the blends were soft and like other laboratory WSP blends, namely WSP4 and WSP5.

Later small deformation rheology was carried out on constituent components and WSP blends, both laboratory and commercial grades. Viscosity measurements were made for components as this was part of the quality testing for these materials from the supplier, and would be carried out in the pharmaceutical industry as part of their own quality assurance.

As with the penetration testing where MW was overall stiffer (higher penetration force) than PW, and with increased congeal point, stiffness also increased. In viscosity testing, MW was shown to have greater viscosity values overall, especially at higher shear rates of 100 s^{-1}. When testing at a low shear rate of 0.01 s^{-1} constituent components showed much closer values in viscosity, except MWH. MWH although containing higher viscosity values, it was also most affected by increasing shear rates by decreasing viscosity, where other samples appear to reach a plateau in viscosity at 1 s^{-1} and remain unchanged as shear rate continues to increase.

As experienced in penetration testing, the crystal presence plays a role in the material, in viscosity testing it is likely that for MWH, even though tests were carried out at 100 °C there are crystals still present in the molten wax, causing the increased recording of viscosity.

Following from viscosity testing, oscillatory testing was carried out on select WSP blends made in the laboratory (WSP3, WSP4, WSP5 and WSP9), and the two commercial blends (WSP10 and WSP11). WSP3, WSP4 and WSP9 were chosen as they are extreme blends made with high congeal point (WSP3 and WSP9) or low congeal point waxes (WSP4), WSP5 has been found to be most like commercial blends and as a way of comparison WSP5 was measured against WSP10 and WSP11 for greater evidence of similarities seen in penetration testing.

Oscillation testing found that WSP5 was, as shown in previous measurements, like WSP10 and WSP11. WSP4, containing PWL and MWL and WSP5, containing PWL and MWM showed a marked difference in G’ values under testing, with WSP4 showing lower values overall, one exception being at 20 °C where values were similar. Stiffer samples, WSP3 and WSP9 recorded higher G’ values, so much that at temperatures of 50 °C where WSP5 was within a viscoelastic region, WSP3 and WSP9 were solid both recording G’ values ≥ 1000000 Pa.

Ultimately PW had a greater influence on viscoelastic regions of WSP blends, with higher congeal point PW causing a narrow range of viscoelastic region to exist for a model blend. MW had influence over the overall stiffness and

melting points of the model blends, with increasing congeal points causing increases in melting points and stiffness, as also seen in penetration testing.

Also notable is that soft WSP model blends had greater potential for hysteresis after storage and after temperature cycling, while stiffer model blends, although experienced hysteresis after storage, when cycling temperature hysteresis was lost and model blends became uniform.

As described, thermal analysis was required for WSP and its constituent components to fully understand the characterisation of these wax materials. From dynamic temperature ramp (rheology) testing it was also evident that WSP is highly temperature dependent, therefore, to test in static (without oscillation) the phase changes, differential scanning calorimetry (DSC) was carried out.

From previous results MW was a stiffer sample, had the greatest congeal point overall, and was expected to contain greater energy requirements, however, in this investigation, it was found that PW contained greater energy than MW.

Constituent components when tested also showed no correlation to the WSP model blends made from the components. The variability of PW having increased enthalpy also caused increased enthalpy in WSP model blends as congeal point increased. Similarly, MW has shown to affect the melting and crystallisation points, within increasing congeal point, so does the melting and crystallisation points. This effect was seen in the WSP model blends, as with blends containing high congeal point MW so did the melting and crystallisation points increase.

As described before, combining constituents in model blends appeared not to give the same enthalpy results when using calculated values based on singular constituent components. Therefore, it was believed that crystal material was being dissolved in the oil phase contained in the model WSP, added as part of the blending process. This dissolving crystal material is likely to have remained in the crystal phase upon melting and re-crystallisation of the WSP model blend being tested.

When comparing to commercial WSP blends the model WSP blends were found not to follow the same similarities seen in other characteristic tests. In

rheological testing WSP10 is like WSP5, however, within DSC testing, WSP10 is most like WSP3 in terms of energy and enthalpy results.

Believing that crystal material was being dissolved in the oil phase of the WSP model blends, the following work was carried out investigating the solubility of the constituent components and WSP blends.

PWM, PWH, MWL and MWM showed to contain components that are most compatible with decahydronaphthalene, most likely due to the higher molecular weight and double ring structure of this solvent. Curiously in MWH acetonitrile showed most affinity, which is also most prevalent in toluene, indicating a component of these materials were similar.

WSP blends have better solubility in lower molecular weight solvents with medium dispersion force strength. Heptane is a better solvent for WSP blends and pure hydrocarbon materials, this suggests larger content of component materials in the blends, such as the oils, has an affinity for the lower mW solvents.

Raman spectroscopy has previously been used as a fingerprint method to identify compound types within WSP and its components. Raman is often a useful tool for identification of impurities in samples, and as such can be implemented as a quality assurance step for WSP processing helping to reduce WSP blend long term issues.

As seen in the previous chapters WSP is much more complicated than was considered before this project. WSP is not just a mix of few wax materials but multiple components of waxes, not only is this an issue but each wax will have its own physical, thermal and chemical signature. As such Raman spectroscopy was found to not be invasive enough for these materials and would require other techniques such as GC-MS.

Recorded data indicated that the bending of C-C bonds is prevalent and the manipulation of CH_2 bonds is strong, however, the bending of CH_2 and CH_3 bonds occurs in little values, compared to those expected from previous authors. Both PWL and MWL were most affected by the Raman spectroscopy experiment and experienced expanded broad peaks at lower wavenumbers. There were

similar trends within the samples compared with the higher congeal point materials, however, data was possibly lost in the scan compared to the others.

Ultimately this project had the aim of characterising WSP and its constituent components with regards to ointments, and this should be considered with the scope of a product within the pharmaceutical industry, suitable for consumer end use. A factory process investigation was carried, aspects concentrated on were the overloading of model WSP blends, WSP4, WSP5 and WSP6. Also, a long term high temperature stability study was completed, to find failures in the chemical and physical nature of WSP blends and constituent components.

When overloading WSP model blends, the addition of oil resulted, notably, in syneresis on the surface of the WSP, however softer blends were subject to a breakdown of lattice structure at an earlier stage of oil overloading. Visually the model blends also changed, changing from a bright coloured blend to a dull matt colour, due to crystal lattice size changing, possibly decreasing, causing less light reflection.

For stiffer blends, addition of oil can help to optimise the blend, creating a model WSP that would be suitable for consumer end use (within quality assurance parameters), the swelling and strengthening of the crystal lattice allows greater qualities of the WSP, however further addition of oil still found an overload and syneresis was evident.

After long term storage of 12 months at 100 °C, all previous testing methods were carried out, with cone penetration testing all waxes and WSP blends showed evidence of the breakdown of the physical characteristics. Stiffer samples suffered the largest loss of structure, however, this is likely due to having the greatest potential for loss within their structure. Overall considering percentage loss of stiffness, all materials suffered the same losses.

Over long term storage, viscosities of waxes do not alter, however, viscoelastic properties are effects, and WSP blends show evidence of loss of G’ values.

Raman spectroscopy did show some similarities in waxes, with peaks shown for components expected, and seen in 0 month storage materials,

however, results were not conclusive due to colour changes in the sample, creating difficulties in sample measurement.

Finally, when observing constituent components and WSP blends under cross polar microscopy, evidence showed that crystal size decreased in samples after long term storage, while also decreasing the packing density of lattices, due to the reduction in crystal size. However, melting and crystallisation points appeared to not be affected by long term storage when observed under the microscope.

7.2 Future Work

This project in its entirety has covered many aspects of characterisation of WSP and its constituent components, however, it has opened, as well, many research areas important for investigation in future. The following outlines possible research areas for greater understanding and use of WSP blend and components;

- Now that the base constituents have been studied, it will be needed to include further wax materials to the overall physical, thermal and chemical characterisation,
    - Obtained wax from multiple suppliers can help to distinguish the difference in waxes.
    - Possibly obtain samples from across the globe to obtain a large (true) scope of the wax characteristics, and to perform a worldwide database of WSP
- The inclusion of wax appearance temperature tests would be useful at the various temperature step used in the temperature profile used throughout this body of work.
    - The WAT could be correlated with the G’ and temperature profiles that have been investigated already.
- Including further chemical analysis of waxes and WSP blends to help determine recognisable patterns and “fingerprints” between the constituent components and results blends
    - MS/GCMS has been shown to work for lower Mw hydrocarbons, with few attempts as such high Mw materials and their blend mixes.

- Extension of Raman spectroscopy, to include WSP model blends.
    - To correlate constituent components with WSP model blends made of them
- In this work, the baseline for solubility work was set, however, this line of research could be further explored by;
    - Adding a wider range of solvents would be needed to obtain values of compound solubility, especially ones of different;
        i. Hydrogen bonding strength.
        ii. At least six of strong, medium and weak hydrogen bonding solvents.
        iii. Solvents with differing intermolecular forces.
- Extend oil overload testing to more model WSP blends;
    - An optimisation stage could be found, such that a critical oil addition level can be given as a QC point within processing.
- With greater model blends made and/or optimised blend should be tested under ambient “normal” conditions;
    - Conditions expected from consumer use should be tested over a reasonable amount of time, to obtain “true” data of stability in WSP model blends.
- Develop better images analysis for greater magnification of crystals may show how crystals can change over time and with the inclusion of different waxes and oil ratios, into blend makeup.

Chapter 8 References

Abbott, S., Hansen, C.M. and Yamamoto, H. 2013. *Hansen solubility parameters in practice complete with eBook , software and data*.

Al-shemmeri, T. 2010. *Engineering Thermodynamics*. Ventus Publishing ApS.

Al-Zahrani, S.M. 2000. Utilization of Polyethylene and Paraffin Waxes as Controlled Delivery Systems for Different Fertilizers. *Industrial and Engineering Chemistry Research*. [Online]. **39**(3),pp.367–371. Available from: http://pubs.acs.org/doi/abs/10.1021/ie980683f%255Cnhttp://pubs3.acs.org/acs/journals/doilookup?in_doi=10.1021/ie980683f.

Anghel, E.M., Georgiev, A., Petrescu, S., Popov, R. and Constantinescu, M. 2014. Thermo-physical characterization of some paraffins used as phase change materials for thermal energy storage. *Journal of Thermal Analysis and Calorimetry*. **117**(2),pp.557–566.

Ashbaugh, H.S., Radulescu, A., Prud'homme, R.K., Schwahn, D., Richter, D. and Fetters, L.J. 2002. Interaction of paraffin was gels with random crystalline/amorphous hydrocarbon copolymers. *Macromolecules*. **35**(18),pp.7044–7053.

ASTM 2016. Standard Test Method for Needle Penetration of Petroleum Waxes. *ASTM International*. [Online]. [Accessed 11 June 2017]. Available from: http://www.astm.org/cgi-bin/resolver.cgi?D1321.

Babaei, H., Keblinski, P. and Khodadadi, J.M. 2013. Improvement in thermal conductivity of paraffin by adding high aspect-ratio carbon-based nano-fillers. *Physics Letters, Section A: General, Atomic and Solid State Physics*. [Online]. **377**(19–20),pp.1358–1361. [Accessed 13 November 2013]. Available from: http://linkinghub.elsevier.com/retrieve/pii/S0375960113003253.

Barry, B.W. 1970. Recent Advances in Pharmaceutical Rheology. *Journal of Texture Studies*. [Online]. **1**(4),pp.405–430. [Accessed 12 December 2013]. Available from: http://onlinelibrary.wiley.com/doi/10.1111/j.1745-4603.1970.tb00740.x/abstract.

Barry, B.W. and Grace, A.J. 1971a. Rheological and sensory evaluation of work softening and recovery of pharmaceutical white soft paraffins. *Journal of pharmaceutical sciences*. [Online]. **60**(8),pp.1198–203. Available from: http://www.ncbi.nlm.nih.gov/pubmed/5127094.

Barry, B.W. and Grace, A.J. 1971b. Rheological properties of white soft paraffin. *Rheologica Acta*. [Online]. **10**(1),pp.113–120. [Accessed 10 December 2013]. Available from: http://link.springer.com/article/10.1007/BF01972487.

Barry, B.W. and Grace, A.J. 1971c. Structural, Rheological and Textural Properties of Soft Paraffins. *Journal of Texture Studies*. **2**(3),pp.259–279.

Barton, A. 1975. Solubility Parameters. *Chem. Rev.* **75**,pp.731–753.

Berneis, K.H., Munzel, K. and Waaler, T. 1964. Kegelpenetration Praktischer Fliesspunkt Von Kohlenwasserstoff-Salbengelen. *Pharmaceutica Acta Helvetiae*. **39**(10),p.604.

Bourne, M.C. and Bourne, M.C. 2002. Chapter 6 – Viscosity Measurement *In*: *Food Texture and Viscosity*., pp. 235–256.

Brame, E. and Graselli, J. 1976. *Infrared and Raman spectroscopy (Practical spectroscopy series)*.

Briker, Y., Ring, Z., Iacchelli, A., McLean, N., Fairbridge, C., Malhotra, R., Coggiola, M.A. and Young, S.E. 2001. Diesel fuel analysis by GC-FIMS: Normal paraffins, isoparaffins, and cycloparaffins. *Energy and Fuels*. [Online]. **15**(4),pp.996–1002. [Accessed 12 December 2013]. Available from: http://pubs.acs.org/doi/abs/10.1021/ef010057m.

Buhse, L., Kolinski, R., Westenberger, B., Wokovich, A., Spencer, J., Chen, C.W., Turujman, S., Gautam-Basak, M., Kang, G.J., Kibbe, A., Heintzelman, B. and Wolfgang, E. 2005. Topical drug classification. *International Journal of Pharmaceutics*. **295**(1–2),pp.101–112.

Carvalho, S.P., Lucas, E.F., González, G. and Spinelli, L.S. 2013. Determining hildebrand solubility parameter by ultraviolet spectroscopy and microcalorimetry. *Journal of the Brazilian Chemical Society*. [Online]. **24**(12),pp.1998–2007. Available from: http://www.gnresearch.org/doi/10.5935/0103-5053.20130250.

Cerezo, A. and Suñe, J. 1970. Rheological Evaluation of Pomade Excipients by Penetrometry. *Trav. Soc. Pharm. Montpellier*. **30**(5).

Chang, G., Koo, J. and Song, K. 2003. Wall slip of vaseline in steady shear rheometry. *Korea-Australia Rheology …*. [Online]. **15**(2),pp.55–61. [Accessed 10 December 2013]. Available from: http://infosys.korea.ac.kr/PDF/KARJ/KR15/KR15-2-0055.pdf.

Chang, K.C., Chiang, Y.W., Yang, C.H. and Liou, J.W. 2012. Atomic force microscopy in biology and biomedicine. *Tzu Chi Medical Journal*. [Online]. **24**(4),pp.162–169. Available from: http://dx.doi.org/10.1016/j.tcmj.2012.08.002.

Clavell-Grunbaum, D., Strauss, H.L. and Snyder, R.G. 1997. Structure of model waxes: Conformational disorder and chain packing in crystalline multicomponent n-alkane solid solutions. *Journal of Physical Chemistry B*. **101**(3),pp.335–343.

Delonca, H., Dolique, R. and Bardet, L. 1967. Determination of thixotropy of vehicles for ointments. *Annales pharmaceutiques françaises*. **25**(3),pp.225–235.

Deman, J.M. and Beers, A.M. 1987. Fat Crystal Networks: Structure and Rheological Properties. *Journal of Texture Studies*. **18**(4),pp.303–318.

Dudkiewicz, A., Tiede, K., Loeschner, K., Jensen, L.H.S., Jensen, E., Wierzbicki, R., Boxall, A.B.A. and Molhave, K. 2011. Characterization of nanomaterials in food by electron microscopy. *TrAC - Trends in Analytical Chemistry*. [Online]. **30**(1),pp.28–43. [Accessed 15 January 2014]. Available from: http://linkinghub.elsevier.com/retrieve/pii/S0165993610002967.

Edwards, H.G.. and Falk, M.J.. 1997. Fourier-transform Raman spectroscopic study of unsaturated and saturated waxes. *Spectrochimica Acta Part A: Molecular and Biomolecular Spectroscopy*. **53**(14),pp.2685–2694.

Edwards, R.T. 1957. Crystal Habit of Paraffin Wax. *Industrial & engineering chemistry*. **49**(4),pp.750–757.

Faoláin, E.Ó., Hunter, M.B., Byrne, J.M., Kelehan, P., Lambkin, H.A., Byrne, H.J. and Lyng, F.M. 2005. Raman Spectroscopic Evaluation of Efficacy of Current Paraffin Wax Section Dewaxing Agents. *The Journal of Histochemistry & Journal of Histochemistry & CytochemistryJ Histochem Cytochem*. [Online]. **53**(53),pp.121–129. Available from: http://www.jhc.org.

Ferris, S.W. and Cowles, H.C. 1945. Crystal Behavior of Paraffin Wax. *Industrial & Engineering Chemistry*. [Online]. **37**(11),pp.1054–1062. Available from: http://pubs.acs.org/doi/abs/10.1021/ie50431a016.

Flaherty, B. 1971. Characterisation of waxes by differential scanning calorimetry. *Journal of Applied Chemistry and Biotechnology*. [Online]. **21**(5),pp.144–148. Available from: http://dx.doi.org/10.1002/jctb.5020210507.

Freund, M., Csikós, R., Keszthelyi, S. and Mózes, G.Y. 1982. *Paraffin Products Properties, Technologies, Applications* [Online]. Available from: http://www.sciencedirect.com/science/article/pii/S0376736108701481.

Gallagher, P., Brown, M. and Kemp, R. 1998. *Handbook of Thermal Analysis and Calorimetry: Volume 1 - Princples and Practice*.

Genovese, A. and Shanks, R.A. 2007. Time-temperature creep behaviour of poly(propylene) and polar ethylene copolymer blends. *Macromolecular Materials and Engineering*. **292**(2),pp.184–196.

GlaxoSmithKline 2013. *GSK Infomation Pack v1.1*.

Hansen, C.M. 2000. Solubility Parameters — An Introduction. *Hansen Solubility Parameters: A User's Handbook*.,pp.1–24.

Hansen, C.M. and Smith, A.L. 2004. Using Hansen solubility parameters to correlate solubility of C60 fullerene in organic solvents and in polymers. *Carbon*. **42**(8–9),pp.1591–1597.

Hawlader, M.N.A., Uddin, M.S. and Khin, M.M. 2003. Microencapsulated PCM thermal-energy storage system. *Applied Energy*. [Online]. **74**(1–2),pp.195–202. Available from: http://linkinghub.elsevier.com/retrieve/pii/S0306261902001460.

He, B., Martin, V. and Setterwall, F. 2004. Phase transition temperature ranges and storage density of paraffin wax phase change materials. *Energy*. [Online]. **29**(11),pp.1785–1804. [Accessed 14 November 2013]. Available from: http://linkinghub.elsevier.com/retrieve/pii/S0360544204000775.

Heertje, L., Leunis, M. and Heertje, I. 1997. Measurement of Shape and Size of Fat Crystals by Electron Microscopy. *LWT - Food Science and Technology*. [Online]. **30**(2),pp.141–146. Available from: http://linkinghub.elsevier.com/retrieve/pii/S0023643896901449.

Hildebrand, J.H. 1979. An improvement in the theory of regular solutions. *Proceedings of the National Academy of Sciences of the United States of America*. **76**(12),pp.6040–6041.

Hildebrand, J.H. 1934. Experimental Tests of a General Equation for Solubility. .

57(1),pp.866–871.

Hildebrand, J.H. 1916. Solubility. *Journal of the American Chemical Society*. [Online]. **38**(8),pp.1452–1473. Available from: http://pubs.acs.org/doi/abs/10.1021/ja02265a002.

Hildebrand, J.H. and Lamoreaux, R.H. 1974. Solubility of Gases in Liquids: Fact and Theory. *Industrial & Engineering Chemistry Fundamentals*. [Online]. **13**(2),pp.110–115. Available from: http://dx.doi.org/10.1021/i160050a004.

Hildebrand, J.H. and Scott, R.L. 1979. Solutions of Nonelectrolytes. *A Textbook of Physical Chemistry*. [Online]. **1**(1),pp.301–352. Available from: http://linkinghub.elsevier.com/retrieve/pii/B9780120442621500141.

HIMRAN, S., SUWONO, A. and MANSOORI, G.A. 1994. Characterization of Alkanes and Paraffin Waxes for Application as Phase Change Energy Storage Medium. *Energy Sources*. [Online]. **16**(1),pp.117–128. [Accessed 13 November 2013]. Available from: http://www.tandfonline.com/doi/abs/10.1080/00908319408909065.

Hoffmann, R., Amundsen, L., Huang, Z., Zheng, S. and Fogler, H.S. 2012. Wax deposition in stratified oil/water flow. *Energy and Fuels*. **26**(6),pp.3416–3423.

Ibrahim, A.A. and Jibril, B.Y. 2005. Controlled Release of Paraffin Wax/Rosin-Coated Fertilizers. *Industrial & Engineering Chemistry Research*. [Online]. **44**(7),pp.2288–2291. Available from: http://pubs.acs.org/doi/abs/10.1021/ie048853d.

Ijeomah, C.E., Dandekar, A.Y., Chukwu, G.A., Khataniar, S., Patil, S.L. and Baldwin, A.L. 2008. Measurement of wax appearance temperature under simulated pipeline (dynamic) conditions. *Energy and Fuels*. **22**(4),pp.2437–2442.

Imai, T., Nakamura, K. and Shibata, M. 2001. Relationship between the hardness of an oil-wax gel and the surface structure of the wax crystals. *Colloids and Surfaces A: Physicochemical and Engineering Aspects*. **194**(1–3),pp.233–237.

Jafari Ansaroudi, H.R., Vafaie-Sefti, M., Masoudi, S., Jafari Behbahani, T. and Jafari, H. 2013. Study of the morphology of wax crystals in the presence of ethylene-co-vinyl acetate copolymer. *Petroleum Science and Technology*. **31**(6),pp.643–651.

Jalili, N. and Laxminarayana, K. 2004. A review of atomic force microscopy imaging systems: Application to molecular metrology and biological sciences. *Mechatronics*. **14**(8),pp.907–945.

Jennings, D.W. and Weispfennig, K. 2005. Experimental solubility data of various n-alkane waxes: Effects of alkane chain length, alkane odd versus even carbon number structures, and solvent chemistry on solubility. *Fluid Phase Equilibria*. **227**(1),pp.27–35.

Jiang, Z., Hutchinson, J.M. and Imrie, C.T. 2001. Measurement of the wax appearance temperatures of crude oils by temperature modulated differential scanning calorimetry. *Fuel*. **80**(3),pp.367–371.

Kané, M., Djabourov, M., Volle, J.L., Lechaire, J.P. and Frebourg, G. 2003. Morphology of paraffin crystals in waxy crude oils cooled in quiescent conditions and under flow. *Fuel*. **82**(2),pp.127–135.

Kok, M. V., Létoffé, J.M., Claudy, P., Martin, D., Garcin, M. and Volle, J.L. 1996. Comparison of wax appearance temperatures of crude oils by differential scanning calorimetry, thermomicroscopy and viscometry. *Fuel*. **75**(7),pp.787–790.

Krupa, I., Miková, G. and Luyt, A.S. 2007. Phase change materials based on low-density polyethylene/paraffin wax blends. *European Polymer Journal*. **43**(11),pp.4695–4705.

Kumar, S., Agrawal, K.M., Khan, H.U. and Sikora, A. 2004. Study of Phase Transition in Hard Microcrystalline Waxes and Wax Blends by Differential Scanning Calorimetry. *Petroleum Science and Technology*. [Online]. **22**(3–4),pp.337–345. Available from: http://www.tandfonline.com/doi/abs/10.1081/LFT-120024390.

Larkin, P. 2011. Chapter 1 - Introduction: Infrared and Raman Spectroscopy Vibrational *In*: *Infrared and Raman Spectroscopy* [Online]. Elsevier, pp. 1–

5. [Accessed 28 November 2016]. Available from: http://linkinghub.elsevier.com/retrieve/pii/B9780123869845100011.

Laux, H., Matthäi, M., Weil, B. and Butz, T. 2005. Influences on the Needle Penetration of Petroleum Wax. *Petroleum Science and Technology*. [Online]. **23**(1),pp.29–37. Available from: http://www.tandfonline.com/doi/abs/10.1081/LFT-20009686220.

Lehmann, U. and Kreipe, H. 2001. Real-time PCR analysis of DNA and RNA extracted from formalin-fixed and paraffin-embedded biopsies. *Methods (San Diego, Calif.)*. [Online]. **25**(4),pp.409–18. [Accessed 13 November 2013]. Available from: http://www.sciencedirect.com/science/article/pii/S1046202301912630.

Li, C., Liu, Q., Mei, Z., Wang, J., Xu, J. and Sun, D. 2009. Pickering emulsions stabilized by paraffin wax and Laponite clay particles. *Journal of Colloid and Interface Science*. [Online]. **336**(1),pp.314–321. [Accessed 13 November 2013]. Available from: http://www.ncbi.nlm.nih.gov/pubmed/19428022.

Lide, D.R. 2003. *CRC Handbook of Chemistry and Physics, 84th Edition Edited by David R. Lide (National Institute of Standards and Technology). CRC Press LLC: Boca Raton. 2003. 2616 pp. $139.95. ISBN 0-8493-0484-9.* CRC Press.

Long, D.A. 1977. *Raman Spectroscopy*. New York (N.Y): McGraw Hill.

Luyt, A.S. and Krupa, I. 2007. Thermal behaviour of low and high molecular weight paraffin waxes used for designing phase change materials. *Thermochimica Acta*. **467**(1–2),pp.117–120.

Luyt, A.S., Krupa, I., Assumption, H.J., Ahmad, E.E.M. and Mofokeng, J.P. 2010. Blends of polyamide 12 and maleic anhydride grafted paraffin wax as potential phase change materials. *Polymer Testing*. [Online]. **29**(1),pp.100–106. [Accessed 13 November 2013]. Available from: http://linkinghub.elsevier.com/retrieve/pii/S0142941809001603.

Mahmoud, R., Gierycz, P., Solimando, R. and Rogalski, M. 2005. Calorimetric probing of n-alkane - Petroleum asphaltene interactions. *Energy and Fuels*. **19**(6),pp.2474–2479.

Martos, C., Coto, B., Espada, J.J., Robustillo, M.D., Gómez, S. and Peña, J.L. 2008. Experimental determination and characterization of wax fractions precipitated as a function of temperature. *Energy and Fuels*. [Online]. **22**(2),pp.708–714. [Accessed 5 December 2013]. Available from: http://pubs.acs.org/doi/abs/10.1021/ef7003927.

Matthäi, M., Laux, H. and Hildebrand, G. 2001. An investigation of the dependence of penetration on the temperature and composition of paraffin waxes. *European Journal of Lipid Science and Technology*. [Online]. **103**(5),pp.292–298. [Accessed 4 December 2013]. Available from: http://dx.doi.org/10.1002/1438-9312(200105)103:5%253C292::AID-EJLT292%253E3.0.CO%255Cn2-1.

McBride, W. 1961. Thalidomide and Congenital Abnormalities. *The Lancet*. [Online]. **278**(7216),pp.1358–1358. Available from: https://doi.org/10.1016/S0140-6736(61)90927-8.

Mian, S. a., Colley, H.E., Thornhill, M.H. and Rehman, I.U. 2014. Development of a de-waxing protocol for tissue engineered models of the oral mucosa used for Raman spectroscopic analysis. *Applied Spectroscopy Reviews*. [Online]. (November),pp.00–00. Available from: http://dx.doi.org/10.1080/05704928.2014.882348.

Musser, B.J. and Kilpatrick, P.K. 1998. Molecular Characterization of Wax Isolated from a Variety of Crude Oils. *Energy & Fuels*. [Online]. **12**(4),pp.715–725. [Accessed 11 December 2013]. Available from: http://pubs.acs.org/doi/abs/10.1021/ef970206u.

Mutimer, M.N., Riffkin, C., Hill, J.A. and Cyr, G.N. 1956. Modern Ointment Base Technology I.:Properties of Hydrocarbon Gels*. *Journal of the American Pharmaceutical Association (Scientific ed.)*. [Online]. **45**(2),pp.101–105. Available from: http://linkinghub.elsevier.com/retrieve/pii/S0095955315338087.

Neto, D. and Neto, B. 2009. Determination of Wax Appearance Temperature (Wat) In Paraffin-Solvent Systems by Photoelectric Signal and Viscosimetry. *Brazilian Journal of Petroleum and Gas*. **3**(4),pp.149–157.

O Faolain, E. 2005. Raman Spectroscopic Evaluation of Efficacy of Current Paraffin Wax Section Dewaxing Agents. *Journal of Histochemistry and Cytochemistry*. [Online]. **53**(1),pp.121–129. Available from: http://www.jhc.org/cgi/doi/10.1369/jhc.4A6536.2005.

Van Ooteghem, M. 1965. Measurement of the Yield Values of Petrolatums and Lanolins with the Penetrometer. *Pharm. Acta Helv*. **40**,p.543.

Pahlavan, F., Mousavi, M., Hung, A. and Fini, E.H. 2016. Investigating molecular interactions and surface morphology of wax-doped asphaltenes. *Phys. Chem. Chem. Phys.* [Online]. **18**(13),pp.8840–8854. Available from: http://xlink.rsc.org/?DOI=C5CP07180A.

Park, E.K. and Song, K.W. 2010. Rheological evaluation of petroleum jelly as a base material in ointment and cream formulations: Steady shear flow behavior. *Archives of Pharmacal Research*. [Online]. **33**(1),pp.141–150. [Accessed 1 April 2014]. Available from: http://www.cheric.org/research/tech/periodicals/view.php?seq=855615.

Pharmacopoeia, E. 2005. 2.9.9. MEASUREMENT OF CONSISTENCY BY PENETROMETRY *In*: *European Pharmacopoeia 5.0*., pp. 235–237.

Pu, G. and Severtson, S.J. 2009. Dependency of contact angle hysteresis on crystallinity for n-alkane substrates. *Journal of Physical Chemistry C*. **113**(16),pp.6673–6680.

Ruoff, R.S., Doris, S.T., M, R. and L, D.C. 1993. Solubility of C60 in a Variety of Solvents. *J. Phys. Chem.* **97**,pp.3379–3383.

Sánchez, P., Sánchez-Fernandez, M.V., Romero, A., Rodríguez, J.F. and Sánchez-Silva, L. 2010. Development of thermo-regulating textiles using paraffin wax microcapsules. *Thermochimica Acta*. [Online]. **498**(1–2),pp.16–21. [Accessed 13 November 2013]. Available from: http://linkinghub.elsevier.com/retrieve/pii/S0040603109003529.

Sarker, D.K. 2013. Creams and ointments *In*: *A Drug Developer's Toolbag*. John Wiley & Sons, Ltd, pp. 69–76.

Sato, T., Araki, S., Morimoto, M., Tanaka, R. and Yamamoto, H. 2014.

Comparison of hansen solubility parameter of asphaltenes extracted from bitumen produced in different geographical regions. *Energy and Fuels*. **28**(2),pp.891–897.

Schramm, G. 1994. *A Practical Approach to Rheology and Rheometry* [Online]. [Accessed 1 April 2014]. Available from: http://www.polymer.cn/bbs/File/UserFiles/UpLoad/200904010309415s.pdf.

Sharma, Y.R. 2007. *Elementary Organic Spectroscopy* [Online]. S. Chand Limited. Available from: https://books.google.co.uk/books?id=aoIrDAAAQBAJ.

Socrates, G. 2004. *Infrared and Raman characteristic group frequencies*.

Speight, J.G. 2011. *Handbook of Industrial Hydrocarbon Processes* [Online]. Elsevier. [Accessed 4 December 2013]. Available from: http://www.sciencedirect.com/science/article/pii/B978075068632710009X.

Statista 2016. 2015 Ranking of the Global Top 10 Oil and Gas Companies Based on Revenue. *Financial Times*. [Online]. [Accessed 23 November 2016]. Available from: http://www.statista.com/statistics/272710/top-10-oil-and-gas-companies-worldwide-based-on-revenue/.

Turrell, G. 1972. *Infrared and Raman Spectra of Crystals*. Academic Pr.

Venkatesan, R., Nagarajan, N.R., Paso, K., Yi, Y.B., Sastry, A.M. and Fogler, H.S. 2005. The strength of paraffin gels formed under static and flow conditions. *Chemical Engineering Science*. **60**(13),pp.3587–3598.

Vilasau, J., Solans, C., Gómez, M.J., Dabrio, J., Mújika-Garai, R. and Esquena, J. 2011. Influence of a mixed ionic/nonionic surfactant system and the emulsification process on the properties of paraffin emulsions. *Colloids and Surfaces A: Physicochemical and Engineering Aspects*. [Online]. **392**(1),pp.38–44. [Accessed 21 November 2013]. Available from: http://linkinghub.elsevier.com/retrieve/pii/S0927775711005899.

Xiang, J. and Drzal, L.T. 2011. Investigation of exfoliated graphite nanoplatelets (xGnP) in improving thermal conductivity of paraffin wax-based phase change material. *Solar Energy Materials and Solar Cells*. [Online].

95(7),pp.1811–1818. [Accessed 13 November 2013]. Available from: http://linkinghub.elsevier.com/retrieve/pii/S0927024811000675.

Zbik, M., Horn, R.G. and Shaw, N. 2006. AFM study of paraffin wax surfaces. *Colloids and Surfaces A: Physicochemical and Engineering Aspects*. [Online]. **287**(1–3),pp.139–146. [Accessed 13 November 2013]. Available from: http://linkinghub.elsevier.com/retrieve/pii/S0927775706002585.

Zhang, Q., Zhao, Y. and Feng, J. 2013. Systematic investigation on shape stability of high-efficiency SEBS/paraffin form-stable phase change materials. *Solar Energy Materials and Solar Cells*. [Online]. **118**,pp.54–60. [Accessed 13 November 2013]. Available from: http://linkinghub.elsevier.com/retrieve/pii/S0927024813003814.

Zheng, M. and Du, W. 2006. Phase behavior, conformations, thermodynamic properties, and molecular motion of multicomponent paraffin waxes: A Raman spectroscopy study. *Vibrational Spectroscopy*. [Online]. **40**(2),pp.219–224. Available from: http://www.sciencedirect.com/science/article/pii/S0924203105001360.